THE UNIVERSITY OF MANITOBA

CONSTANT MEAN EFFECTIVE STRESS TESTS ON SAND BENTONITE SPECIMENS AT ELEVATED TEMPERATURE

by

DARREN YARECHEWSKI

A THESIS

SUBMITTED TO THE FACULTY OF GRADUATE STUDIES

IN PARTIAL FULFILLMENT OF THE REQUIREMENTS FOR THE DEGREE OF

MASTER OF SCIENCE

DEPARTMENT OF CIVIL ENGINEERING

WINNIPEG, MANITOBA

MARCH, 1993

ISBN 0-315-81760-7

Canada

Name DARREN YARECHEWSKI

Dissertation Abstracts International is arranged by broad, general subject categories. Please select the one subject which most nearly describes the content of your dissertation. Enter the corresponding four-digit code in the spaces provided.

GEOTECHNOLOGY
SUBJECT TERM

0428
SUBJECT CODE

U·M·I

Subject Categories

THE HUMANITIES AND SOCIAL SCIENCES

COMMUNICATIONS AND THE ARTS
Architecture 0729
Art History 0377
Cinema 0900
Dance 0378
Fine Arts 0357
Information Science 0723
Journalism 0391
Library Science 0399
Mass Communications 0708
Music 0413
Speech Communication 0459
Theater 0465

EDUCATION
General 0515
Administration 0514
Adult and Continuing 0516
Agricultural 0517
Art 0273
Bilingual and Multicultural 0282
Business 0688
Community College 0275
Curriculum and Instruction 0727
Early Childhood 0518
Elementary 0524
Finance 0277
Guidance and Counseling 0519
Health 0680
Higher 0745
History of 0520
Home Economics 0278
Industrial 0521
Language and Literature 0279
Mathematics 0280
Music 0522
Philosophy of 0998
Physical 0523
Psychology 0525
Reading 0535
Religious 0527
Sciences 0714
Secondary 0533
Social Sciences 0534
Sociology of 0340
Special 0529
Teacher Training 0530
Technology 0710
Tests and Measurements 0288
Vocational 0747

LANGUAGE, LITERATURE AND LINGUISTICS
Language
- General 0679
- Ancient 0289
- Linguistics 0290
- Modern 0291

Literature
- General 0401
- Classical 0294
- Comparative 0295
- Medieval 0297
- Modern 0298
- African 0316
- American 0591
- Asian 0305
- Canadian (English) 0352
- Canadian (French) 0355
- English 0593
- Germanic 0311
- Latin American 0312
- Middle Eastern 0315
- Romance 0313
- Slavic and East European 0314

PHILOSOPHY, RELIGION AND THEOLOGY
Philosophy 0422
Religion
- General 0318
- Biblical Studies 0321
- Clergy 0319
- History of 0320
- Philosophy of 0322

Theology 0469

SOCIAL SCIENCES
American Studies 0323
Anthropology
- Archaeology 0324
- Cultural 0326
- Physical 0327

Business Administration
- General 0310
- Accounting 0272
- Banking 0770
- Management 0454
- Marketing 0338

Canadian Studies 0385
Economics
- General 0501
- Agricultural 0503
- Commerce-Business 0505
- Finance 0508
- History 0509
- Labor 0510
- Theory 0511

Folklore 0358
Geography 0366
Gerontology 0351
History
- General 0578
- Ancient 0579
- Medieval 0581
- Modern 0582
- Black 0328
- African 0331
- Asia, Australia and Oceania 0332
- Canadian 0334
- European 0335
- Latin American 0336
- Middle Eastern 0333
- United States 0337

History of Science 0585
Law 0398
Political Science
- General 0615
- International Law and Relations 0616
- Public Administration 0617

Recreation 0814
Social Work 0452
Sociology
- General 0626
- Criminology and Penology 0627
- Demography 0938
- Ethnic and Racial Studies 0631
- Individual and Family Studies 0628
- Industrial and Labor Relations 0629
- Public and Social Welfare 0630
- Social Structure and Development 0700
- Theory and Methods 0344

Transportation 0709
Urban and Regional Planning 0999
Women's Studies 0453

THE SCIENCES AND ENGINEERING

BIOLOGICAL SCIENCES
Agriculture
- General 0473
- Agronomy 0285
- Animal Culture and Nutrition 0475
- Animal Pathology 0476
- Food Science and Technology 0359
- Forestry and Wildlife 0478
- Plant Culture 0479
- Plant Pathology 0480
- Plant Physiology 0817
- Range Management 0777
- Wood Technology 0746

Biology
- General 0306
- Anatomy 0287
- Biostatistics 0308
- Botany 0309
- Cell 0379
- Ecology 0329
- Entomology 0353
- Genetics 0369
- Limnology 0793
- Microbiology 0410
- Molecular 0307
- Neuroscience 0317
- Oceanography 0416
- Physiology 0433
- Radiation 0821
- Veterinary Science 0778
- Zoology 0472

Biophysics
- General 0786
- Medical 0760

EARTH SCIENCES
Biogeochemistry 0425
Geochemistry 0996
Geodesy 0370
Geology 0372
Geophysics 0373
Hydrology 0388
Mineralogy 0411
Paleobotany 0345
Paleoecology 0426
Paleontology 0418
Paleozoology 0985
Palynology 0427
Physical Geography 0368
Physical Oceanography 0415

HEALTH AND ENVIRONMENTAL SCIENCES
Environmental Sciences 0768
Health Sciences
- General 0566
- Audiology 0300
- Chemotherapy 0992
- Dentistry 0567
- Education 0350
- Hospital Management 0769
- Human Development 0758
- Immunology 0982
- Medicine and Surgery 0564
- Mental Health 0347
- Nursing 0569
- Nutrition 0570
- Obstetrics and Gynecology 0380
- Occupational Health and Therapy 0354
- Ophthalmology 0381
- Pathology 0571
- Pharmacology 0419
- Pharmacy 0572
- Physical Therapy 0382
- Public Health 0573
- Radiology 0574
- Recreation 0575
- Speech Pathology 0460
- Toxicology 0383

Home Economics 0386

PHYSICAL SCIENCES
Pure Sciences
Chemistry
- General 0485
- Agricultural 0749
- Analytical 0486
- Biochemistry 0487
- Inorganic 0488
- Nuclear 0738
- Organic 0490
- Pharmaceutical 0491
- Physical 0494
- Polymer 0495
- Radiation 0754

Mathematics 0405
Physics
- General 0605
- Acoustics 0986
- Astronomy and Astrophysics 0606
- Atmospheric Science 0608
- Atomic 0748
- Electronics and Electricity 0607
- Elementary Particles and High Energy 0798
- Fluid and Plasma 0759
- Molecular 0609
- Nuclear 0610
- Optics 0752
- Radiation 0756
- Solid State 0611

Statistics 0463

Applied Sciences
Applied Mechanics 0346
Computer Science 0984
Engineering
- General 0537
- Aerospace 0538
- Agricultural 0539
- Automotive 0540
- Biomedical 0541
- Chemical 0542
- Civil 0543
- Electronics and Electrical 0544
- Heat and Thermodynamics 0348
- Hydraulic 0545
- Industrial 0546
- Marine 0547
- Materials Science 0794
- Mechanical 0548
- Metallurgy 0743
- Mining 0551
- Nuclear 0552
- Packaging 0549
- Petroleum 0765
- Sanitary and Municipal 0554
- System Science 0790

Geotechnology 0428
Operations Research 0796
Plastics Technology 0795
Textile Technology 0994

PSYCHOLOGY
General 0621
Behavioral 0384
Clinical 0622
Developmental 0620
Experimental 0623
Industrial 0624
Personality 0625
Physiological 0989
Psychobiology 0349
Psychometrics 0632
Social 0451

Nom _____

Dissertation Abstracts International est organisé en catégories de sujets. Veuillez s.v.p. choisir le sujet qui décrit le mieux votre thèse et inscrivez le code numérique approprié dans l'espace réservé ci-dessous.

_____ ☐☐☐ U·M·I

SUJET — CODE DE SUJET

Catégories par sujets

HUMANITÉS ET SCIENCES SOCIALES

COMMUNICATIONS ET LES ARTS
Architecture 0729
Beaux-arts 0357
Bibliothéconomie 0399
Cinéma 0900
Communication verbale 0459
Communications 0708
Danse 0378
Histoire de l'art 0377
Journalisme 0391
Musique 0413
Sciences de l'information 0723
Théâtre 0465

ÉDUCATION
Généralités 515
Administration 0514
Art 0273
Collèges communautaires 0275
Commerce 0688
Économie domestique 0278
Éducation permanente 0516
Éducation préscolaire 0518
Éducation sanitaire 0680
Enseignement agricole 0517
Enseignement bilingue et multiculturel 0282
Enseignement industriel 0521
Enseignement primaire. 0524
Enseignement professionnel 0747
Enseignement religieux 0527
Enseignement secondaire 0533
Enseignement spécial 0529
Enseignement supérieur 0745
Évaluation 0288
Finances 0277
Formation des enseignants 0530
Histoire de l'éducation 0520
Langues et littérature 0279
Lecture 0535
Mathématiques 0280
Musique 0522
Orientation et consultation 0519
Philosophie de l'éducation 0998
Physique 0523
Programmes d'études et enseignement 0727
Psychologie 0525
Sciences 0714
Sciences sociales 0534
Sociologie de l'éducation 0340
Technologie 0710

LANGUE, LITTÉRATURE ET LINGUISTIQUE
Langues
- Généralités 0679
- Anciennes 0289
- Linguistique 0290
- Modernes 0291

Littérature
- Généralités 0401
- Anciennes 0294
- Comparée 0295
- Médiévale 0297
- Moderne 0298
- Africaine 0316
- Américaine 0591
- Anglaise 0593
- Asiatique 0305
- Canadienne (Anglaise) 0352
- Canadienne (Française) 0355
- Germanique 0311
- Latino-américaine 0312
- Moyen-orientale 0315
- Romane 0313
- Slave et est-européenne 0314

PHILOSOPHIE, RELIGION ET THÉOLOGIE
Philosophie 0422
Religion
- Généralités 0318
- Clergé 0319
- Études bibliques 0321
- Histoire des religions 0320
- Philosophie de la religion 0322

Théologie 0469

SCIENCES SOCIALES
Anthropologie
- Archéologie 0324
- Culturelle 0326
- Physique 0327

Droit 0398
Économie
- Généralités 0501
- Commerce-Affaires 0505
- Économie agricole 0503
- Économie du travail 0510
- Finances 0508
- Histoire 0509
- Théorie 0511

Études américaines 0323
Études canadiennes 0385
Études féministes 0453
Folklore 0358
Géographie 0366
Gérontologie 0351
Gestion des affaires
- Généralités 0310
- Administration 0454
- Banques 0770
- Comptabilité 0272
- Marketing 0338

Histoire
- Histoire générale 0578
- Ancienne 0579
- Médiévale 0581
- Moderne 0582
- Histoire des noirs 0328
- Africaine 0331
- Canadienne 0334
- États-Unis 0337
- Européenne 0335
- Moyen-orientale 0333
- Latino-américaine 0336
- Asie, Australie et Océanie 0332

Histoire des sciences 0585
Loisirs 0814
Planification urbaine et régionale 0999
Science politique
- Généralités 0615
- Administration publique 0617
- Droit et relations internationales 0616

Sociologie
- Généralités 0626
- Aide et bien-être social 0630
- Criminologie et établissements pénitentiaires 0627
- Démographie 0938
- Études de l' individu et de la famille 0628
- Études des relations interethniques et des relations raciales 0631
- Structure et développement social 0700
- Théorie et méthodes. 0344
- Travail et relations industrielles 0629

Transports 0709
Travail social 0452

SCIENCES ET INGÉNIERIE

SCIENCES BIOLOGIQUES
Agriculture
- Généralités 0473
- Agronomie. 0285
- Alimentation et technologie alimentaire 0359
- Culture 0479
- Élevage et alimentation 0475
- Exploitation des pâturages 0777
- Pathologie animale 0476
- Pathologie végétale 0480
- Physiologie végétale 0817
- Sylviculture et faune 0478
- Technologie du bois 0746

Biologie
- Généralités 0306
- Anatomie 0287
- Biologie (Statistiques) 0308
- Biologie moléculaire 0307
- Botanique 0309
- Cellule 0379
- Écologie 0329
- Entomologie 0353
- Génétique 0369
- Limnologie 0793
- Microbiologie 0410
- Neurologie 0317
- Océanographie 0416
- Physiologie 0433
- Radiation 0821
- Science vétérinaire 0778
- Zoologie 0472

Biophysique
- Généralités 0786
- Medicale 0760

SCIENCES DE LA TERRE
Biogéochimie 0425
Géochimie 0996
Géodésie 0370
Géographie physique 0368
Géologie 0372
Géophysique 0373
Hydrologie 0388
Minéralogie 0411
Océanographie physique 0415
Paléobotanique 0345
Paléoécologie 0426
Paléontologie 0418
Paléozoologie 0985
Palynologie 0427

SCIENCES DE LA SANTÉ ET DE L'ENVIRONNEMENT
Économie domestique 0386
Sciences de l'environnement 0768
Sciences de la santé
- Généralités 0566
- Administration des hôpitaux 0769
- Alimentation et nutrition 0570
- Audiologie 0300
- Chimiothérapie 0992
- Dentisterie 0567
- Développement humain 0758
- Enseignement 0350
- Immunologie 0982
- Loisirs 0575
- Médecine du travail et thérapie 0354
- Médecine et chirurgie 0564
- Obstétrique et gynécologie 0380
- Ophtalmologie 0381
- Orthophonie 0460
- Pathologie 0571
- Pharmacie 0572
- Pharmacologie 0419
- Physiothérapie 0382
- Radiologie 0574
- Santé mentale 0347
- Santé publique 0573
- Soins infirmiers 0569
- Toxicologie 0383

SCIENCES PHYSIQUES
Sciences Pures
Chimie
- Généralités 0485
- Biochimie 487
- Chimie agricole 0749
- Chimie analytique 0486
- Chimie minérale 0488
- Chimie nucléaire 0738
- Chimie organique 0490
- Chimie pharmaceutique 0491
- Physique 0494
- PolymÈres 0495
- Radiation 0754

Mathématiques 0405
Physique
- Généralités 0605
- Acoustique 0986
- Astronomie et astrophysique 0606
- Électronique et électricité 0607
- Fluides et plasma 0759
- Météorologie 0608
- Optique 0752
- Particules (Physique nucléaire) 0798
- Physique atomique 0748
- Physique de l'état solide 0611
- Physique moléculaire 0609
- Physique nucléaire 0610
- Radiation 0756

Statistiques 0463

Sciences Appliqués Et Technologie
Informatique 0984
Ingénierie
- Généralités 0537
- Agricole 0539
- Automobile 0540
- Biomédicale 0541
- Chaleur et thermodynamique 0348
- Conditionnement (Emballage) 0549
- Génie aérospatial 0538
- Génie chimique 0542
- Génie civil 0543
- Génie électronique et électrique 0544
- Génie industriel 0546
- Génie mécanique 0548
- Génie nucléaire 0552
- Ingénierie des systèmes 0790
- Mécanique navale 0547
- Métallurgie 0743
- Science des matériaux 0794
- Technique du pétrole 0765
- Technique minière 0551
- Techniques sanitaires et municipales 0554
- Technologie hydraulique 0545

Mécanique appliquée 0346
Géotechnologie 0428
Matières plastiques (Technologie) 0795
Recherche opérationnelle 0796
Textiles et tissus (Technologie) 0794

PSYCHOLOGIE
Généralités 0621
Personnalité 0625
Psychobiologie 0349
Psychologie clinique 0622
Psychologie du comportement 0384
Psychologie du développement 0620
Psychologie expérimentale 0623
Psychologie industrielle 0624
Psychologie physiologique 0989
Psychologie sociale 0451
Psychométrie 0632

CONSTANT MEAN EFFECTIVE STRESS TESTS ON SAND BENTONITE SPECIMENS AT ELEVATED TEMPERATURE

BY

DARREN YARECHEWSKI

A Thesis submitted to the Faculty of Graduate Studies of the University of Manitoba in partial fulfillment of the requirements for the degree of

MASTER OF SCIENCE

ACKNOWLEDGEMENTS

The author wishes to express his appreciation to his wife, Charlie, for her patience and understanding during the course of his studies and laboratory tests.

The wisdom and guidance provided by the author's advisor, Dr. James Graham, have proven invaluable and is gratefully acknowledged. The financial support he provided through the AECL research grant is also greatly appreciated.

The construction and modifications performed to the laboratory equipment were provided through the talents of Narong Piamsalee, Martin Green, Steve Meyerhoff, and Ed Lemke.

The author would like to extend his gratitude to Brian Lingnau, Naoto Tanaka, Jim Oswell, and Tom Crilly for the many constructive discussions regarding the buffer testing program. The assistance of Alan Wan, David Dixon, Bruce Kjartanson, and Ingrid Trestrail is also appreciated.

ABSTRACT

A series of ten triaxial tests has been conducted at the University of Manitoba on buffer specimens at elevated temperatures of 65°C and 100°C and with high pressures up to a maximum effective stress of 3.0 MPa. The buffer is a sand-bentonite mixture to be used to seal canisters containing high-level radioactive fuel waste deep within the crystalline rocks of the Canadian Shield. The high temperature (100°C) of the radioactive fuel waste necessitates testing the buffer at elevated temperatures to determine its strength and volume change characteristics. The specimens were sheared under a relatively uncommon stress path in which the mean effective stress p' was kept constant.

The equipment, specimen forming procedures, and the test methodology are described in detail. Membrane diffusion tests were performed on silicone rubber membranes used to seal the specimen from the cell fluid. All test results are presented in a detailed systematic manner.

The shear strength envelopes show only small variation with temperature, and are broadly comparable with the results of previous researchers. The Critical State Lines are dependent on temperature with decreased clay specific volume being produced with increased temperature. The Normal Consolidation Lines show evidence of shrinking yield loci with increased temperature, and this agrees with results shown by other researchers on different clays. The Normal Consolidation Lines and Critical State Lines agree generally with results obtained by Lingnau and Saadat using different test procedures.

LIST OF CONTENTS

LIST OF TABLES

LIST OF FIGURES

LIST OF SYMBOLS

e	Void ratio
CID'	Consolidated isotropic drained tests at constant mean effective stress
CIU	Consolidated isotropic undrained tests with pore pressure measurement
Ci	Curie
CSL	Critical state line
DPT	Differential pressure transducer
E_{50}	Young's modulus at $q = 0.5\ q_{max}$
G_{50}	Shear modulus at $q = 0.5\ q_{max}$
G_c	Specific weight for clay
{ I }	Unit tensor
LSG	Lateral strain gauge
LVDT	Linear variable differential transformer
M	Slope of critical state line in q-p' space
N	Location of normal consolidation line in V_c:ln p' plane
OCR	Overconsolidation ratio
PRV	Pressure relief valve
p'	Mean effective stress $(\sigma'_1 + 2\ \sigma'_3)/3$
p'_c, p'_{cons}	Consolidation pressure
p'_{cs}	Mean effective stress at critical state
q	Deviator stress$(\sigma_1 - \sigma_3) = (\sigma'_1 - \sigma'_3)$
q_{cs}	Deviator stress at critical state
rad	radiation absorbed dose
rem	roentgen equivalent for man
RTD	Resistance thermal device
Sv	Sievert

u, u_b	Pore water pressure, back pressure
V	Specific volume
V_c	Clay specific volume
V_o	Initial specimen volume
α	Angle of shear planes to the major principal axis
α	Alpha particles (Appendix A only)
β	Beta particles
β_{cw}	Thermal expansion coefficient for pore water
β_s	Thermal expansion coefficient for mineral solids (average)
γ	Gamma particles
γ_c	Effective clay dry density
γ_w	Unit weight of water
Γ	Location of critical state line in V_c:ln p' plane
$\varepsilon_1,\varepsilon_2,\varepsilon_3$	Principal strains
$\dot{\varepsilon}_1$	Axial strain rate
ε_s	Shear strain
ε_v	Volumetric strain
$\delta\varepsilon_v^p$	Plastic volumetric strain increment
η	Stress ratio = q/p'
κ	Slope of unload-reload line in V_c:ln p' space
λ	Slope of normal compression line and critical state line in V_c:ln p' plane
ν	Poisson's ratio
$\sigma_1,\sigma_2,\sigma_3$	Principal total stresses
$\sigma_1',\sigma_2',\sigma_3'$	Principal effective stresses
ϕ	Angle of shearing resistance

CHAPTER 1

INTRODUCTION

This thesis deals with one aspect of the proposed Canadian concept for burying nuclear waste in the hard rocks of the Canadian Shield. It involves laboratory tests on one of the materials that will be used to seal radioactive waste from the inhabited environment. The introductory material presented in Section 1.1 and 1.2 originally came from a term paper for course 23.716 Environmental Impact. The term paper is presented in its entirety in Appendix A.

1.1 Nuclear Energy

Nuclear reactors harness the energy that is produced by fission of Uranium-235. The heat produced through the fission process is used to convert water to steam which turns a turbine to produce electricity. Fission is a process where atoms are split by neutrons. The splitting of the atom releases neutrons, radiation, and radioactive fragments called fission products.

The reactors that Canada produces are called CANDU reactors (CANadian Deuterium Uranium). These reactors employ natural uranium which contains 0.7% U-235 and 98.3% U-238. Power comes from fission of Uranium-235. Uranium-238 is not fissile material but absorbs neutrons and decays to fissile Plutonium-239. The uranium is processed into fuel bundles that can be used in the CANDU reactor. The natural uranium is formed into ceramic pellets which are housed in zirconium tubes and arranged to form a fuel bundle.

Each time fission occurs 2 to 3 neutrons are released that can take part in another fission. The splitting of a single atom creates the potential to split more atoms and is called a chain reaction. The fuel is considered spent when the number of neutrons that are absorbed by the fission products becomes greater than the number of neutrons being released.

The spent fuel contains a variety of fission products that emit harmful radiation. The radiation levels decay with time and the radioactive elements become more stable. The decay process for some elements can take a very long time with the reduction of half the radioactive elements being called the half-life. Elements such as iodine-129 and plutonium-239 have half-lives of 17,000,000 and 24,000 years, respectively.

The objective of research undertaken at Atomic Energy of Canada Limited (AECL) in Pinawa, Manitoba is to develop a safe and permanent method for disposal of nuclear waste. Currently spent fuel bundles are stored in pools or in above-ground concrete canisters. These storage methods are safe but require maintenance and monitoring. Who will monitor the waste 10,000 years from now? Can we be assured that the type of society that we know will exist in the future? The answers to these important questions are outside the scope of this thesis.

1.2 Proposed Method for Nuclear Waste Disposal in Canada

In Canada, the investigation into a suitable permanent method to dispose of high-level radioactive waste began in 1977 with the Hare Report. The committee was formed by the Canadian Government to investigate the disposal options that exist.

The report recommends that the waste be contained deep in a crystalline rock formation.

AECL has investigated the characteristics of granite plutons in the area known geologically as the Canadian Shield. The Shield has been stable for hundreds of millions of years and contains about 1500 plutons. Plutons are formed at depths of several kilometres when magma wells upward and then solidifies. The magma cools slowly to form crystalline igneous rock which is later exposed at the ground surface by erosion and uplift. Since the rock forms as a massive body it contains few fractures and joints. It is proposed that vaults be excavated in a granite pluton 1000 m below the ground surface to contain the nuclear fuel waste. The current proposal is that boreholes would be excavated within the floor of the vaults to allow emplacement of nuclear waste containers, although further options are under examination.

The Canadian disposal concept consists of a number of barriers which are designed to retard the flow of the nuclear waste. The barriers will prevent the waste from migrating to the biosphere before the radioactive elements have decayed to a safe level. The barriers include (1) a stable waste form, (2) the container, (3) seals, and (4) granite rock.

The spent fuel bundles will be stored directly in titanium containers. The fuel is 99% contained in the ceramic pellets with 1% existing within the interior of the zirconium tubes. Therefore the radionuclides that are free to be solubilized and transported are the 1% that are not contained within the pellet. The container is designed to withstand the vault conditions for 500 years. Once the canister corrodes, the radionuclides are contained by a sand-clay mixture called buffer

whose properties are investigated in this thesis. The buffer surrounds the container within the emplacement borehole and will retard the groundwater flow. Beyond the buffer, the remaining transport paths for the radionuclides are through the backfill that is used to seal the vault, and the granite rock.

1.3 The Role of Buffer in Nuclear Waste Containment

The sand-clay mixture (that is, the buffer) will seal the annulus between the titanium container and the granite rock. The buffer also supports the canister and prevents it from settling within the borehole. Bentonite makes up the clay portion of the buffer and is used for its swelling properties.

During the initial stages after emplacement, the canister temperature will increase to 100°C and the buffer will dry. Once the waste disposal site is decommissioned the original groundwater levels will be restored and water will be reintroduced to the buffer. The buffer will swell and reseal any cracks that were formed during the drying stage. It is anticipated that the resaturation period will be less than the life span of the container. The buffer will experience conditions of elevated temperature, and water pressures up to 10 MPa.

1.4 Past Research on Buffer

The buffer has been a topic of research at the University of Manitoba since 1984. A series of MSc and PhD dissertations have been based on examination of various aspects of the buffer properties. The purpose of the research has been to determine the characteristics of the buffer and to be able to model the buffer

numerically. The following provides an overview of previous research on buffer at the University of Manitoba.

Sun (1986) conducted triaxial tests on buffer specimens with a dry density of 1.50 Mg/m^3. The tests he performed include incremental isotropic consolidation, undrained strain controlled, and drained load controlled tests (with constant mean effective stress p'). These tests examined the pseudo-elastic bulk modulus, strength envelope, and the shear modulus of the buffer up to a confining pressure of 1.0 MPa at ambient temperatures.

Wan (1987) performed similar triaxial tests to Sun but with an increased confining pressure of 3.0 MPa at ambient temperature. A technique for forming specimens that equilibriate faster was examined by varying the dry density and water content. He extended the swelling pressure-effective clay dry density relationship and investigated the applicability of the effective stress concept. The critical state model as it relates to the buffer was investigated.

Saadat (1989) examined the validity of the effective stress concept and developed a conceptual model for the buffer. The pressure-clay dry density relationship was extended to a confining pressure of 10 MPa on specimens with dry densities of 1.50 Mg/m^3 and also the AECL reference, 1.67 Mg/m^3. His triaxial tests included isotropic consolidation, undrained strain controlled, and drained stress controlled tests. The tests were performed at room temperature with some tests being performed at back pressures as high as 7 MPa. The rock-buffer-container-backfill interaction was examined through preliminary finite element modelling.

Yin (1990) developed an elastic visco-plastic model for triaxial stressing. The model predicts creep, strain rate, and relaxation in consolidation and shear. The model was calibrated with existing data from tests performed at room temperature.

Oswell (1991) performed a variety of tests to examine the elastic plastic behaviour of the buffer at room temperature. He studied the elastic moduli, yield locus, flow rule, plastic potential, hardening law, and failure criterion. The tests were performed on specimens with densities of 1.49 Mg/m^3 and 1.67 Mg/m^3.

Lingnau is currently writing up a testing program that for the first time investigated the response of buffer to elevated isothermal temperatures of 65°C and 100°C. Triaxial tests were performed on buffer specimens compacted to 1.67 Mg/m^3 dry density with a maximum confining pressure of 10 MPa. The specimens were consolidated and then sheared undrained using a constant rate of strain.

Tanaka and Crilly have recently begun research programs that will investigate the effect of temperature on yielding and also the effect of thermal ramping. Thermally ramped tests will model the conditions in the vault better than isothermal tests. The temperature of the buffer will gradually increase to a maximum of 100°C in the vault, approach isothermal conditions, and then begin cooling. These tests will initially be performed using illite rather than bentonite to gain a better understanding of thermal effects on a less active clay. The bentonite contains montmorillonite which has a similar basic structure to illite. However, illite has less significant swelling characteristics because it contains sheets of aluminum-silica units that are weakly bound by potassium ions instead of water. It is expected that the less active behaviour of illite will

lead to a clearer understanding of temperature effects on clay without the additional complexity introduced by the creep behaviour of the bentonite.

1.5 The Need for this Research

The previous section has outlined the work of past researchers and provides a precedence for the types of laboratory testing that are conducted. Predominantly, two types of triaxial test are conducted at the University of Manitoba. These are (1) undrained strain controlled tests and (2) drained stress controlled tests with either the cell pressure or the mean effective stress held constant. The purpose of performing triaxial tests using two methods is to ensure that the strength envelope is independent of the chosen stress path.

The testing necessary to characterize the buffer at ambient temperatures is now virtually complete. Since the buffer will experience temperatures approaching a maximum of 100°C it is necessary to advance the testing program to encompass thermal effects. Presently, Lingnau has completed isothermal triaxial tests at elevated temperatures using just one stress path in undrained strain controlled tests.

Using the philosophy outlined earlier, it follows that triaxial tests along a second stress path are necessary to advance the research. The research program described in this thesis was designed to investigate buffer characteristics at elevated temperatures along a second independent stress path. This stress path, similar to the ambient temperature test programs, is at a constant mean effective stress, but now the tests were performed at elevated temperatures. Results should hopefully be corroborated by Lingnau's results when they are finalized.

The constant mean effective stress tests have been performed in a manner similar to that used by Sun, Wan, and Saadat. The specimens were cylinders of buffer with height 100 mm and diameter 50 mm, formed at a dry density of 1.66 Mg/m^3. The specimens were first consolidated isotropically and subsequently sheared with five increments of stress under drained conditions. The specimens were initially consolidated isothermally at 26°C, and then the temperature was increased to 65°C or 100°C to allow further consolidation at elevated temperature. The purpose was to observe the thermal effects on consolidation, independent of pressure changes. Lingnau's tests were done slightly differently by increasing the specimen temperature at the start of the test.

The effective stress concept has been examined at elevated temperature by increasing the back pressure to 7.0 MPa while maintaining a constant mean effective stress, similar to Saadat's tests. This was done for two tests at temperatures of 26°C and 65°C. These specimens were consolidated and then sheared in the usual way at the elevated back pressure. This is probably the first time that tests of this nature have been performed.

CHAPTER 2

LITERATURE REVIEW

As mentioned in Chapter 1, the Canadian concept for disposal of high-level radioactive waste includes a sand-bentonite barrier called buffer surrounding the waste container. The buffer has a low hydraulic conductivity at $\approx 10^{-12}$ m/s (Cheung et al. 1985, Dixon et al. 1987) which will impede the flow of radionuclides from the depository. Buffer consists of bentonite (from Avonlea, Saskatchewan) which contains 80% sodium montmorillonite, and 10% illite, with smaller amounts of quartz, feldspar, gypsum, and carbonates. Sodium bentonite is an active clay which swells or compresses, depending on the imposed effective confining pressure, until volumetric equilibrium is reached. The sand particles are 60% retained between sizes of 0.2 mm to 1.0 mm. The sand is well-graded with a uniformity coefficient of 4.0 (Dixon et al. 1985).

The two components of the buffer, silica sand and sodium bentonite, occur separately in nature. As a result, the buffer is an engineered material and experience is limited as to how it will perform compared to common natural soils. Graham et al. (1989) showed that the behaviour of the buffer is controlled by the clay fraction, and that the sand grains are not in direct contact, but merely act as filler. The purpose of the sand is to reduce shrinkage, increase the thermal conductivity, and decrease the hydraulic conductivity of the buffer (Dixon and Gray 1985, Radhakrishna 1984).

The behaviour of the buffer has been modelled using the theories of Critical State Soil Mechanics (CSSM) which was first introduced by Roscoe et al. (1958). CSSM uses three parameters to define the current state of the soil, namely the mean effective stress p', deviator stress q, and specific volume V (these variables are defined below). In triaxial compression tests, it can be assumed that the major principal total stress σ_1 corresponds to the axial stress. From the conditions imposed in the test cell, it is also assumed that the intermediate and minor principal total stresses σ_2 and σ_3 are equal, with magnitude equal to the applied confining pressure.

The applicability of the effective stress concept as it pertains to the buffer was examined by Oswell (1991). He concluded that the effective stress concept could be applied to the buffer provided that conditions of constant volume or constant volume straining rate, constant temperature, and constant chemistry are met (Graham et al. 1992). Therefore the effective stress σ' can be calculated as,

$$\{\sigma'\} = \{\sigma\} - u\{I\} \qquad .....(1)$$

where u is the porewater pressure and { I } is the unit tensor. The effective stress is taken to include interparticle and physico-chemical forces.

The equations for p' and q are shown below for both total and effective stress.

Total stress (axial symmetry, $\sigma_2 = \sigma_3$; $\varepsilon_2 = \varepsilon_3$)

$$p = (\sigma_1 + \sigma_2 + \sigma_3) / 3 = (\sigma_1 + 2\,\sigma_3) / 3 \qquad .....(2)$$

$$q = \sigma_1 - \sigma_3 \qquad .....(3)$$

Effective stress

$$p' = ((\sigma_1 - u) + 2\,(\sigma_3 - u)) / 3 = (\sigma_1' + 2\,\sigma_3') / 3 \quad .....(4)$$

$$q = (\sigma_1 - u) - (\sigma_3 - u) = \sigma_1' - \sigma_3' \quad .....(5)$$

Volume and shear strains are respectively defined by

$$\varepsilon_v = \varepsilon_1 + 2\,\varepsilon_3 \quad .....(6)$$

$$\varepsilon_s = 2\,(\varepsilon_1 - \varepsilon_3)/3 = \varepsilon_1 - \varepsilon_v / 3 \quad .....(7)$$

Specific volume is the third parameter required to determine the "state" of the specimen (Wroth and Houlsby 1985) and is a measure of the soil particle spacing. The specific volume is the volume occupied by unit volume of solids and can be represented as,

$$V = 1 + e \quad .....(8)$$

where e is the void ratio = (volume of voids) ÷ (volume of solids). Since the behaviour of the buffer is dominated by the clay fraction it is appropriate to use the specific volume of the clay-water phase V_c to describe the particle spacing of the soil. Specimens can also be examined based on the dry density of the clay-water phase γ_c. The clay-water specific volume can be calculated based on the following equation,

$$V_c = G_c\,\gamma_w / \gamma_c \quad .....(9)$$

where G_c is the specific weight (called "relative density" in SI) of the clay phase, γ_c is the effective clay dry density, and γ_w is the unit weight of water. The specific weight G_c has been taken as 2.75 for the clay particles.

Critical State Soil Mechanics uses elastic-plastic theories to link the shear strength of a soil with its deformation characteristics. The five components used to form the elastic-plastic model include (1) elastic behaviour, (2) yield criterion, (3) plastic potential, (4) hardening law, and (5) failure rule. Elasticity is the recoverable response of the specimen after deformation has taken place. The elastic region is bounded by a curved yield locus in p'-q space or a yield surface if considering the 3-dimensional case in p'-q-V_c space. The yield surface marks the boundary between elastic and plastic deformation, that is, between recoverable and nonrecoverable deformations. Yield loci were defined by Graham, Noonan, and Lew (1983) for Winnipeg clay. The results showed that yield loci could be normalized with respect to preconsolidation pressure, defined as the yield point in a 1-dimensional consolidation test.

Once the state of the specimen reaches a current yield locus the specimen begins to strain plastically and deformations are not entirely recoverable. The ratio between increments of plastic volumetric strain and plastic shear strain defines the plastic strain increment vector, and can be used to determine the magnitude and direction of the plastic shear strain if plastic volumetric strains are known from the hardening law. The plastic potential is a locus joining lines that are orthogonal to the plastic strain increment vector. If the plastic potential coincides with the yield locus the plastic strains are said to be associated. The hardening law also determines relative changes in the size of the yield surface. Expansion of the yield locus due to plastic straining is called strain hardening, while shrinking of the yield surface is strain softening.

Oswell (1991) determined that the elastic behaviour of buffer at ambient temperature after unloading was generally isotropic (see also Wan 1987). That is

the yield locus meets the p'-axis in p'-q space at approximately a right angle. He normalized the yield locus for specimens with two different dry densities and found that the shape is the same for both. That is, the shape of the yield locus is independent of specimen dry density. The yield surface is also located well below the failure envelope for the buffer, and this indicates that plastic straining always occurs between yielding and failure of the specimen. The plastic potential for the buffer is non-associated.

A simplification of the general CSSM soil model is given by the Cam Clay model. The Cam Clay model makes assumptions with regard to the shape of the curves in p'-q-V_c space. The shape of the yield locus in p'-q sections is taken to be elliptical. This model is therefore, for an isotropic soil since the yield loci are orthogonal to the p'-axis. It assumes linear relationships exist for the elastic unload-reload lines in ln p'-V_c sections with slope κ. Likewise, the hardening law assumes a linear relationship between the specific volume and preconsolidation pressure with slope λ. The Cam Clay model assumes that the shape of the yield locus remains elliptical during plastic straining. The plastic potential is taken to be associated with the yield locus.

A final aspect of the Cam Clay model is its treatment of the "critical state" condition. Once a soil has yielded it begins to deform plastically. Shear stresses can continue to change until a condition is reached where only incremental plastic shear strains occur, and the volume is constant. This condition is called critical state, when continued shear strains occur without change in effective stress p', shear stress q, pore water pressure u, and specific volume V. Different initial stresses cause specimens to define a locus of critical states called the critical state line (CSL). For the Cam Clay model, the CSL has slope M in p'-q

space and passes through the origin ($q_{cs} = M\ p'_{cs}$). From the requirement that $\delta\varepsilon_v^p = 0$ and the assumption of associated flow, the CSL passes through the top of each yield locus. The critical state line in ln p'-V space is parallel to and on the "dry" side (lower V_c) of the hardening law line (slope λ) defining preconsolidation pressures.

The next requirement in buffer-related research is to gain an understanding of the effects of different temperatures on the parameters of this soil model. Thermal effects on buffer have been examined by Lingnau for undrained strain controlled triaxial tests at elevated specimen temperatures of 65°C and 100°C. Graham et al. (1990) showed that in the pressure range from 0.6 to 3.0 MPa the isotropic consolidation behaviour in log p_c'-V_c space gives parallel lines with a slope $\lambda = 0.171$. The lines produce smaller values of V_c with increased temperature, and this indicates shrinkage of the yield surface with heating.

Research into the effects of elevated temperature on soil properties has been performed during the 1980's with regard to the safe disposal of radioactive waste. The research has been performed in Italy by Dr. T. Hueckel at ISMES, Bergamo; in the United States by Dr. S. Houston at Sandia Laboratories; and in Canada by Dr. J. Graham at the University of Manitoba. The proposed nuclear waste disposal concept in Italy is to deposit the nuclear waste in continental clay. The concept for Houston's work is to dispose of high-level nuclear waste in canisters 30 m below the sea floor, at an ocean depth of approximately 4000 to 6000 m.

Hueckel and Pellegrini (1989) examined the effect of heating undrained specimens with a constant deviator stress and constant total isotropic stress. They determined that the specimens could fail thermally with increasing specimen

temperature. The temperature increase elevates the porewater pressure which reduces the mean effective stress in the specimen. The yield locus was found to soften due to increased temperature, and harden with decreased temperature. The increased pore pressure effect has been observed in Athabasca oil sand by Agar (1986) who found that the pore fluids expand more rapidly than the solid particles. Agar also found that the pore pressure-temperature relationship is non-linear under a constant confining stress, and linear under a constant effective confining stress. Increased porewater pressure has also been examined by Campanella and Mitchell (1968) and Plum and Esrig (1969).

According to Yong et al. (1969) increased temperature up to 45°C on kaolinite results in increased swelling pressure. This is of importance when considering that the sodium bentonite is a swelling clay. Aylmore et al. (1969) determined that the sorptive properties of illite can be reduced by heating. This was indicated by a water content decrease from 200% to 35% when the clay was preheated to 400°C.

Shrinkage of the yield locus (at constant specific volume) has been shown to occur in 1-dimensional oedometer tests with an increase in temperature (Erikkson 1989). This was also confirmed by Tidfors and Sällfors (1989) who also found that specimens with higher liquid limit produce a more pronounced decrease in preconsolidation pressure. The λ-lines are shown to be parallel. The unload-reload lines (slope κ) are shown to be approximately parallel by Demars and Charles (1982), Plum and Esrig (1969), and Campanella and Mitchell (1968). (However, more recent studies by doctoral candidate Tanaka suggests this may not always be true.) Thermal effects drive the κ-line to lower specific volumes with

increased temperature. Therefore, at a given preconsolidation pressure the elastic region decreases with temperature.

A decrease in volume with increased temperature was found to occur in drained tests on normally consolidated clays by Campanella and Mitchell (1968) and Hueckel et al. (1987). Plum and Esrig (1969) investigated thermal effects on specimens formed from slurry. They found that heating a normally consolidated soft soil increases the compressibility and produces volume decreases. Cooling of the specimen was found to make the specimen behave as though it were overconsolidated. This lends support to the idea that the yield locus expands on cooling. Expansion of the yield locus for a normally consolidated specimen would appear to make the specimen overconsolidated. Demars and Charles (1982) determined that a portion of the volumetric strains from thermal cycling are nonrecoverable. The amount of nonrecoverable volume strain increases with decreasing OCR and plasticity. Campanella and Mitchell (1968) show that the nonrecoverable volumetric strains accumulate with repeated heating-cooling cycles for a normally consolidated soil.

The shear strength of oil sand was found not to change significantly due to temperature (Agar et al. 1987). Paaswell (1967) suggested that for a low plastic clay, temperature increases reduce the viscosity of the pore fluid resulting in decreased shearing resistance. Wöhlbier and Henning (1969) found that pretreating kaolinite by heating produced higher shear strengths. Lingnau's test program also suggests that the undrained shear strength for the buffer increases with elevated temperature.

This literature review shows that a good experimental framework exists for understanding the effects of elevated temperatures on normal clay soils. However,

nothing exists in the literature for highly plastic natural clays, or for the engineered mixture of bentonite and sand that forms the buffer. The work described in this thesis is complementary to the concurrent experimental program which has just been completed at the University of Manitoba by Lingnau. This is the first program to be reported on the shear behaviour of the Canadian buffer at elevated temperatures.

CHAPTER 3

TEST EQUIPMENT

3.1 Triaxial Cells for High Temperature Testing

The geotechnical laboratories at the University of Manitoba have three triaxial cells that operate under pressures up to 10 MPa and maximum temperatures of 100°C. A schematic of the triaxial cell is shown in Figure 3.1. The early stages of this program involved commissioning the third of these cells before beginning the testing program. Another of the three cells became available for this program in December 1991, allowing two tests to be performed simultaneously. This speeded the work greatly because testing periods have lasted between 19 to 71 days, and production was slow with only a single cell. Another feature of the cell design allows inspection of the specimen alignment during the installation process. The specimen and top cap can be mounted onto the pedestal and the piston can be brought in contact before the outer sleeve is installed and the cell pressure raised. This ensures that all the components are aligned prior to testing. The cells were also designed to accommodate an internal load cell which eliminates measurement of piston-seal friction when the specimen is sheared, and lateral displacement transducers.

The cell in Figure 3.1 is constructed of nickel-plated mild steel with a stainless steel piston, top cap, and pedestal. The cell consists of two thick circular plates which are connected by four rods. The lower end of the rod is threaded into the cell base while the upper end is machined with a shoulder which supports the

top plate. To enclose the cell, a steel sleeve slips around the outside of the plates and is seated in a groove in the cell base. A thinner plate is bolted to the top plate with four large nuts on the rods. This upper plate rests on the top plate and the top edge of the sleeve and, in conjunction with the rods, holds the cell together when it is filled with cell fluid and then pressurized.

The cell is sealed with nitroxille U-cup seals; the seals are located around the piston, rods, top plate, and cell base. In the past, it was found that seals with different chemical compositions became brittle and cracked either due to heat, or contact with water or silicone oil. The nitroxille seals are designed to withstand these conditions. A concave portion of these seals faces towards the pressurized chamber. Increasing the cell pressure causes the concave portion to open and exert pressure against the walls of the groove, thus providing a seal. This is physically apparent when the piston is to be brought in contact with the top cap for the beginning of shear. The axial load required to overcome the cell pressure exerted on the piston can be calculated. However, additional loads must be applied to overcome the friction between the seal and the piston. The use of a load transducer inside the cell is designed to overcome uncertainties in the piston friction force.

Testing procedures used with this equipment are evolving continuously. The following sections of the thesis have been written at Dr. Graham's request to place on record the procedures that had been found most successful up to mid-1992.

The specimen sits on a stainless steel pedestal which is removable (if required) from the cell base. Three viton sealing rings are used to separate the pore fluid from the cell fluid and the atmosphere. One ring is located slightly inside the

periphery of the pedestal and two smaller rings are located around each of the two ports that supply water to the specimen. The pedestal is connected to the cell base with two bolts which are located within the large diameter sealing ring and outside the rings that seal the ports. With this arrangement the rings at the ports seal the pore fluid from the atmosphere, while the exterior ring seals cell fluid from the atmosphere. As an added precaution, the countersunk bolt holes that contain the bolts for the pedestal are threaded and sealed with brass plugs. This prevents any pore fluid losses past the portal sealing rings to the atmosphere.

Axial loads are applied to the specimen through a 25 mm diameter stainless steel piston with a submersible load cell threaded to the lower end. The load cell is housed between two steel plates. The lower plate contains a steel ball which contacts the load cell button and the bevelled top cap on the specimen. Bolts pass up through the load cell and thread into the upper plate which threads onto the piston. A steel ball is also placed at the top of the piston during assembly. The steel balls used in the axial assembly prevent eccentric loads from being applied to the specimen.

The piston can be locked vertically in place by turning a locking collar downward. This forces the tapered interior, as shown in Figure 3.2, to bear on two brass collets which grip the piston. A steel sleeve couples the lock collar to the thick top plate. A teflon tube is contained between the sleeve and the piston to ensure axial alignment of the piston. It was found that the teflon expanded with heat and wedged between the sleeve and piston. This resulted in either a stick-slip motion of the piston as seen later in test specimen T1302 or a completely immobile piston as was the case for T1305, causing the test to end after consolidation. Later

tests were performed without the teflon bushing and relied only on the brass collets to ensure the specimen is loaded axially.

Silicone oil is used as the cell fluid for all high temperature testing in the University Laboratory. The reasons for using silicone oil as opposed to water or antifreeze are: (a) thermal stability, (b) low electrical conductivity, (c) nonflammability (flashpoint 500°C), (d) low compressibility, (e) viscosity (500 centipoise), (f) inertness, and (g) non-toxicity. The low electrical conductivity allows electrical devices to be used inside the cell. The inertness of the oil prevents corrosion of nitroxille/viton seals and steel components.

All pressures applied during testing originate from nitrogen tanks which can satisfy the test requirements of 10 MPa maximum cell pressure. An added benefit to using nitrogen tanks is that tests can be operated independently and do not rely on one source such as a compressor. The nitrogen pressure is applied through a wall-mounted regulator, accumulator, pressure transducer, and the cell coupled in series. The accumulator, which can withstand a maximum pressure of 21 MPa, contains a diaphragm that acts as an interface between the nitrogen and silicone oil. The accumulator performs two functions by: (1) preventing silicone oil from backing up into the regulator and (2) in the event of a major cell fluid leak the nitrogen gas could not move past the accumulator, thus preventing an explosive gas failure at the cell. The pore pressure is applied directly to the water surface in a back pressure burette which will be described in detail in Section 3.2.2.

Axial load is applied to the specimen using a system of hangers, levers, and weights. The triaxial tests in this research program are performed under a constant mean effective stress p', which requires constant deviator, cell, and pore

pressures during each stage of shearing. The lever system provides an 8:1 ratio between the load exerted on the piston and the hanger load.

The plumbing for the triaxial cell consists of a variety of tubing, fittings, and valves. Copper and stainless steel tubing (3.18 mm-diameter) are used for the pore water and back pressure lines. Stainless steel tubing and fittings are used to connect the cell base to the brass pore pressure block which houses the porewater pressure transducer. This line encounters the largest thermal effects. Therefore the use of only stainless steel parts, means that differential expansion does not create leakage problems. Copper tubing is used for the remaining lines. Metallic rather than plastic tubing is used to withstand the maximum back pressure of 7 MPa which has been used in these tests. (Back pressure is the controlled test pressure that is applied to the pore fluid inside the specimen to ensure saturation, and mimic the porewater pressure expected in the field.) Hydraulic hose is used between the regulator, accumulator, and the cell to transmit pressure from the nitrogen tank to the silicone oil cell fluid. Swagelock compression fittings and pipe threaded connections are used to join components together.

The valves used on the triaxial cells are brass Nupro valves which are right-angle valves that produce no volume change when opened or closed. On delivery, the valves contain teflon-coated sealing rings. Viton rings are installed as replacements if the sealing rings become damaged. Both these materials can withstand temperatures in excess of 100°C, with the teflon-coated rings being preferrable in applications with corrosive liquids. The valves are directional; this means that they must be opened from high to low pressure according to the direction indicated on the valve. Opening a valve that has higher pressure on the

opposite side results in tearing of the sealing ring and the valve will not seal when closed again.

3.2 Instrumentation and Calibration

The specimen and its surrounding environment are monitored using a variety of DC electrical devices. Each device is plugged into a main power board on the test frame which is connected, by one main cord to a data acquisition computer. Voltage or resistance readings are converted into engineering units with a Basic program called Datalog, and then stored in a file on the computer's hard drive. The data are later imported into a Lotus spreadsheet. With the aid of macros, the lotus files and their graphs can be updated routinely and inspected readily. This facilitates careful monitoring during the course of the experiment.

The computer system uses a Basic program called Voltmetr which was supplied with the Hewlett Packard hardware in the data acquisition system. This is used to measure the voltage output of a device during calibration when, for example, a known pressure is applied to a pressure transducer and the corresponding voltage is measured. The transducers are manufactured to provide a linear relationship between the measured parameter and signal output. The slope of this line is called the gain, and is used in the Datalog program to convert the voltage measurement into engineering units. The zero in the Datalog calibration routine is the voltage reading when atmospheric pressure is applied to the transducer. The zero does not correspond to the Y-intercept of the line plotted on the pressure vs. voltage graph.

3.2.1 Pressure

All pressures are measured as close to the specimen as possible with the aid of brass junction blocks mounted on the cell base. Each block contains four outlets which are equipped with valves to transfer either pore or cell fluid. A fifth outlet located in the bottom of the block contains a Micro Gage P-102 pressure transducer which has a capacity of 14 MPa. The pressure transducer is temperature compensated to 100°C and is accurate to within 0.25% of full scale (or 35 kPa). The benefit of having pressure transducers mounted on the cell base (rather than in the more customary wall-mounted units) is that they allow more accurate measurements because of lower compliance in the measuring system. However, there is greater risk that cell-base mounted valves and fittings may leak when subjected to elevated temperatures.

The pressure transducers are calibrated using a portable dead weight tester (Ashcroft model 8130) which has a capacity of 7 MPa. The accuracy of the dead weight tester is 0.03% of the actual reading. The dead weight tester operates using a capstan to apply hydraulic pressure beneath a vertical piston. The piston has a small base plate at the end which is used to support circular weights which are engraved with specific pressures. When the capstan is turned inward, the pressure increases beneath the vertical piston, forcing the piston and the weights upward. The weights are brought above a marked height and the pressure transducer voltage is measured. The sum of the marked pressures on the weights corresponds to the pressure in the hydraulic oil.

3.2.2 Volume

The change in specimen volume is determined by measuring the volume of water that travels between the Differential Pressure Transducer shown in Figure 3.3 and the specimen. The volume measurement contains two components which are (a) the Differential Pressure Transducer (DPT) and (b) the back pressure burette. The DPT's used in this laboratory are Rosemount and Fisher brands. They employ an instrumented diaphragm between two chambers. Nitrogen is contained on one side of the diaphragm while water is in the opposite chamber. The DPT measures a change in hydraulic head which is provided by a column of water in the back pressure burette. Gain and zero screws on the DPT housing can be used to set the maximum and minimum elevation of the column of water that will be measured. For the tests in this program, the DPT is set to measure the visible volume change that can be seen in the graduated glass burette. A narrower gain setting produces more sensitive volume measurements.

The DPT is calibrated using the graduated glass burette inside the back pressure burette. The calibration of the DPT depends on pressure level and therefore must be calibrated for different back pressures used during testing. In general, a back pressure of 1 MPa is used, although specimens T1303 and T1307 were consolidated and sheared with a back pressure of 7 MPa. The change in the gain is 0.001 ml/mV for a pressure change from 1 MPa to 7 MPa. There is also a shift in the zero of -0.225 ml over the same pressure range.

As shown in Figure 3.3, the back pressure burette consists of a glass, graduated burette which is sealed in a clear acrylic tube with brass end caps and sealing rings. The end caps are threaded on the tube to compress the sealing rings. The

glass burette is sealed in the bottom cap with a sealing ring while the top is open. Therefore, when the acrylic tube is pressurized with nitrogen, pressure is applied to the interior and exterior of the glass burette.

The acrylic tubing was originally purchased for the back pressures up to 1 MPa. To perform tests with higher back pressures up to 7 MPa, the acrylic portion of the back pressure burette had to be redesigned. It was determined that the burette could withstand the 10 MPa back pressure, if the acrylic were made with a sufficient opening to allow only the glass burette to pass inside with nominal clearance. The necessary calculations were based on elastic thick-walled theory.

Thick-walled acrylic tubes were manufactured to replace the existing tubes by purchasing rods of clear acrylic and drilling a hole along the axis to fit the glass burette. The burette was pressure tested up to 10 MPa in a shielded case to ensure that theory corresponded with reality. The burettes have performed well, for periods as long as 15 days at 7 MPa back pressure, and to this point show no indication of fatique such as the crazing that is evident in some of the low pressure burettes. The thicker wall makes seeing the graduations on the glass burette slightly more difficult, especially in areas where the manufacturing process of drilling the tube has scarred the interior of the clear acrylic.

3.2.3 Temperature

Resistance Thermal Devices (RTD) are used to measure the temperature of the specimen. The devices are lightly attached to the outer membrane using a silicone rubber band. The lead wires pass through the cell base via a bulkhead connector.

The purpose was to locate the sensor as close to the specimen as possible to measure the specimen temperature as opposed to the cell temperature.

A three wire RTD consists of a ceramic base overlain with platinum windings and is similar in appearance to a strain gauge. Changes in temperature cause a resistance change in the platinum that can be measured by the computer. Unlike thermocouples which measure the temperature difference between the leads and the tip, the RTD is compensated for lead wire resistance and measures the actual temperature.

Calibration of the RTD requires a temperature bath of a known temperature and a resistance measuring device. The RTD is heated and cooled in the bath and the resistance is read at intervals from Channels 7 and 9, on the data acquisition computer, the two channels that are assigned to measure the signals as resistance rather than voltage. The RTD's are accurate to ±0.1°C and can withstand temperatures up to 500°C.

The differential temperature across the length of the specimen is measured using two bridged thermocouples. A copper-constantan thermocouple is attached to the specimen using a silicone rubber band and the tips are positioned near the top and bottom of the specimen. When the temperatures are equal at both tips the voltage reading is zero. Calibration is performed by placing each tip in a separate temperature bath. The temperature difference between the two baths is recorded and the voltage measured. The thermocouple is accurate to ±0.1°C.

The cell temperature is controlled using programmable ramp and soak temperature controllers. The two brands of controller that are currently in use are the Thermoelectric Tempstar II and the Microscan 200. The cell temperature is input to

the controller through the RTD and in turn power is supplied to a 150 watt silicone rubber heater band. The band has sufficient power to maintain a cell temperature of 65°C with a power output of about 50%. At 100°C it is necessary to use a base heater to supplement the power output. The base heater is a stove element which is attached to the base of the cell and supplies power through a transformer. The transformer maintains constant base heater power, allowing the controller to adjust the power output to the heater band, thus maintaining the programmed temperature.

The controller operates using three principles of control theory to maintain the target temperature which are: (1) proportional (P), (2) integral (I), and derivative (D) response. The proportional band is a controller setting that controls the temperature oscillations about the setpoint value. The setpoint value is the target temperature that is to be maintained. The controller supplies a proportion of 100% power to the heater, depending on the location of the actual temperature within the proportional band. As the temperature approaches the upper limit of the band the power output reduces until there is no power supplied to the heater. In the opposite sense, if the temperature drops towards the lower limit, power output increases to 100%. The proportional response may cause the temperature to stabilize anywhere within the bandwidth. The reset function which has units of repeats/minute is used to bring the temperature to the setpoint value. As the temperature cycles about the setpoint value, integral and derivative response can be used to smooth the oscillations.

The proportional band used for these triaxial systems is 2% which is considered a low value, and is suitable for the slowly changing temperatures in this program. This is due to the size and thermal inertia of the system. The reset rates for the Thermoelectric and Microscan are 0.01 and 0.1 rpt./min., respectively. These

values are the lowest manufacturer's settings for both controllers. The cycle time is the oscillation time for the output relay. The Thermoelectric controller has a single pole double throw relay which is a mechanical switch. If the cycle time was set too fast, the relay was found to overheat and require replacment. As a result, a cycle time of 60 seconds is used with the Thermoelectric controller. The Microscan contains a solid state relay which cannot overheat, therefore the cycle time is set at 1 second. The integral and derivative response were set to 0.2 minutes and zero for the Thermoelectric and zero for the Microscan. It was found that the Microscan did not require any integral or derivative response because the reset rate was higher than the Thermoelectric value.

3.2.4 Axial Strain

The axial movement of the specimen is measured during shear using a Linear Variable Differential Transformer (LVDT). Since the tests are performed under isothermal conditions, it is appropriate to consider the cell components to be in thermal equilibrium. As a result, axial displacement of the piston is measured relative to the top of the cell without concern about thermal changes in the dimensions of the reference points and LVDT supports. The LVDT (Transtek model 0244-000 and Hewlett Packard 7DCDT-1000) is supported by an aluminum bracket which is connected in turn to a steel rod and the cell top plate. The drop rod rests on an aluminum plate which is attached to the piston. All components are assembled prior to the beginning of shear to ensure that they are all in temperature equilibrium so that only axial movement of the piston is measured, and not thermal expansion of the components.

The LVDT has a displacement range of 25 mm. The device is located outside of the insulated container and does not experience significant heating. The LVDT is specified for temperatures ranging between -53°C and 121°C. Calibration is performed using a series of gauge blocks immediately prior to the beginning of shear.

3.2.5 Lateral Strain

The lateral specimen displacement is measured at mid-height using a Lateral Strain Gauge (LSG) as shown in Figure 3.4. The LSG's were built in the University Laboratories using a design from Kolymbas and Wu (1989) which came from an original design by El-Ruwayih (1976). When the specimen changes diameter, the thinner bands flex and the strains are measured by the strain gauges. The strain gauge converts the flexure into an electical signal which can be measured at the computer.

The LSG consists of four short lengths of spring steel which are 11 mm wide and 80 mm long with two thick and two thin bands. Two bands have a thickness of 0.76 mm while the two thinner sections have a thickness of 0.10 mm. The thin sections are curved to meet the stiff sections which are held against the specimen with metal springs. The sections are soldered together and where the stiff sections contact the specimen brass chocks soldered to the stiff bands prevent the device from moving horizontally. Strain gauges (300 Ω) are attached to the inside and outside of the curved section and produce a linear response to the lateral movements of the specimen.

The LSG is calibrated using three brass cylinders of known diameter. Initially, some hysteresis is present when commissioning the device but with continued flexing

repeatable results are obtained. The device is also calibrated for temperatures ranging from 26°C to 100°C since shifts of zero and gain are dependent on temperature. The calibration procedure entails placing the LSG mounted on the brass cylinder in a silicone oil temperature bath and measuring the cylinder diameter, temperature, and voltage at 10°C intervals.

3.2.6 Load

Axial load measurements during shear are made using a 22.2 kN capacity model 1211 Interface submersible load cell. The load cell is temperature compensated for the temperature range from -9°C to 46°C and has a working range from -54°C to 93°C. Although these temperatures do not extend to 100°C the manufacturer claims that the load cell will work in this application. It has also been found that the load cell can operate under repeated 100°C temperatures and produce consistent results. The accuracy of the load cell is 0.05% of full scale within the temperature compensated range.

The load cell is calibrated using a compression frame in the structures laboratory at the University of Manitoba. Removing the load cell from the triaxial cell requires that the top plate be removed to lift the load cell upwards. The load cell can not be inserted from the side between the steel rods that support the top plate. The load cells are calibrated with the plate and ball apparatus mounted to the load cell as it would be used during testing.

3.3 Loading System

The loading procedure for a triaxial test, where the mean effective stress p' is held constant, involves applying increments of deviator stress. A constant deviator stress is maintained during each load increment and the cell pressure is adjusted to maintain a constant p'. In the tests in this research program, five equal increments of deviator stress were chosen. At the fifth and final increment, the specimen is predicted to fail, based on the strength envelope provided by other researchers such as Saadat (1989). Failure is determined when the specimen exhibits excessive continuous axial straining, with a maximum strain of 15% being used to define the "end of test".

The increments of deviator stress are applied as axial loads using the system of hangers, levers, and weights, as shown in Figure 3.5. The hanger consists of a horizontal steel bar across the top of the piston. A steel ball is located between the bar and piston to prevent eccentric loading. Threaded 11 mm diameter steel rods are bolted to the top bar, and extend below the base of the triaxial cell where they are bolted to a second cross-bar. Thrust bearings are located between the bottom nuts and the lower cross-bar.

The lever arm consists of a 660 mm long beam with a cross-sectional height of 51 mm and width of 13 mm. Triangular steel pins extend through the beam at three locations. These pins provide the contact points that are used to transmit the load from the weights to the piston. The two pins directly beneath the cell are spaced 76 mm apart with the top of the end pin contacting the frame that supports the cell. The bottom of the middle pin contacts the piston hanger. The pin at the

opposite end of the beam supports a small hanger which carries the weights actually used to apply the axial load.

The distance between the two end pins is 608 mm which provides an 8:1 lever ratio (608 mm ÷ 76 mm) between the applied hanger load and the load exerted at the middle pin. Although this is correct in principle, loads measured at the load cell inside the test cell will be less than predicted due to friction from the U-Cup seal that encircles the piston. The friction losses depend on the cell pressure. A higher cell pressure causes the U-shaped seal to open laterally and generate its sealing by exerting greater force against the piston. The internal load cell allows measurement of the actual axial load on the specimen. This is a considerable improvement on the more usual external load cells which would require load corrections to be performed by subtracting the friction losses at the seal.

The lever arm is maintained in a horizontal position when the specimen is being sheared to ensure that a constant deviator stress q is applied. During shear, the piston moves downward and the lever arm tilts away from the cell. The lever is restored to a horizontal position by tightening the lower nuts on the piston hanger. Thrust bearings, immediately above the nuts, reduce the amount of torque required when the hanger rods are loaded.

A steel box around the lever arm is used to support the lever arm: (a) during consolidation when the unloaded lever is forced upward due to the cell pressure acting on the piston, (b) to support the lever arm when the load cell is brought in contact with the specimen, and (c) when the specimen fails rapidly at the end of shearing to prevent excessive axial movements and instrumentation damage. The top of the box is welded to a steel bolt which extends through the flange in the

supporting frame. The height of the box can be fixed by nuts located above and below the flange.

3.4 Heat Resistant Silicone Membranes

The triaxial tests in this program were performed isothermally at temperatures of 26°C, 65°C, and 100°C. The mechanism of sealing traditionally used is latex membranes, with Buna sealing rings holding the membrane tightly against the top cap and the pedestal. Latex membranes will not withstand elevated temperatures. During T1307 and T1306, at 65°C and 100°C, respectively, a section of latex was installed to cover the height of the specimen between two full length silicone membranes that were developed in the laboratories at the University of Manitoba by Lingnau. At 65°C, the colour of the latex was darkened from a light yellow to a dark brown with some pitting on the exterior. At 100°C, the latex was black in colour and had been totally remoulded during heating. The latex was soft, sticky, and had taken the shape of the silicone membranes where they had folded during shear. When the latex membrane was removed, it did not hold any of its original shape.

Research into an appropriate rubber mix to replace the latex was performed by Lingnau (1992) and after some experimentation it was decided to use silicone rubber TC5050 from BJB Enterprises of California, USA. This particular rubber was found to be more resistant to tearing and was flexible enough to facilitate sealing against the top cap and pedestal.

3.4.1 Manufacturing

The TC5050 silicone rubber is purchased in two components that are to be mixed in a 10:1 ratio by weight. The white bulk component and the blue hardener are combined and mixed until the color is consistently blue.

When mixing is complete, the mix is poured into the bottom of the mould shown in Figure 3.6. The mould is constructed of aluminum and is split lengthwise with a top and bottom cap. The mould is sealed along its length with a sheath of plastic, and at the base with a silicone rubber gasket (formed with the same silicone rubber material). After the mix is introduced to the mould, it is placed in a deairing chamber under a vaccuum of about 100 kPa for one hour. This removes air that was entrained during mixing. The amount of air in the mix can easily be seen during the first minute of deairing when the mix exhibits frothing.

The mould is removed from the deairing chamber and a piston is slid inside. The piston is a solid piece of aluminum with pins at the sides, near the top and bottom. The pins are designed to keep the piston a distance of about 1.3 mm away from the walls of the mould, which is the thickness of the membrane once the mix has cured. A compression frame is used to force the piston to the bottom of the mould. Considerable effort would be required if the piston were pushed manually due to the viscosity of the mix and the small opening between the piston and the mould. The piston is forced into the mould at a slow constant rate to allow any air that may be remaining in the mix an opportunity to escape.

After the piston is fully seated in the mould, the silicone rubber gasket and top cap are bolted to the top of the mould to seal the vessel. The mould is then

pressurized to 280 kPa to compress any remaining air bubbles and create as dense a membrane as possible. The mix remains pressurized during the curing period which lasts for about 24 hours at room temperature. During the early stages of membrane manufacturing, when the mould was not pressurized, air bubbles were occasionally found which rendered the membranes useless. After curing, the membrane is removed from the mould and inspected visually for obvious flaws.

3.4.2 Sealing and Diffusion Tests

The ten specimens that were tested in this program were sealed from the cell fluid with two layers of silicone membrane. With the exception of T1301 and T1302, all the tests used viton sealing rings with a cross-sectional diameter of 3.2 mm to seal the membrane against the top cap and pedestal. Hose clamps were used as the sealing device in T1301 and T1302. It was found later that these clamps allowed silicone oil to leak into the pore fluid after about four days, and their use was discontinued.

Viton sealing rings can withstand temperatures ranging between -29°C to 204°C and are used with an inside diameter of 38 mm which is 75% of the top cap and pedestal diameters. The ASTM D4767-88 standard for performing a Consolidated-Undrained Triaxial Compression Test on Cohesive Soil recommends that the inside diameter of the sealing rings be between 75% and 85% of the top cap and pedestal diameters. After the first use, the sealing rings stretch slightly, but the inside diameter remains within the specified limits. Five rings are used to seal the top of the membrane and seven sealing rings to seal the bottom. As many sealing rings are used as can physically be applied to the top cap and pedestal.

The membranes were subjected to diffusion tests to determine if fluid transport occurs through the membrane. A single membrane was used for the diffusion tests instead of the two membranes that are used during a regular triaxial test. Also, the buffer was replaced with a steel cylinder of the same dimensions as the buffer specimens, and was installed with filter strips and stones. This allows separation of volume changes occurring in the buffer from apparent volume changes caused by diffusion through the membranes. Details of the installation procedure will be described in Chapter 4.

The diffusion tests were performed in a simpler cell, known colloquially as "The Bomb", which has been used for high pressure consolidation tests with a maximum cell pressure of 10 MPa. It has no piston, and so cannot be used for shear tests. The cell is constructed of two main components which are (1) the cover and (2) the base. The cover consists of four steel pieces which are welded together. The base is constructed of aluminum and contains a groove for a large diameter viton sealing ring. The two pieces are clamped together with four large nuts and bolts. The brass pedestal is bolted to the cell base with two allen screws. The counter sunk bolt holes in the aluminum cell base are sealed with brass plugs to contain the pore water. A viton sealing ring with a 3.2 mm cross-sectional diameter is seated between the base of the pedestal and the cell base to separate the pore fluid from the cell fluid. The pore water line from the pedestal to the pore pressure transducer consists of a bore within the aluminum cell base rather than tubing.

The new sealing apparatus shown in Figure 3.7 was designed to seal the membrane against the top cap and pedestal. The reason for this new design was to ensure that any fluid transport that occurred was not moving past the sealing rings that are typically used. The design principle is to use the cell pressure to provide a

better seal. The brass ring around the pedestal contains a groove on the bottom in which a viton sealing ring is placed. The ring is bolted to the aluminum cell base and the sealing ring is compressed. The top of the brass ring is machined into a conical shape that comes close to the side of the pedestal at the bottom and flares outwards at the top. The membrane is placed on the pedestal and is curled back on itself. A viton sealing ring with a cross-sectional diameter of 5.1 mm is placed in the fold at the bottom of the membrane and is then pushed into the tapered brass ring. In cross-section, the 5.1 mm diameter sealing ring is wedged between the membrane, brass ring, and the pedestal. When the cell pressure is exerted on the large diameter sealing ring it is forced further into the taper. The pocket of air between the two sealing rings on the brass ring maintains a pressure that is less than the cell pressure, thus keeping a positive differential pressure across the large diameter sealing ring. Similar arrangements have been provided for the top cap.

Diffusion tests were performed on both latex and silicone membranes. The results of these tests are shown in Figures 3.8 to 3.13. The latex membrane has a thickness of 1.3 mm, the same as the silicone membrane. The temperature was held constant at 26°C during the latex diffusion test which was performed for 27 days, with the exception of the the first 3 days which were subject to room temperature conditions in the range 22°C to 23°C. As shown in Table 3.1, five different mean effective stresses ranging from 0.6 MPa to 9.0 MPa were applied and the corresponding volumetric strains measured.

For the latex membrane, Figure 3.10 shows that each pressure increment was accompanied by an immediate or elastic volumetric response which was followed by static conditions. The elastic volumetric changes are due to a change in cell

pressure and decrease markedly above an effective stress of 6.0 MPa. It is believed that this elastic response is due to compliance of the system. The first four increments show slightly expansive volumetric strains while the last two increments are slightly compressive. (Volume strain is defined by the ratio of volume change to the volume of the 100 mm high by 50 mm diameter specimen.) During the 27 day test period, the fluctuation in volumetric strain is approximately 0.2% if the initial elastic volume change due to the first application of a higher cell pressure is excluded.

It is difficult to determine, with certainty, whether the small tendencies towards volume change observed during the latex membrane test are diffusion or externally related properties, since the volume measurements are on the boundary of what the equipment can measure accurately. External effects include fluctuations in the room temperature, cell temperature, back pressure, and cell pressure. However, it is interesting to observe that changes in room temperature coincide with the volumetric changes. As shown in Table 3.1, slightly expansive volumetric strains are accompanied by cooling room temperatures and compressive strains parallel warming room temperatures. Only cell temperatures have been controlled during this program while burette and DPT readings are subjected to diurnal and seasonal changes in room temperature. It seems reasonable to conclude that the diffusion of silicone oil through a single latex membrane is minimal at room temperatures when external factors such as temperature changes and pressure changes are considered.

Results from Saadat (1989) shows a leakage rate of 0.005%/day at room temperature using two 1.3 mm latex membranes with silicone oil cell fluid. These results were obtained with a confining pressure of 10 MPa and back pressures ranging from 1 to 7 MPa. Saadat's sealing system used Buna sealing rings to seal the latex

membranes. Differences between Saadat's and these new tests may lie in the different sealing techniques or the effects of room temperature fluctuation.

Immediately following the diffusion test on latex a silicone membrane was installed in the "Bomb" using identical sealing techniques. Initially five pressure increments were applied while maintaining a constant cell temperature of 26°C, matching the procedure used during the diffusion test on latex. Following the application of pressure increments at 26°C the specimen temperature was increased to 65°C and then 100°C. The specimen temperature was held constant during each temperature and three pressure increments of 0.6, 1.5, and 3.0 MPa were applied. The results in Figure 3.13 show that compressive apparent volumetric strains occur approximately linearly with time. Table 3.1 shows that for the 26°C temperature results that an increased effective stress produces a greater volumetric strain rate until the effective stress reaches 6.0 MPa. Beyond an effective stress of 6 MPa the volumetric strain rate remains constant.

The apparently compressive nature of the volumetric strains suggests that silicone oil is being transported into the pore water. The rate of temperature change with time was not calculated for the silicone membrane test in Table 3.1, since the magnitude of the volumetric strain rates masks the effect of room temperature fluctuations.

At an effective stress of 0.6 MPa, the volumetric strain rate did not change with cell temperature. Faster volumetric strain rates occur with increased temperature for effective stresses of 1.5 and 3.0 MPa; between temperatures of 26°C and 65°C, the volumetric strain rate increases by 100% while between 65°C and 100°C, the rate increases by about 55%. The majority of the volumetric strain rates shown in

Table 3.1 for the silicone membrane, are greater than 0.1%/day which is the rate used to define the end of consolidation for the buffer. This raises fundamental questions about the effectiveness of these membranes. Further development work is being undertaken by current research students Tanaka and Crilly.

3.5 Leakage Tests

The triaxial cells are tested to ensure that the pore fluid and cell fluid lines do not leak prior to conducting tests on the buffer. The cell fluid line is tested by plugging the port in the cell base and pressurizing the line to 10 MPa. The presssure is maintained for at least one day and all fittings are inspected for leaks. The cell fluid line is tested after any modifications have been performed.

The pore water lines are leak tested using two methods. The first method tests the water lines from the back pressure burette to the junction block mounted on the cell base. The line is sealed by closing a valve between the junction block and the cell base, and is pressurized for a minimum of one day. The burette is pressurized to 1 MPa or 7 MPa depending on whether the standard or high pressure burette is used. The level in the burette is monitored using the DPT. A drop in the water level indicates a leak in the system.

The second method used to perform leakage tests on the pore fluid lines involves sealing the port in the pedestal. A small plug fitted with a sealing ring is seated in the pedestal port. The plug is held in place by applying an axial load with the hanger system. Similar to the first method, the line is pressurized up to 7 MPa and the water level monitored for any indication of leakage. One or other of these two procedures has generally been performed before each test. The tests show

the pore fluid lines to be free of leaks at ambient temperatures up to pressures of 7 MPa.

In addition, two full scale leakage tests have been conducted. These tests are similar in all aspects to a conventional triaxial test with the exception that the specimen is replaced by an aluminum cylinder. The cylinder has the same dimensions as the buffer specimen with a diameter of 50 mm and height of 100 mm. By using the aluminum cylinder, any volume changes that occur can be attributed to the system as opposed to the buffer. The test is performed using two silicone rubber membranes sealed against the top cap and pedestal with viton sealing rings.

The results of the two full scale leakage tests are shown in Figures 3.14 to 3.23. The purpose of the tests was to determine if the pore fluid system leaks at elevated temperatures of 100°C. The tests were conducted on the two different triaxial systems simultaneously. The conditions imposed on the mock specimens were the same for both cells. The cells were pressurized to 1.6 MPa with a back pressure of 1.0 MPa (p' = 0.6 MPa) and heated to 100°C on the first day of the tests. Apparent dilative volumetric strains were measured once the specimen temperature had reached thermal equilibrium at 100°C. Dilative volumetric strains are measured as a drop in the burette water level which indicates that a leak exists in the system. The leakage rate was -0.6%/day in both cells.

The balance of the testing time was spent searching for the source of the leakage. The water lines in both cells had been tested prior to the full scale tests using the second method outlined earlier whereby the pedestal port is sealed with an axial load at ambient temperatures. To ensure that the pore water line did not develop a leak due to heating of the cell the valve between the block and cell base

was closed for a period of one hour. The volumetric strain remained constant while the porewater pressure decreased by about 0.1 MPa. This indicated that the leak was located beyond the transducer block.

It was suspected that the two bolts that anchor the pedestal to the cell base may not be applying adequate compression to the sealing rings beneath the pedestal. To test whether this was actually the case, an axial load of about 1.7 MPa was applied to both mock specimens to determine if the volumetric strain rate would decrease. The volumetric strain rate decreased slightly to -0.5%/day but the general trend of flow out of the pore fluid lines remained. Therefore the pedestal rings were not perceived to be the source of leakage. As described previously the holes in the cell base that are used to secure the pedestal are sealed with plugs. Therefore, if water were able to leak past the seal rings surrounding the port beneath the pedestal it would be contained. The total volume of water lost during each test was about 12 ml which is far greater than can be stored in the chamber beneath the pedestal.

For the remainder of the discussion regarding the two full scale leakage tests the results will be presented for one test since the results are generally the same for both tests. It is interesting to note that although the triaxial systems are similar in general configuration each apparatus is entirely unique once the parts are assembled. For example, the valves and fittings that make up the system are constructed with adequate quality control to make the parts virtually identical when they arrive from the manufacturer. However, the valves and fittings on the two systems were connected by different individuals in the University Laboratory which creates differences between the cells. Since the results from these two

tests are the same this implies that the leaks may not originate from any specific connection but may be caused by a material property of one of the components.

The test continues with the temperature being decreased to 26°C. The volumetric strains become constant. Therefore, the leakage rate is influenced by temperature. The water line from the transducer block was replaced previously with stainless steel tubing. At the time of replacement brass fittings were left in place beneath the cell brass. Suspecting that differential thermal expansion between the brass and steel may open a leak upon heating the fittings were replaced with stainless steel. The back pressure was reduced to zero with the cell pressure reduced to 0.6 MPa to maintain the same effective stress. The cell was hoisted and with the valve at the transducer block closed the brass fittings were replaced.

Once the fittings were replaced the cell and pore pressures were restored to 1.6 MPa and 1.0 MPa, respectively, and the cell was heated to 100°C. The leak continued until the cell pressure was increased to 2.5 MPa. At an effective stress of 1.5 the volumetric strain became constant. When the effective stress was restored to 0.6 MPa the leakage continued. Therefore, the leakage rate is affected by the effective stress.

The back pressure was increased to 7 MPa with the effective stress maintained at 0.6 MPa to determine if the leakage rate is affected by the magnitude of the back pressure. The leakage rate was unchanged by the back pressure. The effective stress was subsequently increased to 1.5 MPa at elevated back pressure and the volumetric strain became constant. The effective stress was restored to 0.6 MPa at elevated back pressure and an axial stress of about 2.7 MPa was applied. The leakage rate was restored.

During the last stages of the full scale tests different results are obtained between the two tests. For Triaxial Cell #2, the deviator stress was increased to 3.9 MPa with the back pressure reduced to 1 MPa at an effective stress of 0.6 MPa. The specimen temperature was reduced to 68°C. The volumetric strain became constant and remained constant when the deviator stress was removed. The results near the end of the test on Triaxial Cell #3 show that the leakage rate remains constant regardless of the axial stress imposed and regardless of the back pressure as long as the effective stress remains constant at 0.6 MPa.

In summary, the two full scale leakage tests indicate that water moves out of the pore water lines at an effective stress of 0.6 MPa and specimen temperature of 100°C. The leak stops at an effective stress of 1.5 MPa. The leakage rate does not appear to be affected by the magnitude of the back pressure or by axial stress. The exact location of the leak has not been determined despite considerable effort, but it is known that the leak occurs between the specimen and the transducer block. Since fittings beneath the cell base appear to be sound and the compression of the sealing rings beneath the pedestal does not affect the volumetric strain, the double silicone membranes are perhaps allowing water to diffuse through to the silicone oil. These results are contrary to those obtained during the diffusion tests in "The Bomb", where a single membrane allowed silicone oil to pass through to the pore water and produce apparent compressive volumetric strains. The test setup was different in "The Bomb" because only a single membrane was tested whereas double membranes were used in these tests. In a follow-up program, Tanaka is developing new membranes, and new detailing for the pedestal.

CHAPTER 4

EXPERIMENTAL PROGRAM

4.1 Triaxial Tests with Constant Mean Effective Stress

The research program described here consists of ten triaxial tests on buffer at three constant mean effective stresses. The testing procedure can be divided into three distinct sections which include (1) specimen preparation, (2) consolidation, and (3) shear. The procedures will be reported in some detail to place on record the careful techniques that must be adopted.

The buffer is first mixed in the laboratory with a water content of about 23% prior to compaction, and the specimen is then formed in five layers using a rigid mould and compaction frame. The height of the specimen during the compaction process is carefully controlled to ensure the specimen has uniform density and high saturation.

Immediately after the specimen is formed it is seated on the pedestal in the triaxial cell and sealed with silicone membranes before beginning the consolidation process. The triaxial cell is filled with silicone oil and then pressurized to the target cell pressure. At the same time, a back pressure is applied to the pore water. Specimens are consolidated isotropically under the surrounding cell pressure until volumetric equilibrium has been attained. In all the work at the University of Manitoba, this has been arbitrarily taken to be when the volumetric strain rate decreases to 0.1%/day. For tests at elevated temperature, the specimen

is consolidated initially at about 26°C until volumetric equilibrium is reached, and then the specimen temperature is increased to either 65°C or 100°C. The consolidation process is complete when volumetric equilibrium is attained at the elevated isothermal conditions.

As mentioned in Chapter 3, once consolidation is complete the specimen is sheared by applying axial loads in five increments. Each additional load increment is added when the logarithm of the axial strain rate approaches a constant with time. The specimen fails when axial strains increase drastically with time. The test is concluded when axial strains reach about 10% to 15%.

4.2 Specimen Preparation

The techniques used to form the high density buffer specimens are based on methods devised by Yarechewski (1988), Wan (1987), and Sun (1986). The buffer specimens are formed to a dry density of 1.67 Mg/m^3, which is 95% of ASTM Modified Standard Dry Density and is the target density specified for "Reference Buffer Material" (RBM) by Atomic Energy of Canada Limited (AECL). The water content is controlled to produce specimens with high saturations. The specimens are formed in five lifts using static compaction techniques.

The specimens contain equal amounts of clay and sand measured by dry weight. The crushed silica sand has a grain size distribution which corresponds with the specifications from Dixon, Gray, and Thomas (1985). In the University Laboratory, the sand is obtained in separate grain sizes which are subsequently weighed and mixed to produce the required gradation.

Atterberg Limit Tests were performed on the bentonite that was used during this experimental program to determine its liquid limit, plastic limit, and plasticity index. The tests were performed by N. Piamsalee who also performed similar tests for Oswell and Lingnau in previous years. The results are presented in Table 4.1 and show that the clay is highly plastic (classified as a CH soil according to the Unified Soil Classification System). The results are consistent between researchers with the exception of the oven-dried sample in 1992. The dried sample (oven temperature 110°C) has a 28% lower liquid limit and plasticity index. This shows that oven drying may affect the plasticity of the clay.

The process for mixing the buffer begins by oven-drying the clay and sand for 24 hours at 110°C. Water used for the buffer mixture is distilled and deaired under a vacuum. The water is deaired to reduce the amount of air in the specimen and therefore increase the saturation. After drying, the materials are removed from the oven, sealed, and allowed to cool. The addition of water when the material is warmer than room temperature causes accelerated evaporation and greater deviation from the targetted water content. Sealing the containers during cooling prevents the bentonite from drawing moisture from the air.

The sand is weighed into a stainless steel mixing bowl and the clay into a beaker. Distilled water is added to the sand to produce a final specimen with a water content of 23.5%. The sand-water and clay are taken to a cool humid room (3°C) for mixing. The relative humidity of the room is maintained close to 100% by a water spraying apparatus. Mixing in the controlled environment of the cool room helps to maintain predictable moisture losses. The water contents after mixing are generally about 0.8% lower than the targetted value.

The clay is added gradually to the sand/water mixture while stirring with a spoon. The clay tends to produce lumps if it is added too quickly. Once all the clay is added, mixing continues for about 15 minutes until uniform colour and consistency are obtained. Nodules of buffer are ground with the spoon until the internal colour matches the general colour of the mix, indicating uniform water distribution. The consistency is determined qualitatively by tipping a heaping spoonful of buffer sideways. If the loose buffer clings to the spoon, demonstrating uniform cohesiveness, the buffer is considered to be uniformly mixed.

Once mixing is complete, the buffer is placed inside two (that is, doubled) plastic bags and sealed with masking tape. The buffer is cured for three days in the humidified cool room to allow the water to distribute evenly throughout the mix. On the second day of curing a sample of the buffer is removed to determine its water content. On the third and final day of curing, the dried soil sample taken on the previous day is weighed and the water content used to calculate the required amount of soil to form the specimen to the target dry density of 1.67 Mg/m^3.

Specimens are formed in a split mould using the compaction frame shown in Figure 4.1. The compaction frame consists of three steel plates with connecting tie rods and contains a hydraulic cylinder which is used to apply axial pressure to the buffer. A manually operated hydraulic jack supplies pressure to the cylinder which is measured with a dial gauge. A dial caliper is used to measure the height of the specimen relative to the bottom of the mould. The mould is centered in a recess at the base and a middle plate surrounds the top. A split mould is used to provide uniform stress release when the specimen is removed from the mould. In the case of a tubular mould, extrusion of the specimen causes nonuniform stress release across the length of the specimen.

The specimen is compacted in five lifts with each lift containing an equal mass of soil. The target height of the specimen is 100 mm with a diameter of 50 mm. The height of each lift can be measured at the time of compaction with the dial caliper on the compaction frame. It was determined by Yarechewski (1988) that specimens compacted using five equal 20 mm lifts produced denser layers towards the bottom of the specimen.

Uniform density of the specimen is obtained by using two techniques which are referred to as (a) recompaction and (b) varied layer height. The recompaction technique is used to compensate for the rebound of the specimen when the final lift is compacted. As shown in Table 4.2, the specimen rebounds by 0.57 mm once it has been compacted to the target height of 100.00 mm. The rebounded height is measured by offloading the specimen and then lowering the piston until light resistance is felt in the jack handle. The target height is obtained by repeatedly compacting the specimen below the previous height and measuring the rebounded height. The procedure is iterative and is a function of the researcher's familiarity with the specimen response.

The varied layer height technique is used to compact each lift to a different height rather than using a constant 20 mm lift height. Varying the height of the lifts produces a specimen with consistent density along its length. The first stage of the procedure determines quantitatively the target heights that will produce a uniform specimen. This is performed by first compacting a specimen using five equal 20 mm lifts and measuring the actual layer heights after compaction. As shown in Table 4.3, the thickness of the lower lifts is less than the upper lifts; therefore the lower lifts are denser than the upper lifts. The Layers numbered 1 and 5 correspond to the top and bottom of the specimen.

The height measurements from the specimen that was compacted in equal lifts is used to determine the compaction heights for a uniform specimen. To form a specimen of consistent density, the lower lifts are initially compacted to heights greater than 20 mm while the top lifts are compacted to heights less than 20 mm. The compaction of each subsequent lift also compacts the underlying layers. Therefore it is intended that compaction of the upper layers will cause the lower layers to decrease in height with the final height approaching 20 mm for all the layers.

The height measurements from the specimen compacted in equal lifts are inverted from top to bottom and used as the target heights for the specimen of uniform density. These measurements, as shown in Table 4.3, have a sum of 100.79 mm which is greater than the target height of 100 mm. This occurs because after compaction the specimen is separated into the five layers to measure the thickness of each lift. When the lifts are separated, the formerly interlocking soil grains are exposed as a rough surface which is included in the height measurement. The target heights are corrected by dividing the 0.79 mm height difference by 5 and subtracting this value from each of the target heights as shown in the fourth column of Table 4.3.

The specimen compacted using the varied layer heights had consistent heights along the length of the specimen as shown in column five of Table 4.3. The corresponding dry densities for both equal and varied target heights are shown in Table 4.4. The dry density variation is reduced from ± 0.016 Mg/m^3 in a specimen compacted with 20 mm layer heights to ± 0.003 Mg/m^3 when the varied layer height technique is used. The variation in the specimen water content is $\pm 0.1\%$, which indicates good water content control.

4.3 Specimen Installation

A system of drainage materials is used to facilitate water flow from the specimen to the back pressure burette as shown in Figure 4.2. The materials include Whatman 54 filter paper, filter stones, and Mirafi 140NS matt weave geotextile strips. The filter paper is placed against the top and bottom of the specimen to prevent migration of soil particles into the water lines and still allow the flow of water. Filter stones are used to provide drainage from the top and bottom of the specimen. The geotextile strips round the circumference of the specimen allow full radial drainage by contacting both filter stones.

The specimen is installed in the triaxial cell immediately after compaction. Geotextile drainage strips are placed around the side of the specimen to permit radial drainage. Oswell et al. (1991) performed tests on different types of radial drains, including geotextile, to determine whether confining pressures acting on the strips can close the drainage path. It was found that the geotextile can maintain a flow path with confining pressures as high as 6 MPa. The geotextile strips are attached to the specimen with narrow silicone rubber bands and are arranged in a spiral configuration. The spiral configuration allows the strips to shorten when the specimen strains axially and therefore do not reinforce the specimen. After the strips are mounted on the specimen, a dry filter stone is temporarily placed at each end of the specimen and the strips are trimmed to a length that will fully contact the side of the stone but not extend beyond the outer edge.

Prior to installing the specimen in the triaxial cell, all drainage lines are flushed with distilled water from the back pressure burette. This ensures that the

lines are free of air and not blocked by any debris. When flushing is complete a bead of water is created on the top of the pedestal that covers both drainage ports. The pressure transducers are opened to the atmosphere and a reading is taken at the computer. The calibration factors are then adjusted to have the transducers read zero pressure.

During the installation procedure the drainage valves are closed to prevent the specimen from swelling. Allowing the specimen free access to water at low confining stress causes the specimen to swell, and alters the initial specimen conditions from those measured at the end of compaction. The second drainage port in the pedestal is traditionally used to flush any remaining air out of the bottom stone and drainage lines prior to beginning consolidation. The buffer specimens are not flushed during this research program because of their tendency to swell at low confining pressures. For this reason the secondary port is sealed and the back pressure is used to compress any remaining air in the system.

The filter stones used for the test are soaked in deaired water for 24 hours to saturate the stones. When the specimen is ready to be installed the bottom stone is slid onto the pedestal. A disc of Whatman 54 filter paper is soaked in distilled water and then slid onto the filter stone. The specimen along with the attached dry geotextile strips is seated on the filter paper. A soaked disc of filter paper is slid onto the top of the specimen followed by another filter stone and the top cap.

The cylindrical surface of the pedestal is dried with a paper towel to ensure that the contact surface between the membrane and steel is dry. Prior to installation, the top cap and pedestal surfaces are cleaned with a degreasing agent, rinsed with

water, and then dried. All surfaces are maintained clean and dry to ensure sealing.

The first silicone rubber membrane is mounted onto a stretcher to install the membrane over the specimen. The stretcher is a steel tube with small diameter steel pipe extending outward from a hole in the side. A flexible hose is attached to the pipe. The membrane is slipped inside the steel tube and stretched over the ends. Suction is applied to the flexible hose which draws the membrane in contact with the inner wall of the steel tube. The membrane is lowered into position over the specimen and then the suction is released. The membrane is slid off the ends of the tube and the stretcher is removed.

Viton sealing rings with an inside diameter between 75% and 85% of the top cap diameter are used to seal the membrane against the steel. The sealing rings are rolled on to the edge of the membrane stretcher and then snapped onto the top cap or pedestal. On the first membrane, three sealing rings are used on the pedestal and two sealing rings are used near the upper edge of the top cap. A second membrane is installed and sealed with four viton rings on the pedestal and three rings on the top cap.

Once the specimen is sealed to the pedestal it is instrumented with a lateral strain gauge, two resistance thermal devices (RTD), and a differential temperature thermocouple. The lateral strain gauge is placed at mid-height on the specimen and is held lightly in place by springs that secure the two stiff steel bands. The RTD's are held near the mid-height of the specimen with silicone rubber bands. One RTD is designated for the temperature controller while the second RTD is connected to the computer. The temperature controller is not linked directly to the data

acquisition system. The differential temperature thermocouple is located with the tips an equal distance from the mid-height of the specimen and against the outer membrane.

When it is assured that all the instrumentation is operational, the final assembly of the cell is performed. The load cell is lowered to within 50 mm of the top cap and locked in place with the locking collar. The steel sleeve is lowered over the top plate of the cell and slid into the groove in the cell base. An overhead crane is used to lift the heavy sleeve. The four nuts on the 25 mm diameter tie rods are removed and the top plate that secures the sleeve is installed. The tie rod nuts are then reinstalled and tightened. (Recent modifications to the cells have made this latter step redundant.)

The top cross bar of the hanger is placed in contact with a ball atop the piston, and bolted to the hanger rods. The lower cross bar has to be supported during the assembly of the load apparatus since the locking collar cannot support the weight of the hanger system. The steel box that is used to support the lever arm is adjusted to allow a small amount of free play. When the cell is pressurized the load cell and piston are forced upwards and the lever prevents the load cell from contacting the top plate of the cell. The locking collar is then disengaged to allow free movement of the piston when the specimen is sheared.

The cell is filled with silicone oil using a 13 mm O.D. tube from a 38 litre tank. The oil is forced into the cell using an air pressure of about 500 kPa which is supplied from the Engineering Building compressor. The cell is filled in approximately 10 minutes. Prior to beginning the consolidation process the cell is insulated with a sheet metal canister that contains foil-backed insulation. The

insulation prevents heat loss when the cell is heated and helps to maintain isothermal conditions around the specimen.

4.4 Consolidation

The consolidation process consists of applying a surrounding pressure, called the cell pressure, to the specimen and allowing the specimen to drain. During isotropic consolidation $\sigma_1=\sigma_2=\sigma_3$, and has the magnitude of the applied cell pressure. The piston that is used to apply axial loads during shear does not contact the top of the specimen during this stage, and therefore only the cell pressure acts on top of the specimen. A back pressure, u_b, is applied to the pore water inside the specimen to fully saturate the system by compressing and dissolving any trapped air that remains after installation. The specimens are generally consolidated with a back pressure of 1.0 MPa, and an appropriate cell pressure applied to maintain the targetted effective stress.

Consolidation begins when the drainage valve is opened to allow water to move in or out of the specimen in response to the applied cell pressure. Before opening the drainage valve, the pore pressure is measured to determine the pressure within the specimen as a result of filling the cell. With a cell pressure of 500 kPa from the building air pressure, a pore pressure of approximately 120 kPa is commonly developed with the drain closed. The pore pressure is considerably lower than the cell pressure because the specimen is not flushed during installation and the back pressure at this point has not been applied to saturate the system. The back pressure supplied by the nitrogen tank is regulated to match the existing pore pressure within the specimen. Matching the pressure on both sides of the drainage valve prevents a water surge either in or out of the specimen. Once the drain is

opened the cell and back pressure are increased incrementally until the required mean effective stress is imposed on the specimen. The process of pressurizing the cell takes approximately 20 minutes.

The consolidation procedure continues until the volumetric strain rate is 0.1%/day. This is an arbitrarily set value which is used to reconcile long consolidation periods with the need to produce a number of tests in a finite time period. When consolidation is complete, the excess pore pressures are minimal and the specimen is very close to equilibrium with its surrounding conditions. Further straining at less than 0.1%/day is considered to be creep straining at essentially constant effective stress.

4.4.1 Thermal Consolidation

All specimens are initially consolidated at temperatures of 26°C. Once the volumetric strain rate is 0.1%/day the temperature is increased to either 65°C or 100°C. This is performed by adjusting the setpoint of the temperature controller and, for the 100°C tests, connecting the base heater on the cell.

Heating of the cell causes the silicone oil to expand and pressures to increase within the cell. The pressure regulators used with the triaxial cell control pressure by increasing the pressure towards the set value but have very limited capability to reduce pressure if the set value is exceeded. To reduce the cell pressure during heating, pressure relief valves (PRV) are used to allow oil to escape when the pressure exceeds a set value. The PRV operates with springs which are designated for different pressure ranges. The "cracking" pressure is the pressure at which the valve will be wide open. The cracking pressure can be set by

turning the top cap of the valve. If the top cap is tightened completely the PRV will crack at the maximum pressure specified for the spring while loosening the cap will decrease the cracking pressure towards the minimum specified spring pressure.

The PRV reseals, or begins to bleed oil, at about 90% of the cracking pressure. It has been found that the heating process is generally slow and that the PRV can bleed excess pressures without reaching the cracking pressure. This provides smoother pressure adjustment than if the valve were to open and close abruptly as is the case when the cracking pressure is reached. During heating, the pressure regulator is set to a lower pressure than 90% of the cracking pressure. This is to avoid having the regulator activate the PRV rather than the thermal expansion of the silicone oil. If the regulator was set high enough to cause the PRV to bleed, the accumulator would eventually be depleted of oil and the cell pressure would decrease. Once heating is complete, a valve is closed between the cell fluid line and the PRV and cell pressure control is returned to the regulator.

4.4.2 Consolidation at Elevated Back Pressure

During two of the tests (T1303 and T1307) the back pressure during consolidation was increased from 1.0 MPa to 7.0 MPa and maintained for the duration of the test. This was performed to determine whether the effective or total stress concept is a valid method of analysis under elevated temperature. The total stress for these tests was also increased by 7.0 MPa, so the effective stress was held constant.

T1303 was performed at a temperature of 26°C, and T1307 was performed at 65°C. Once the volumetric strain rates had reached 0.1%/day at the end of thermal consolidation the back pressure was increased. The pressures were increased using

0.3 MPa increments for T1303 which had an effective stress of 0.6 MPa and 1.0 MPa increments for T1307 at an effective stress of 1.5 MPa. The pressures were adjusted by first increasing the back pressure and then the cell pressure to the required effective stress. Therefore, during the 30 minutes of pressure adjustment the mean effective stress was either equal to the required effective stress or lower. This is almost certainly the first time anywhere, that the validity of the effective stress concept for use with dense bentonite has been tested at elevated temperatures. Results from these procedures will be discussed more fully in Section 6.2.

4.5 Shear

The specimen is sheared by applying incremental axial loads until the specimen fails. The loads are applied in five increments using the hanger and lever system described previously. The failure load can be estimated from the undrained shear tests of past researchers. For this experimental program the failure load was estimated from Saadat's (1989) relationship for peak failure stress which shows:

$$q_p = 2.59 \, (p')^{0.80} \qquad \text{....(10)}$$

with units of kPa. The term q_p is the peak deviator stress. This relationship is for high density (1.67 Mg/m^3) specimens at ambient temperatures. To maintain a constant mean effective stress the following two equations must be satisfied where:

$$q = \sigma_1' - \sigma_3' \qquad \text{..(5bis),(11)}$$

$$p' = (\sigma_1' + 2 \, \sigma_3') / 3 \qquad \text{..(4bis),(12)}$$

with p' = constant.

To allow increases in the deviator stress q while keeping p' constant, the cell pressure must be decreased by one-third the amount of the deviator stress changes ($\Delta\sigma_1 = -2\ \Delta\sigma_3$). With the test arrangement being used, the cell pressure represents the minor principal stress σ_3. The major principal stress is axial, with magnitude $\sigma_1 = \sigma_3 + q$.

The cross-sectional area changes as the specimen compresses during shear, and is calculated from the volumetric and axial measurements. The axial load is measured from the internal load cell, and equals the deviator stress q multiplied by the cross-sectional area. From equation (3), σ'_1 can be calculated to give the required deviator stress, and the cell pressure σ_3 is then determined to maintain a constant mean effective stress p'.

The methodology that is used to put the theory into the actual operation of the triaxial cell will now be described. Prior to beginning shear, the load cell is lowered into contact with the top cap on the specimen. The load cell voltage is monitored using the Basic program Voltmetr to determine the instant that the load measurements increase, indicating contact with the specimen.

Weights are added to the hanger system to counterbalance the cell pressure that forces the piston upward. The piston is moved downward by pressing on the lever arm until contact is made between the lever arm and the steel support box. If no load is measured during this interval the lever is released to its former position and the piston is lowered by tightening the nuts on the hanger. The piston is lowered by approximately the distance that the lever had moved the piston. This process is continued until a load is measured at the load cell. The reason that the hanger nuts are not used as the sole means to lower the piston is that the

lever is a more sensitive device to determine the contact point. The axial stress applied during this procedure is less than 5% of the maximum deviator stress at p' of 0.6 MPa, and less than 2% at p' of 3.0 MPa.

Once the contact point is located the lever is adjusted to a horizontal position with the hanger nuts. The steel support box holds the lever near the contact point with no axial load applied to the specimen. The lever is maintained in a horizontal position during the entire shearing process. This allows consistent loads to be applied by the lever system and, with the aid of a bubble level, provides a quick visual reference for determining the movements of the piston.

The LVDT used to measure the axial movements of the piston is attached to the top of the cell by a mounting bracket. A steel rod threaded into the top plate of the cell is joined to the LVDT by an aluminum bracket. An aluminum plate is attached to the top of the piston, immediately below the cross-bar of the hanger. The LVDT rod contacts the aluminum plate and measures the linear displacement of the piston. The LVDT and its apparatus are mounted on the triaxial cell prior to the heating phase during consolidation. This is to allow the equipment to reach thermal equilibrium before the beginning of shear and to prevent measurement of component expansion. The LVDT is located outside the insulated container of the cell and maintains a temperature close to room temperature. It is for this reason that the LVDT is not secured to the piston which is generally close to cell temperature.

The LVDT is calibrated immediately prior to the beginning of shear with gauge blocks. The calibration is performed with the mounting apparatus and LVDT in place. This ensures that the LVDT measurements are accurate and are not influenced by variations in the axial alignment of the mount.

Once the preparatory work is completed, weights are applied to the lever to produce the first increment of deviator stress. The weights consist of steel plates that are notched to accommodate the rod from the hanger. The weights are added slowly in small increments to avoid producing high pore pressures in the specimen. Rapid loading creates an undrained condition in the specimen and produces elevated pore pressures that can drive the specimen closer to failure. Once the final value of required load increment is added, the cell pressure is decreased to maintain a constant p' according to equation (2).

Successive load increment are added when the axial strain rate during the previous increment approaches a constant with time. Generally, the specimens failed at maximum deviator stresses that were somewhat higher than predicted from Saadat's equation for room temperature specimens. As a result, most specimens had to be loaded above the fifth increment. This was done by adding small amounts of load, and monitoring the axial strain rate for 10 minutes. If the axial strain rate decelerated rapidly, another small load increment was added. If the axial strain rate accelerated or strained at a fast constant rate no further loads were added and the specimen was monitored until strains of 10 to 15% were attained. Care was taken to ensure that q was kept constant during rapid compression by adding small additional weights to take account of increasing cross-sectional area.

The criteria used to determine when the specimen had failed include large axial strains, and an inability for the specimen to support further loads. A maximum axial strain of 10% was used for earlier tests and 15% was used for later tests. Determining whether the specimen can support additional loads can be found in two ways (1) load measurements from the load cell do not increase with the addition of weights on the external hanger, and (2) upon adding a weight, the lever arm falls

away smoothly and rests on the support box. In general, the specimen was allowed to deform until 15% axial strain was reached whether the axial strain rate was accelerating or decelerating.

4.6 Cooling and Specimen Removal

After the specimen has failed the hanger weights are removed, and the load cell raised above the specimen a distance that returns the LVDT reading to zero. The triaxial cell is then cooled and the specimen removed. The drainage conditions are open during the cooling phase and closed immediately prior to removing the specimen. Lingnau, during his research program, removed the specimen from the triaxial cell when the temperatures were 65°C or 100°C. It was decided for this program to allow the triaxial cell to cool prior to removing the specimen, since a cool triaxial cell is easier and safer to disassemble. Another benefit to removing a cool specimen is that less moisture loss can occur if the specimen is at room temperature. This improves the control of water contents and specific volumes.

When the triaxial cell is cooled, the silicone oil cell fluid contracts and the diaphragm drops lower in the accumulator. If the diaphragm reaches the bottom of the accumulator, the cell pressure would be lost, and the membranes balloon. To avoid this, the accumulator is filled prior to cooling the cell. It has been found that a 50°C drop in cell temperature will cause the diaphragm to contact the bottom of the accumulator. The maximum volume of the accumulator is 0.7 litres. Therefore, the silicone oil undergoes approximately a 1 litre change in volume when the cell temperature is decreased from 100°C to 25°C under a constant cell pressure.

Once the cell is cooled, the specimen is removed and its weight and dimensions are recorded. The water content of the specimen is measured by dividing it in five sections along its axis and coring each section using a steel tube and hydraulic press. The water content is determined for the interior and exterior of each section. The filter stones are placed on paper towels to determine if silicone oil contamination (caused by leakage or diffusion through the membranes) exists within the specimen. After one day any liquid in the stone is soaked into the paper towel, with the water evaporating, and silicone oil leaving a dark stain.

CHAPTER 5

TEST RESULTS

5.1 Introduction

Ten triaxial tests have been conducted at the University of Manitoba for this research program. The results from the tests are shown in Figures 5.1 to 5.56, which have been arranged to present the results from Specimens T1301 to T1310 in a complete, systematic manner. The tests were conducted at three mean effective stresses of 0.6, 1.5, and 3.0 MPa with three temperatures of 26, 65, and 100°C. No test was performed at a mean effective stress of 3.0 MPa and 26°C. These tests are the first to be reported on buffer compacted to 1.67 Mg/m^3. Wan and Saadat performed similar tests on buffer compacted to 1.51 Mg/m^3 at ambient temperature.

As is customary in Dr. Graham's laboratory, each test is designated by a number such as T1301 where the first portion T13 indicates the test series performed by the author (researcher number 13), while the latter portion 01 represents the test number in his test program. The suffix CID' attached to the test number represents the triaxial test conditions which for this program refers to Consolidated Isotropic tests sheared with Drained conditions. The apostrophe is added to indicate that the tests are sheared with constant mean effective stress and are not conventional drained triaxial tests.

All tests were performed using the same general techniques described in detail in Chapter 4. The specimens were first consolidated to equilibrium at a controlled

temperature of 26°C which is slightly above average room temperature. The temperature was then increased, and the specimen again allowed to come to volumetric equilibrium. Shearing began after all consolidation had been completed. It consisted of applying five (or more) increments of axial load until the specimen began to strain rapidly and accelerate towards failure. The onset of accelerating axial straining was defined as "failure", and represents the maximum deviator stress that the specimen could support.

Table 5.1 summarizes the test conditions for each specimen. The following overview outlines variations from the general procedure.

T1301: The specimen was consolidated isotropically at a mean effective stress of 1.5 MPa at ambient temperatures. The average specimen temperature was 27°C ± 0.8°C during consolidation and 25°C ± 1.4°C during shear. This is the only specimen that did not use the temperature controller to maintain the specimen temperature within ±0.1°C. When the specimen was sheared axial strains increased rapidly with the application of the third load increment. An error in calculating the required axial stress resulted in an actual mean effective stress of 1.7 MPa during shear.

T1302: Consolidation of T1302 was performed in two stages, initially with a specimen temperature of 26°C and then at an elevated temperature of 65°C. An apparent leak was observed during thermal consolidation and the triaxial cell was hoisted to replace a possibly faulty pore fluid line beneath the cell base. The back pressure was reduced to atmospheric pressure and the cell pressure was decreased to 1.5 MPa to maintain a constant effective stress. After the repair, the pore pressure was restored to 1 MPa with p'

equal to 1.5 MPa but the leak continued. As a result, the lateral strain gauge was used to determine when the specimen had attained volumetric equilibrium at the end of consolidation and to calculate the cross-sectional area of the specimen during shear. This specimen, similar to T1301, was sheared at a mean effective stress of 1.7 MPa. The erratic loading pattern shown in Figure 5.28a was caused by binding of the piston due to expansion of the teflon sleeve. The piston was twisted regularly to release the friction.

T1303: The test was conducted at a mean effective stress of 0.6 MPa and at a controlled temperature of 26°C. During consolidation the back pressure and cell pressure were increased to 7 MPa and 7.6 MPa, respectively. The first load increment applied during shear was again miscalculated and the specimen strained rapidly to an axial strain of 7%. The load was removed and the specimen was reconsolidated until volumetric equilibrium was achieved. Shearing was then recommenced with correct loads.

T1304: This specimen was consolidated at an effective stress of 0.6 MPa at temperatures of 26°C and 65°C. The specimen was sheared at 65°C and failed at the seventh increment.

T1305: During the early stages of consolidation the cell pressure was accidently fixed at 2.1 MPa and the effective stress was maintained at 1.1 MPa until volumetric equilibrium was observed. The specimen was then consolidated again at a revised effective stress of 0.6 MPa at specimen temperatures of both 26°C and 100°C. After consolidation, the piston jammed in the top of the triaxial cell in the same way as during T1302, but this time with much

greater friction. It was decided that the specimen could not be sheared at a temperature of 100°C and the test was discontinued at the end of consolidation.

T1306: The mean effective stress was 0.6 MPa and the specimen temperature 100°C in this test. Lateral strain readings were discontinued on the 11th day of consolidation due to a broken connection on the transducer inside the cell. A total of eight load increments was needed to fail the specimen.

T1307: This specimen was consolidated initially at 26°C and then at a temperature of 65°C. Once volumetric equilibrium was observed at 65°C the back pressure and cell pressure were increased by 7 MPa and a constant mean effective stress of 1.5 MPa was maintained. The specimen was sheared at elevated pressure and temperature and failed when the sixth load increment was applied.

T1308: In this case, the mean effective stress was 3.0 MPa and the specimen temperature 100°C. Lateral strain measurements ceased on the 6th day of consolidation when the specimen was being heated, due to a broken connection. This specimen failed at the fifth load increment.

T1309: This specimen was consolidated to an effective stress of 1.5 MPa at a temperature of 100°C. The specimen failed at a load which corresponded to the sixth increment.

T1310: The mean effective stress during this test was 3.0 MPa with a specimen temperature of 65°C. Similar to T1308, the lateral strain readings were

discontinued when a connection broke on the 4th day of consolidation during the heating stage. The specimen failed at about 4.5 increments rather than the fifth load increment.

5.2 Initial Specimen Conditions

Table 5.2 shows the initial condition of each specimen. These results correspond to the period immediately after compaction when the specimen has been removed from the mould. The water contents are based on the average between two samples of loose buffer which are taken the day before compaction and at the end of compaction. The results show that good control of the water content was obtained with an average water content of 22.7% and a standard deviation of 0.1%. The buffer was always mixed with a 23.5% water content which reduced by about 0.8% during mixing in the cool room. This consistent water loss shows that mixing in a controlled environment with standardized procedures can eliminate variations in water content between specimens.

The average measured dry density of the specimens is 1.660 Mg/m^3 with a standard deviation of 0.003 Mg/m^3. The target dry density is 1.67 Mg/m^3 which is 95% of maximum modified Proctor dry density. Specimens were compacted to a height of 100 mm in the split mould using the recompaction technique described in Section 4.2. Once the specimen is removed from the mould the specimen rebounds and the measured height is slightly greater than 100 mm producing a slightly reduced dry density. The values shown in Table 5.2 represent a high level of control during specimen preparation and compaction.

The rebound of the specimen once it is removed from the mould produces a network of small cracks that can be observed on the surface of the specimen. Immediately after the specimen is removed from the mould the surfaces show no indication of cracks. However, after approximately 5 minutes, when the specimen is being weighed and measured, hairline cracks begin to appear on the specimen surface. These small cracks are closely spaced and cover the entire specimen. The crack pattern does not appear to be related to the geometry of the specimen. The presence of the cracks is likely related to the release of total stress that occurs when the specimen is removed from the rigid mould.

The saturation of the specimen is about 98% at the end of compaction. The calculation is based on an average specific gravity of 2.70 for the soil particles. The sand has a specific gravity of 2.65 while the clay has a specific gravity of about 2.75. The average specific gravity can be used since equal masses of sand and bentonite are combined to make the buffer specimens. High saturation at the end of compaction reduces the period of time required for the back pressure to saturate the system during initial stages of the triaxial test. The back pressure compresses air bubbles and moves air into solution in the pore water to ensure that the specimen is saturated. Saturated specimens allow accurate volume change measurements during testing since only the volume of water movement is measured. This represents changes in pore volume directly when specimens are saturated.

5.3 Consolidation

The temperature control during the triaxial tests was generally maintained within ±0.1°C as specified with the controller settings. The temperature controller monitors the specimen temperature with an RTD mounted at approximately mid-height

on the exterior of the specimen. The temperature measured at the controller is independently confirmed with a second RTD mounted at the same location. The signal from the second RTD is measured with the data acquisition computer. The room temperature during the triaxial tests was generally below 26°C and fluctuated by about ±1°C with a maximum fluctuation of about ±3°C occurring during T1301. The room temperature fluctuations shown in Figure 5.19b and 5.53b for T1310 are typical for this experimental program, with diurnal changes of about ±0.5°C.

The differential temperature along the length of the specimen was measured with two copper-constantan thermocouples. The differential temperature was monitored to ensure that the specimens were subjected to isothermal conditions. When the specimen temperature was constant the temperature difference between the ends of the specimens was about 0.8°C. During the heating stage of the test the bottom of the specimen was slightly warmer, producing a temperature differential of about 1.4°C. When the specimen was cooled after shearing, the top of the specimen would be warmer by about 2.8°C until isothermal conditions were again restored. Since the temperature differentials along the length of the specimen were small during the course of the tests, it can be assumed that isothermal conditions prevail.

Table 5.3 shows the results of mass balance calculations between the beginning and the end of the test. The initial water content was measured at the time of compaction, and the final water contents measured when the specimens were removed from the triaxial cell. At the end of each test, the specimen was divided axially into five sections, and these were then cored with a steel tube. The buffer inside the tube is used to measure the final internal water content shown in Table 5.3. This is taken to be the most accurate available representation of the water content of the specimen. The external water contents (from the outer shells) are generally

lower than the internal values (from the tube cores) and indicate that some drying occurs during the build-out process.

The calculated initial and final water contents in Table 5.3 are based on volumetric strains measured during triaxial testing. The initial value is calculated backwards from the final measured water content, while the final calculated water content is determined by working forward from the water content measured at compaction. It is generally accepted by researchers at the University of Manitoba that calculating specimen water content by working backwards from the final measured water content is the more accurate method. Some delay during installation may leave the specimen slightly drier than the measured water content after compaction, or alternatively, it may gain moisture from the filter stones, drains, cell base, etc. The water content calculated at the end of the triaxial test is taken from the interior of the specimen without allowing any time for drying. Therefore the final measured water content is generally more accurate. The differences between the calculated and measured initial and final water contents are rather larger than those found by previous researchers testing at constant ambient temperatures of 26°C. Concurrent work revealed some problems with the silicone rubber membranes that were used as discussed in Sections 3.4.2 and 3.5.

Calculations of clay specific volume V_c during this research program were conducted using both initial and final water contents since the mass balances in Table 5.3 show some discrepancies. The initial water contents are used to calculate the clay specific volume through to the end of the first consolidation stage at 26°C. The clay specific volume at the peak deviator stress and the end of thermal

consolidation (or the beginning of shear) is calculated by using the final water content and calculating backwards.

Consolidation results for each test are shown in Figures 5.1 to 5.20. Table 5.4 summarizes the volumetric and lateral strains that occurred during consolidation. Positive strains are compressive while negative strains are expansive. The results in Table 5.4 show that lateral strains were slightly compressive during 26°C consolidation regardless of whether the specimen was swelling or compressing volumetrically. This is possibly due to anisotropy that was built into the specimen during the compaction process.

The duration of the consolidation period depended on whether the specimens were dilative or compressive. Specimens that swelled to volumetric equilibrium generally took longer periods to reach equilibrium than compressive specimens. The time taken to complete thermal consolidation was typically faster than initial consolidation at 26°C and this was independent of whether the specimen was dilative or contractive. During thermal consolidation, the volumetric strains tended to be either compressive or expansive in the same manner as during the 26°C consolidation period, and to be of similar magnitude. The lateral strains during 26°C consolidation were compressive, while during thermal consolidation at elevated temperature the lateral strains were generally expansive regardless of the volumetric strain direction or mean effective stress.

The consolidation results are summarized in Figure 5.57 which plots clay specific volume against the natural logarithm of mean effective stress. The figure shows relationships for a) after compaction, b) the end of first consolidation at 26°C, and c) the end of second thermal consolidation at 26°C, 65°C, or 100°C. The

initial clay specific volume is about 2.25 as defined by measurements at the end of compaction. During the first consolidation, Figure 5.57 shows that specimens swell or compress until volumetric equilibrium is attained under the imposed mean effective stress. The transition between expansive and compressive strains is at an effective stress of 1.5 MPa which is thought to be about the swelling equilibrium pressure for the reference buffer (1.67 Mg/m^3) at 26°C. Above this pressure, specimens compress; and below, specimens swell until volumetric equilibrium is reached.

Ideally, the "first consolidation" line and the 26°C "end of thermal consolidation" lines in Figure 5.57 should coincide. The differences shown in the Figure arise from (1) differences in the way the specific volumes were calculated, whether forwards from the beginning of testing, or backwards from the end of testing, and (2) the limited number of tests from which the figure was prepared. Later, in Chapter 6, these data will be compared with parallel but not identical tests run by Lingnau. The pattern shown in Figure 5.57 agrees generally with Lingnau's results from a larger number of tests.

Figure 5.58 shows three relationships for thermal consolidation at 26°C, 65°C, and 100°C. The lines for each temperature are close to parallel with increased temperature producing decreased clay specific volume. The equations for all consolidation lines are presented below. It is recalled that clay specific volumes after compaction and at the end of first consolidation were calculated using the initial water content, whereas the end of consolidation results were calculated backwards from the final water content.

Beginning of consolidation

V_c = Constant = 2.25 ...(13)

End of first consolidation period at 26°C before heating

$V_c^{26°C} = 2.281 - 0.081 \ln p'$ (p' in MPa) $R^2 = 0.95$ ...(14)

$V_c^{26°C} = 2.841 - 0.081 \ln p'$ (p' in kPa)

End of thermal consolidation at 26°C, 65°C, and 100°C

$V_c^{26°C} = 2.404 - 0.084 \ln p'$ (p' in MPa) Fitted ...(15)

$V_c^{26°C} = 2.981 - 0.084 \ln p'$ (p' in kPa)

$V_c^{65°C} = 2.291 - 0.076 \ln p'$ (p' in MPa) Fitted ...(16)

$V_c^{65°C} = 2.818 - 0.076 \ln p'$ (p' in kPa)

$V_c^{100°C} = 2.151 - 0.091 \ln p'$ (p' in MPa) Fitted ...(17)

$V_c^{100°C} = 2.778 - 0.091 \ln p'$ (p' in kPa)

During the heating phase the water and system components expand slightly. The leakage tests described in Section 3.5 show volumetric strains of about 0.4% during heating and cooling cycles which would correspond to an apparent change in clay specific volume of about 0.01. The specimen used for the leakage tests was an aluminum cylinder, so any measured change in volume during heating was due entirely to expansion of water and test cell components. During heating, buffer specimens show apparent compressive volumetric strains of +0.3% at 65°C and +0.7% at 100°C. The changes in volume measured during heating and cooling cycles were reversible during the full scale leakage tests. However during the tests on buffer the expansive volumetric strains during cooling were slightly less than the

corresponding compressive strains. Average volumetric strains measured during cooling of specimens at 65°C were about -0.2% and about -0.5% at 100°C. The volumetric strains during heating and cooling are included in all the results presented since the effect in terms of specific volume is small.

To gain a sense of the effect of temperature on the diffuse double layer within the pore water, simple calculations were made to determine what portion of lateral strains were due to thermal expansion and to changes in the diffuse double layer. The volumetric thermal expansion of pore water (herein considered to be bulk water) was calculated using a thermal expansion coefficient β_{cw} of 9.23 x 10^{-4}/°C and 1.162 x 10^{-3}/°C at 65°C and 100°C, respectively, based on work by Dixon (Baldi et al. 1990). Since the average volumetric expansion coefficient for the mineral solids β_s is very small (3.9 x 10^{-5}/°C) compared with the pore water coefficient it was neglected. The units for the coefficients are volumetric strain per degree Celsius with positive values representing expansion (this deviates from the practice used in this thesis where positive strains represent compression or a volume reduction). To use the volumetric expansion coefficients to calculate lateral strains, the specimen was assumed to be isotropic and the volumetric coefficients were divided by three.

The calculated lateral expansion of the porewater is -1.20% at 65°C and -2.86% at 100°C. The calculations were based on an initial specimen temperature of 26°C. The average measured lateral strain due to heating was -0.64% at 65°C and -1.67% at 100°C. The measured expansive strains are generally less than the predicted expansion of the pore water. This is likely caused by contraction of the diffuse double layer which in turn allows more void space to be occupied by bulk water. Contraction of the diffuse double layer appears to account for the 0.56% and 1.19%

lateral strain that was not manifested during heating to 65°C and 100°C, respectively. These results also corroborate the decrease in volume with increased temperature found by Campanella and Mitchell (1968) and Hueckel (1987) as discussed in Chapter 2.

The pore pressure coefficient $B = \Delta u/\Delta\sigma_{cell}$ describes the change in pore pressure Δu that occurs due to a change in cell pressure $\Delta\sigma_{cell}$ under undrained conditions. It is commonly used as a quality control check to ensure the validity of undrained shear tests. The so-called "B-Test" is performed at the end of consolidation to determine if a specimen is saturated or if leakage exists between the cell fluid and pore water. To perform a B-Test, the drainage valve is closed, and initial pore pressure and cell pressure measured to define conditions at the beginning of the test. Once initial pressure readings have been taken, the cell pressure is increased and the resulting pore pressure response is measured. If the pore pressure increases by the same amount as the cell pressure then B = 100%, and the specimen can be considered completely saturated. A B-value less than 100% indicates that the specimen is not completely saturated, while a B-value greater than 100% indicates either leakage exists between cell fluid and pore water, or incomplete equilibration of pore water pressures generated during the earlier consolidation period. As a general guideline, a minimum B-value of 98% is required for research testing, while 95% has been generally accepted for commercial tests.

Values of B measured by Saadat (1989) and Lingnau (Graham et al. 1991) for buffer at the end of consolidation are generally about 99% to 100% with a back pressure of 1 MPa. Measurement of B was attempted during this research program, but accurate measurements could not be obtained. At the end of consolidation the drainage valve was closed and the pore pressure monitored to ensure that the pore pressure was at

equilibrium prior to beginning the B-Test. It was found that the pore pressure decreased with time, and this would create abnormally low B-values.

From the leakage tests described in Section 3.5 it is believed that diffusion of pore water through the membranes to the cell fluid results in a decrease in pore pressure when the drainage valve is closed. The high values of saturation shown in Table 5.2 suggest that B will be about the same as measured by Saadat and Lingnau, that is, between 99% and 100% at the end of consolidation. The need for high B-values is not as great in the drained tests in this program, compared with the undrained tests done by other researchers. The tests during this program are conducted with drained conditions, and therefore the pore pressure is equal to the back pressure. In undrained triaxial tests it is necessary to measure the pore pressure during shear to determine the mean effective stress.

5.3 Shear

Results from the incremental shear portion of the drained triaxial tests are shown in Figures 5.21 to 5.56. Table 5.5 summarizes these results. Most of the tests failed when the axial strains were still less than 5%. Volumetric strains during shearing depended on consolidation pressure and temperature, and ranged from +1.9% to -3.3%. Similarly, the lateral strains ranged from +0.5% to -3.9%. (Positive signs represent compression.)

Figure 5.59 shows the peak shear strength results. Tests at higher temperature tend to give slightly higher strengths (see Graham et al. 1992 Report) but the effect appears to be small. The strength envelope can be expressed by the power law function shown below.

Peak shear strength

$q_{peak} = 0.84\ p'^{\,0.56}$ (p' in MPa) $R^2 = 0.96$ ...(18)

$q_{peak} = 18.01\ p'^{\,0.56}$ (p' in kPa)

Figure 5.60 shows the clay specific volume versus mean effective stress at failure. The results show that the clay specific volume depends on the specimen temperature. Equations relating V_c and p' are shown below for each temperature. The line for the two 26°C tests in Figure 5.60 has been drawn only through the point for T1301. However, comparison with the 65°C and 100°C curves suggests this would be a reasonable approximation. These lines are compared later with equivalent results from Lingnau's program.

Clay specific volume at peak shear strength at 26°C, 65°C, and 100°C are presented below.

$V_c^{26°C} = 2.422 - 0.160 \ln p'$ (p' in MPa) Fitted ...(19)

$V_c^{26°C} = 3.527 - 0.160 \ln p'$ (p' in kPa)

$V_c^{65°C} = 2.312 - 0.153 \ln p'$ (p' in MPa) Fitted ...(20)

$V_c^{65°C} = 3.369 - 0.153 \ln p'$ (p' in kPa)

$V_c^{100°C} = 2.230 - 0.160 \ln p'$ (p' in MPa) Fitted ...(21)

$V_c^{100°C} = 3.335 - 0.160 \ln p'$ (p' in kPa)

Table 5.6 shows the calculated values of the shear modulus G_{50} and Young's modulus E_{50}. The behaviour of the buffer, as of all soils, is non-linear, so the values of G and E vary during shearing. As a simplification, and for comparison purposes, values of G and E in Table 5.6 have been calculated at the point where the deviator stress is 50% of the maximum deviator stress, hence the use of the terms G_{50} and E_{50}. This is also a reasonable assumption since the buffer will likely function at some working stress near $0.5q_{max}$.

The shear modulus is calculated by plotting deviator stress versus shear strain, while Young's modulus is determined from a plot of deviator stress versus axial strain. Since the deviator stress is constant during the duration of each load increment, the strains in this case are taken from the readings after 1-day and 2-days of loading. Wan (1987) and Saadat (1989) have shown that 1-, 2-, and 3-day load durations plot as curves with similar shape. The initial sections of the stress-strain curves are reasonably linear and have a decreased slope (increased displacements) with increasing time. During this program, load increments were generally applied for 2 days, and so readings for 3-day intervals were not obtained. Two methods are currently used at the University of Manitoba to calculate E_{50} and G_{50}. The first method calculates the moduli by determining the slope of a secant from $q = 0$ to $q = 0.5q_{max}$. The second method determines the slope of the local tangent at $q = 0.5q_{max.}$ The slope of deviator stress q versus shear strain ε_s curve is equal to 3G; while the slope of the deviator stress versus axial strain is E. The values of shear modulus G_{50} and Young's modulus E_{50} in Table 5.6 were calculated using both the secant and tangent methods, and are for 1- and 2-day load durations. The results for G_{sec} and E_{sec} for 1-day load durations from Table 5.6 are plotted in Figure 5.61 and 5.62. Figure 5.61 shows some tendency for the shear moduli to increase with mean effective stress p' and to

decrease with temperature, although the measurements are not unambiguous. Figure 5.62 shows a small tendency for E_{50} to increase with mean effective stress in these tests with no distinct relationship to temperature.

The lateral strain gauge measures the radial displacement of specimens during shear. As usual, it is assumed that the specimen retains the shape of a right cylinder during shear. Comparison between axial and lateral strains show that during the initial stages of shear Poisson's ratio ν varies from about 0.4 to 0.6, that is, at close to constant volume. The values of ν were calculated using a secant method. This is the first time such results have been available from the University of Manitoba laboratories. A value of 0.5 for ν assumes that the buffer acts isotropically as a perfectly elastic material such as rubber. Beyond the initial stages of shear Poisson's ratio tends to increase above 0.5. Generally, during the final load increments ν ranges from about 0.5 to 1.4. The averaged values of ν, during the entire shear stage, range from 0.4 to 0.9 with the average for the T1300 series being about 0.6. The results indicate that ν is not affected by the dilative or compressive nature of the specimens.

The axial strain rate during each load increment was calculated when the axial strain became approximately linear with time. Figure 5.63 shows stress ratio $\eta = q/p'$ versus axial strain rate $\dot{\varepsilon}_1$. Generally the axial strain rates equilibriate at slightly higher values with increased deviator stress. The axial strain rate typically does not exceed 0.17%/day prior to failure. The relationships shown in Figure 5.63 do not appear to be affected systematically by temperature.

The dilative and compressive nature of the buffer dictates that specimens will fail in different manners depending on the consolidation pressure and temperature. It can be hypothesized that specimens consolidated below the swelling equilibrium pressure may not be completely at equilibrium when the shearing process begins. As a result, the lower portion of the specimen will be allowed to swell to equilibrium while the upper portion will be somewhat drier. This will result in shear planes developing in the lower portion of the specimen since it will be wetter and weaker along with more significant deformation than the upper portion. Specimens that are compressive or consolidated above the swelling equilibrium pressure should exhibit more uniform failure patterns with shear planes concentrated along the specimen mid-section.

The shape of the specimen at the end of shear seems to depend on the mean effective stress and on the specimen temperature during the triaxial test. There are three predominant specimen shapes which include (1) barrel, (2) widened base, and (3) shear plane. Figures 5.64 to 5.66 shows a sketch and photographs of three different specimens at the end of shear, each exhibiting one of the failure shapes. The barrel shape, as the name implies, is a widening of the middle portion of the specimen with only slight widening at the ends. Specimens that have a widened base begin to bulge at a distance of about 55 mm below the top of the specimen and flare outwards to the bottom. The upper portion of the specimen above the bulge tapers slightly towards the top but predominantly retains its originally cylindrical shape. Shear planes cut through the cross-section of the relevant specimens at an angle α to the major principal axis. The parts of the specimen above and below the shear plane slide in opposite directions along the shear surface. The angle of shearing resistance ϕ can be calculated as $2\alpha - 90°$.

Specimens T1301, T1302, and T1307 exhibited a barrel shape at the end of shear. Specimens T1301 and T1302 were sheared at a mean effective stress of 1.7 MPa with specimen temperatures of 27°C and 65°C. It is recalled that T1301 and T1302 were sheared with higher initial load increments than the correct load increments. T1307 was sheared at a mean effective stress of 1.5 MPa, at an elevated back pressure of 7 MPa and a temperature of 65°C. These suggest that the specimen shape seems to be independent of the loading method and the total stress.

Specimens T1303, T1304, and T1306 had a widened base at the end of shear. The mean effective stress was 0.6 MPa for all three tests, with specimen temperatures being 26°C, 65°C, and 100°C, respectively. The location of the bulge begins at a distance of about 55 mm below the top of the specimen. The total height of the specimens is about 95 mm for T1303, T1304, and 86 mm for T1306. The difference between the diameter of the specimen at the top and bottom of the taper is about 4 mm for T1303, T1304, and 11 mm for T1306. Specimen T1303 failed on the first load increment and was subsequently reconsolidated and sheared with an elevated back pressure of 7 MPa. About 5.3% axial strain was unrecoverable when the specimen initially failed. However, the shapes of the three specimens at the end of shear were similar, with the bulges in virtually the same location. Also, the difference in diameter between the top and bottom of the bulge is almost equal to the amount of permanent axial deformation. Lingnau (see for example Graham et al 1992) has suggested that bulging of this type indicates non-homogeneous swelling specimens in which expansive consolidation straining was not totally complete. With p'_{cons} = 0.6 MPa, all these specimens swelled during consolidation. If this process had not completely terminated at the beginning of shearing, then the lower part of the specimen would be wetter than the upper part. Shear strains would therefore concentrate in the weaker, low part of the specimen.

Shear planes were identified in specimens T1308 and T1309. Specimen T1308 exhibited some bulging along the mid-section, and a measured angle α of about 47°. This suggests an angle of shearing resistance ϕ equal to 4°. The specimen was sheared at an effective stress of 3.0 MPa, and a temperature of 100°C. Specimen T1309 showed evidence of a failure plane at an effective stress of 1.5 MPa and temperature of 100°C. The failure shape for T1309 was a combination of a widening base and a shear plane. In this case, the failure plane was less defined than for T1308, and this is likely related to the combined failure mechanism. The angle α for T1309 was about 78° which corresponds to an angle of shearing resistance of 66°. As has been found frequently in other studies, determination of ϕ by measuring the angle of the shear plane does not give consistent results.

Specimen T1310 exhibits a combination of failure mechanisms between barrelling and widening of the base. It was sheared at an effective stress of 3.0 MPa at 65°C. The specimen began to bulge at a distance of 31 mm below the top as opposed to 55 mm mentioned previously. The specimen diameter begins to taper downward at about 20 mm above the base thus showing some indication of the barrelling mechanism.

It seems that the shapes of specimens at the end of shearing depend on both the mean effective stress and temperature. Effective stresses of 1.5 MPa and 3.0 MPa produce shear planes at elevated temperature, with the most clearly defined shear plane occurring at an effective stress of 3.0 MPa at 100°C. At an effective stress of 0.6 MPa the final shape of the specimen is less clearly dependent on temperature, with both barrelling and bulging modes being observed.

The specimen shapes indicate that specimens at higher effective stress and temperature may strain soften during shearing, that is, may become more brittle. Specimens that develop a barrel shape at the end of shear are more ductile, that is they should strain harden during shear. The load controlled procedures used in these tests do not permit observations of strain softening behaviour.

CHAPTER 6

DISCUSSION

6.1 Introduction

Research into the effects of temperature on buffer behaviour began at the University of Manitoba with Lingnau, and followed Saadat's tests at ambient temperatures. Lingnau's experimental program consisted of three series of undrained triaxial compression tests performed at temperatures of 26°C, 65°C, and 100°C. The purpose of the program presented in this thesis was to conduct drained stress controlled triaxial compression tests under temperature and pressure conditions that were similar to Lingnau's, and to compare the strength relationships for buffer specimens tested using this different stress path.

This chapter will summarize the results presented in Chapter 5 and discuss their relationship with results from Lingnau and Saadat. The method of testing, although significantly different from that used in undrained tests, produces comparable consolidation and shear strength results.

6.2 Consolidation

During this program, consolidation of buffer specimens was performed in two stages. Initially, the specimens were consolidated at a controlled temperature of 26°C which is approximately room temperature. Once the first stage of consolidation was complete, they were heated and allowed to reach volumetric equilibrium at elevated

temperatures of either 65°C or 100°C. Specimens were taken to be at volumetric equilibrium when their volumetric strain rates were less than 0.1%/day. The purpose of dividing the consolidation process into two parts was to measure the effect of temperature on the buffer when consolidated initially at room temperature and then heated to an elevated temperature. During Lingnau's program, specimens were heated immediately after consolidation pressures were applied, so volume changes due to pressure and temperature could not be readily separated. The specimens from Lingnau and Saadat's programs, as with this program, were formed by static compaction to a dry density of 1.67 Mg/m^3, but differed slightly with some variation in mixing and compaction techniques from those described in Chapter 4.

In general, the application of heat to a buffer specimen that is in pressure and volumetric equilibrium produces small volumetric change in the specimen. As shown in Figure 5.57, no net volume change seems to occur at a mean effective stress of 1.5 MPa for specimens consolidated at 26°C. The results in Figure 5.58 show three distinct relationships between specimens consolidated at three different temperatures of 26°C, 65°C, and 100°C. These relationships reflect shrinking yield loci at constant specific volume with increasing temperature as shown by other researchers in Chapter 2. The consolidation lines can be considered parallel for different temperatures. The equations for the normal consolidation lines are presented again below for comparison later (p' in kPa).

Beginning of consolidation

V_c = Constant = 2.25 ...(13bis),(22)

End of first consolidation period at 26°C before heating

$V_c^{26°C} = 2.841 - 0.081 \ln p'$ $R^2 = 0.95$ ...(14bis),(23)

End of thermal consolidation at 26°C, 65°C, and 100°C

$V_c^{26°C} = 2.981 - 0.084 \ln p'$ Fitted ...(15bis),(24)

$V_c^{65°C} = 2.818 - 0.076 \ln p'$ Fitted ...(16bis),(25)

$V_c^{100°C} = 2.778 - 0.091 \ln p'$ Fitted ...(17bis),(26)

The equations for the normal consolidation lines as determined by Saadat and Lingnau are presented below (p' in kPa). The equations from Lingnau's larger data base also show a small trend towards a shrinking yield locus with increasing temperature, that is, lines for increasing temperatures are at successively lower specific volumes.

Saadat (1988), ambient temperatures

$V_c^{26°C} = 3.541 - 0.171 \ln p'$ $R^2 = 0.95$ ...(27)

Lingnau

$V_c^{26°C} = 3.102 - 0.121 \ln p'$ $R^2 = 0.94$ ...(28)

$V_c^{65°C} = 3.050 - 0.121 \ln p'$ Fitted ...(29)

$V_c^{100°C} = 2.950 - 0.121 \ln p'$ Fitted ...(30)

The consolidation results presented are plotted in Figure 6.1 and show good agreement between the different researchers. The slope λ of Saadat's normal consolidation line is greater than Lingnau's and the results from this research program. The results are also summarized in Table 6.1.

6.2.1 The Effective Stress Concept

The validity of the effective stress concept was examined during consolidation of two of the specimens (T1303 and T1307) by increasing the back pressure from 1 MPa to 7 MPa while maintaining a constant mean effective stress. The purpose of this procedure was to confirm that the behaviour of the specimens is governed by changes in effective stress rather than total stress.

Specimen T1303 was consolidated at an elevated back pressure at 26°C, similar to Saadat's procedure with ambient temperatures, and T1307 was consolidated at an elevated temperature of 65°C. The results for T1303 are shown in Figures 5.5 and 5.6. Figure 5.5a shows that both the cell and back pressures were increased by 7 MPa on the eleventh day of the test. If the effective stress concept is valid, it would be expected that no further volume change would occur in the specimen since the effective stress was constant. The volumetric strains measured during consolidation are shown in Figure 5.6a and show that the specimen continues to dilate at about the same rate after the change in total stress. The lateral strain measurements in Figure 5.6b show that the specimen did not change in diameter. Evidence from the membrane diffusion tests indicate that membrane diffusion occurs at a mean effective stress of 0.6 MPa at elevated temperatures. Given the doubt that membrane diffusion places on the volumetric measurements, the lateral strain gauge is considered a more reliable measure of the actual performance of the specimen at a mean effective stress of 0.6 MPa. These readings support the applicability of the effective stress concept.

The order of consolidation events followed three stages for specimen T1307, and included consolidation at (a) room temperature, (b) elevated temperature to 65°C,

and (c) elevated back pressure to 7 MPa. The back pressure during the first six days of the test was held at 1 MPa with an effective stress of 1.5 MPa as shown in Figure 5.13a. The specimen reached volumetric equilibrium after about four days and was then heated to 65°C as shown in Figure 5.13b. Figure 5.14a shows an "apparent" compressive strain of about 0.4 % on the fourth day which is primarily due to expansion of the pore water and system components during the heating phase. After heating was complete the specimen maintained a relatively constant volume and after 2 days volumetric equilibrium was confirmed. The cell and back pressure were then increased to 8.5 MPa and 7 MPa, respectively. Figure 5.14a shows an instantaneous volumetric response to the pressure change with virtually no volume change afterward. The lateral strain results for T1307 are presented in Figure 5.14b and show that the specimen expanded laterally by about 0.1% due to heating. On the fifth day of consolidation the specimen "apparently" dilated laterally by about 0.6% during a short time period. However, the pressure, temperature, and volume strains during the fifth day were relatively constant. The change in the diameter of the specimen on the fifth day is, therefore, presumed to be unique to the lateral strain gauge and may be caused by a shift in the location of the device due to the change in temperature. After the pressure was elevated the diameter of the specimen remained constant.

The consolidation results for specimens T1303 and T1307 show that the buffer is governed by effective stresses since no significant volume or lateral strains occurred due to a 7 MPa increase in total stress. This is especially evident for T1307 since the applied effective stress of 1.5 MPa is approximately equal to the swelling equilibrium pressure for the buffer. If total stresses governed the volume change of the specimen, then large volume strains due to the 7 MPa increase

in total stress would have been observed but in reality the specimen maintained its state of volumetric equilibrium.

6.3 Shear

The specimens in this program were sheared at a series of constant mean effective stresses along vertical stress paths in p':q-space. They were sheared by applying equal increments of axial load which correspond to (almost) constant increments of deviator stress. The size of the increments was chosen so that failure could be expected after the fifth increment was added. The maximum deviator stress was predicted from Saadat's (1988) equation for the peak strength of the buffer which is $q_p = 2.59\ p'^{0.80}$. (Saadat's equation is based on triaxial tests at ambient temperature on buffer specimens with an initial dry density of 1.67 Mg/m^3.) The deviator stress was held constant during each load increment, and subsequent increments added only when the axial strain rate became relatively constant.

The specimens were sheared with drainage leads open, and typically exhibit small volumetric strains since the mean effective stress is held constant. The lateral strains generally mirror the shape of the axial strains, with Poisson's ratio being approximately 0.5 (Section 5.3), at least in the early portions of the test. Determination of Poisson's ratio from lateral strain measurements is reasonably accurate during the initial stages of shear when the specimen shape does not deviate significantly from a right cylinder. Quite good sensitivity appears to have been achieved from the newly developed lateral strain indicators.

The measured axial strains and axial strain rates show that the specimens strain at a relatively fast rate immediately after loading. In all but the final increment,

this is followed by deceleration to an approximately constant axial strain rate (see for example Figure 5.35). Under the final increment, the axial strain rates accelerate until large, unacceptable, strains are attained. The specimen is said to have failed when axial strain is accelerating, or the specimen can sustain no further loads. The tests were terminated at axial strains of 15%. Axial strains at failure were generally less than 6%, with several specimens failing at less than 3%. Relatively good control of the mean effective stress and deviator stress was possible considering that any fluctations in cell pressure are linked directly to the applied axial load. An increase in cell pressure will create greater impetus for the piston to be pushed from the cell and has the effect of reducing load on the specimen.

Until this testing program, only moderately compacted buffer specimens (1.54 Mg/m^3, 85% Modified ASTM Dry Density) had been sheared at the University of Manitoba under constant mean effective stresses. Tests on low density specimens were performed by Wan (1987) and Saadat (1989). The cross-sectional areas of the specimens during shear were calculated from volume change measurements only. Axial loads were adjusted to maintain a constant mean effective stress with increasing cross-sectional area. As the specimen approached failure and began to strain rapidly the axial loads were adjusted more frequently. When the final load increment was applied to low density specimens, the axial strain initially decelerated at the same rate as for previous load increments. However, after periods of a few hours, the axial deformations of these specimens accelerated until, as mentioned earlier, the end of test was reached at about 15% axial strain.

High density buffer specimens fail differently, in a more abrupt and brittle manner. Specimens that failed at the predicted deviator stress exhibited a dramatic

response, with the lever and weights of the loading system swinging downward rapidly until they were checked by a mechanical stop. If the load increment was insufficient to cause the specimen to fail almost immediately after application of the load, axial straining would not accelerate. As in the earlier tests, load increments prior to failure caused the high density buffer specimens to strain at constant, and successively faster axial strain rates.

Some specimens did not fail at the expected deviator stresses, and it was necessary to apply additional loads to cause failure. Fractions of a full load increment were applied to these specimens and the axial strains were then monitored to determine if the axial deformation accelerated. If the axial deformation decelerated, further loads were applied and the deformations again monitored. The response was immediate (within 5 minutes) when a load was applied that would produce accelerating axial strains.

The shear failure results from the nine tests that were successfully sheared in the program were presented in Figure 5.59. (Results for T1305 are not presented since this specimen was not sheared due to malfunctioning of the cell.) The results show little systematic variation in strength between buffer specimens sheared at different temperatures. Figure 6.2 shows the results compared to peak strength relationships for CIU (Consolidated Isotropically, sheared Undrained with pore pressure measurement) tests presented by Saadat for ambient temperatures, and by Lingnau for 65°C and 100°C. The equations for all the curves are presented below. The results from Lingnau show that increased temperatures produce somewhat higher peak strength envelopes, although the differences are not large.

Peak shear strength (q and p' in kPa):

Yarechewski, 26°C, 65°C, and 100°C

$q_{peak} = 18.01\ p'^{0.56}$ $R^2 = 0.96$ ...(18bis),(31)

Saadat (1987), ambient temperatures

$q_{peak} = 2.59\ p'^{0.80}$ $R^2 = 0.94$ ...(32)

Lingnau

65°C Temperature

$q_{peak}^{65°C} = 4.93\ p'^{0.72}$ $R^2 = 0.96$ ...(33)

100°C Temperature

$q_{peak}^{100°C} = 6.67\ p'^{0.71}$ $R^2 = 0.98$ ...(34)

Results from this program show that in the mean effective stress from 0 to 1 MPa, the test data compare closely with Lingnau's curve for specimens sheared at 100°C. The curve for the constant p' tests then rejoins Lingnau's 65°C and Saadat's 26°C curves at about 3 MPa. At a mean effective stress of 3.2 MPa, the constant p' curve and Lingnau's 65°C curve cross below Saadat's 26°C curve. However, the differences are not large, and may lie simply in the scatter in the results. Lingnau's and Saadat's curves were drawn for a larger data base than was possible in the current test series.

The equations for the peak strength lines were plotted in Figure 5.60 in V_c:p'-space and are now compared with critical state results from Saadat and Lingnau in Figure 6.3. Since the change in volume between the peak and end-of-test

is small during constant-p' tests the peak strength lines in Figure 5.60 may be assumed to approximate the critical state lines for 26°C, 65°C, and 100°C.

Critical state lines at 26°C, 65°C, and 100°C (p' in kPa):

Yarechewski

$V_c^{26°C} = 3.527 - 0.160 \ln p'$ Fitted ...(19bis),(35)

$V_c^{65°C} = 3.369 - 0.153 \ln p'$ Fitted ...(20bis),(36)

$V_c^{100°C} = 3.335 - 0.160 \ln p'$ Fitted ...(21bis),(37)

Saadat (1989)

$\ln V_c^{26°C} = 1.763 - 0.126 \ln p'$ $R^2 = 0.97$ ...(38)

$V_c^{26°C} = 4.363 - 0.279 \ln p'$

Lingnau

$V_c^{26°C} = 3.102 - 0.121 \ln p'$ Fitted ...(39)

$V_c^{65°C} = 3.020 - 0.121 \ln p'$ Fitted ...(40)

$V_c^{100°C} = 2.930 - 0.121 \ln p'$ Fitted ...(41)

Lingnau regressed a best-fit line through his 26°C data. "Best-fit" lines were then fitted to the 65°C data and 100°C data with the same slope, 0.121. Table 6.2 presents the above results in the form $V_c = \Gamma - \lambda \ln p'$. The results show similar slopes for the critical state lines and a trend towards decreased clay specific

volume with increased temperature. Some detailed differences in the values of Γ may result from the way different researchers prepare their data.

6.3.1 Shear of Specimen T1303

Specimen T1303 initially was sheared with higher applied loads due to a miscalculation. As a result, the specimen was failed on the first application of the load and experienced axial strain to about 7% with only 1.7% recoverable upon unloading. Strains of this magnitude during this program usually indicate that the specimen has failed through plastic straining. The maximum deviator stress calculated during this initial loading was 0.55 MPa. After unloading, the specimen was allowed to reconsolidate istropically at the original mean effective stress of 0.6 MPa. Upon application of the correct loads, the specimen was sheared to a maximum deviator stress of 0.59 MPa as shown in Figure 5.32a which is comparable with results from other tests as shown in Figure 5.59.

The results of this test show that the specimen can recover structurally after being strained excessively. This is partly because the nature of the specimen forming procedure produces a fairly homogeneous material with no inherent structure. Another reason for this recovery is likely owing to the swelling capabilities of the sodium bentonite to heal (or at least seal) the shear bands that developed within the specimen. This self-healing capability will play an important role within the life of the nuclear waste disposal vault to impede the flow of radionuclides.

CHAPTER 7

CONCLUSIONS AND RECOMMENDATIONS FOR FURTHER WORK

As is customary, only the principal conclusions will be listed here. More detailed conclusions have been presented at appropriate places in the discussion. It is appreciated that tests are few and statistically questionable, yet reasonably clear trends have been established that support work by other researchers. The principal conclusions are as follows.

- Constant mean effective stress triaxial tests can be performed on sand-bentonite specimens at elevated temperatures of 26°C, 65°C, and 100°C.

- The effect of temperature on the strength of the buffer is small in these tests. The strength envelope can be represented by a single relationship, which is independent of temperature.

- The shear strength results from these CID' tests are comparable to the results of Lingnau and Saadat.

- The Critical State Lines show a trend towards reduced clay specific volume V_c with increased temperature.

- The effective stress concept appears to be useful for describing the behaviour of buffer at elevated temperatures.

- Buffer specimens consolidated at elevated temperatures exhibit behaviour which can be interpreted as representing a shrinking yield locus with increased temperature.

- The buffer has self-healing capabilities which allow it to be failed under large axial strains, reconsolidated, and then resheared without a reduction in peak strength.

- The Shear Modulus G_{50} increases slowly with increased mean effective stress but no obvious dependency on temperature has been noted from these tests. The Young's Modulus is approximately constant. Again there is no obvious dependency on temperature.

- Silicone oil cell fluid diffuses through two silicone membranes at a mean effective stress of 0.6 MPa at 100°C. The direction of the diffusion path is from the lower back pressure to the higher cell pressure.

- Dilative specimens exhibit a failure mechanism in which local bulging is seen at the base of the specimens. Compressive specimens exhibit shear planes.

- Further research should be undertaken to determine the effects of temperature change on the elastic properties of the buffer, and the effect of cyclic or ramped temperatures.

- Calibration of thermal expansive strains should be described and related to diffuse double layer strains.

- Diffusion of silicone oil should be arrested by locating a more resistant membrane material.

- The conical sealing ring should be employed if current sealing practices allow passage of silicone oil into the pore water.

- The teflon bushing in the triaxial cell head should be replaced with a system that exhibits less deformation with the application of heat.

- Scatter in the data is still relatively large.

- A stronger conceptual and numerical model of constitutive behaviour should be developed.

REFERENCES

Aylmore, L.A.G., Quirk, J.P., and Sills, I.D. 1969. Effects of heating on the swelling of clay minerals. Highway Research Board, Special Report **103**, pp. 31-38.

Agar, J.G., Morgenstern, N.R., and Scott, J.D. 1986. Thermal expansion and pore pressure generation in oil sands. Canadian Geotechnical Journal, **23**, pp. 327-333.

Agar, J.G., Morgenstern, N.R., and Scott, J.D. 1987. Shear strength and stress-strain behaviour of Athabasca oil sand at elevated temperatures and pressures. Canadian Geotechnical Journal, **24**, pp. 1-10.

Baldi, G., Hueckel, T., Peano, A., Pellegrini, R. 1990a. Developments in modelling of thermo-hydro-geomechanical behaviour of Boom clay and clay based buffer materials. Vol. I, submitted to Commissione delle Comunita' Europee by ISMES, Progretto ASP-4361, Doc. n. RAT-DMM-149.

Baldi, G., Hueckel, T., Peano, A., Pellegrini, R. 1990b. Further check and development of the thermo-hydro-geomechanical model for Boom clay and clay based buffer materials with an emphasis on the thermo-mechanics of water-solid systems. Vol. II, submitted to Commissione delle Comunita' Europee by ISMES, Progretto ASP-4361, Doc. n. RAT-DMM-149.

Campanella, R.G., Mitchell, J.K. 1968. Influence of temperature variations on soil behaviour. Journal Soil Mechanics and Foundations Division, ASCE, Vol. 94, No. SM3, Proc. Paper 5958, pp. 709-734.

Cheung, S., Gray, M.N., and Dixon, D.A. 1985. Hydraulic and ionic diffusion properties of bentonite-sand buffer materials. Proceedings. International symposium on the coupled processes affecting the performance of the nuclear waste repository, Lawrence Berkley Laboratories, Berkeley, U.S.A.

Demars, K.R., and Charles, R.D. 1982. Soil volume changes induced by temperature cycling. Canadian Geotechnical Journal, **19**, pp. 188-194.

Dixon, D.A., Gray, M.N. 1985. The use of bentonite in a nuclear fuel waste disposal vault. Proceedings 1st Canadian Engineering Technology Seminar on the Use of Bentonite for Civil Engineering Applications. Regina, Saskatchewan, Canada, pp. 64-74.

Dixon, D.A., Gray, M.N., Thomas, A.W. 1985. A study of the compaction properties of potential clay-sand mixtures for use in nuclear fuel waste disposal. Engineering Geology **21**, pp. 247-255.

Dixon, D.A., Cheung, S.C.H., Gray, M.N., and Davidson, B.C. 1987. The hydraulic conductivity of dense clay soils. Proceedings 40th Canadian Geotechnical Conference, Regina, Saskatchewan, pp. 389-396.

Erikksson, L.G. 1989. Temperature effects on consolidation properties of sulphide clays. Proceedings 12th International Conference Soil Mechanics and Foundation, Rio de Janiero, **3**, pp. 2087-2090.

Graham, J., Noonan, M.L., Lew, K.V. 1983. Yield states and stress-strain relationships in a natural plastic clay. Canadian Geotechnical Journal **20**, pp. 502-516.

Graham, J., Saadat, F., Gray, M.N., Dixon, D.A., and Zhang, Q.-Y. 1989. Strength and volume change characteristics of sand-bentonite mixture. Canadian Geotechnical Journal **26**, pp. 292-305.

Graham, J., Yin, J.-H., Oswell, J.M., and Lingnau, B.E. 1990. Constitutive modelling of sand-bentonite buffer (RBM). Unpublished Contract Report WS-27J-62961 to Atomic Energy of Canada Limited.

Graham, J., Lingnau, B.E., Yarechewski, D.S., and Tanaka, N. 1992. Thermo-elastic-plastic modelling of sand-bentonite buffer for use in underground disposal of nuclear fuel waste. Unpublished Contract Report WS-30J-79981 to Atomic Energy of Canada Limited.

Hueckel, T., Borsetto, M., and Peano, A. 1987. A study of thermo-plastic hydraulic coupling in clays applied to nuclear waste disposal. Proceedings 2nd International Conference on Constitutive Laws for Engineering Materials, Theory and Application, **1**, pp. 311-318.

Hueckel, T., and Pellegrini, R. 1989. Modelling of thermal failure of saturated clays. Numerical Models in Geomechanics. S. Pietruszczak and G.N. Pande, eds. Elsevier, New York, NY, pp. 81-90.

Oswell, J.M. 1991. Elastic plastic behaviour of a sand-bentonite mixture. PhD Thesis, University of Manitoba, Department of Civil Engineering.

Paaswell, R.E., 1969. Transient temperature influences on soil behaviour. Highway Research Board, Special Report **103**, pp. 220-230.

Plum, R.T., and Esrig, M.I. 1969. Some temperature effects on soil compressibility and pore water pressure. Highway Research Board, Special Report **103**, pp. 231-242.

Radhakrishna, H.S. 1984. Thermal properties of clay-based buffer material for a nuclear fuel waste disposal vault. Atomic Energy of Canada Limited Report AECL-7805.

Roscoe, K.H., Schofield, A.N., and Wroth, C.P. 1958. On the yielding of soils, Geotechnique **8**, pp. 22-52.

Saadat, F. 1989. Constitutive modeling of the behaviour of a sand-bentonite mixture. PhD Thesis, University of Manitoba, Department of Civil Engineering.

Sun, B.C.-C. 1986. Stress-strain properties in sand-clay buffer materials. MSc Thesis, University of Manitoba, Department of Civil Engineering.

Tidfors, M., and Sällfors, G. 1989. Temperature effect on preconsolidation pressure. Geotechnical Testing Journal, **12**, pp. 93-97.

Wan, A.W. 1987. Compaction and strength characteristics of sand-clay buffer material formed at swelling pressure-water content equilibrium. MSc Thesis, University of Manitoba, Department of Civil Engineering.

Wöhlbier, H., and Henning, D. 1969. Effect of preliminary heat treatment on the shear strength of kaolinite clay. Highway Research Board, Special Report **103**, pp. 287-300.

Wroth, D.M., and Houlsby, G.T. 1985. Soil mechanics-property characterization and analysis procedures. Proceedings, 11th International Conference on Soil Mechanics and Foundation Engineering, San Francisco, CA, vol. 1, pp. 1-54.

Yarechewski, D.S. 1988. Quality control tests for making sand-bentonite specimens for nuclear waste containment studies. BSc Thesis, University of Manitoba, Department of Civil Engineering.

Yin, J-H. 1990. Constitutive modeling of time dependent stress-strain behaviour of soils. PhD Thesis, University of Manitoba, Department of Civil Engineering.

Yong, R.N., Chang, R.K., and Warkentin, B.P. 1969. Temperature effects on water retention and swelling pressure of clay soils. Highway Research Board, Special Report **103**, pp. 132-137.

APPENDIX A

THE DISPOSAL OF RADIOACTIVE WASTE

This term project was previously presented on April 18, 1991 at the University of Manitoba for course 23.716 Environmental Impact.

1.0 The Nature of Radioactivity

Radioactive decay is the process whereby unstable atoms release energy to become more stable. The half-life of a radioactive element is the time required for the number of atoms to be reduced by one-half through radioactive decay. There are several types of radiation that are emitted during the decay process. Alpha-particles (α) are large and positively charged. They are composed of helium nuclei (2 protons and 2 neutrons) and cannot penetrate the body or clothes. Beta-particles (β) consist of electrons which can penetrate 1 to 2 cm into water and flesh. Although both of these particles are not very harmful externally, they can cause significant damage to sensitive tissue if they enter the body. Gamma-radiation (γ) can penetrate through the body and is used to kill cancer cells and tumors. Gamma-radiation and x-rays are part of the electromagnetic spectrum, which includes visible light, but have much greater penetrating power.

When radiation collides with other atoms in the human body, ions are produced which may react with the strands of DNA molecules. This type of radiation is called ionizing radiation. The broken DNA strands are repaired regularly, but if damaged beyond repair, the regulation system of the cells becomes unbalanced and cell reproduction occurs in an uncontrolled manner and rate. The damage can be either

somatic or genetic. Somatic damage affects the living organism, while genetic damage refers to defects in chromosomes and genes that can be passed to offspring.

There are several units used for quantifying radiation. The Curie (Ci) is the number of nuclear disintegrations (3.7×10^{10}) that one gram of radium undergoes in one second. The roentgen or rad (radiation absorbed dose) is the amount of energy deposited per kilogram of tissue. A factor called the relative biological effectiveness is used to differentiate between different types of penetrating radiation and is called a rem (roentgen equivalent for man). Rems are a measure of the biological damage caused by energy. A similar unit in the SI system is the sievert (Sv). The average radiation dose received by the public is 2.7 mSv/yr from background radiation. According to Canadian law an additional 50 mSv/yr is allowable for people working with radiation and 5 mSv/yr for the general public. The effects of radiation are presented below. The radiation dosages refer to an instantaneous exposure over the whole body.

10000 mSv	Illness and death within a few weeks.
1000 mSv	1 out of 100 exposures results in nausea, cancer.
100 mSv	Not noticeable.
1 mSv	This represents the minimum dosage on earth due to background radiation. Represented by 1 case of cancer in 100,000.

The estimated average radiation dose rates for the Canadian population are presented in Figure 1 [1]. These doses are based on 1 kW of nuclear energy production per person which is the estimated amount for the 1990's. The figure was taken from a report by Sir Edward Pochin for the United Nations Scientific Committee on the Effects of Atomic Radiation (UNSCEAR) [25]. According to

Figure 1, the radiation dosage from the nuclear energy cycle represents approximately 6 percent of the natural radiation dose rate.

Extensive research has been performed to determine the effect of fallout on organisms and the environment. Radioactive fallout initially collects on the leaves of plants, and as these drop to the forest floor, the radionuclides become attached to the humus and litter. The high surface area to weight ratio of the humus causes the radionuclides to bond strongly with the humus and not penetrate into deeper soils [11]. Unfortunately, most studies concerning radiation effects on flora and fauna have been performed from the perspective of radiation originating from fallout and not from below the ground surface. Therefore, it is not certain what effects radionuclides escaping from buried wastes would have on the biosphere.

Certain fission products (these are the by-products of a nuclear reaction) can be concentrated in organic tissue. The Windscale reprocessing plant in the United Kingdom was releasing low-level liquid wastes into the Irish Sea [4]. The concentration of the radionuclides was low enough that the water was safe for swimming and recreational activities. However, a seaweed used as a source of food in South Wales was found to concentrate ruthenium-106 which is one of the fission products released from the reprocessing plant. This case shows that there are certain plants and animals that will reconcentrate radionuclides, and that dilution of radioactive waste does not necessarily solve the disposal problem.

There are other organisms that are good indicators of contamination levels. Freshwater mussels in northern Italy feed on suspended particles and live in the sediments. These molluscs tend to concentrate cesium and manganese, as revealed from studies after the Chernobyl accident [29]. They are particularly useful

indicators because they occupy a wide area and are not as mobile as fish, making it possible to determine contamination levels in different regions.

2.0 The Nuclear Energy Cycle

The process of generating electricity in nuclear reactors is similar in principle to coal generators where heat is generated to convert water into steam. The steam is passed through a turbine to produce electricity. The CANDU (CANadian Deuterium and Uranium) reactors use natural uranium as fuel for the reactor and deuterium (heavy water) as the moderator and coolant. A schematic representation of how a CANDU reactor produces electricity is shown in Fig. 2 [20]. The deuterium is circulated over the uranium fuel and through a boiler containing light water. The light water is changed to steam which is used to drive a turbine to produce electricity. Once the steam passes through the turbine, it is condensed and the process is repeated. The CANDU 600 reactors can produce a nominal electrical output of 600 Megawatts.

The mined uranium oxide, which is used as fuel in a nuclear reactor, is compressed into ceramic pellets which are placed in zirconium tubes 0.5 m long, as shown in Figure 3 [3]. These tubes are arranged in a 0.1 m diameter circular configuration which is called a fuel bundle and contains about 20 kg of natural uranium. One fuel bundle produces the equivalent amount of energy to 400 tonnes of coal.

Nuclear reactors use uranium fuel to produce heat through the process of fission [17]. Fission is the splitting of nuclei which results in the release of radiation, neutrons, and radioactive fragments called fission products. Uranium-235 is fissile material, that is, a material that will undergo fission and

keep the chain reaction in progess. Naturally occurring uranium contains 0.7% U^{235} and 99.3% U^{238}. The uranium-238 does not support fission, but absorbs neutrons to produce uranium-239 which decays to fissile plutonium-239. In the nuclear reactor, the uranium-235 atoms are split by neutrons which in turn causes 2 or 3 neutrons to be released. These newly released neutrons can subsequently split other U-235 atoms and release more neutrons. This continued fission process is called a chain reaction. The fission fragments move away rapidly after impact and jostle other uranium atoms which produces heat. During one fission, 200 MeV of electricity is produced [16]. The amount of uranium-235 required for nuclear weapons is 90% and explains why a nuclear reactor cannot explode like a nuclear bomb [35].

For the fission process to take place the neutrons must be slowed otherwise they will not strike the U^{235} atoms. The slowing of the neutrons is accomplished through the use of a moderator, which in CANDU reactors is deuterium. Deuterium is a water molecule with an extra neutron in the nucleus of the hydrogen atoms. As the fast neutrons pass through the deuterium, they bounce between atoms causing them to lose energy and speed. A schematic representation of this process is presented in Figure 4 [17]. It is important that the moderator loop be free of leaks because the deuterium can absorb neutrons and be changed to tritium which is radioactive.

Light water, although much less expensive than deuterium, is not preferred as a moderator because it absorbs too many neutrons, and this reduces the amount of fissioning that can occur. Some nuclear reactors, that use light water as a moderator, require as much as 3 percent of the fuel to be U-235 while there is only about 0.7% in natural uranium deposits. Reactors that require a higher uranium-235 content use enrichment processes to increase the content.

The fission rate in reactors is controlled by neutron-absorbing rods made of cadmium and boron which are lowered between the fuel bundles. By placing the rods deeper within the reactor core, fewer reactions occur because the rods remove neutrons that would otherwise be used for fission. The reaction rate can also be slowed by lowering the level of the deuterium in the reactor core. Less of the moderator means that fewer neutrons are slowed and allowed to take part in the reaction.

The fuel is considered spent when the amount of neutrons absorbed by the fission products begins to outnumber the number of neutrons released by the fissile material. The result is that less energy is produced efficiently. After the fuel has been spent, the uranium content remains virtually unchanged, with 98.7% of the U^{238}, U^{235}, and U^{234} intact.

2.1 Recycling

The spent fuel rods can be recycled by recovering the plutonium fission products produced by the chain reaction. The process consists of dissolving the waste in acid and removing the useful elements. The remaining waste is solidified by vitrification into glass or ceramic and disposed. By using the plutonium as a fuel, the amount of energy obtained from natural uranium can be increased. Alternatively, thorium can be changed into fissile uranium-233 which can be mixed with plutonium and used in CANDU reactors. This is termed a "near-breeder" and could extend the nuclear resources by a factor of ten. The term "breeder" refers to reactors that can create more nuclear fuel by converting fission products. The use of plutonium in reactors reduces the amount of waste, but does not eliminate

the long term hazards, since it is difficult to entirely separate the plutonium. Other long-lived fission products will also remain in the waste.

The need to recycle depends on the cost and availability of the uranium oxide that occurs naturally in Canada. Presently (in 1992), the cost of recycling is greater than the cost of mining and employing natural uranium in a "once-through" fuel process. There is a large natural supply of fissionable material in Canada. This makes it more economical to mine uranium for fuel than to recycle fuel waste.

3.0 Selection of a Site for a Nuclear Reactor

The factors involved with choosing a nuclear reactor location generally fall into three categories which relate to the environmental, economical, and technical efficiency of a location. The environmental concerns that need to be addressed pertain to aquatic, terrestrial, atmospheric, and food chain elements of the biosphere.

The power plant, to be economically feasible, should be close to the main receiver of the electricity. However at the same time, the technical feasibility of the project must be assessed. The site selection process performed by Manitoba Hydro attempts to weigh the factors related to these categories without creating a relationship between cost and environment [20,21]. The impact on the environment is determined by a ranking scheme which is created by members of a committee from various organizations.

There are many effects which must be investigated during the site selection process such as turbine noise, radiation emissions, and cooling operation. Condensing of

steam once it exits the turbine requires approximately 24 m^3/s to 48 m^3/s of water which will be increased in temperature by 15°C to 7.5°C, respectively. If this warmed water is returned to a water body it can affect the aquatic life. A closed cooling system uses towers that allow the steam to be condensed as it falls through cooled air. Some energy is used to condense the steam and some water is lost due to evaporation. This reduces the impact on the aquatic life and requires a smaller water body for supplemental supply. However, it increases the cost to operate the plant and reduces the efficiency.

If thermal discharges occur in a water body, fish will move to better locations and overcrowding will occur. Discharges also produce turbidity which may affect fish reproduction and the fishing industry. The impact on the terrestrial environment could affect unique or rare species and habitat which would include alterations of migratory patterns. Socio-economic impacts such as the influx of people to the area may be based on the ease of commuting to the site and may affect existing populations in the vicinity. Radioactive emissions from a nuclear power plant are small, and generally represent 1% of the allowable specification. An isolation zone extends in a 1 km radius around the power plant. This results in low turbine noise at the plant boundary. Landscaping is used to reduce the visual impact of the site.

The Manitoba Hydro report suggests that the disposal of nuclear waste be either at the plant site or at a common disposal site within the province but did not give further details.

4.0 Waste Treatment

Nuclear waste comes in different forms which are generally grouped into three categories as low, intermediate, and high-level waste. The definitions of these categories depend on the activity and half-lives of the waste. In France, low and intermediate level wastes are disposed in covered trenches or shallow repositories. High-level wastes that have long half-lives and high activity will be stored in deep repositories as shown in Figure 5 [4].

Nuclear waste can originate from other sources besides from the irradiated fuel in the reactor. The wastes with lower activity include such items as light bulbs, rags, paper, and tools that have been exposed to radiation. Liquid wastes originate from cleanup of the reactor coolant and condensate, leaks in the cooling cycle, decontamination operations, floor drains, and water from showers and laundry. Decontamination operations use water jets to remove radioactive material from canisters or other objects.

The wastes are processed into a stable waste form that will allow minimum dispersion of radioactive material into the environment. The process of vitrification combines the radioactive waste with borosilicate glass to create a stable product that can accomodate a wide variety of waste products. Radioactive liquid waste is generally non-volatile and remains attached to salts. The salts are converted to an insoluble form and precipitated using either filters or floc precipitation [5]. Ion exchangers are then used to separate the radioactive particles from the salts. Leaving the salts in the waste produces an unstable waste form which can etch through glass.

The high level liquid waste can be turned into a calcine and mixed with glass frit which is subsequently melted and cast. The final vitrified product is cast into stainless steel containers each holding about 400 kg of product. The containers are welded shut, decontaminated, and subsequently stored in vaults. The gases and liquids evolved from the process require treatment using such technology as scrubbers and filters.

Glass is not completely insoluble but the leach rate can be very low if extreme temperature (500°C) and water contact is avoided. A low leach rate can be accomplished by careful control of the fission product content within the glass and containment within a medium that allows heat transfer. Devitrification can increase the leachability by a factor of 2 to 5 [1]. The high level waste can also be incorporated into other materials such as bitumen, crystalline ceramic, or cement-based encapsulants.

The solid waste form should be free of voids and contain a chemistry which is stable. By preventing solubilization of the waste, storage can be performed in canisters without fear of radionuclide leakage. It is best to remove organics from the waste since they produce acids which can accelerate decay of the container.

Low level waste can be disposed using incineration and clean-up techniques for the gases. Other current methods include baling with two layers of polyethylene and storage. The waste is compacted prior to packaging to reduce the volume. Plant awareness can also be used to reduce the amount of low level waste and prevent its entrance into the waste stream.

5.0 Present Storage Methods

5.1 Pools

Highly radioactive nuclear fuel waste is currently stored in concrete double-walled pools lined with stainless steel and filled with ordinary (as opposed to "heavy") water. The water shields the fuel bundles which are placed on racks consisting of stainless steel or aluminum alloy. The racks contain boron which is used to prevent fission of the uranium by absorbing neutrons released from the bundles. This process has been used for the past 30 years in Canada.

As of 1988, there were about 12,300 tonnes of used fuel in storage, predominantly in pools. The 2,000 megawatt Pickering Generating station in Ontario produces about 260 tonnes of waste each year. All of the fuel waste produced by this plant could be stored in a waterfilled tank 160 metres long, 10 metres wide, and 8 metres deep until the year 2000 [1]. The amount of waste produced by nuclear power plants is not very large in volume or weight.

Nuclear fuel waste stored in pools requires about 2 cubic metres of water volume per tonne. As the waste releases heat, a circulation system cools the water and prevents overheating of the pool. The water is filtered through an ion exchange column to remove any radioactivity that may have escaped from the used fuel and dissolved. Current technology relies predominantly on pool systems. The acquired knowledge about pool storage is quite substantial.

The risks involved with pool storage lies primarily with human error. Should an earthquake occur, the pool may crack and allow the water to drain and the shielding

would be lost. A different scenario might occur if the plant had to be evacuated. The cooling system would be left unattended and in the event of a malfunction the pool water could become hot and boil. Interaction between the zirconium cladding on the rods and steam will release hydrogen. This could result in an explosion that would open the building and the radioactive material to the atmosphere.

5.2 Dry Storage

Concrete canisters are presently used for "dry" storage. These containers consist of 1 m thick concrete walls with two inner steel linings. They are about 2.5 m in diameter, 5 m high, and contain approximately 4.4 tonnes of irradiated fuel. Cooling of the canisters is provided by natural convection of the surrounding air.

Another type of concrete vault contains "thimble" tubes which consist of long vertical tubes arranged in a vertical grid. A series of canisters is stacked vertically within the tubes and welded shut. Cooling is provided by natural air circulation around the tubes.

The advantage of dry storage over pools is (a) the cooling medium is unlimited since it consists of the surrounding air, (b) low corrosion rates for the canisters, (c) no power supply is needed since natural convection can be used, and (d) the system requires very little surveillance.

5.3 Shallow Burial of Waste

France opened a new repository in 1991 for intermediate and low level waste [9]. Intermediate level wastes are stored below the ground surface in concrete boxes,

with low level wastes being placed on top of the boxes. The waste is then covered with an earth mound and grassed. Groundwater will be monitored for contamination and treated if necessary. The wastes are short-lived and will be monitored for a period of 300 years, after which time the land may be reclaimed.

Approximately two-thirds of U.S. high level waste from defence materials is at the Hanford Nuclear Reservation in Richland, Washington. The high level waste is currently vitrified, placed into stainless steel containers, and placed in a repository, while low level wastes are placed in near-surface vaults. Prior to using the vitrification process at Hanford, single-walled carbon steel tanks containing high level liquid waste were buried underground. A total of 450,000 gallons was found to have leaked from 20 of the 149 tanks in 1956. This case reinforces the need to immobilize the waste in a solid stable waste form.

6.0 Proposed Permanent Storage Methods

The key objective of any nuclear waste disposal program is to isolate the material from the biosphere for a sufficiently long time to allow the waste to decay naturally. Some of the decay curves of radioactive isotopes are presented in Figure 6 [23]. There are several alternatives that could be used for permanent disposal, and these are described below.

6.1 Surface Disposal

It is possible to store waste in canisters on the ground surface with a monitoring system in place. This is essentially the method in use today. Any problems that

may occur during the life of the disposal site can be remediated without great difficulty.

The major deficiency with this system is that the site will have to be monitored in perpetuity. This leaves the burden of monitoring the waste of this generation to the generations of the future. There are no guarantees that society in the future will be in a position to guard the waste from the biosphere. The risks of wars, sabotage or other disasters also pose a major hazard.

6.2 Disposal in Glaciers

The nuclear waste could be interred within glaciers such as those in Greenland or the Antarctic. The thickness of the glaciers is 3000 m or more and could provide adequate isolation. The heat generated by the canisters would cause them to sink to the bottom of the glaciers. The glaciers are dynamic systems that migrate with time. When glaciers move over hills and through valleys crevasses open and close. There is a risk that the canisters could be crushed either by movement within the ice or near the ice/ground interface which could accelerate the transmission of radionuclides. Besides the questions of glacier stability there is also problems with the legalities of this proposal. The Antarctic is controlled by an international treaty, and neither Antarctica nor Greenland are Canadian territory.

6.3 Outer Space

With current technology it is possible to send the waste to the sun or other planets. The problem with this idea is that the safety hazards during transportation are enormous. The cargo of nuclear waste could break up within the

earth's atmosphere and cause a global catastrophe. The space shuttle Challenger accident is a grim reminder that space travel is not always safe. The costs involved also make this proposal prohibitive.

6.4 Salt Formations

Salt formations have been investigated in the U.S. as a geologically stable formation for nuclear waste disposal. The existence of the salt, in itself, is an indication that the area has not been subject to groundwater conditions for a long time. At depths of 600 m the salt has self-sealing capabilities and good heat conduction characteristics.

The formations contain traces of water which form brine pockets that could burst due to heating by the waste. The salt is also corrosive and could cause the canister to decay more rapidly. The glass in the vitrified waste may be affected by increased temperature and could be etched by the hot brine. Another difficulty with these formations is that they are generally an indicator of the presence of oil and natural gas. Exploratory drilling in the vicinity of a nuclear waste site would prove hazardous.

6.5 Sea Burial

From 1949 to 1982, the UK dumped waste containers on the sea floor of the north-east Atlantic until a moratorium was imposed in 1985 at the London Dumping Convention [8,10]. Mixing of the oceans is approximately 100 to 1000 years which is too short a time and would result in damage to the ocean biota. As described previously, organisms can reconcentrate radionuclides that were originally dilute

and permit their introduction into the food chain. The decay of the canisters would be accelerated by the ocean salt, thus allowing premature release of radionuclides.

It is also proposed that nuclear waste be stored in canisters within the ocean bed. The sea floor spreads and subsides due to cooling and metalliferous deposition. As a result an abyss is created and is filled by deposition processes with fine red clay sediments. This produces an abyssal plain which is eventually subducted. It is estimated that the entire process of sedimentation and subduction would take about 200 million years.

The proposed site would be located within the central portion of a tectonic plate which is stable from both a climatic and geological perspective. Plate boundaries should be avoided to allow sufficient time for waste decay. It is uncertain how heat will affect the surrounding medium. Should less waste be placed per canister the affect of heating would be reduced, but more canisters would have to be used.

The Sandia National Laboratories is examining various sites on the sea floor to determine the most suitable location for a 10,000 year storage span [14]. The movement of the sea floor is about 100 m in 1000 years or about 10 cm per year. It is possible to predict the location of volcanic activity and few catastrophic geological events occur on the sea floor. The sedimentation process on the ocean bottom is much simpler than on land with the exception of areas of strong bottom currents, slumps, and turbidity. Geochemical data shows the sediments to be uniform over an area as wide as 700 km apart. The deposition rate can be predicted for different locations and depends primarily on climatic conditions.

It is important that the nuclear waste site be in a remote area to avoid accidental disturbance or collisions by passing vessels during waste emplacement. Most commercial fishing is performed along the edges of the oceans, while most oil resources are found along the continental margins. Low grade nodules of trace metals can be found on the ocean floor, but would probably not be considered a valuable resource due to their abundance and accessibility on land.

The United Kingdom is also studying the possibility of deep sea disposal within caverns or boreholes [22]. Access to the caverns would be from the coast or platforms on the sea bed. The main risk with this type of disposal is during the transport phase.

6.6 Crystalline Rock

The waste could be contained within a crystalline geological formation, provided the rock can transmit heat sufficiently to prevent overheating and fracturing. The rock mass should be homogeneous and free of any joints or fractures to ensure a low permeability. As mentioned previously, all areas that are earthquake-prone and near mineral resources should be avoided. The rock should be resistant to changes from irradiation by the waste.

The depth of the site should be sufficient that the waste could not be affected by glaciation, eustasy, or major climatic changes and should be an adequate distance from any activity that may cause crustal instability such as large dams or deep mining [1]. It has been suggested that abandoned mines be used for deep disposal of the waste. This would not be a good alternative since the mine may contain many fractures and openings which were man-made but not recorded.

The only path that radionuclides could follow to the biosphere would be through the groundwater. The rate at which the radionuclide can travel through the groundwater depends on the immobilization of the waste, the rate of groundwater movement through the rock, and the sorption capability of the rock on the radionuclides. A small amount of gas evolves from the migrating waste with the radioactive isotopes representing one-billionth of the total gases.

It is recognized that the sheer distance that the nuclide-laden groundwater would have to travel to reach the biosphere is not enough to isolate the radionuclides. Wastes such as neptunium-237, iodine-129, and plutonium-239 have half-lives of 2.13 million, 17 million, and 24,000 years, respectively. Groundwater would certainly pass through to the biosphere during these time frames. The sorptive capacity of the rock would retard the radionuclide flow and allow them to decay naturally to safe levels below the ground surface prior to release into the environment. The nature of this adsorption depends on the physical and chemical characteristics of the rock and also the mechanical and thermal stresses created during excavation and emplacement.

Experiments with two long-lived wastes, strontium-90 and cesium-137, indicate that strontium moves at less than 3% of the groundwater rate and cesium much slower [16]. The experiment was performed on a sandy unconfined aquifer. Silts and clays were found to retard the flow still further. The flow of the radionuclides can be complicated by the presence of acidic groundwater which can increase the transport rate of some fission products.

There is evidence in nature to suggest that the sorption characteristics of the rock would be sufficient to prevent migration of radionuclides into the biosphere.

A natural uranium ore body was discovered at Cigar Lake, Saskatchewan which had undergone a nuclear reaction 1300 million years ago, similar to the reaction that occurs in a nuclear reactor. The used fuel was 98% unchanged and had not been dissolved or transported by the groundwater.

Six natural reactors were also discovered in Oklo, Gabon, West Africa [3]. The reactions took place 1.7 billion years ago and continued for 100,000 years. The uranium-235 content at the site was less than the normal 0.7% found in ore deposits and was linked to the presence of fission products which were similar to those found in man-made reactors. The plutonium-239 was found to be well sorbed within the rock mass along with about half of the other fission products. Only the highly soluble and poorly sorbed products were released, thus indicating that a good immobilization of the waste is necessary.

Research is currently underway in Canada with regard to deep burial of high level radioactive waste into a stable geological formation such as a granite pluton in the Canadian Shield [2,7]. The 1500 plutons in the Shield have been stable for hundreds of millions of years and will probably continue to be stable. The preferred pluton should contain a high feldspar and a low quartz content, since quartz is sensitive to stress changes and has low adsorption capacity. The burial site would consist of a series of tunnels and vaults approximately 2 km by 2 km at a depth of 1000 m below the ground surface. The deeper the waste can be placed the longer the flow path required for the radionuclide to travel to the biosphere. Depths of about 1200 m should be avoided since there is a risk of rock bursting into the excavated cavity due to pressure release. This site would have a storage capacity of 191,000 tonnes which would meet the production of nuclear waste until the year 2035.

The proposed boreholes of the repository would be 5 m deep and 1.24 m diameter with canisters 2.25 m long and 0.64 m diameter. A sand-bentonite mixture called "buffer" would be used to seal the annular space between the canister and the rock. The mixture, by its nature, tends to swell when in contact with water. This characteristic will seal the area between the canister and the rock, retarding flow. In the United Kingdom researchers are currently studying grouting of the canisters into place. The alkalinity of the concrete slows the corrosion of the canister. It is estimated that the anaerobic corrosion of the steel would be 1 to 5 μm/yr. If cracks form, normal grouts would not have the useful self-healing characteristics of the clay.

The study of clays near volcanoes 1000 m below the island of Götland in Sweden and in Sardinia show that clays can retain their swelling and sealing properties after having been dried and cracked due to volcanic heating. Immediately after emplacement, the buffer will be subjected to a period of heating (maximum 150°C) while awaiting the return of original groundwater levels. These initial stages may cause the buffer to dry and crack, but once the buffer comes in contact with water it will swell and reseal the annulus. During the drying period the nuclear waste will be contained within the canister.

The safeguards of the Canadian containment system comprise several barriers which include the container, sand-clay buffer, backfill, and depth of emplacement. The waste itself is locked in ceramic pellets which are contained in zirconium tubes. The waste distribution within the tube consists of 99% in the pellets and 1% on the inner surface of the cladding. This portion on the cladding is the waste that would be released once the canister corrodes and leaks. The container is designed to be highly insoluble to prevent dissolving of the waste and transportion through

the groundwater. The canister is predicted to have a life of about 500 years and would be composed of titanium or copper. The bundles are placed in carbon steel tubes which are then placed within the canister. The space between bundles is filled with glass beads to provide uniform support. Each canister can hold 72 bundles.

Currently the Underground Research Laboratory at Lac du Bonnet, Manitoba contains experimental rooms at 240 m and 445 m depths, with hydrogeological testing to 1200 m.

It is estimated that 9 billion dollars will be spent on nuclear waste disposal at a typical disposal site over its 70-year life. This represents 1% of the domestic electricity costs. The construction of the facility will employ 1100 people during the 10-year construction period and 600 people during the 40-year waste emplacement period. The vault will be monitored inside and out. Transportation of the waste will be performed with heavy metal casks. Currently, two interim assessments have been made in 1981 and 1985 and presented to regulatory and environmental agencies.

7.0 Discussion

It should be remembered that human beings are fallible creatures, and it follows that their creations are also fallible. Therefore, regardless of the number of redundant safety precautions, human error can still present a risk to the operation of a nuclear reactor and the waste disposal system.

The Nuclear Regulatory Commission (NRC) is the federal agency in the United States that ensures public safety with regard to nuclear energy. Dr. Stephen Hanauer, a

senior official of the NRC, kept a private file of safety problems that came to his attention. This file is called the "Nugget File" and was compiled over a 10 year period from 1966 to 1976 [28]. The file became available to the public under the Freedom of Information Act and shows a variety of "small" accidents that were mainly caused by human error. A few examples are presented below.

-Welding outfit left inside reactor vessel.
-The movement of the control rods was opposite to the switch indicator.
-Hose from a well tap was connected to a radioactive waste tank resulting in contaminated drinking water.
-A tested circuit breaker which should trip open and allow the control rods to be lowered would not function.
-Release of radioactive laundry water due to open valve in transfer line.
-Pressure controlled vent valves open to the atmosphere.
-An emergency core cooling pump would not start because the fuses had been left out.
-Electronics that were considered to have a high reliability failed due to poorly soldered printed circuit boards.
-Incorrectly wired control panel would not allow lowering of control rods.
-Failure of power distribution panel due to water infiltration caused by plugged roof drain.
-Electrical relays inoperable because they were painted.

These incidents did not result in catastrophic failure of the nuclear plants but an accumulation of "small" events could lead to a major disaster. It is important that the regulating bodies enforce the rules on safe plant operation.

8.0 Conclusions

The disposal progam for radioactive nuclear wastes must kept open to public scrutiny, and have environmental safety as the main priority. Interim storage of these wastes cannot be performed indefinitely because there are too many uncertainties regarding the ability of society to maintain these facilities into the future.

Permanent deep disposal of radioactive waste in a geological formation is the preferred option. Deep burial would provide the required isolation with the least risk to public safety.

Further research must be undertaken to determine the characteristics of radionuclide transport from below the ground surface. Specific research must establish the effects more soluble radionuclides such as iodine-129 and technetium-99 have on the environment, and the mobility of these radionuclides through the groundwater.

REFERENCES

[1] Blasewitz, A.G., Davis, J.M., and Smith, M.R. The treatment and handling of radioactive wastes. American nuclear society topical meeting, Richland, Washington, April 19-22, 1982.

[2] Brown, T.L., LeMay, Jr., H.E. Chemistry: The central science. Prentice Hall Inc., Englewood Cliffs, New Jersey, 2nd edition, 1981.

[3] Environment Canada. Ocean dumping control act. Annual report, 1987-88.

[4] Harwell, M.A., Hutchinson, T.C. Environmental consequences of nuclear war, scope 28, physical and atmospheric effects. Vol. 1 and 2, 2nd ed. John Wiley and Sons, Great Britain, 1989.

[5] Lafleur, C.W. Hydrogeological factors to be addressed in disposal guide. Atomic Energy Control Board, December, 1986.

[6] Lutze, Werner, editor. Scientific basis for nuclear waste management V. Proceedings of the materials research society on the scientific basis for nuclear waste management, Volume 11, Berlin, Germany, June 7-10, 1982.

[7] Kennedy, C.C. Atomic energy in Canada. Atomic Energy of Canada Limited, Chalk River, Ontario, 1956.

[8] Manitoba Hydro. Nuclear generating station site selection program, report no. 2, candidate selection. June, 1977.

[9] Manitoba Hydro. Nuclear generation station site selection program, report no. 3, preferred site selection, 3 vols. March, 1978.

[10] Nelkin, D. Nuclear power and its critics: The Cayuga Lake controversey. Cornell University Press, New York, 1971.

[11] Pollard, R.D., ed. The nugget file. Union of Concerned Scientists, Cambridge, Massachusetts, 1979.

[12] Sheppard, S.C. Review of effect of soil on radionuclide uptake by plants. Atomic Energy Control Board, March, 1987.

[13] Shemilt, L.W., chairman. Technical advisory committee on the nuclear fuel waste management program, ninth annual report. Atomic Energy of Canada Limited, July, 1988.

[14] Wagstaff, K.P. The development of criteria for radioactive waste disposal. Atomic Energy Control Board, February, 1985.

[15] Wieser, Anne, editor. Challenges to nuclear waste. Proceedings of the nuclear waste issues conference, Winnipeg, Manitoba, Canada, September 1214, 1986.

[16] Whicker, F.W., and Schultz, V. Radioecology: Nuclear energy and the environment. CRC Press Inc., Vol. 1, 1982.

[17] Hinga, K.R., Heath, G.R., Anderson, D.R., and Hollister, C.D. Disposal of high-level radioactive wastes by burial in the sea floor. Environmental Science and Technology, Vol. 16, No. 1, 1982.

[18] Varley, J. Handling low and medium active waste in East Germany. Nuclear Engineering International, September, 1990.

[19] Riccardi, N., and Ravera, O. Unionidae (molluscs, lamellibranchiata) used as an environmental indicator for radioactive contamination from the Chernobyl accident. Environmental Technology Letters, Vol. 10, pp. 347-353, 1989.

[20] Hileman, B. EPA's rules on radiation. Environmental Science and Technology, Vol. 17, No. 12, 1983.

[21] Jackson, R.E., and Inch, K.J. Partitioning of strontium-90 among aqueous and mineral species in a contaminated aquifer. Environmental Science and Technology, Vol. 17, No. 4, 1983.

[22] Holloway, R.W., and Hayes, D.W. Mean residence time of plutonium in the troposphere. Environmental Science and Technology, Vol. 16, No. 2, 1982.

[23] Oblath, S.B. Leaching from solidified waste forms under saturated and unsaturated conditions. Environmental Science and Technology, Vol. 23, No. 9, 1989.

[24] Penrose, W.R., Polzer, W.L., Essington, E.H., Nelson, D.,M., and Orlandini, K.A. Mobility of plutonium and americium through a shallow aquifer in a semiarid region. Environmental Science and Technology, Vol. 24, No. 2, 1990.

[25] Hileman, B. Nuclear waste disposal. Environmental Science and Technology, Vol. 16, No. 5, 1982.

[26] Smith, R.A., Nyman, D.H., and Anderson, B.N. Getting ready to build the Hanford waste vitrification plant. Nuclear Engineering International, March 1990.

[27] Bradbury, D. Helping to reduce effluent generation. Nuclear Engineering International, September 1989.

[28] Monckton, N. Ensuring the safety of deep repositories. Nuclear Engineering International, February 1989.

[29] Cooper, J.R., McColl, N.P., and Hill, M.D. The radiological impact of the UK nuclear fuel cycle. Nuclear Engineering, Vol. 27, No. 6, pp. 377-384, December 1988.

[30] Aikin, A.M., Harrison, J.M., and Hare, F.K. (chairman). The management of Canada's nuclear wastes. Energy, Mines and Resources Canada, Report EP77-6, 1977.

[31] Cruickshank, A. France pushes ahead with new repositories. Nuclear Engineering International, February 1990.

[32] Atomic Energy of Canada Limited. Managing Canada's nuclear fuel waste. May 1989.

[33] Cameron, D.J. Fuel isolation research for the Canadian nuclear fuel waste management program. Atomic Energy of Canada Limited, AECL-6834, June 1982.

[34] Acres Consulting Services Ltd. A disposal centre for irradiated nuclear fuel: Conceptual design study. Atomic Energy of Canada Limited, AECL-6415, September 1980.

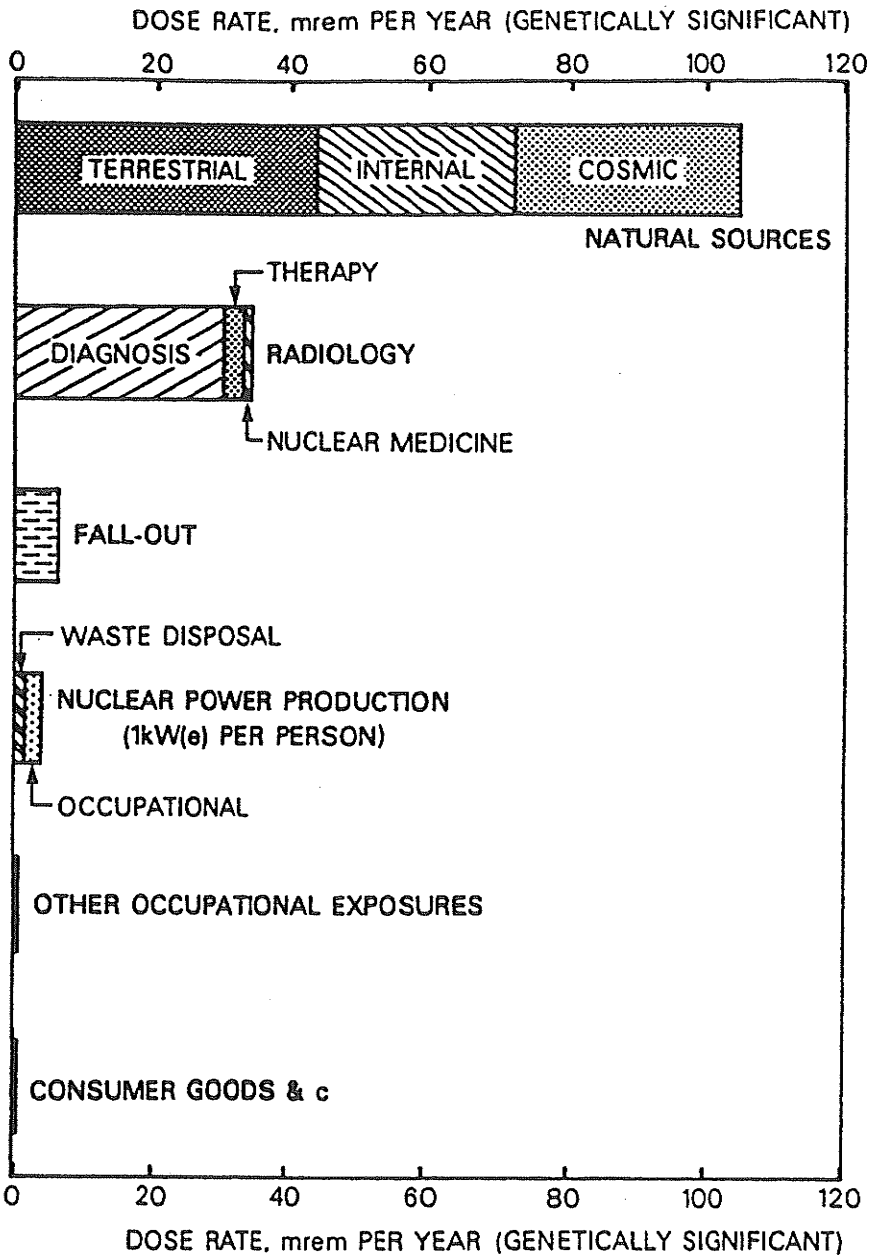

Fig. 1 Dose rate averaged throughout entire Canadian population (Aikin, Harrison, and Hare, 1977).

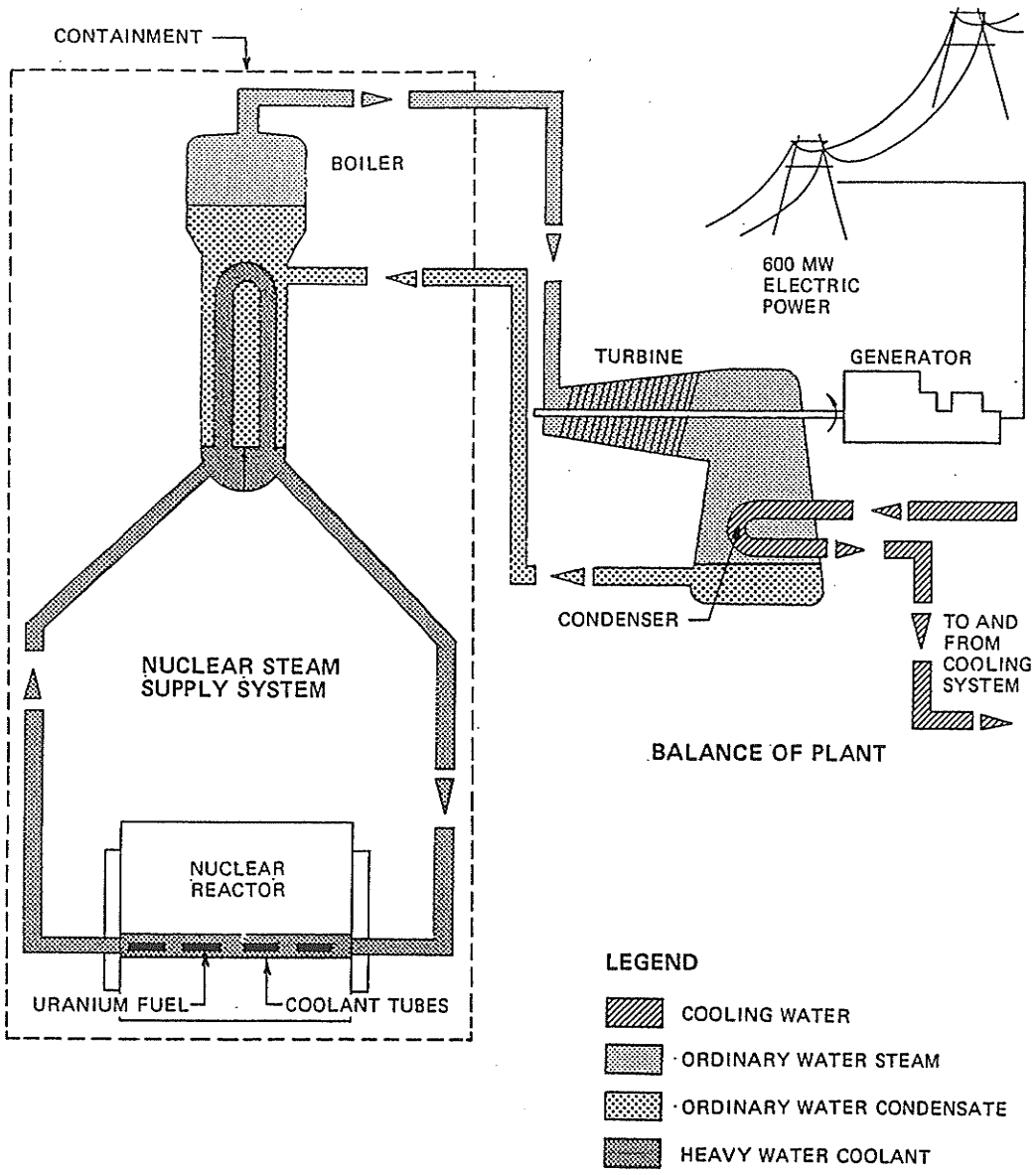

Fig. 2 Basic components of a CANDU nuclear generating station (Manitoba Hydro, 1978).

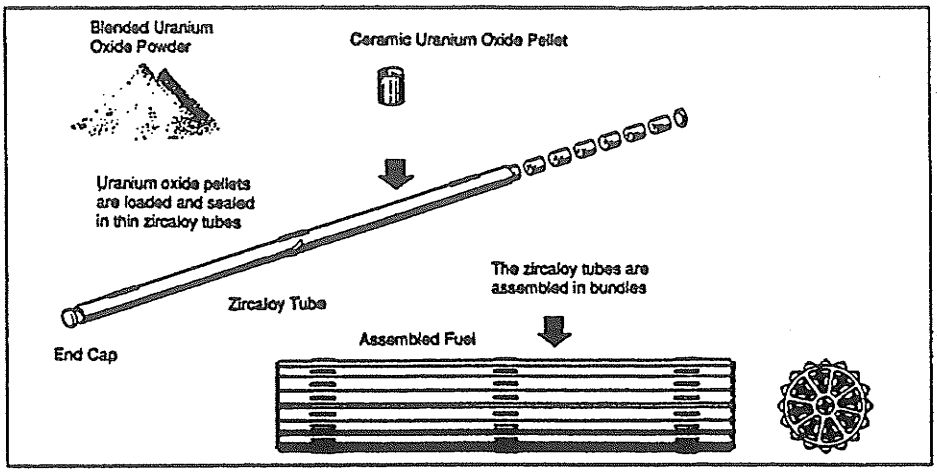

Fig. 3 Construction of fuel bundles for the CANDU nuclear reactor (AECL, 1989).

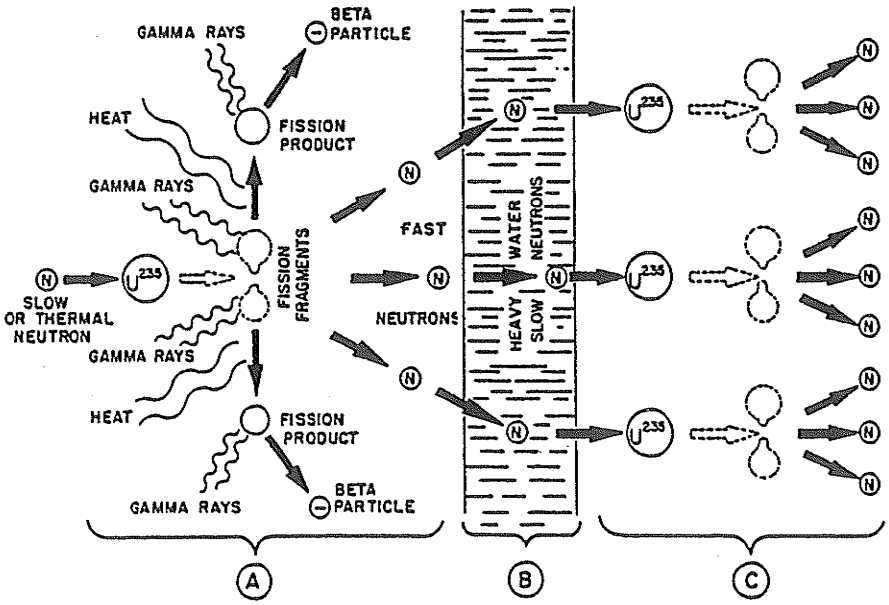

Fig. 4 Schematic representation of a nuclear chain reaction and the moderating of neutrons (Kennedy, 1956).

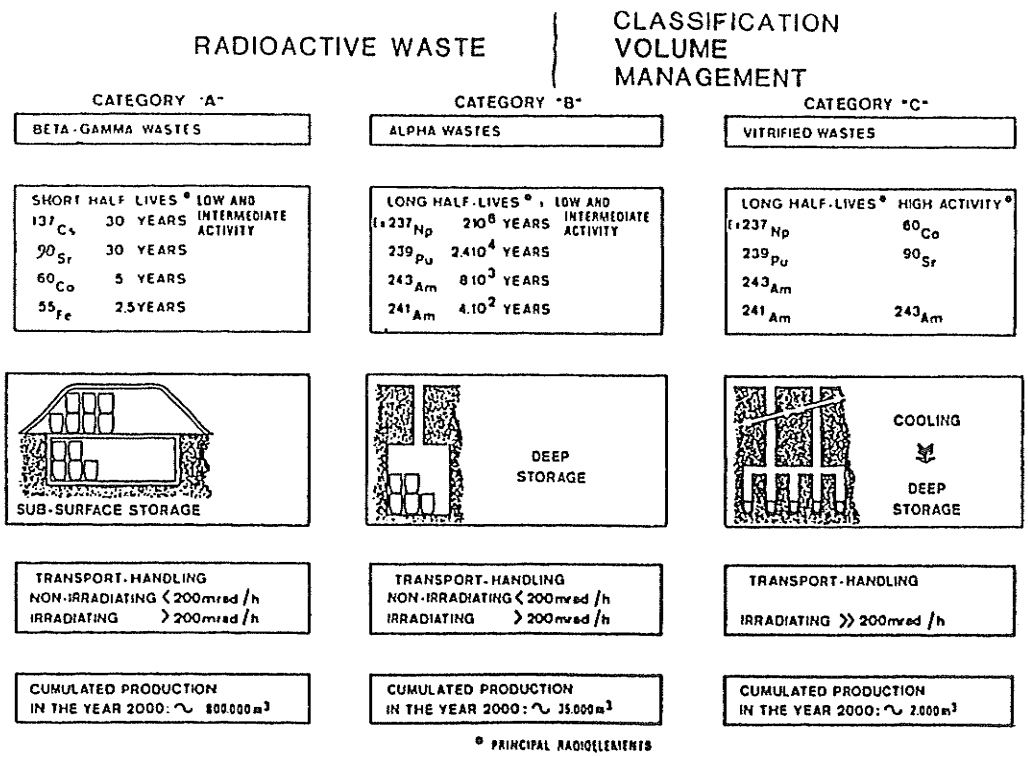

Fig. 5 The classification, volume, and management of radioactive wastes in France (Blasewitz et al., 1982).

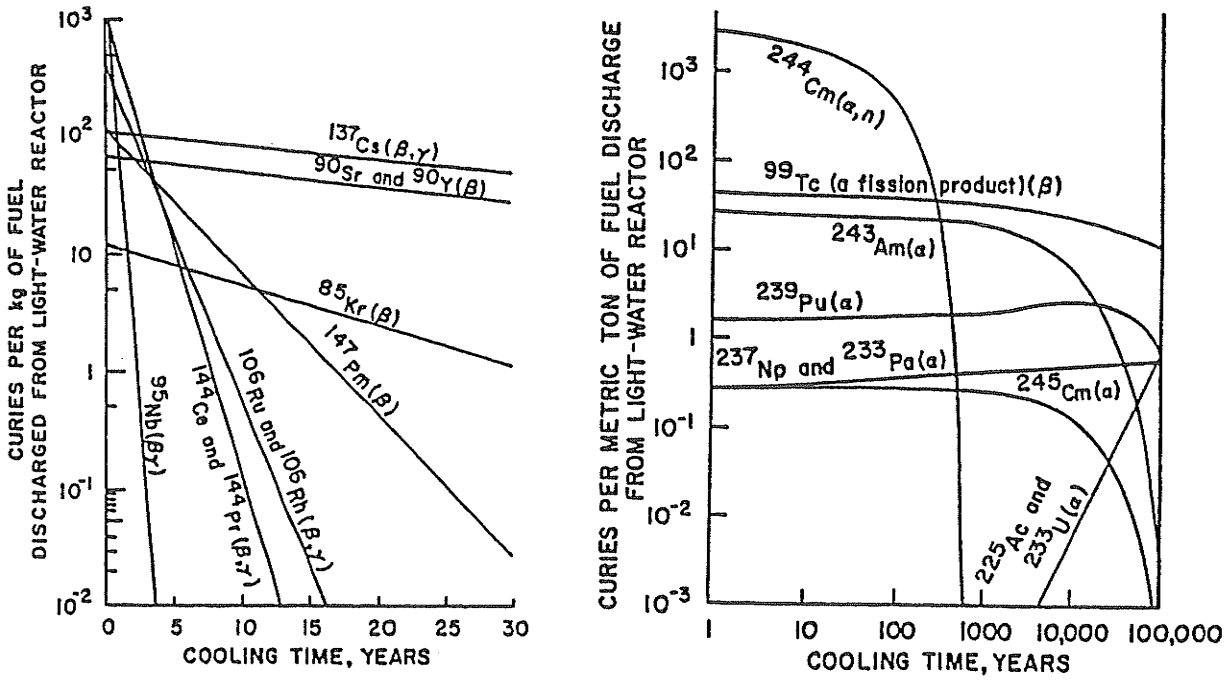

Fig. 6 The change in isotopic activity of fission products with time from a light water reactor (National Academy of Sciences, 1975).

Table 3.1: Diffusion Test Results

LATEX MEMBRANE

Stage	p' (MPa)	Cell Temperature (°C)	Volumetric Strain Rate (%/Day)	Room Temp. Change (°C/Day)
1	0.6	23	-0.0128	-0.42
2	0.6	26	-0.0184	-0.26
3	1.5	26	-0.0191	-0.41
4	3.0	26	-0.0051	0.20
5	6.0	26	0.0003	0.04
6	9.0	26	0.0047	0.08

SILICONE MEMBRANE

Stage	p' (MPa)	Cell Temperature (°C)	Volumetric Strain Rate (%/Day)
1	0.6	26	0.0336
2	1.5	26	0.1094
3	3.0	26	0.1213
4	6.0	26	0.1472
5	9.0	26	0.1473
6	0.6	65	0.0843
7	1.5	65	0.2015
8	3.0	65	0.2752
9	0.6	100	0.0504
10	1.5	100	0.3024
11	3.0	100	0.4389
12	0.6	26	0.0479

Note: For both tests V_o = 200 ml and u_b = 1.0 MPa.

Table 4.1: Results of Atterberg Limit Tests on Sodium Bentonite Clay

Year	Researcher	Liquid Limit (%)	Plastic Limit (%)	Plasticity Index (%)
1989	Oswell	228	N/A	N/A
1990	Lingnau	222	36	186
1992†	Yarechewski	236	40	196
1992‡	Yarechewski	208	40	168

Notes: † Not dried prior to testing.

‡ Oven-dried prior to testing.

Table 4.2: Recompaction Measurements for Final Lift

Compression	Compacted Height (mm)	Rebounded Height (mm)
1	100.00	100.57
2	99.72	100.29
3	99.58	100.14
4	99.56	100.00

Table 4.3: Layer Height Variation

Layer	Initial Target Heights (mm)	Actual Heights (mm)	Inverted Target Heights (mm)	Final Actual Heights (mm)
1	20.00	20.34	19.78	20.15
2	20.00	20.25	19.92	20.10
3	20.00	20.18	20.03	20.11
4	20.00	20.08	20.09	20.11
5	20.00	19.94	20.18	20.01
Sum:	100.00	100.79	100.00	

Table 4.4: Dry Density Variation using Equal and Varied Target Heights

Layer	Dry Density (Mg/m^3)	
	Equal Target Heights	Varied Target Heights
1	1.632	1.677
2	1.645	1.672
3	1.652	1.679
4	1.650	1.674
5	1.682	1.682
Average:	1.652	1.677
Standard Deviation:	0.016	0.003

Table 5.1: Test Conditions at Constant Mean Effective Stress

Test Number	Mean Effective Stress p' (MPa)	Specimen Temperature (°C)	Duration (Days)
T1301†	1.5	27	71
T1302†	1.5	65	34
T1303	0.6	26	55
T1304	0.6	65	57
T1305‡	0.6	100	21
T1306	0.6	100	28
T1307	1.5	65	19
T1308	3.0	100	24
T1309	1.5	100	19
T1310	3.0	65	15

Notes: † Sheared at p' = 1.7 MPa

‡ Consolidation only

All tests conducted with a back pressure of 1 MPa. Specimens T1303 and T1307 were also consolidated and sheared with a back pressure of 7 MPa.

Table 5.2: Initial Specimen Conditions

Test Number	Water Content (%)	Bulk Density (Mg/m^3)	Dry Density (Mg/m^3)	Clay Specific Volume V_c	Saturation (%)
T1301	22.6	2.036	1.661	2.24	97.6
T1302	22.7	2.040	1.663	2.25	98.2
T1303	22.8	2.032	1.654	2.26	97.5
T1304	22.6	2.036	1.660	2.24	97.5
T1305	22.7	2.035	1.658	2.25	97.7
T1306	22.6	2.037	1.661	2.25	97.7
T1307	22.7	2.033	1.657	2.25	97.4
T1308	22.7	2.034	1.658	2.25	97.4
T1309	22.8	2.043	1.664	2.25	98.8
T1310	22.4	2.032	1.660	2.23	96.6
Average	22.7	2.036	1.660	2.25	97.6
Standard Deviation	0.1	0.003	0.003	0.01	0.5

Table 5.3: Specimen Water Contents

Test Number	Water Content (%)					
	Measured			Calculated		
	Initial	Final Internal	Final External	Initial	Final	Difference
T1301	22.6	24.1	23.4	25.6	21.2	2.9
T1302	22.7	22.5	21.6	——	——	——
T1303	22.8	25.7	25.1	22.6	26.0	0.3
T1304	22.6	26.0	25.2	21.0	27.6	1.6
T1305	22.7	24.4	23.9	20.3	26.8	2.4
T1306	22.6	24.5	24.2	19.3	27.9	3.4
T1307	22.7	27.7	25.4	27.5	22.9	4.8
T1308	22.7	19.6	18.8	20.5	21.7	2.2
T1309	22.8	21.6	21.2	20.6	23.8	2.2
T1310	22.4	21.1	21.3	24.0	19.5	1.6

Table 5.4: Consolidation Results

Test Number	Consolidation					
	26°C Temperature			65°C or 100°C Temperature		
	Volumetric Strain (%)	Lateral Strain (%)	Duration (Days)	Volumetric Strain (%)	Lateral Strain (%)	Duration (Days)
T1301	+1.0	+0.1	31	——	——	—
T1302	+0.3	+0.2	1	——	+0.9	12
T1303	-4.1	+1.6	25	——	——	—
T1304	-2.8	+0.1	11	-2.8	-2.6	10
T1305	-1.9	+0.1	14	-4.9	-0.9	7
T1306	-2.7	+0.8	10	-1.5	——	6
T1307	0.0	+0.2	4	+0.4	-0.3	2
T1308	+1.3	+0.3	6	+1.0	——	5
T1309	0.0	+0.2	4	+0.6	-3.0	2
T1310	+1.2	+0.3	4	+1.8	-1.1	7

Table 5.5: Shear Results at Failure

Test Number	Mean Effective Stress p' (MPa)	Specimen Temperature (°C)	Volumetric Strain (%)	Lateral Strain (%)	Axial Strain (%)	Maximum Deviator Stress q_{max} (MPa)
T1301	1.7	27	+0.8	-2.7	5.0	1.10
T1302	1.7	65	+0.4	-2.0	3.7	1.28
T1303	0.6	26	-0.9	-3.9	7.8	0.59
T1304	0.6	65	-1.8	-3.5	2.9	0.59
T1306	0.6	100	-3.3	+0.5	1.6	0.68
T1307	1.5	65	0.0	-1.3	2.7	1.10
T1308	3.0	100	0.0	——	5.0	1.53
T1309	1.5	100	-1.6	-2.4	3.1	1.08
T1310	3.0	65	+1.9	——	6.3	1.41

Table 5.6: Shear Moduli and Young's Moduli at $0.5q_{max}$

	Shear Modulus G_{50} (MPa)				Young's Modulus E_{50} (MPa)			
	1-Day		2-Day		1-Day		2-Day	
Test	Sec.	Tan.	Sec.	Tan.	Sec.	Tan.	Sec.	Tan.
T1301	45	34	35	27	145	114	128	85
T1303	58	52	—	—	246	200	—	—
T1304	39	30	29	23	128	100	102	79
T1306	31	28	—	—	155	111	—	—
T1307	51	43	45	33	162	129	115	91
T1308	50	36	33	26	156	118	99	80
T1309	69	56	51	41	257	203	180	147
T1310	76	54	67	48	186	152	157	114

Table 6.1: Equation Constants for Normal Consolidation Lines.

		Temperature								
	Test	26°C			65°C			100°C		
Researcher	Type	N	λ	R^2	N	λ	R^2	N	λ	R^2
Saadat	CIŪ	3.541	0.171	0.95	—	—	—	—	—	—
Lingnau	CIŪ	3.102	0.121	Fit	3.050	0.121	Fit	2.950	0.121	Fit
Yarechewski	CID'	2.981	0.084	Fit	2.818	0.076	Fit	2.778	0.091	Fit

Note: Equation has the form $V_c = N - \lambda \ln p'$ with p' in kPa.

Table 6.2: Equation Constants for Critical State Lines.

		Temperature								
	Test	26°C			65°C			100°C		
Researcher	Type	Γ	λ	R^2	Γ	λ	R^2	Γ	λ	R^2
Saadat	CIŪ	4.363	0.279	0.97	—	—	—	—	—	—
Lingnau	CIŪ	3.102	0.121	Fit	3.020	0.121	Fit	2.930	0.121	Fit
Yarechewski	CID'	3.527	0.160	Fit	3.369	0.153	Fit	3.335	0.160	Fit

Note: Equation has the form $V_c = \Gamma - \lambda \ln p'$ with p' in kPa.

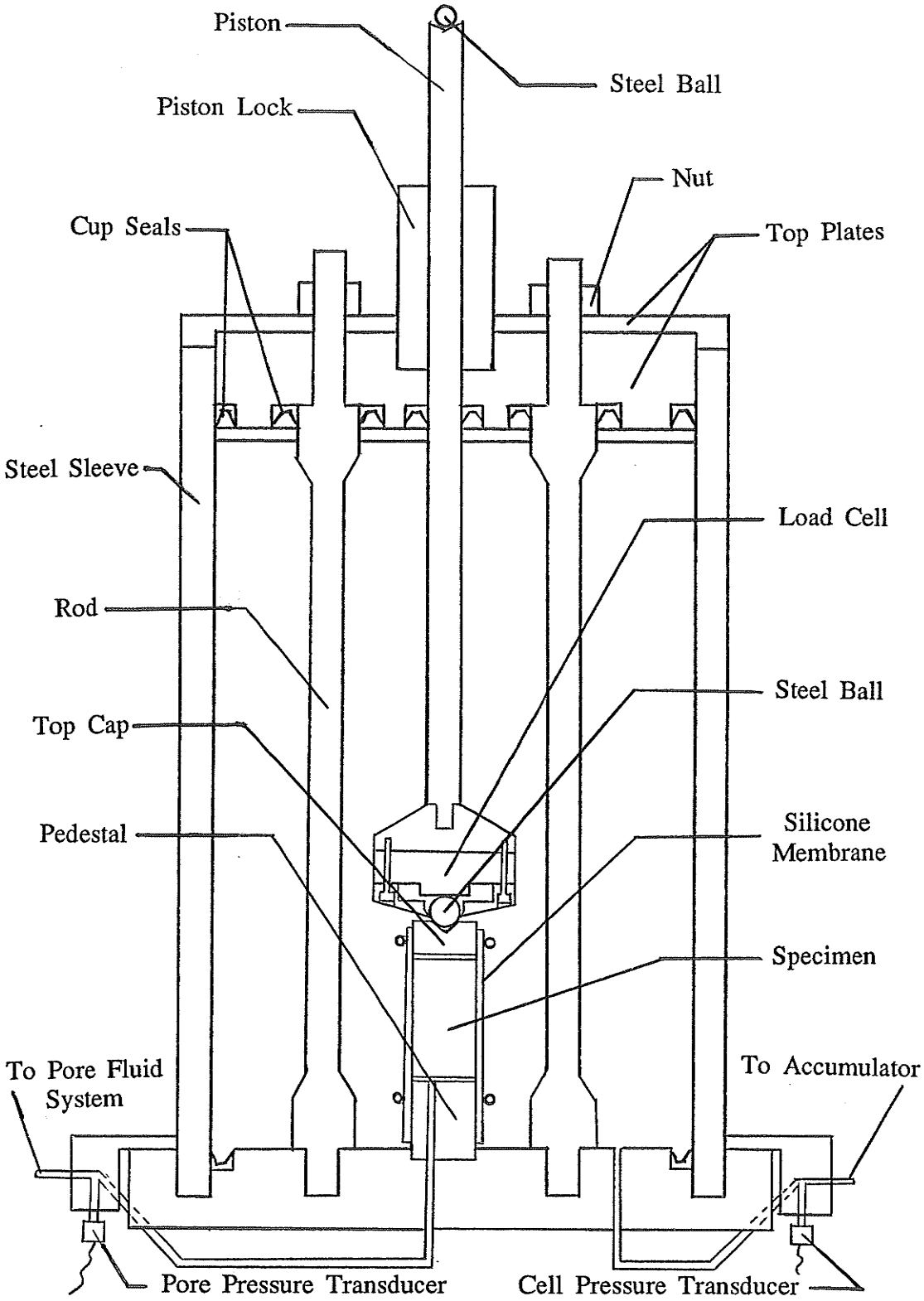

Fig. 3.1 High temperature triaxial cell.

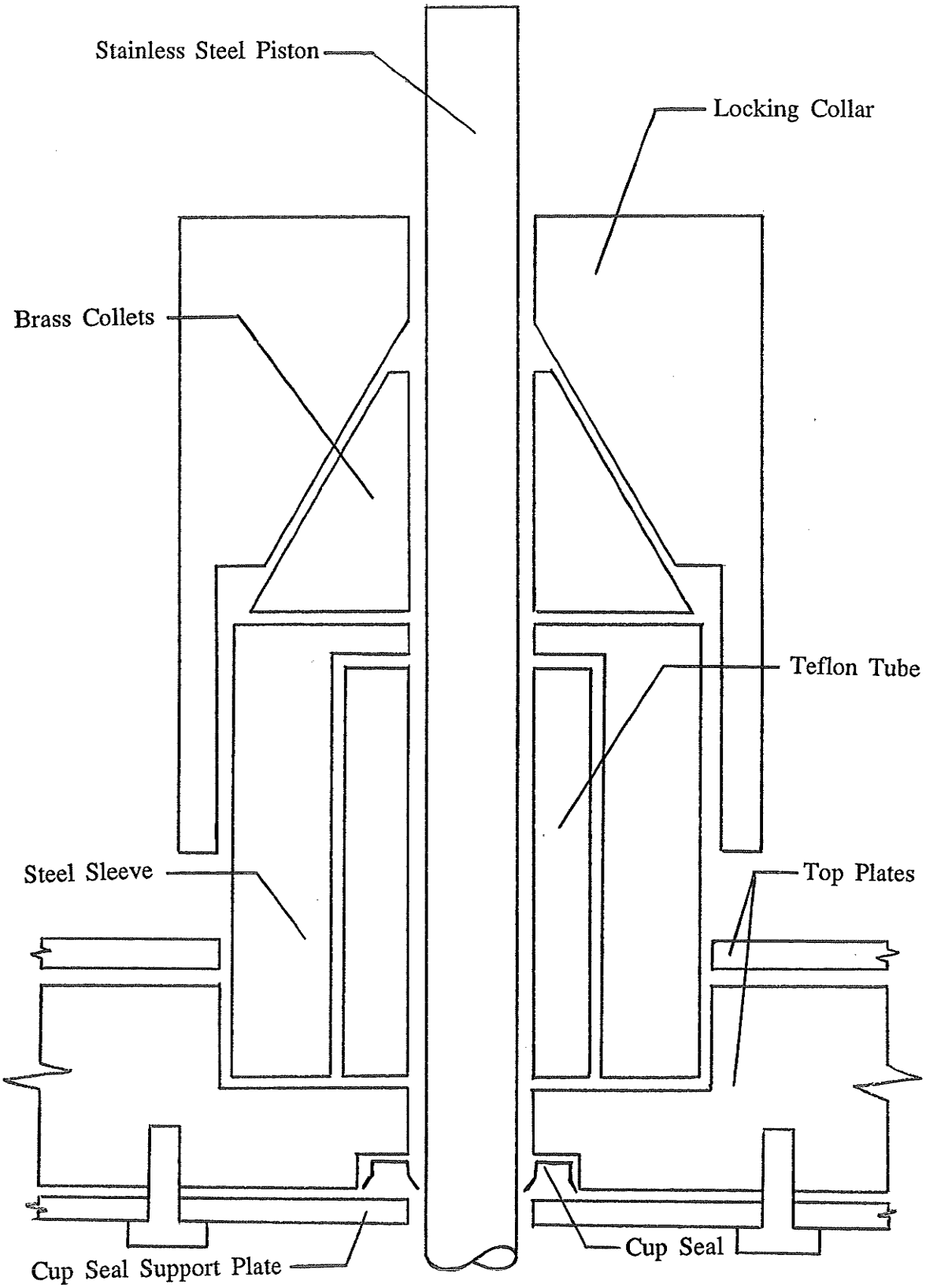

Fig. 3.2 Piston locking mechanism in the head of the triaxial cell.

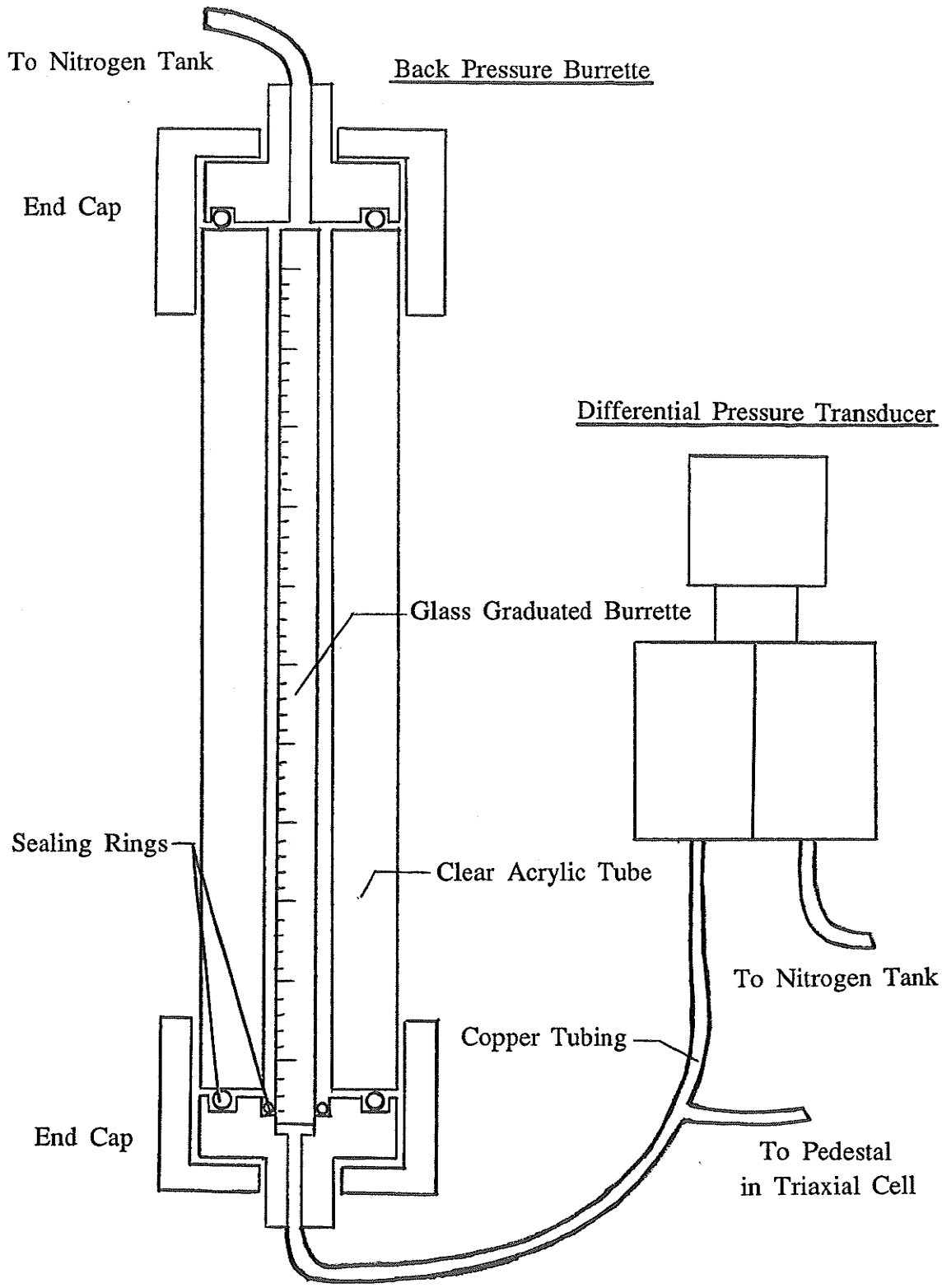

Fig. 3.3 Pore fluid system with Differential Pressure Transducer and Back Pressure Burrette.

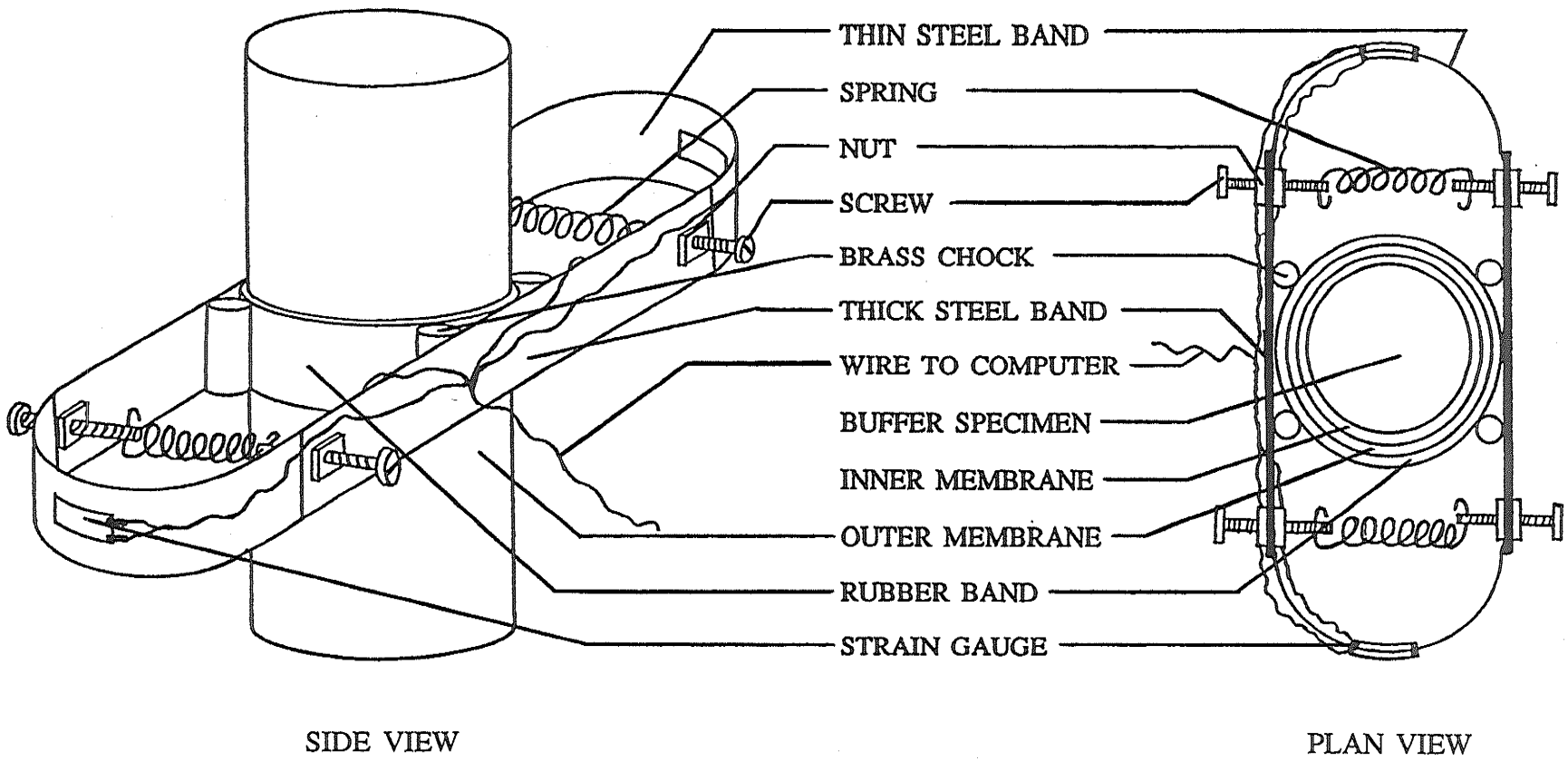

Fig. 3.4 Lateral strain gauge.

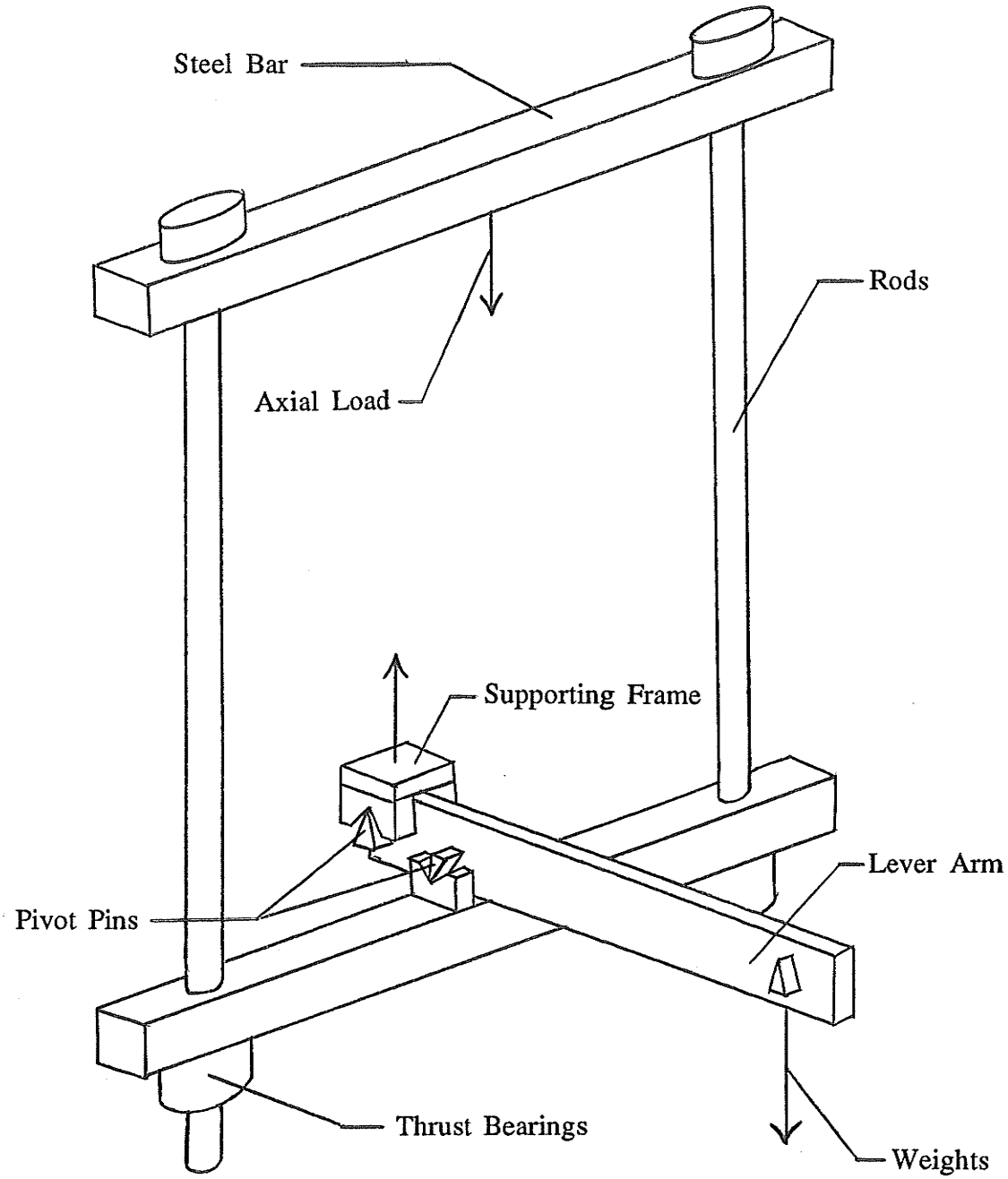

Fig. 3.5 Hanger system for applying axial loads.

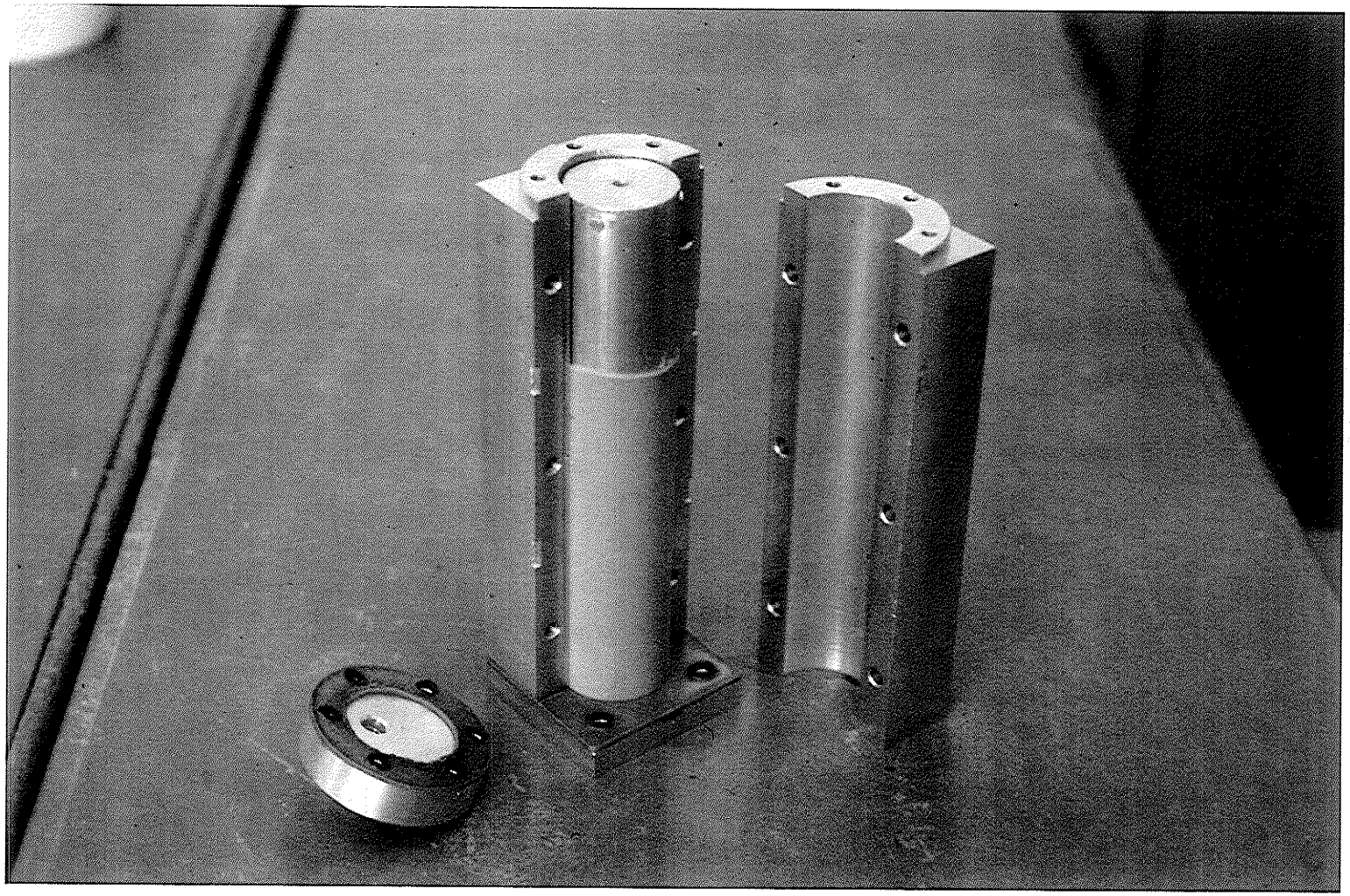

Fig. 3.6 Mould for forming silicone rubber membranes.

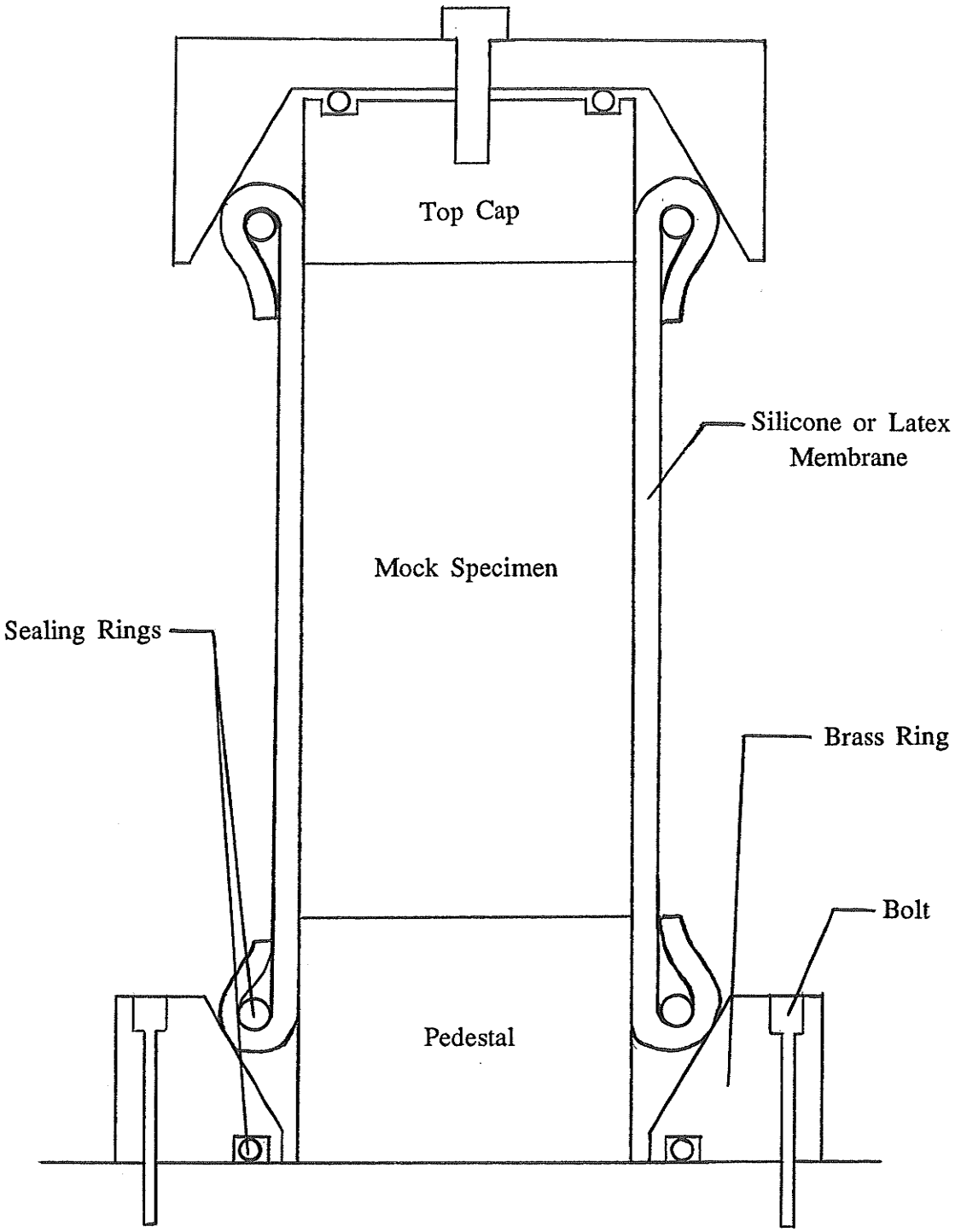

Fig. 3.7 New sealing apparatus employed for membrane leakage tests.

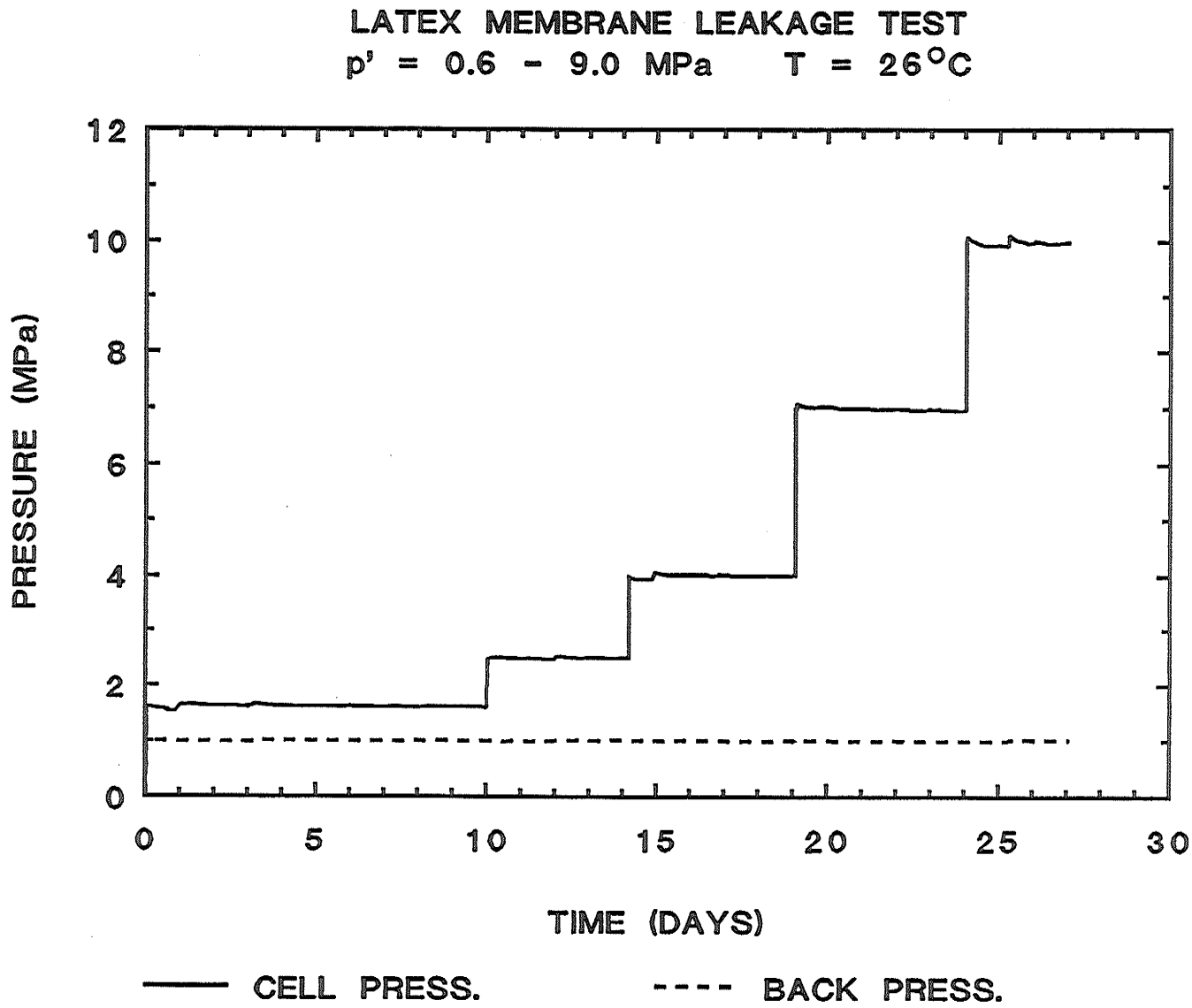

Fig. 3.8 Latex membrane leakage test. Cell and Back Pressure *vs.* Elapsed Time.

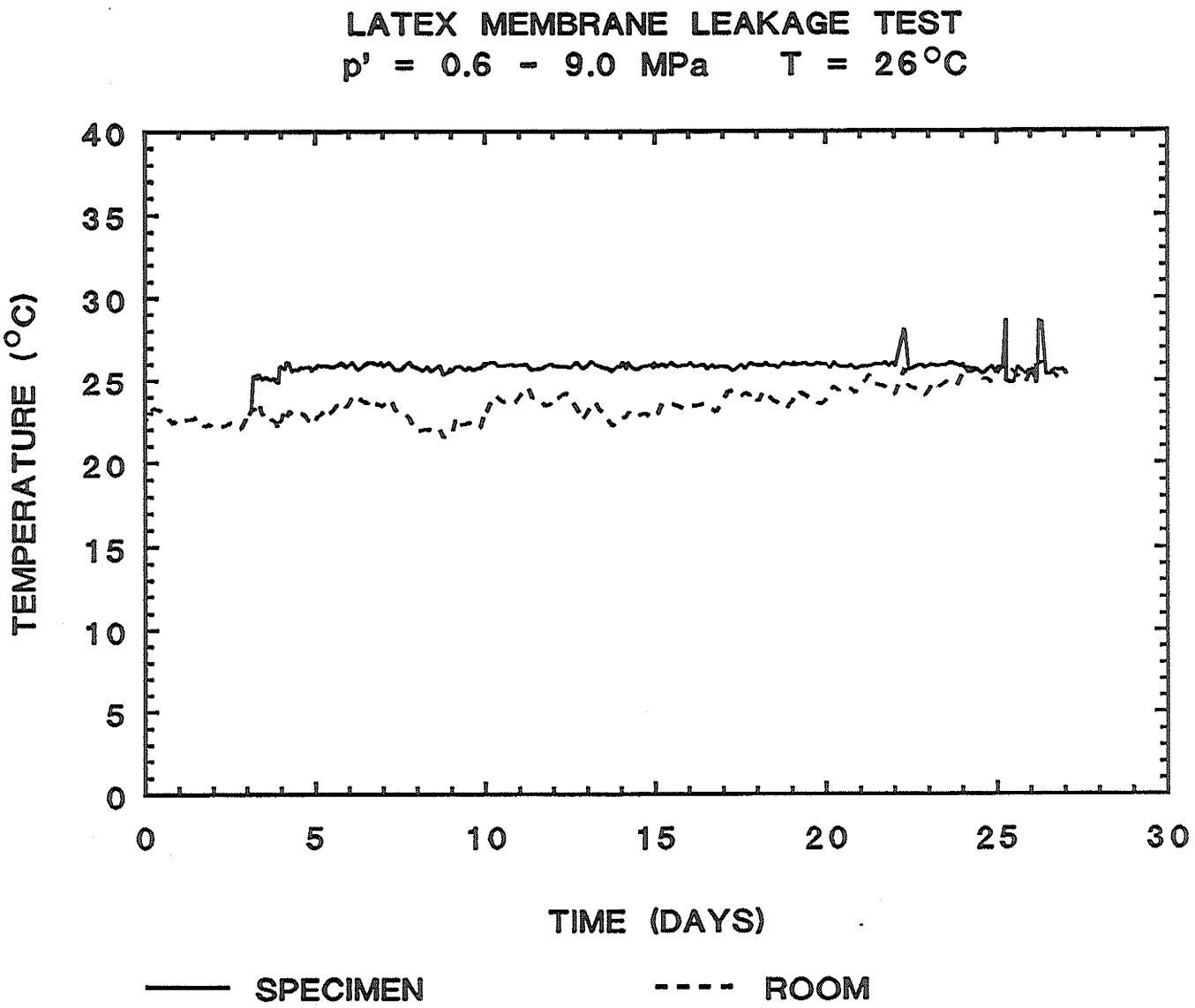

Fig. 3.9 Latex membrane leakage test. Specimen and Room Temperature *vs.* Elapsed Time.

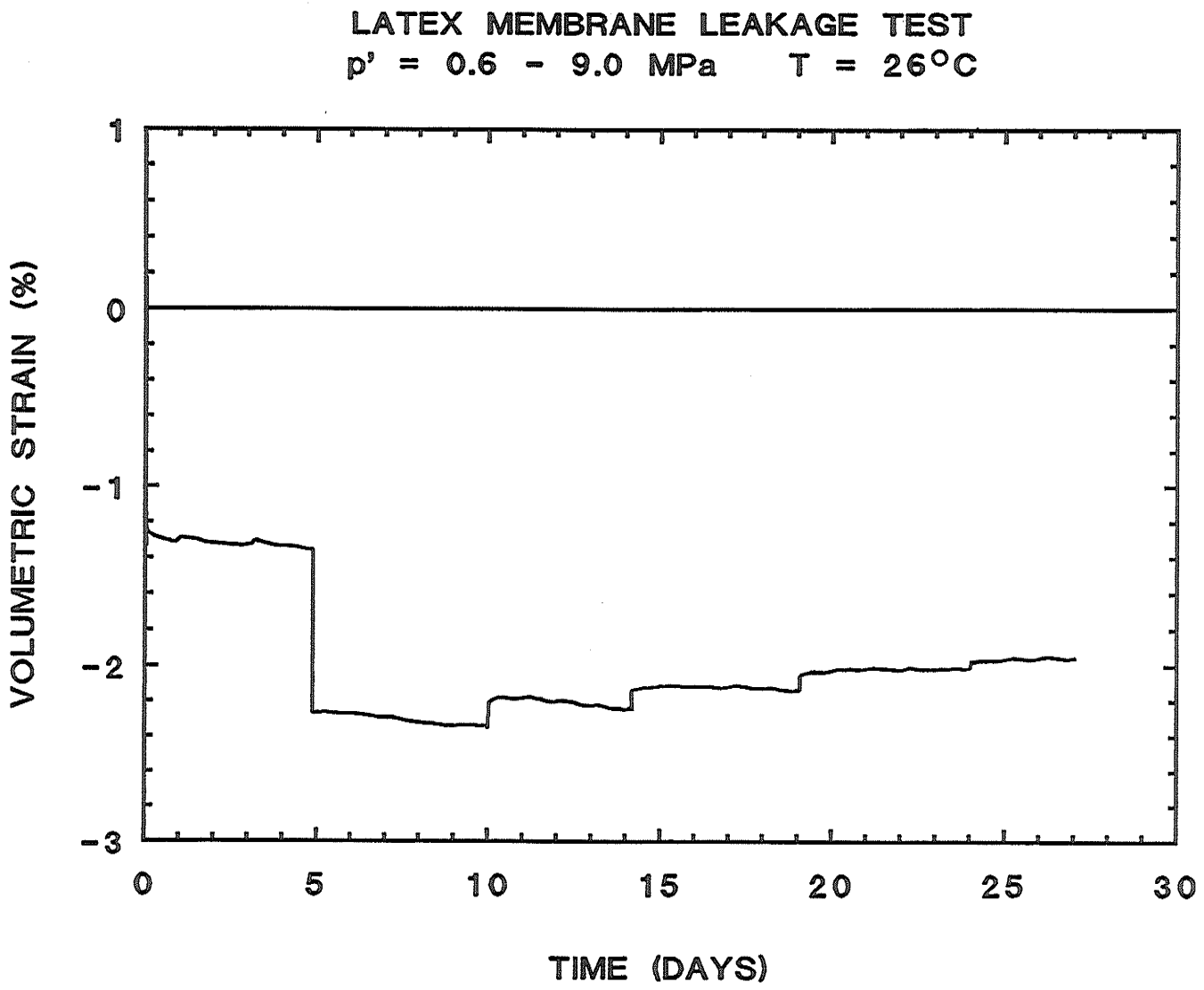

Fig. 3.10 Latex membrane leakage test. Volumetric Strain *vs.* Elapsed Time.

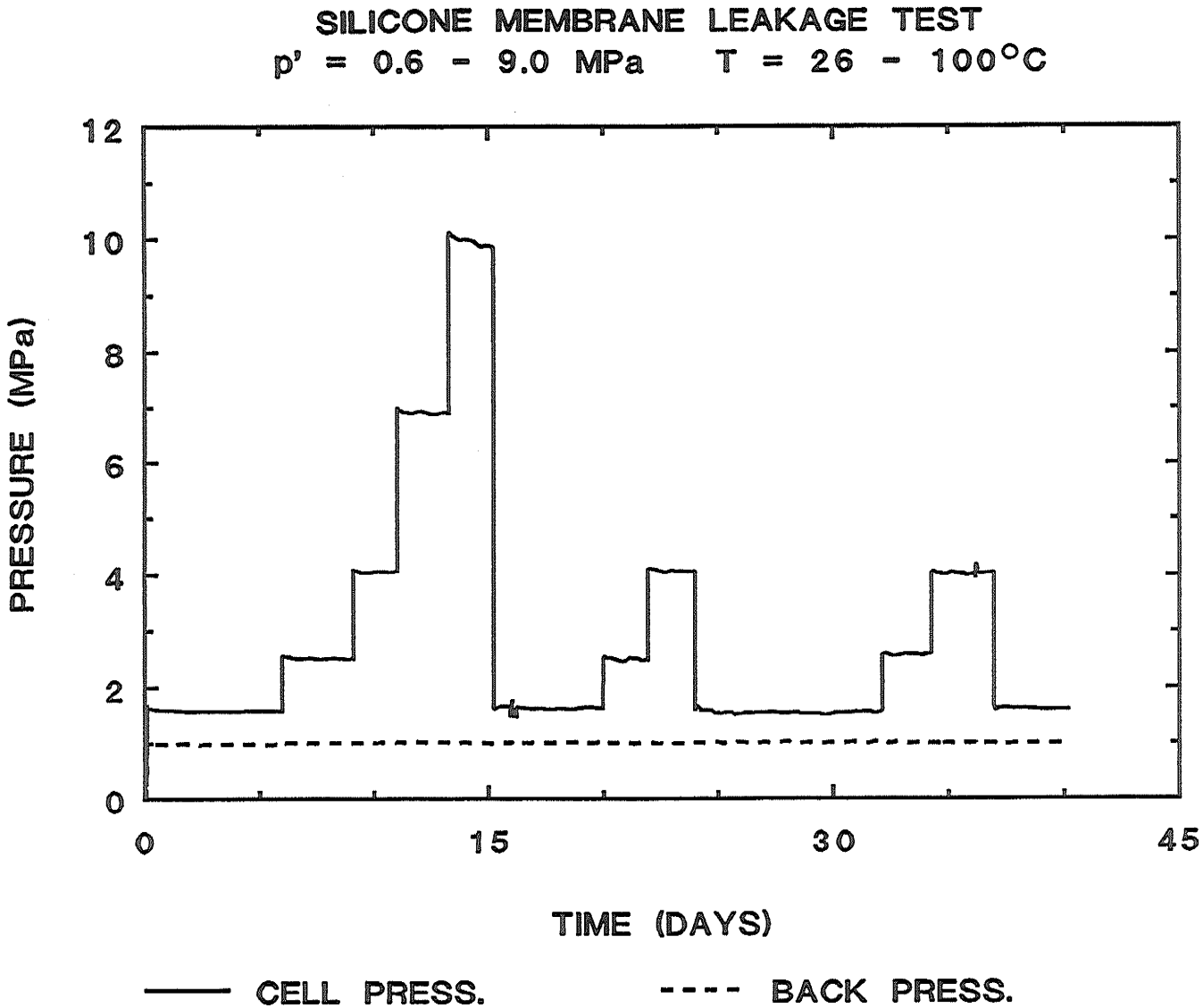

Fig. 3.11 Silicone membrane leakage test. Cell and Back Pressure *vs.* Elapsed Time.

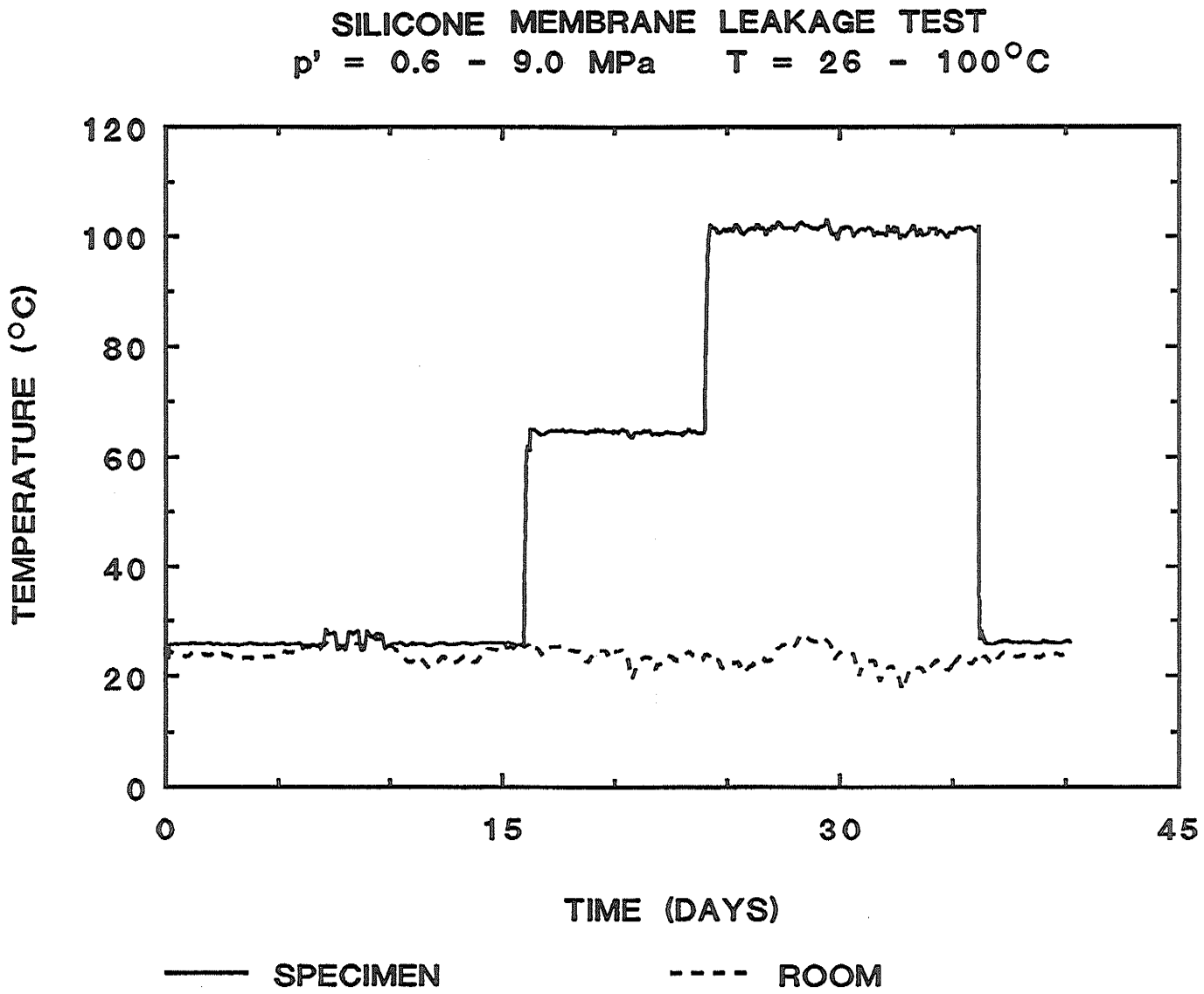

Fig. 3.12 Silicone membrane leakage test. Specimen and Room Temperature *vs.* Time.

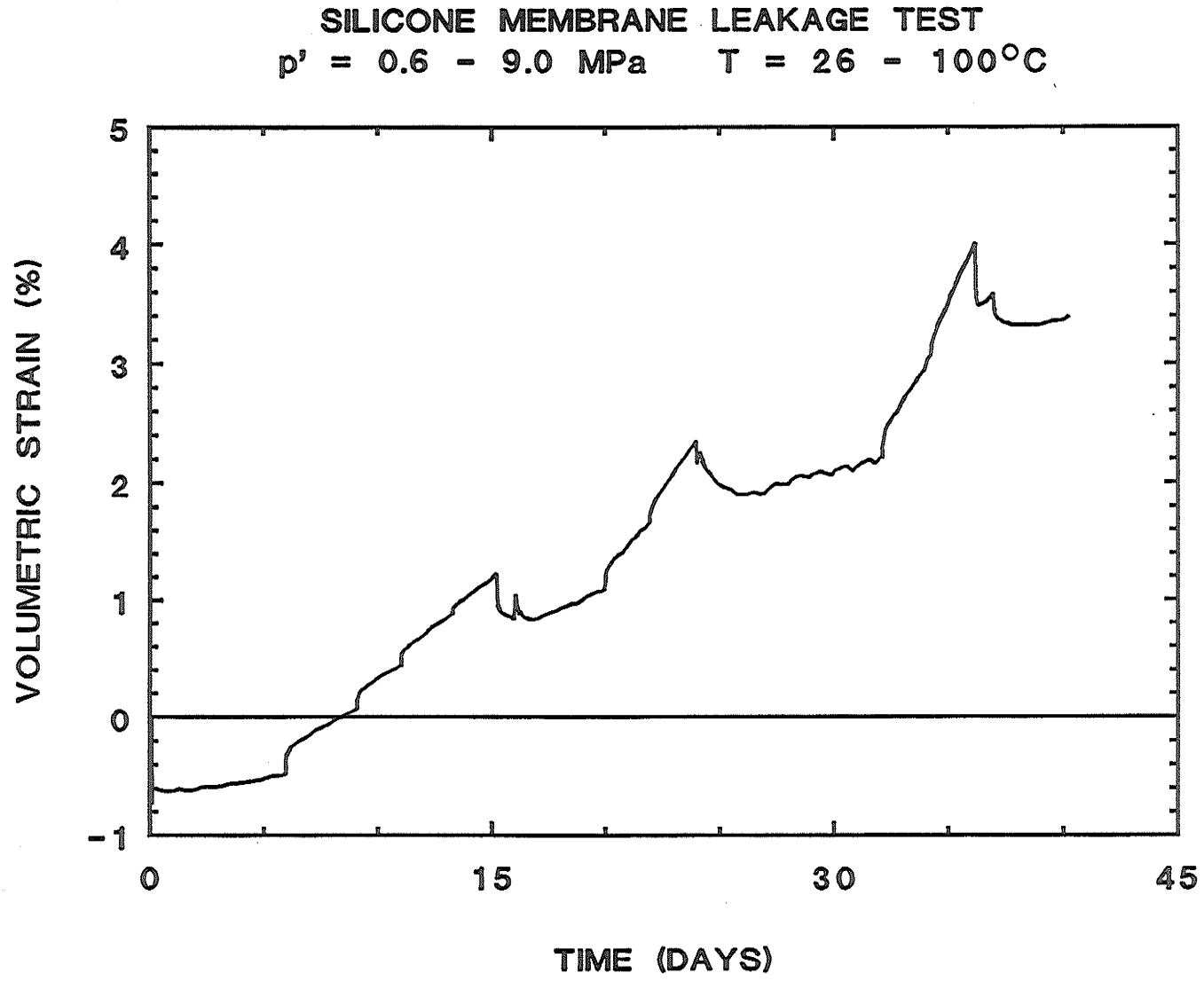

Fig. 3.13 Silicone membrane leakage test. Volumetric Strain *vs.* Elapsed Time.

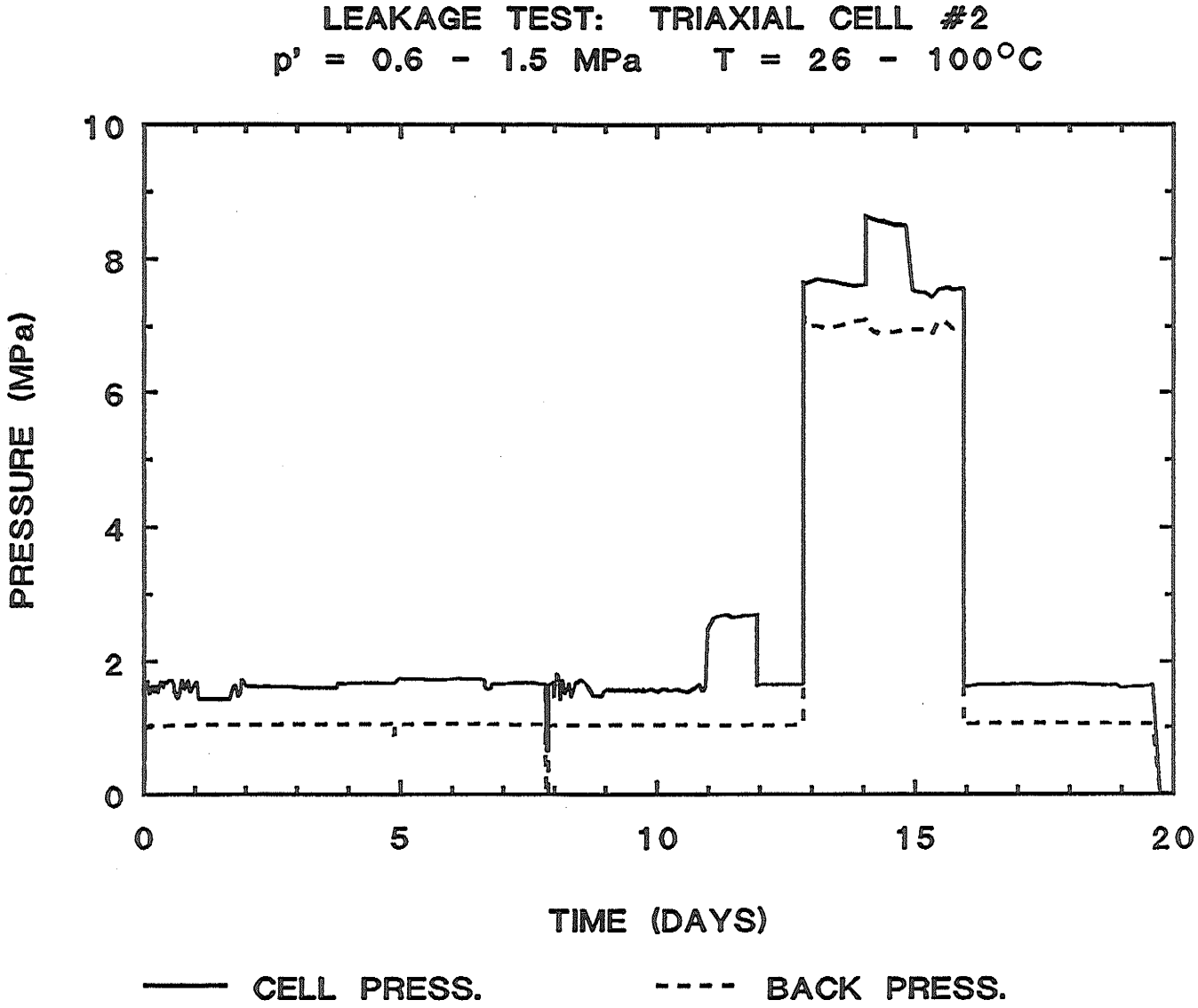

Fig. 3.14 Triaxial Cell #2 Leakage Test. Cell and Back Pressure *vs.* Elapsed Time.

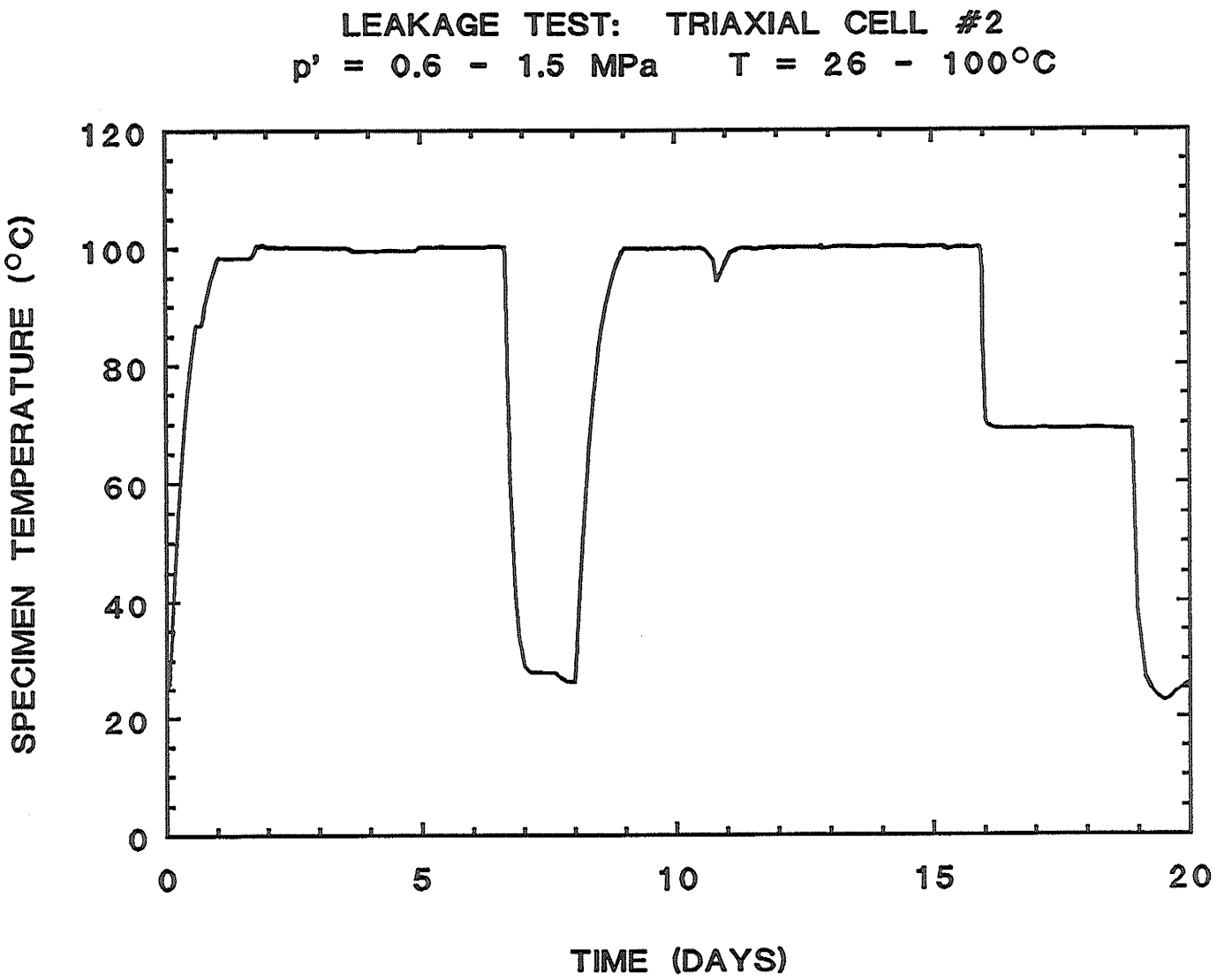

Fig. 3.15 Triaxial Cell #2 Leakage Test. Specimen Temperature *vs.* Elapsed Time.

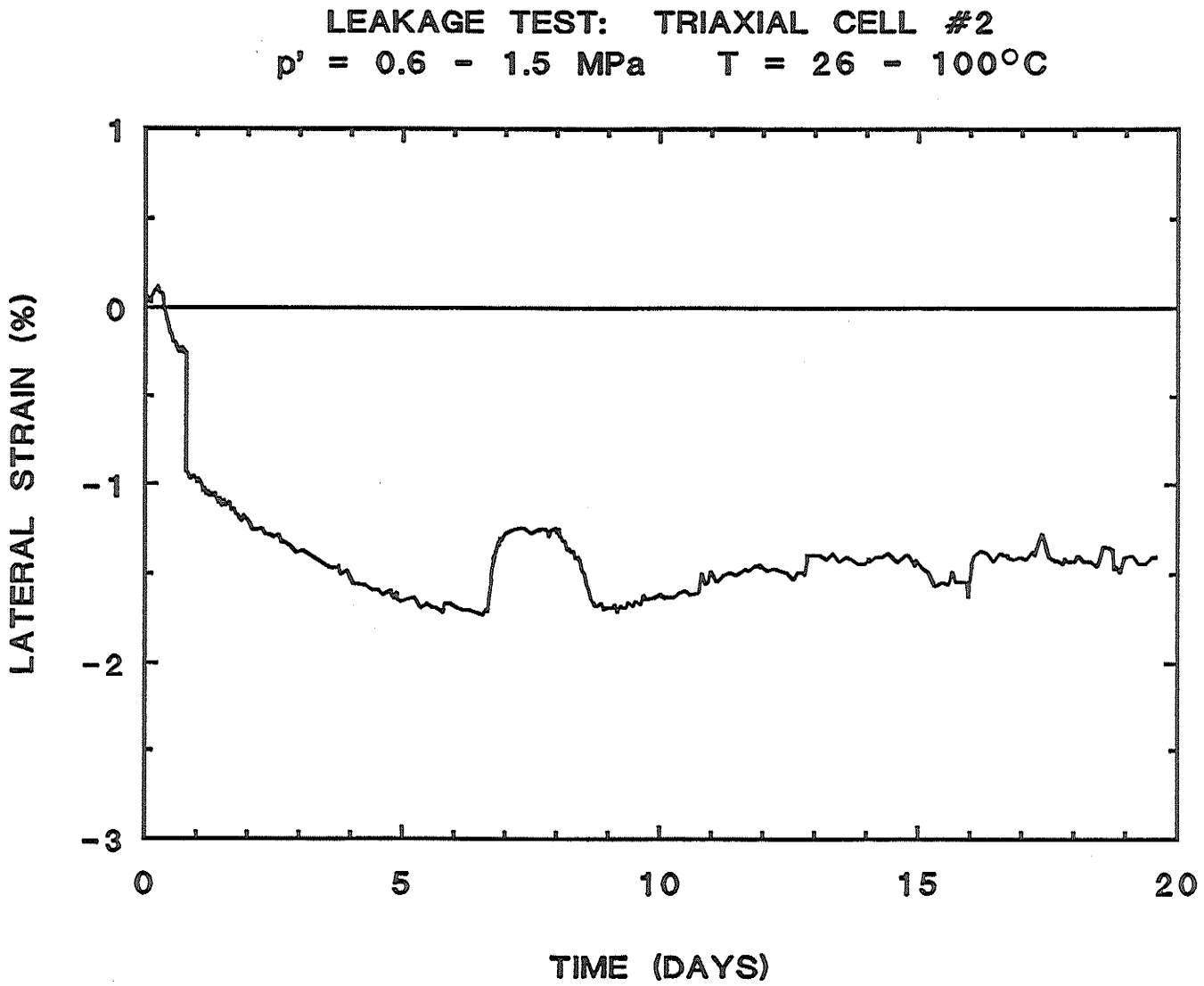

Fig. 3.16 Triaxial Cell #2 Leakage Test. Lateral Strain *vs.* Elapsed Time.

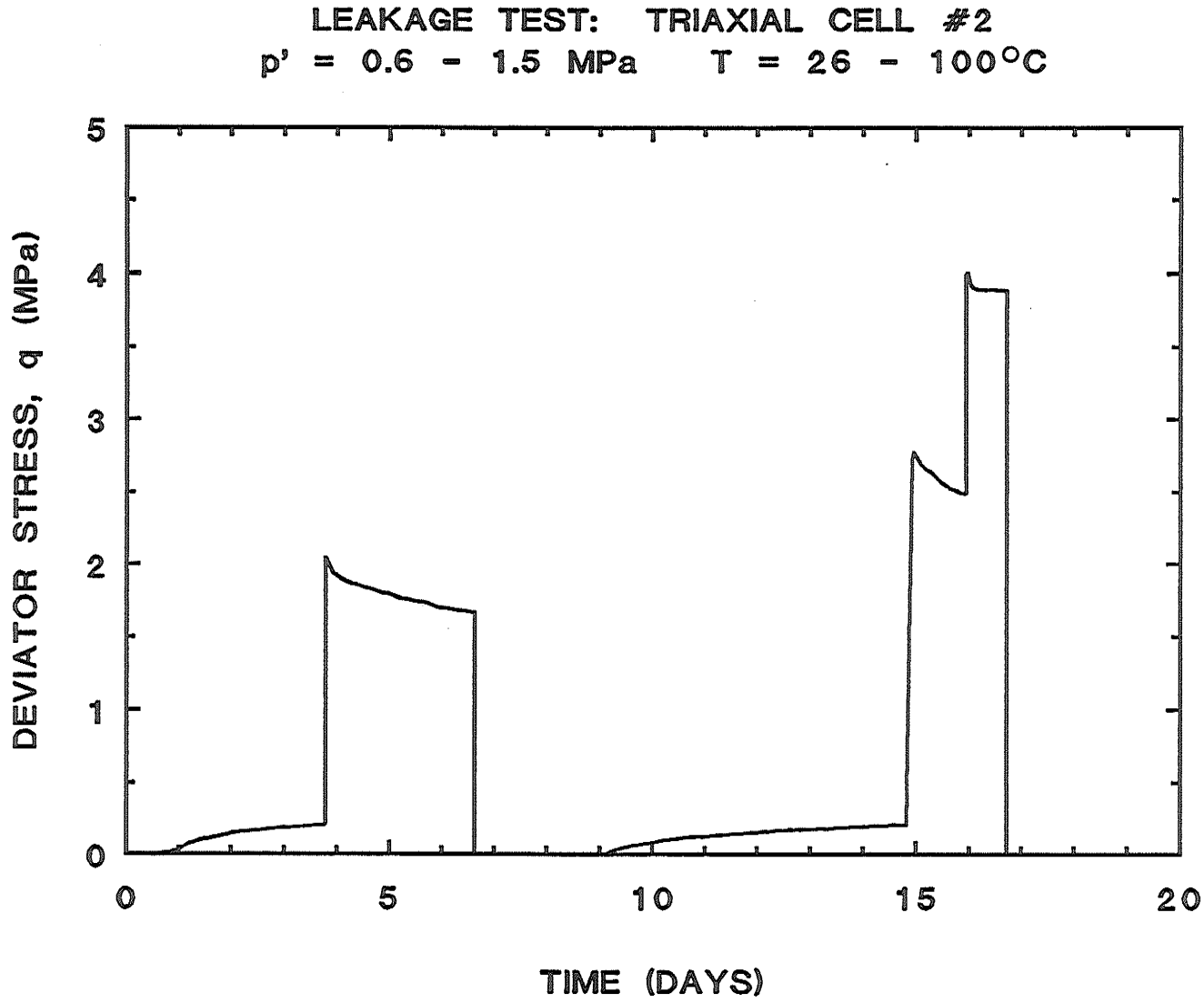

Fig. 3.17 Triaxial Cell #2 Leakage Test. Deviator Stress q *vs.* Elapsed Time.

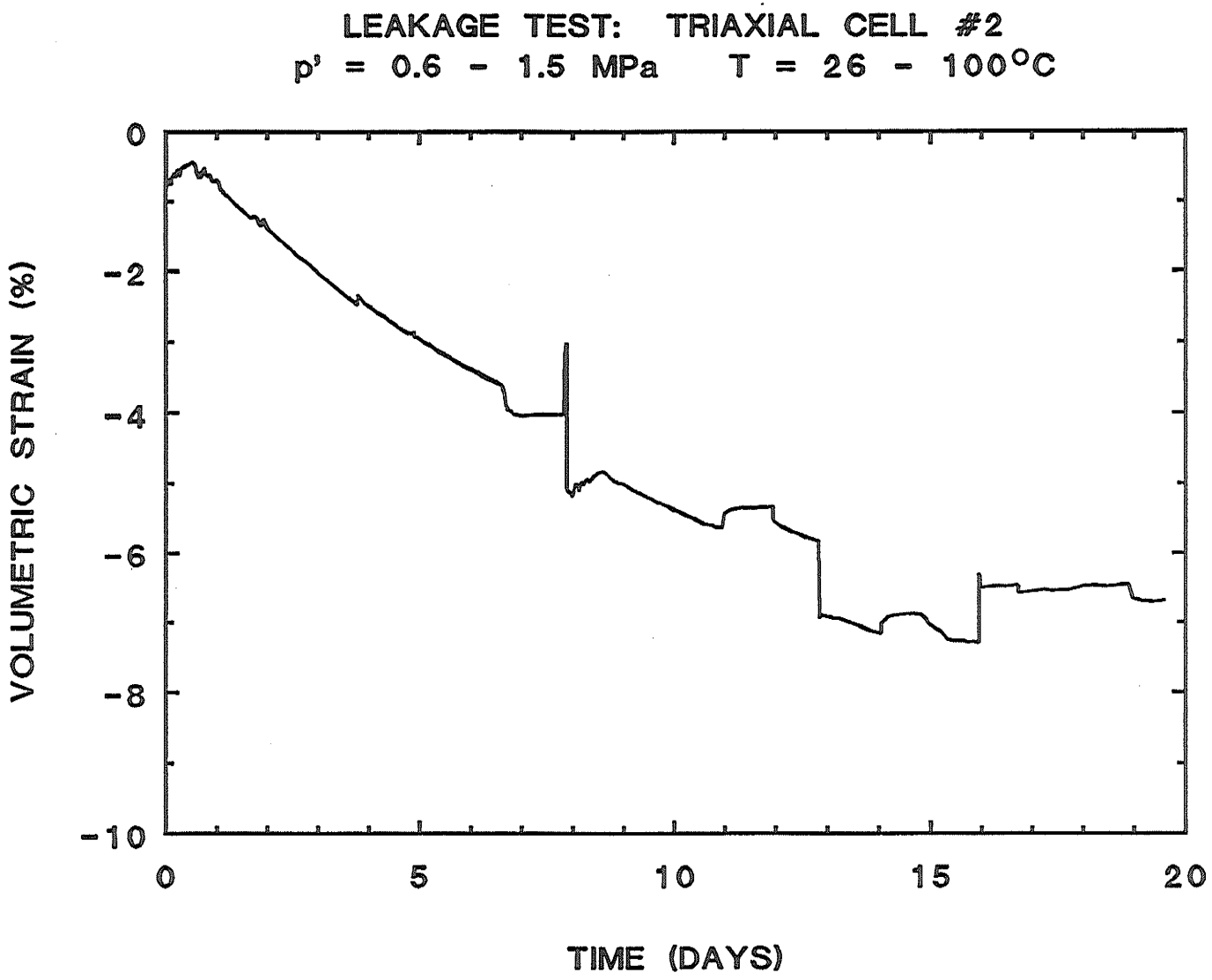

Fig. 3.18 Triaxial Cell #2 Leakage Test. Volumetric Strain *vs.* Elapsed Time.

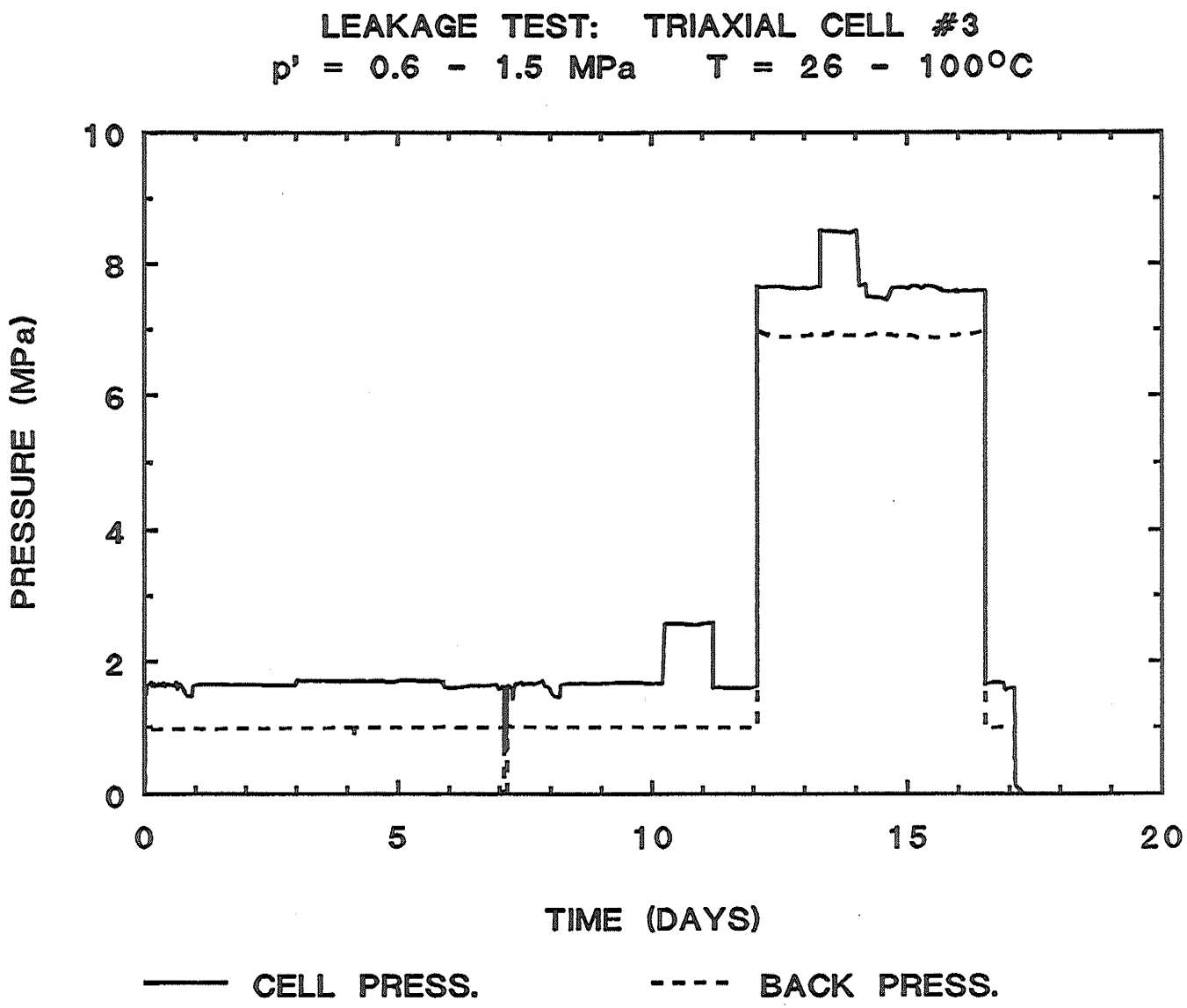

Fig. 3.19 Triaxial Cell #3 Leakage Test. Cell and Back Pressure *vs.* Elapsed Time.

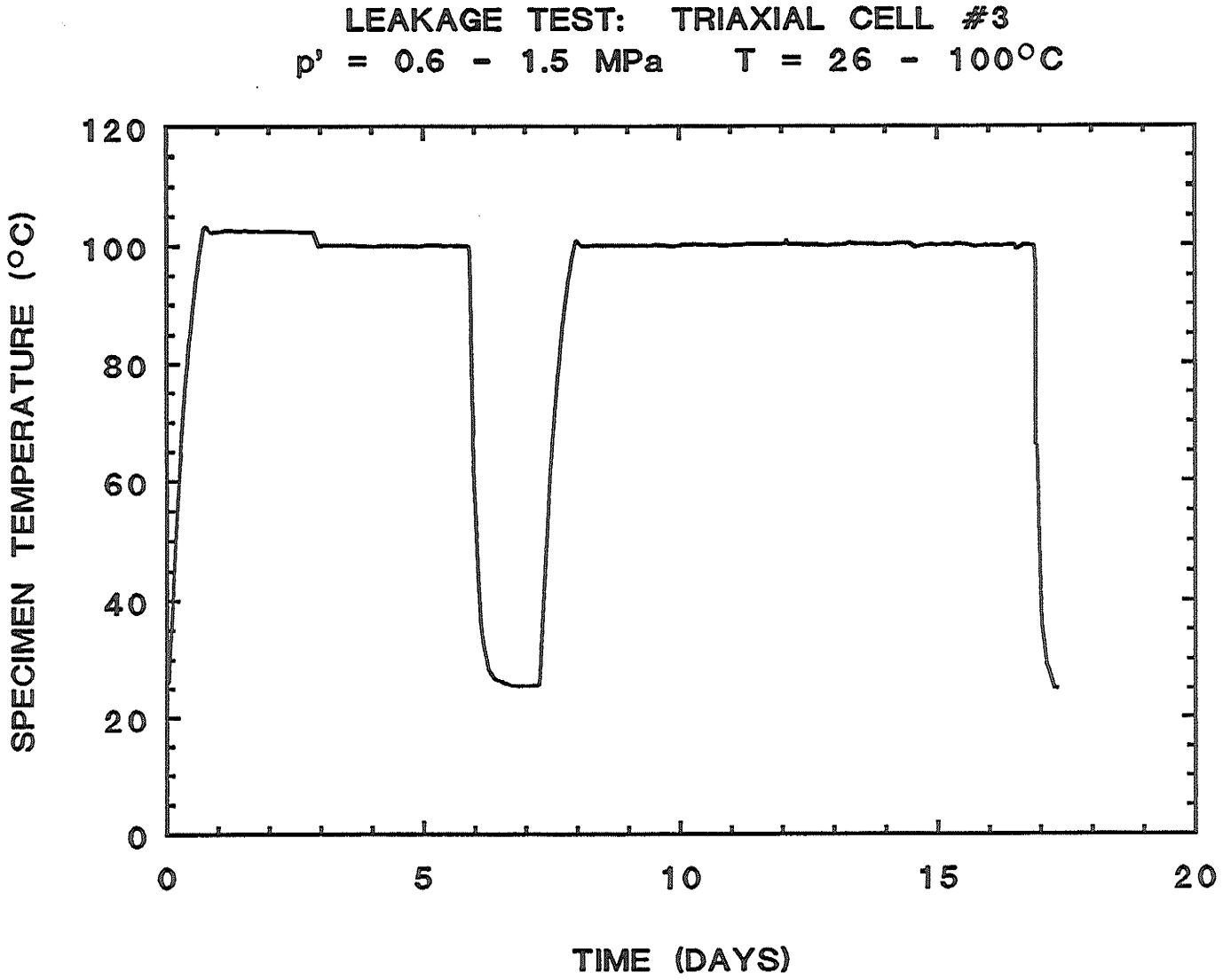

Fig. 3.20 Triaxial Cell #3 Leakage Test. Specimen Temperature *vs.* Elapsed Time.

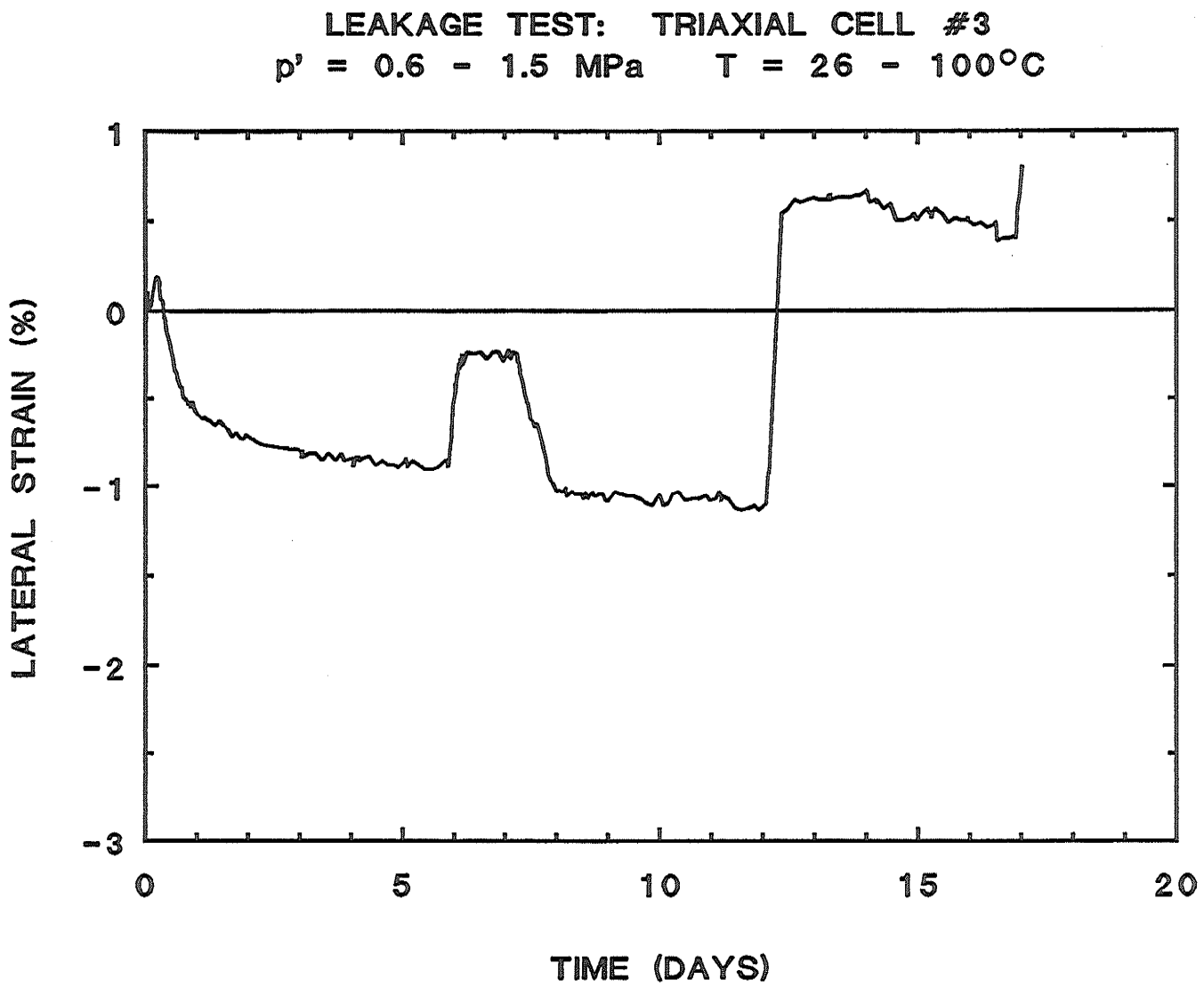

Fig. 3.21 Triaxial Cell #3 Leakage Test. Lateral Strain *vs.* Elapsed Time.

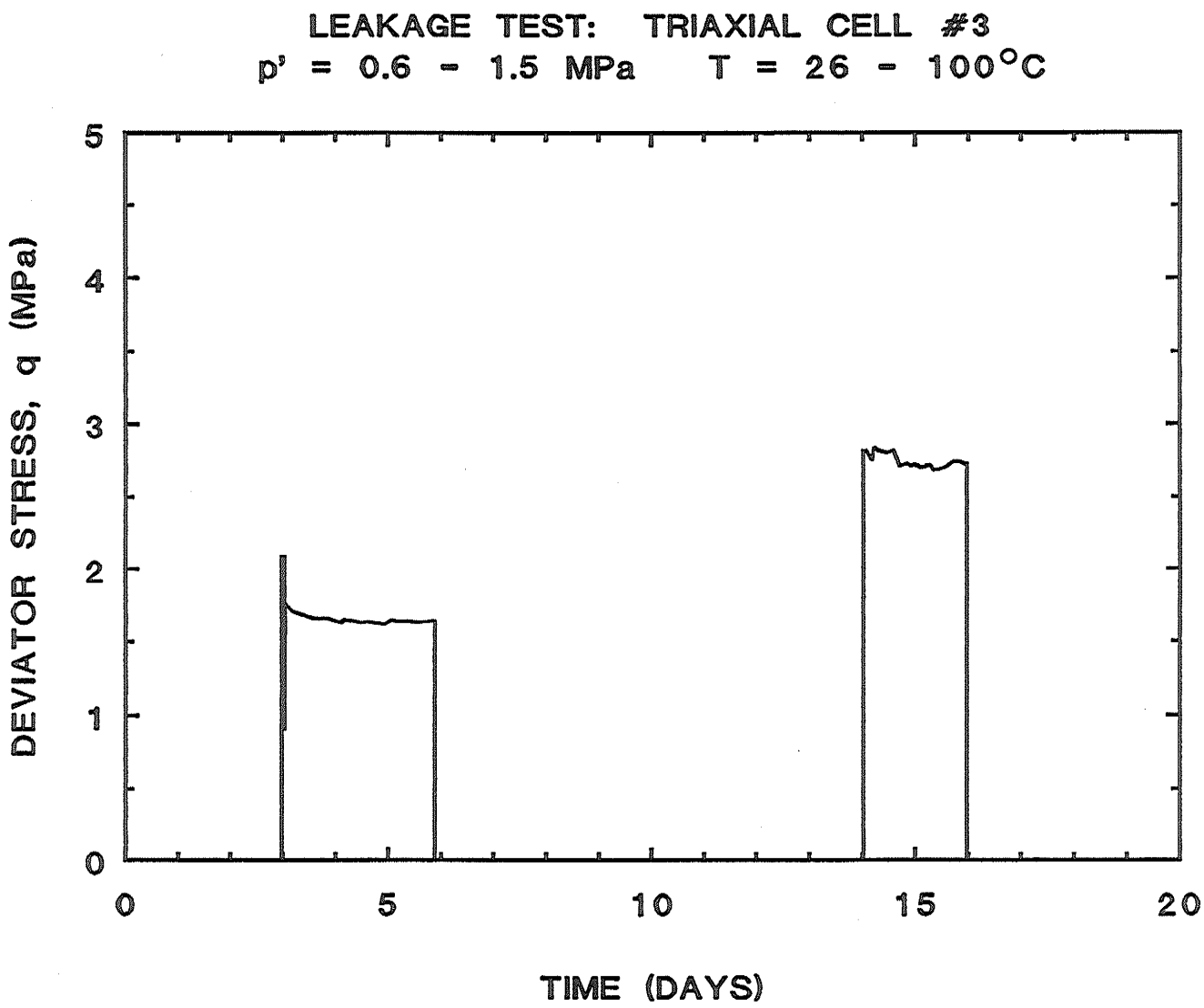

Fig. 3.22 Triaxial Cell #3 Leakage Test. Deviator Stress q *vs.* Elapsed Time.

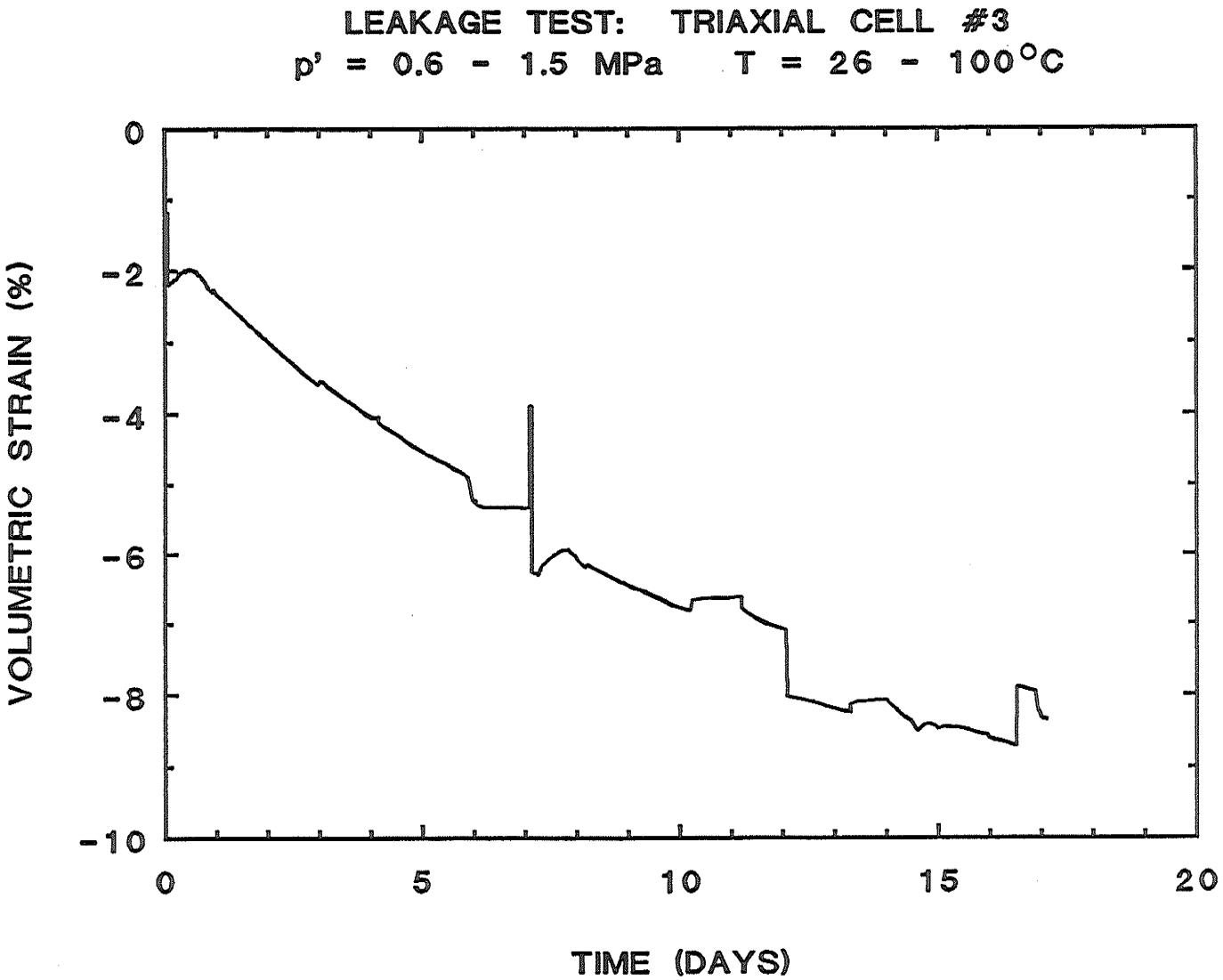

Fig. 3.23 Triaxial Cell #3 Leakage Test. Volumetric Strain *vs.* Elapsed Time.

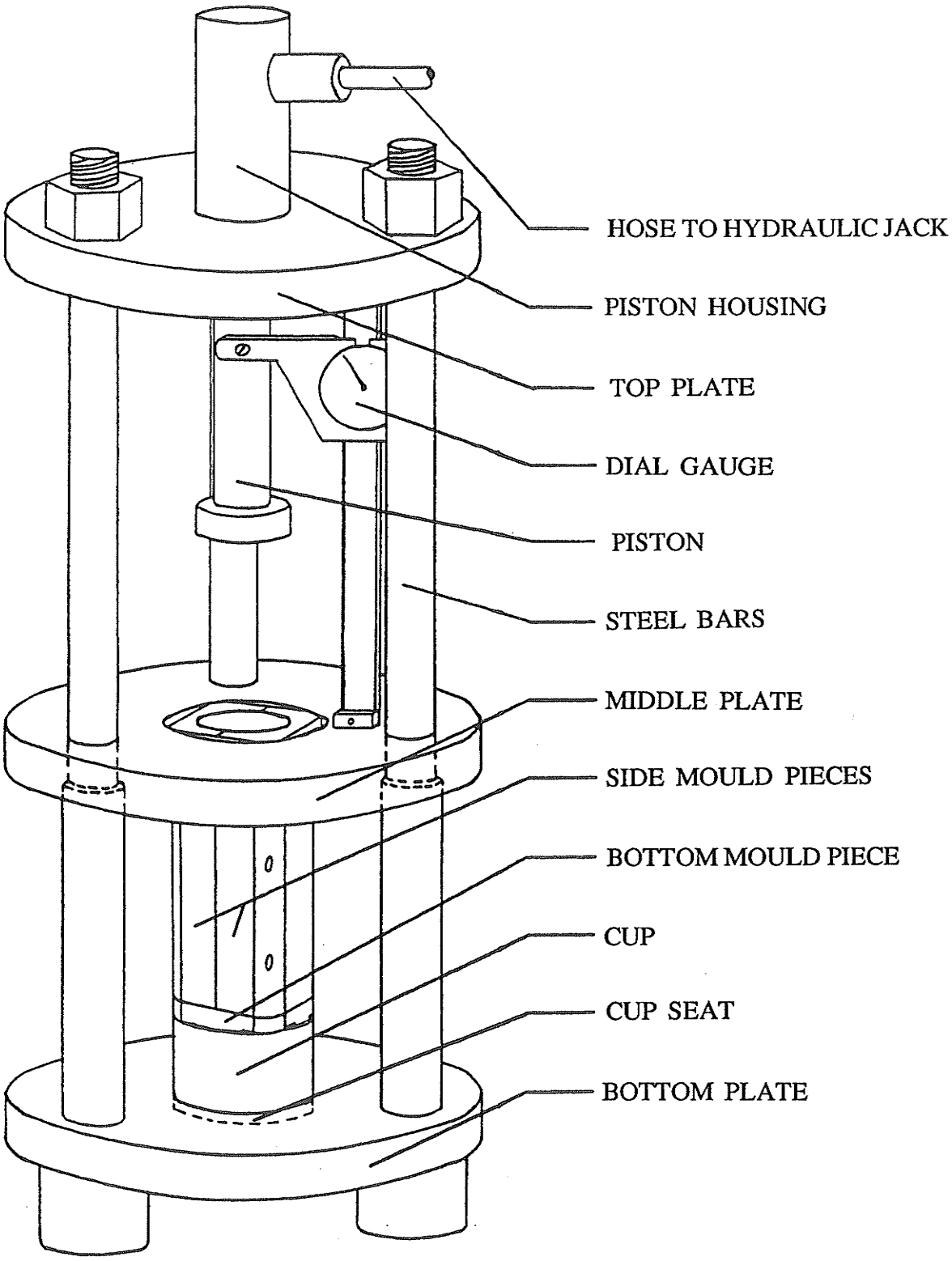

Fig. 4.1 Compaction frame for forming buffer specimens used in triaxial tests.

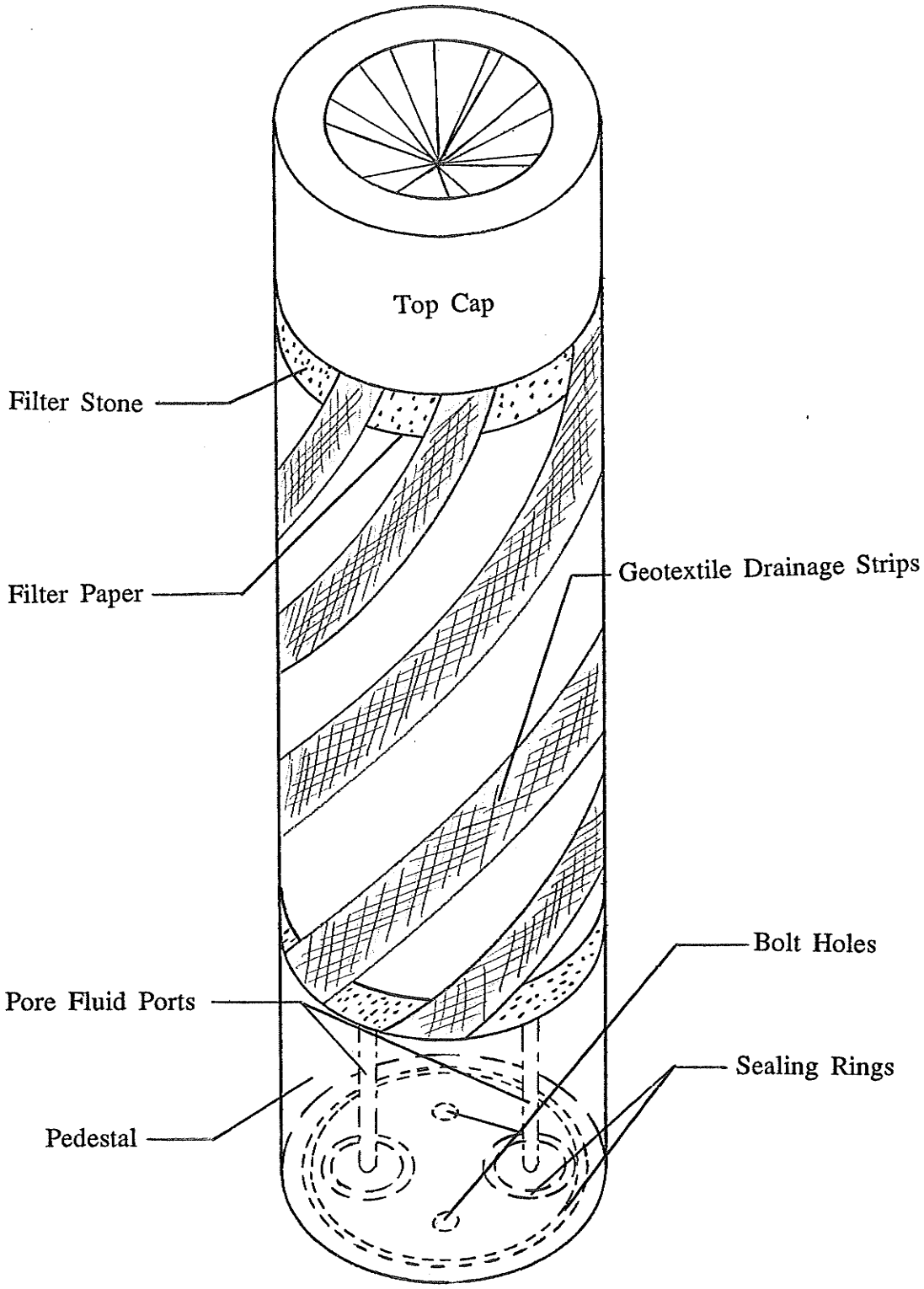

Fig. 4.2 Drainage system components adjacent to buffer specimen.

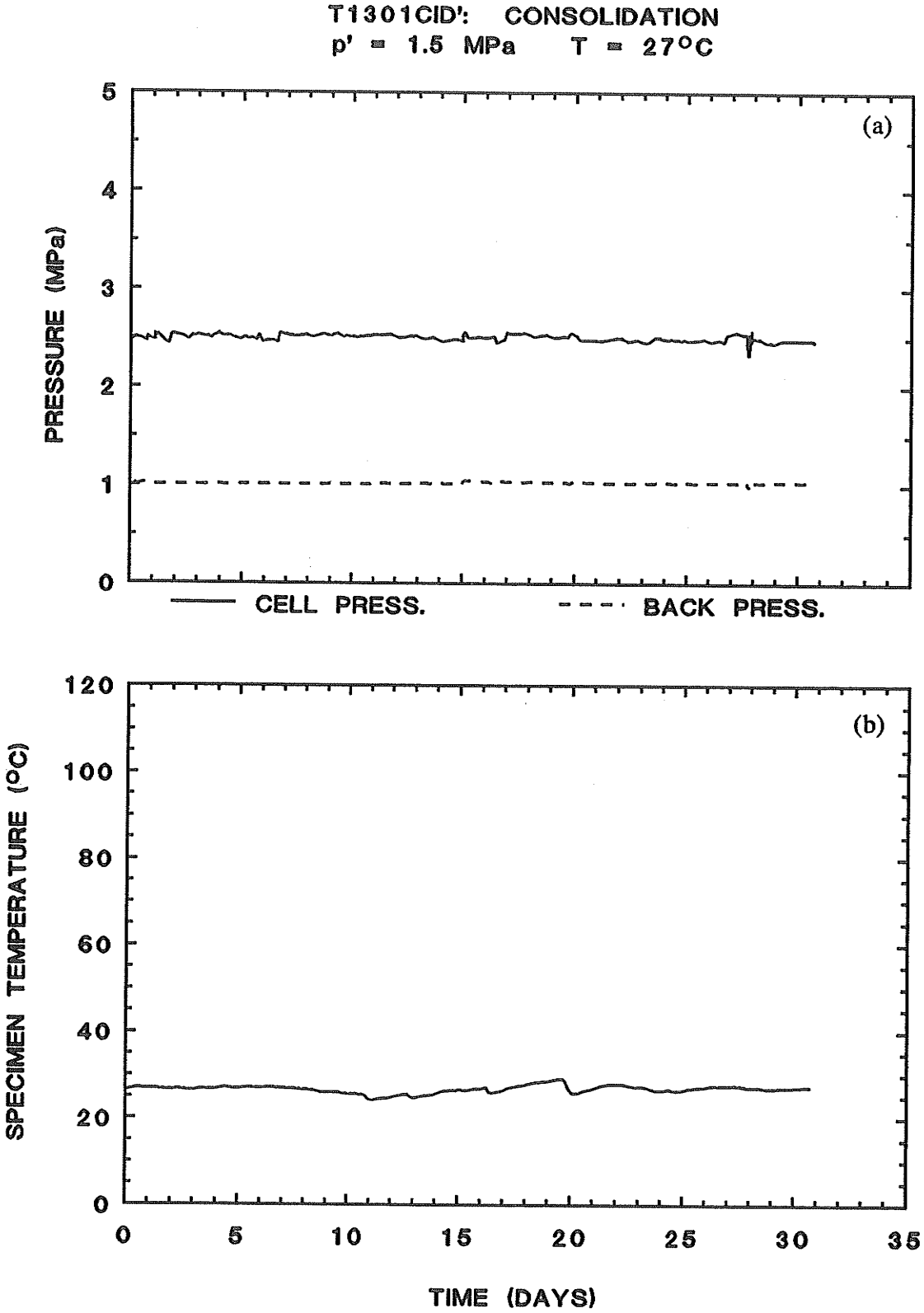

Fig. 5.1 Consolidation T1301. p' = 1.5 MPa, u_b = 1.0 MPa, T = 27°C

a) Cell σ_3 and Back Pressure u_b *vs.* Elapsed Time.

b) Specimen Temperature *vs.* Elapsed Time.

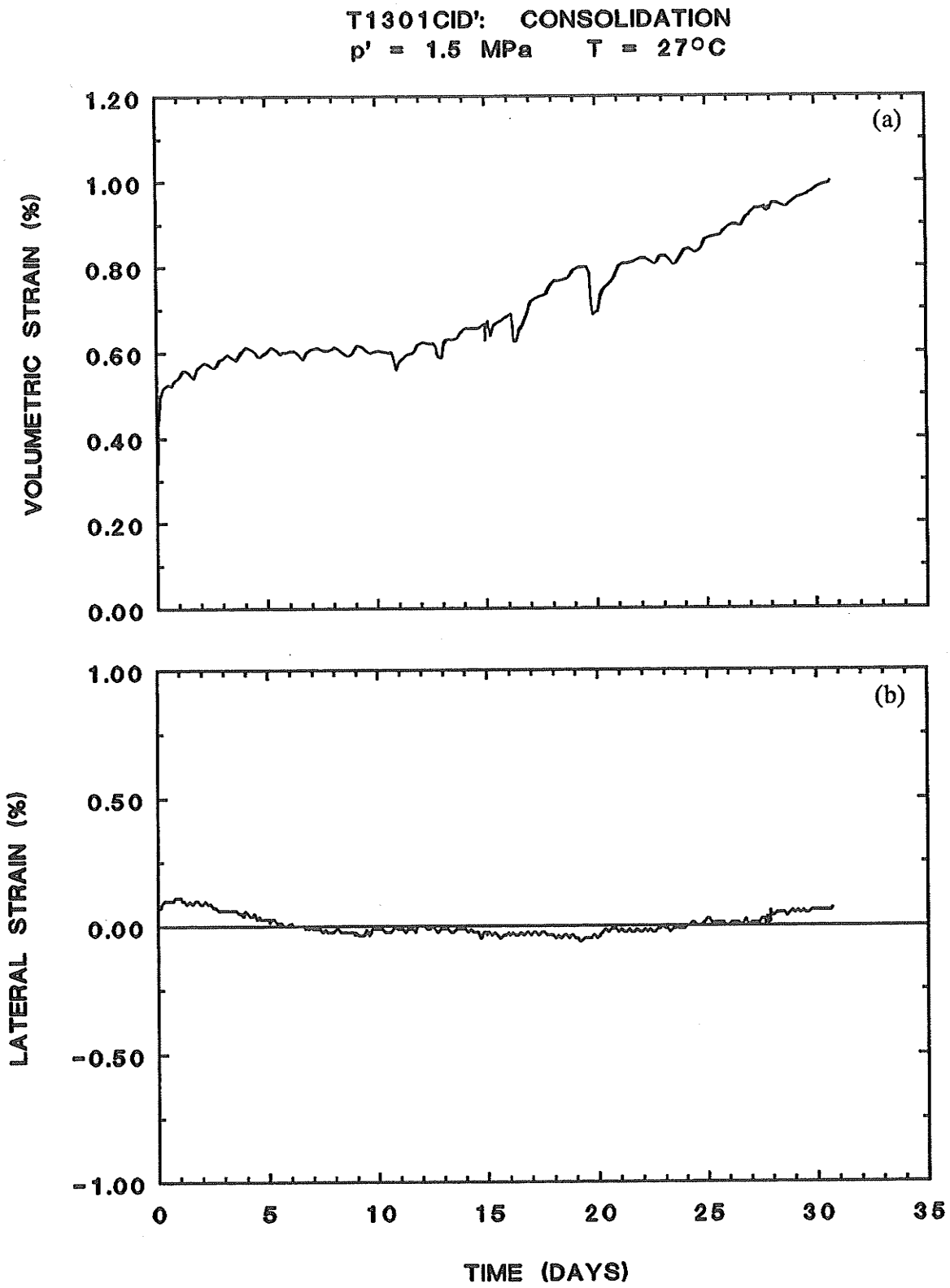

Fig. 5.2 Consolidation T1301. p' = 1.5 MPa, u_b = 1.0 MPa, T = 27°C

a) Volumetric Strain ε_v *vs.* Elapsed Time.

b) Lateral Strain ε_3 *vs.* Elapsed Time.

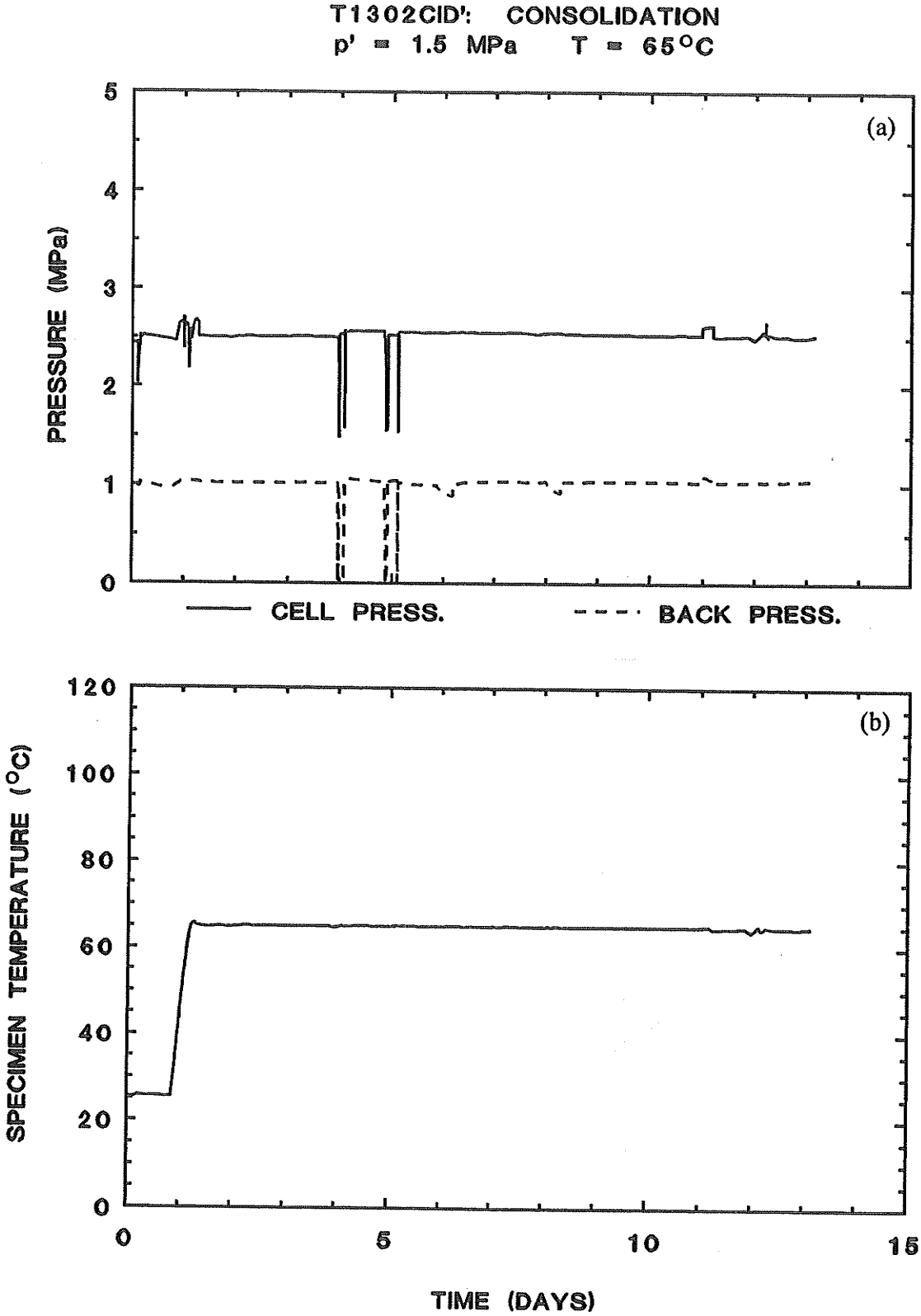

Fig. 5.3 Consolidation T1302. p' = 1.5 MPa, u_b = 1.0 MPa, T = 65°C

a) Cell σ_3 and Back Pressure u_b *vs.* Elapsed Time.

b) Specimen Temperature *vs.* Elapsed Time.

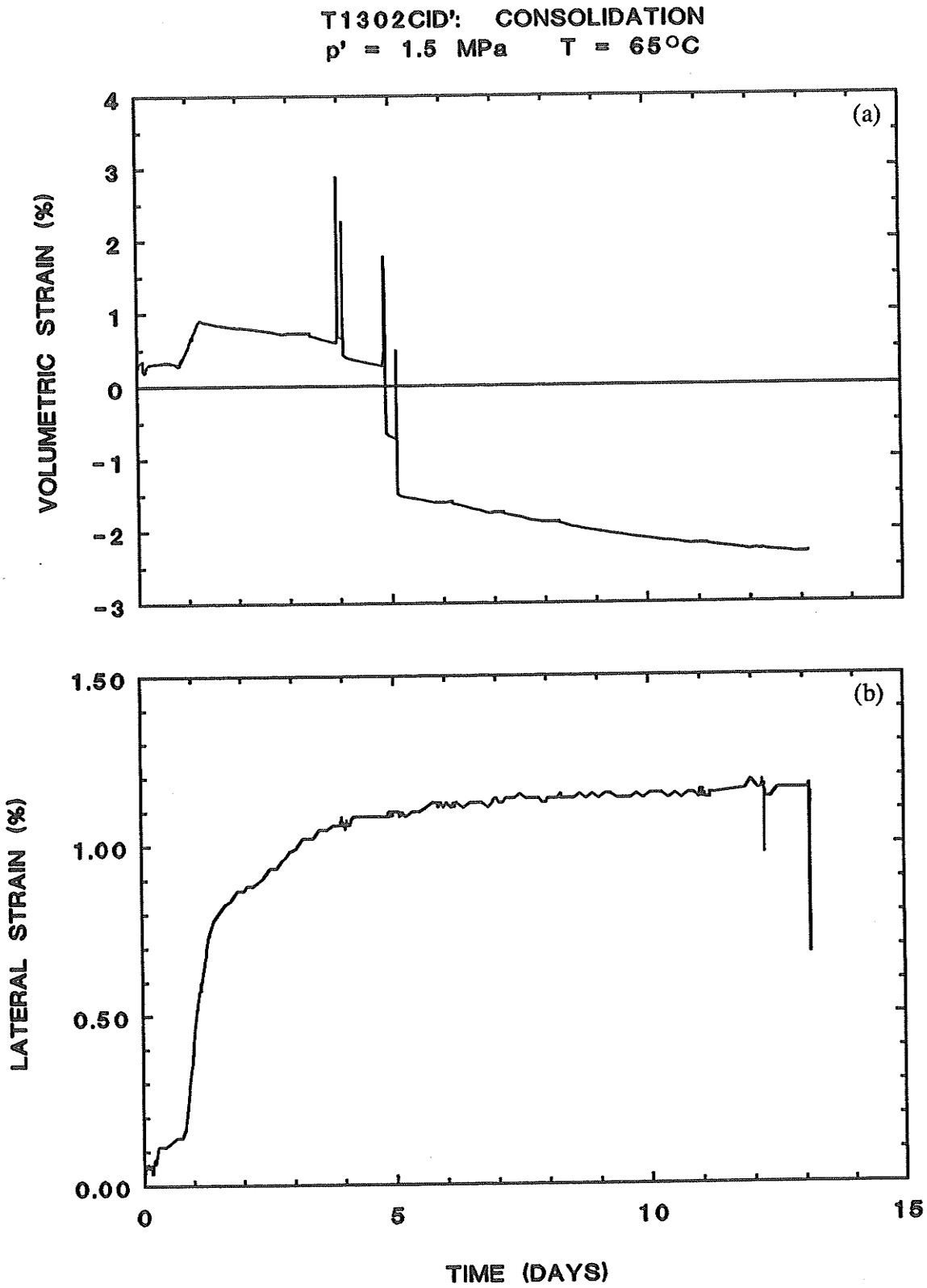

Fig. 5.4 Consolidation T1302. p' = 1.5 MPa, u_b = 1.0 MPa, T = 65°C

a) Volumetric Strain ε_v *vs.* Elapsed Time.

b) Lateral Strain ε_3 *vs.* Elapsed Time.

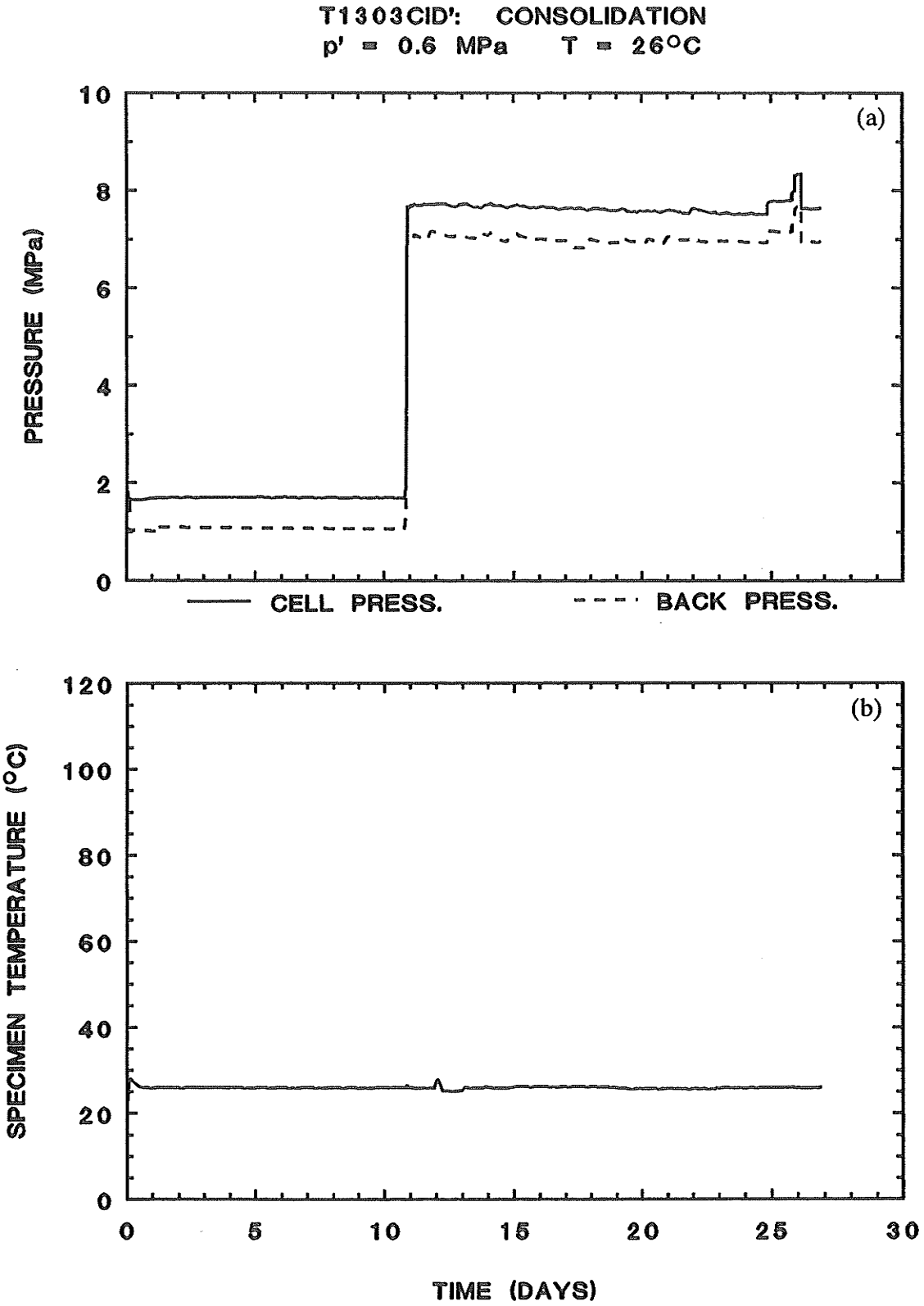

Fig. 5.5 Consolidation T1303. p' = 0.6 MPa, u_b = 1.0 - 7.0 MPa, T = 26°C

a) Cell σ_3 and Back Pressure u_b *vs.* Elapsed Time.

b) Specimen Temperature *vs.* Elapsed Time.

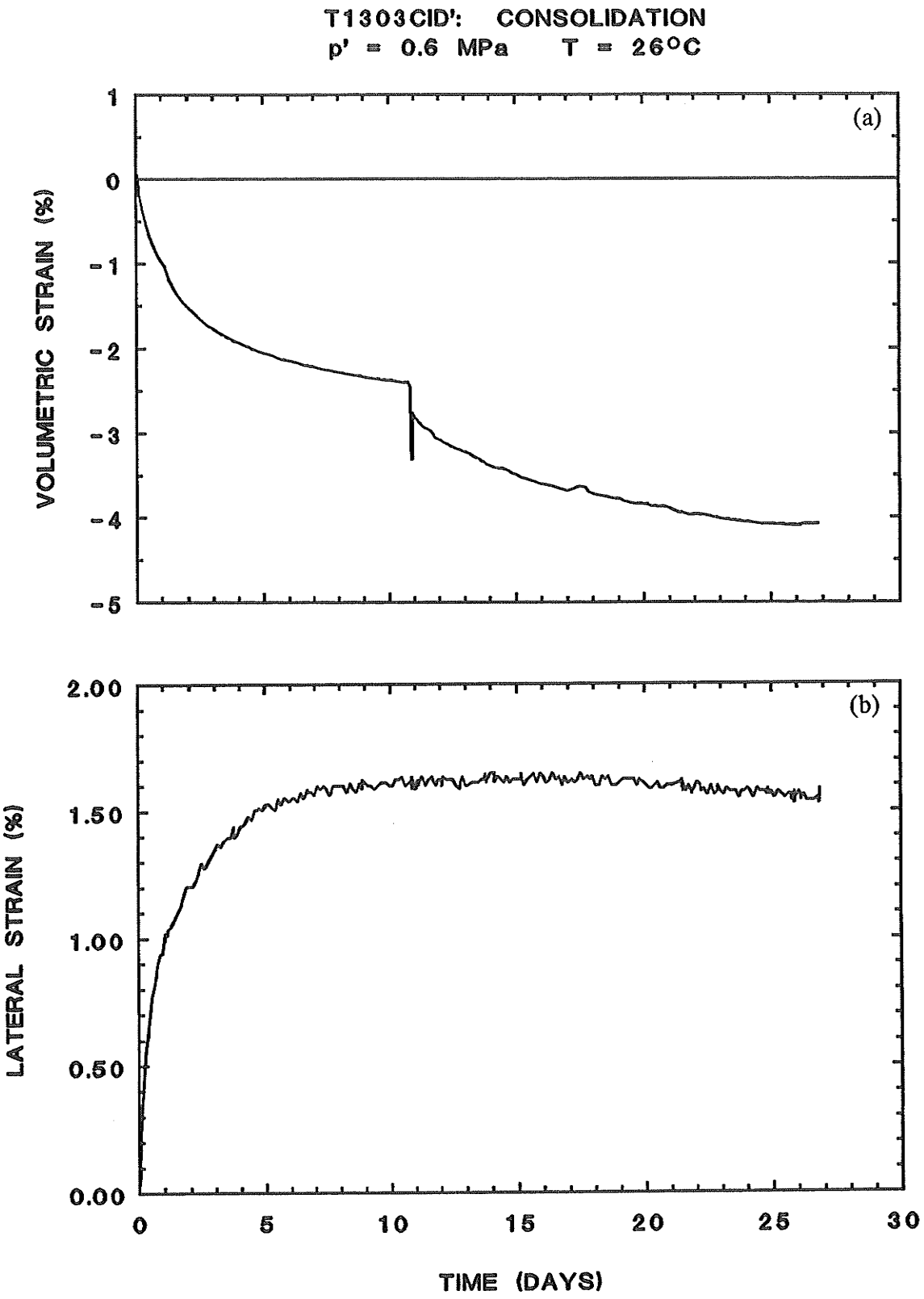

Fig. 5.6 Consolidation T1303. p' = 0.6 MPa, u_b = 1.0 - 7.0 MPa, T = 26°C

a) Volumetric Strain ε_v *vs.* Elapsed Time.

b) Lateral Strain ε_3 *vs.* Elapsed Time.

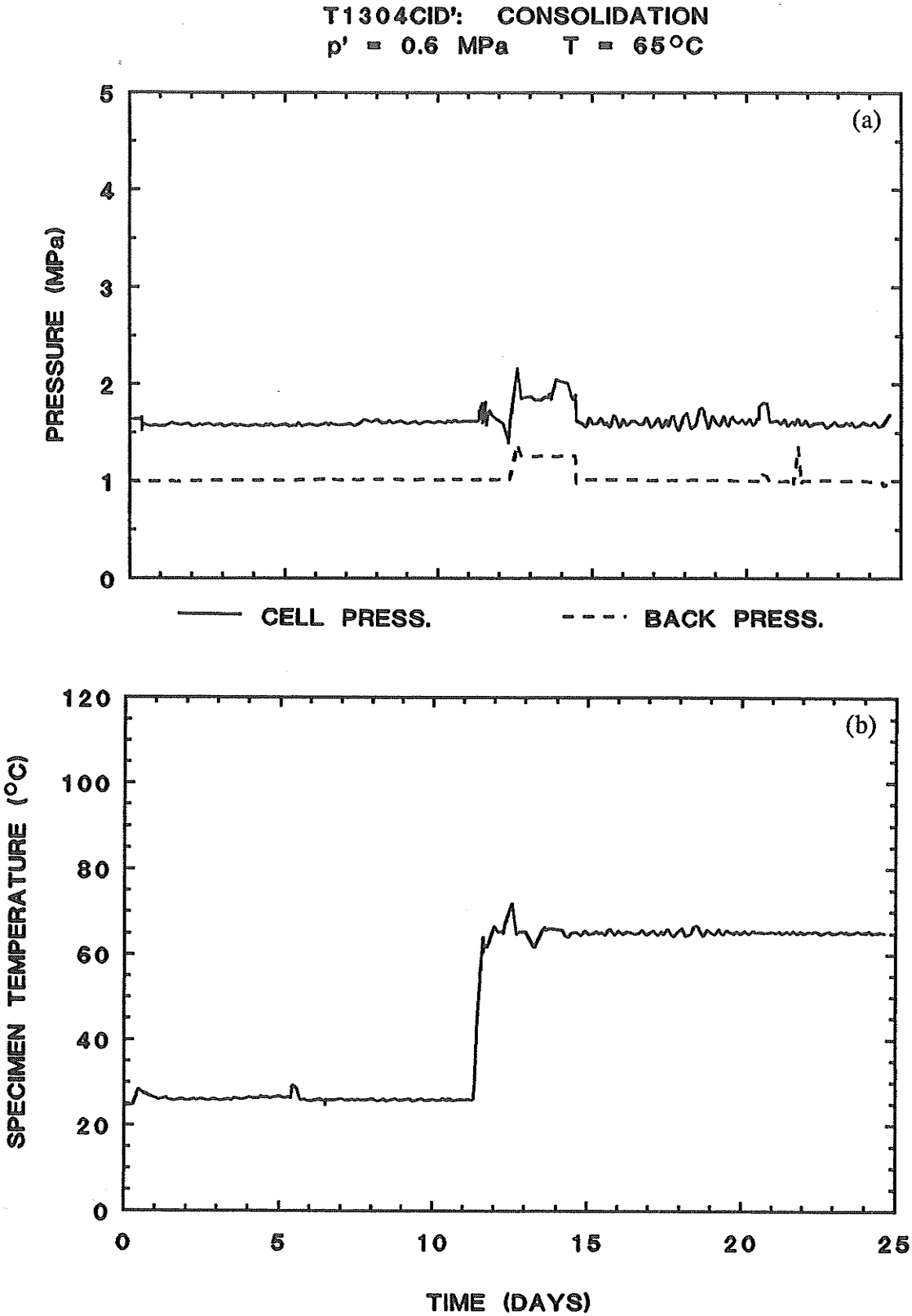

Fig. 5.7 Consolidation T1304. p' = 0.6 MPa, u_b = 1.0 MPa, T = 65°C

a) Cell σ_3 and Back Pressure u_b *vs.* Elapsed Time.

b) Specimen Temperature *vs.* Elapsed Time.

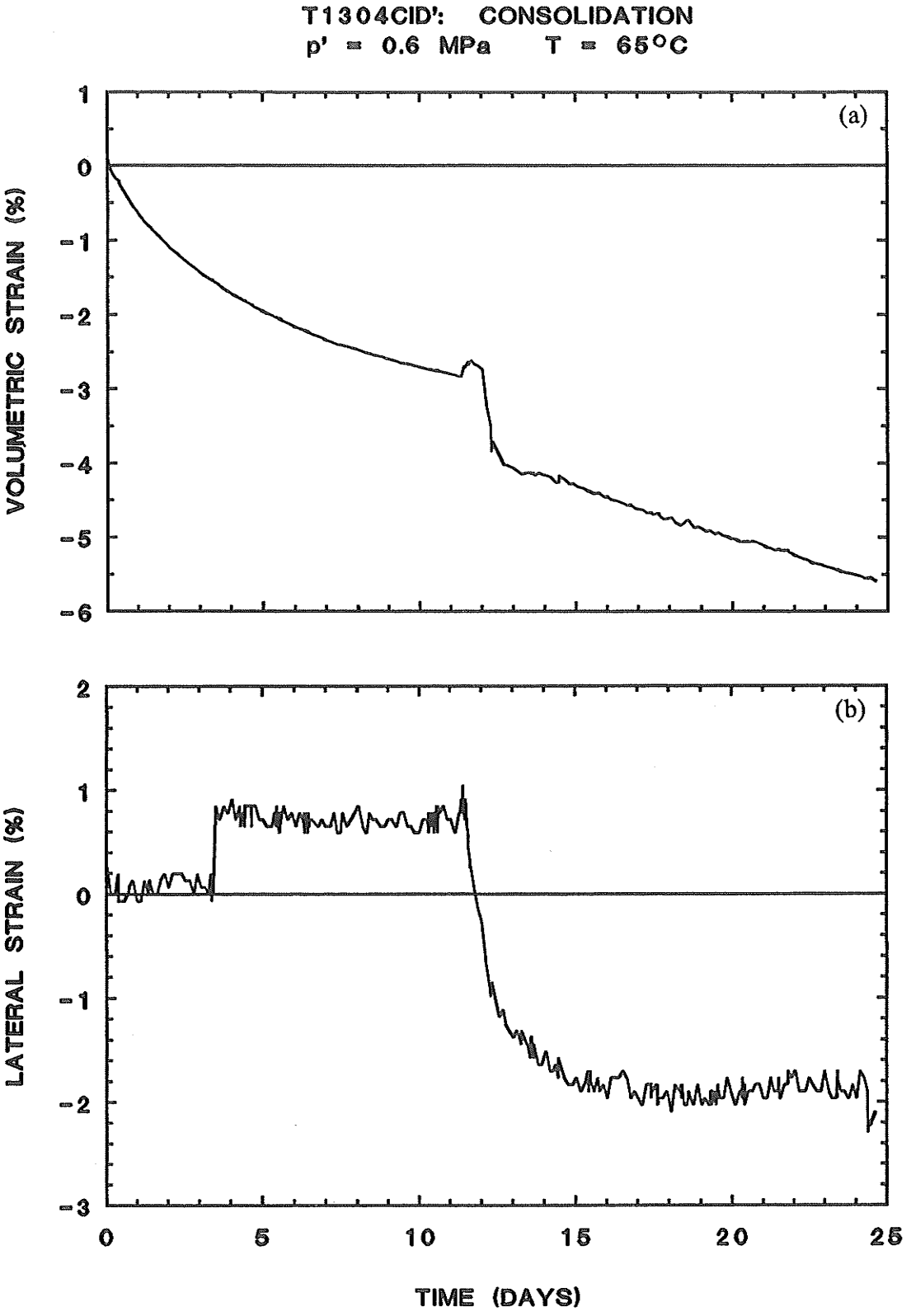

Fig. 5.8 Consolidation T1304. p' = 0.6 MPa, u_b = 1.0 MPa, T = 65°C

a) Volumetric Strain ε_v *vs.* Elapsed Time.

b) Lateral Strain ε_3 *vs.* Elapsed Time.

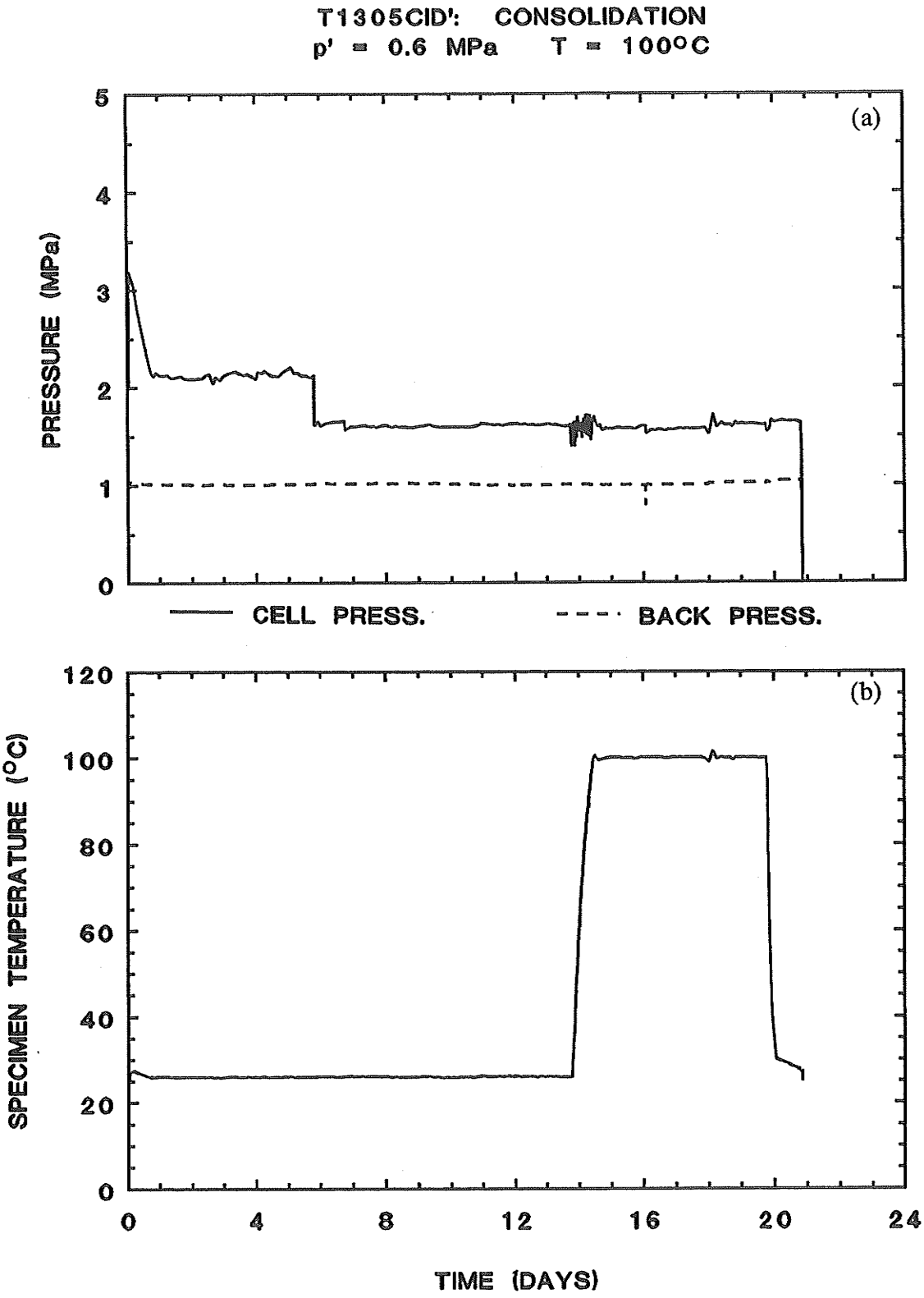

Fig. 5.9 Consolidation T1305. p' = 0.6 MPa, u_b = 1.0 MPa, T = 100°C

a) Cell σ_3 and Back Pressure u_b *vs.* Elapsed Time.

b) Specimen Temperature *vs.* Elapsed Time.

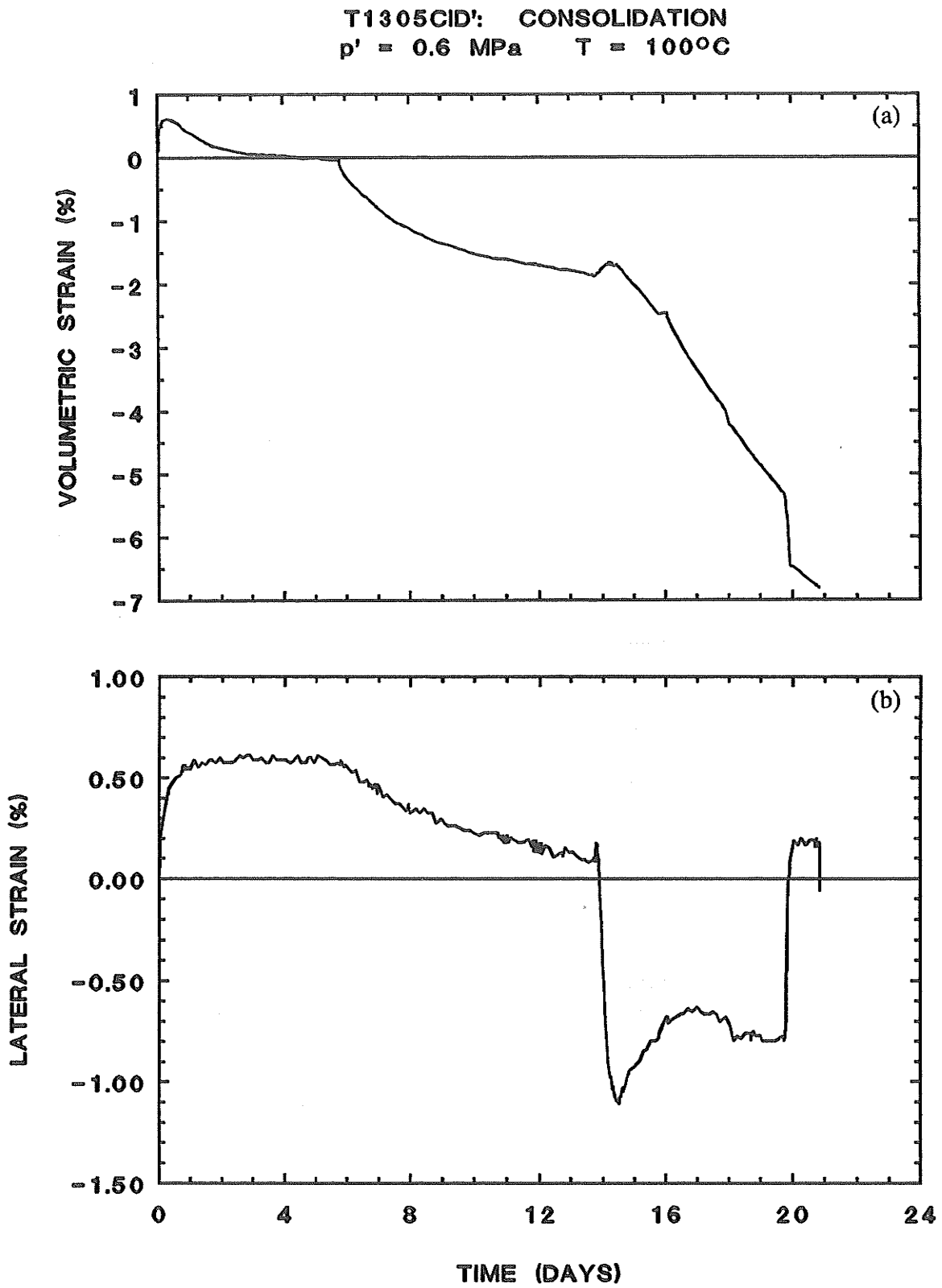

Fig. 5.10 Consolidation T1305. p' = 0.6 MPa, u_b = 1.0 MPa, T = 100°C

a) Volumetric Strain ε_v *vs.* Elapsed Time.

b) Lateral Strain ε_3 *vs.* Elapsed Time.

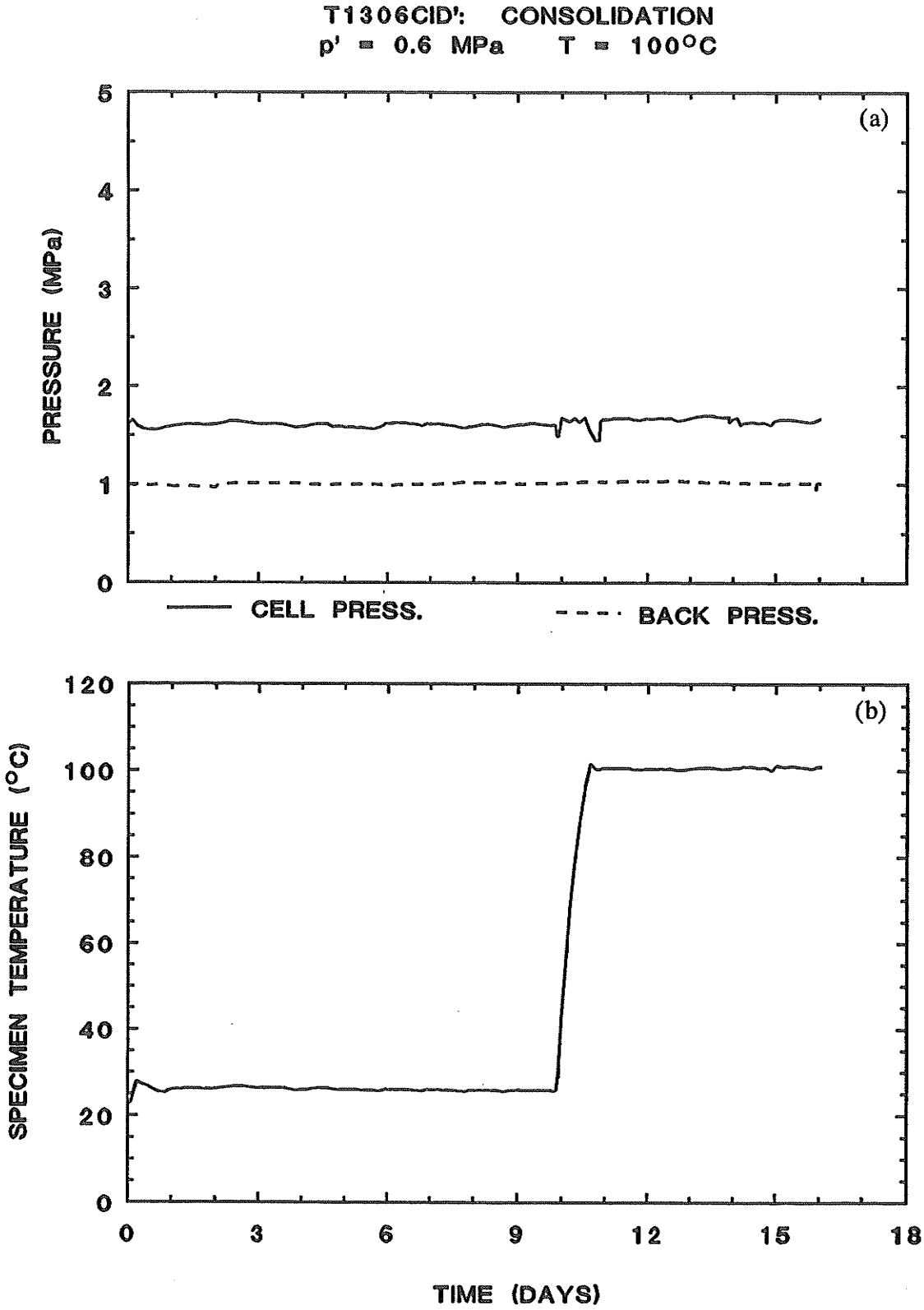

Fig. 5.11 Consolidation T1306. p' = 0.6 MPa, u_b = 1.0 MPa, T = 100°C

a) Cell σ_3 and Back Pressure u_b *vs.* Elapsed Time.

b) Specimen Temperature *vs.* Elapsed Time.

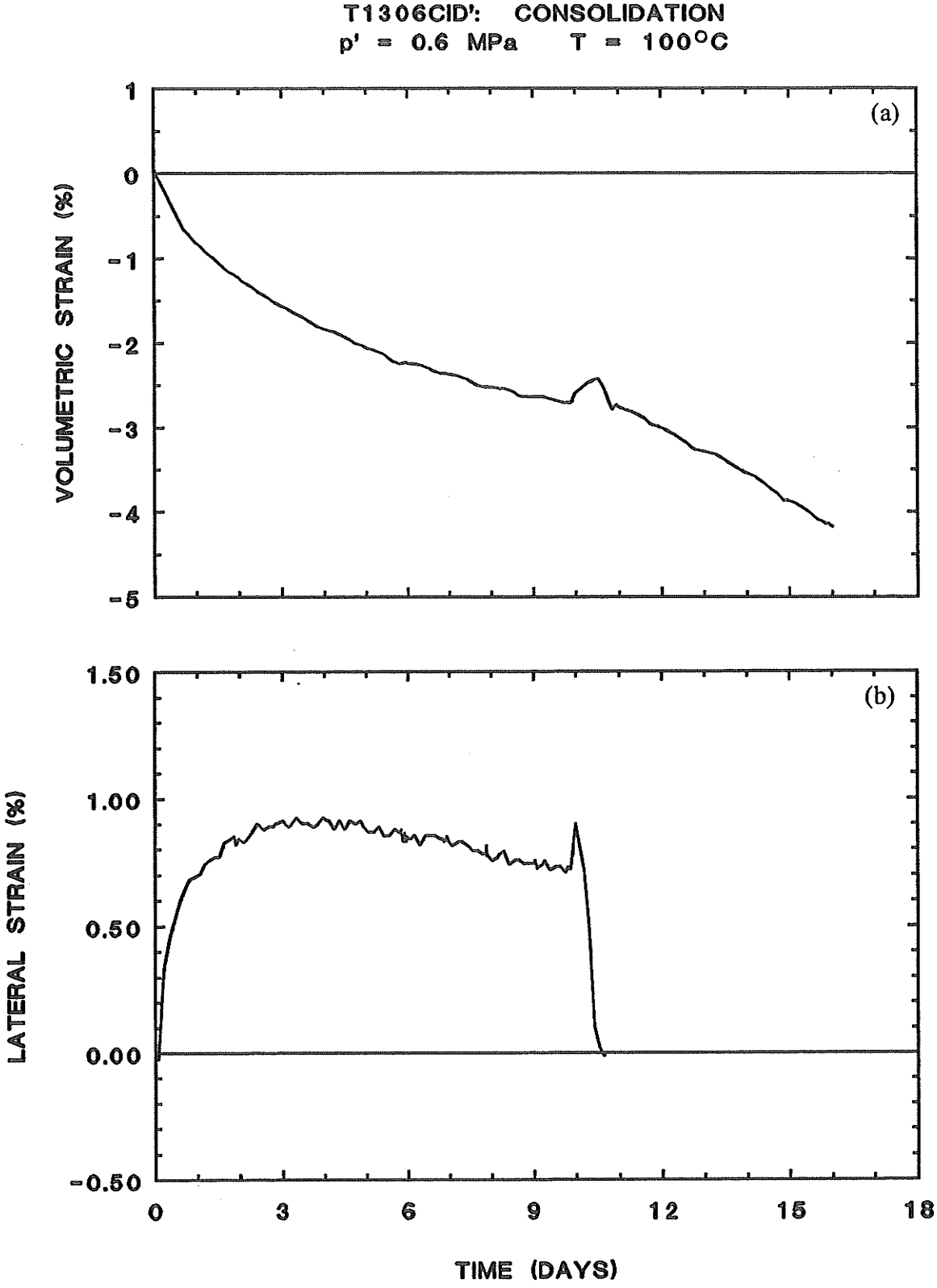

Fig. 5.12 Consolidation T1306. p' = 0.6 MPa, u_b = 1.0 MPa, T = 100°C

a) Volumetric Strain ε_v *vs.* Elapsed Time.

b) Lateral Strain ε_3 *vs.* Elapsed Time.

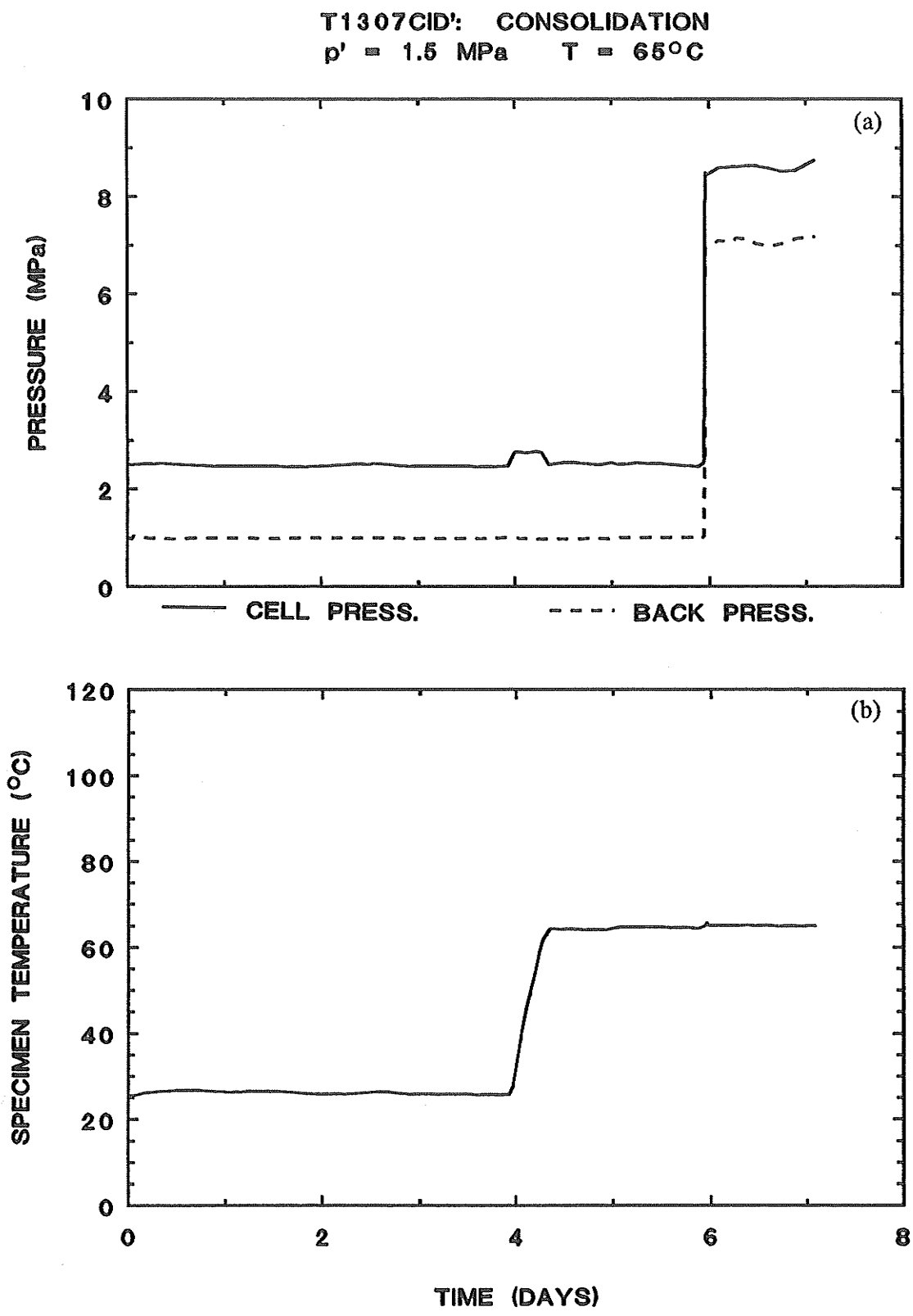

Fig. 5.13 Consolidation T1307. p' = 1.5 MPa, u_b = 1.0 - 7.0 MPa, T = 65°C

a) Cell σ_3 and Back Pressure u_b *vs.* Elapsed Time.

b) Specimen Temperature *vs.* Elapsed Time.

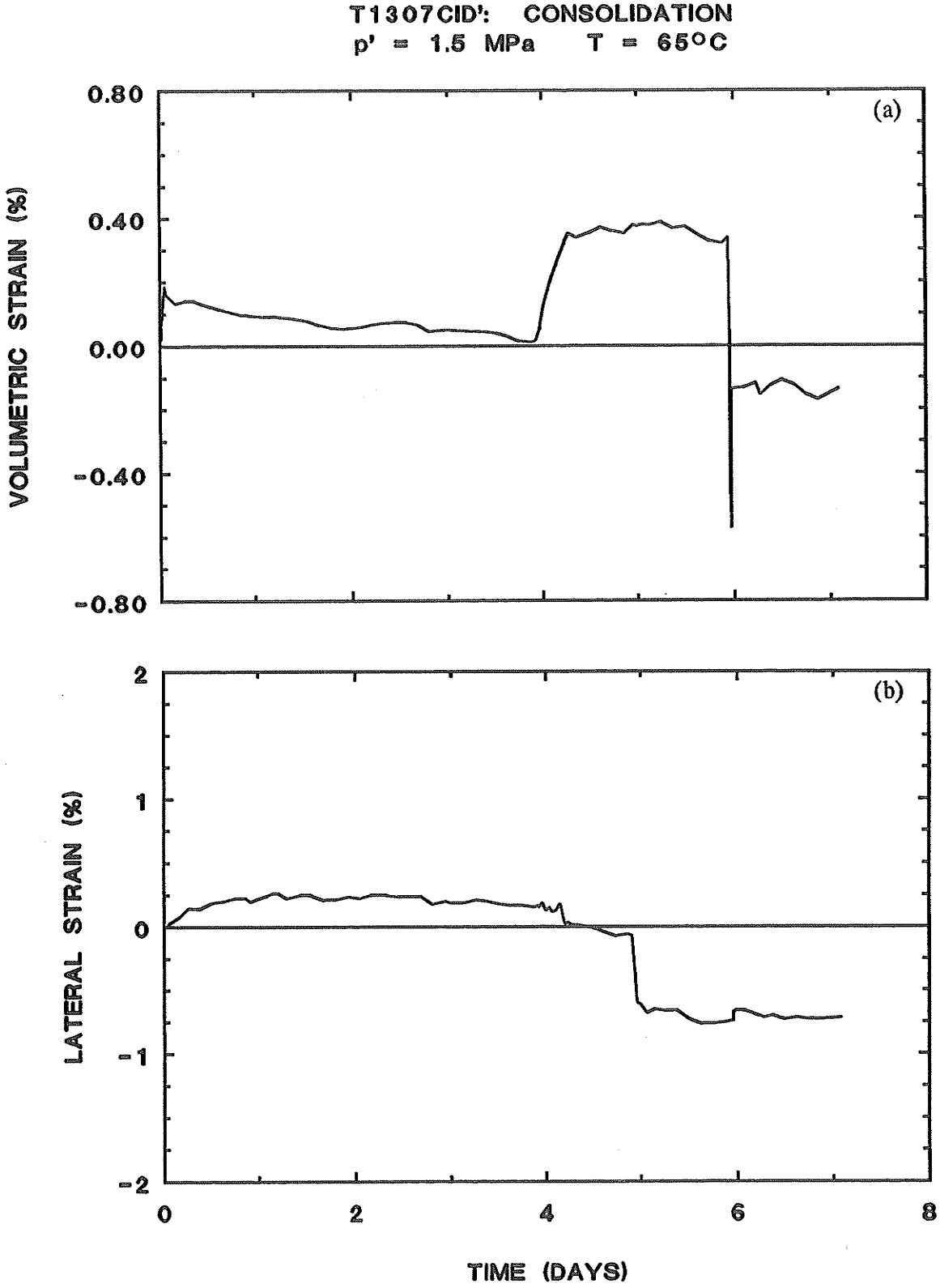

Fig. 5.14 Consolidation T1307. p' = 1.5 MPa, u_b = 1.0 - 7.0 MPa, T = 65°C

a) Volumetric Strain ε_v *vs.* Elapsed Time.

b) Lateral Strain ε_3 *vs.* Elapsed Time.

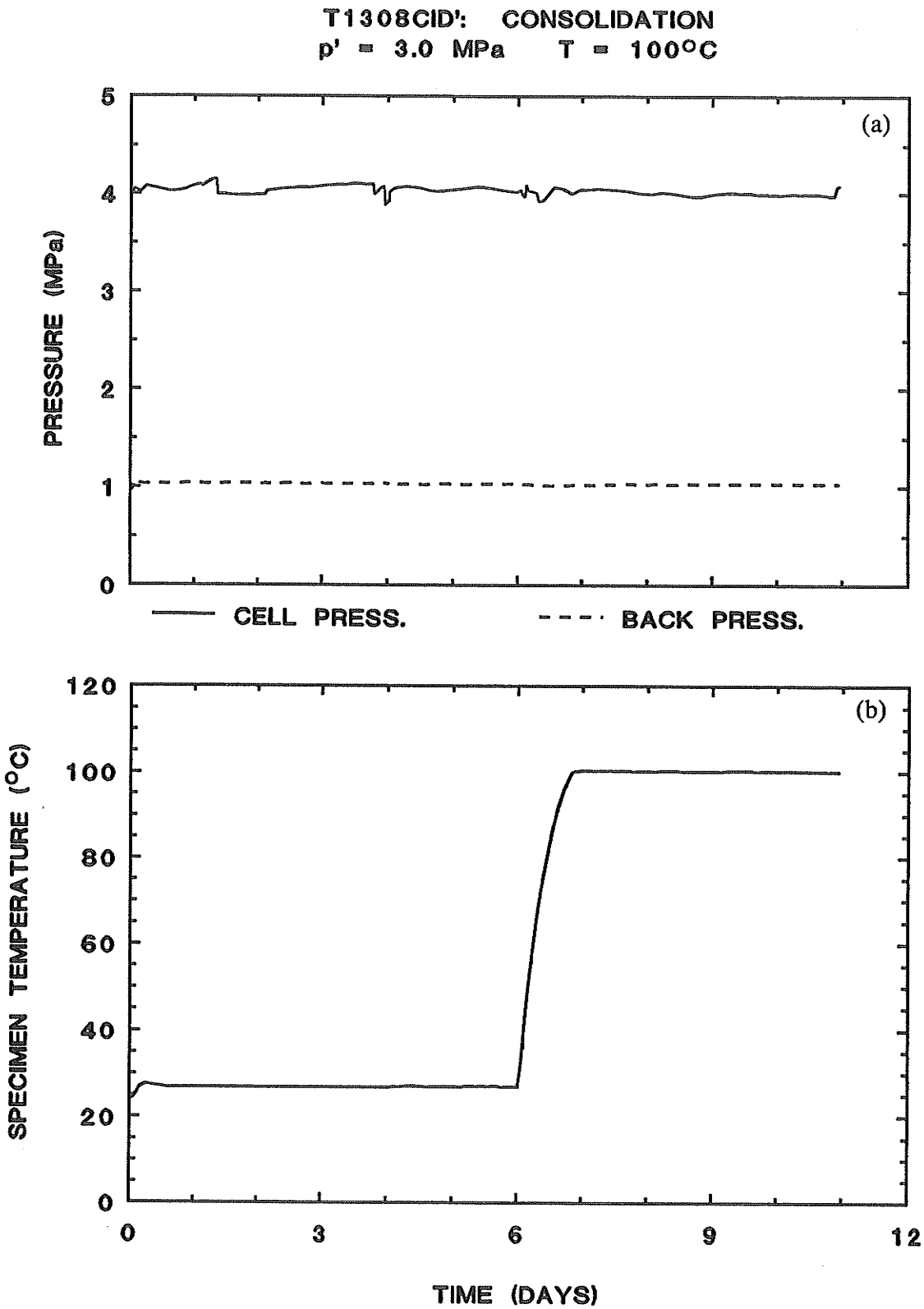

Fig. 5.15 Consolidation T1308. p' = 3.0 MPa, u_b = 1.0 MPa, T = 100°C

a) Cell σ_3 and Back Pressure u_b *vs.* Elapsed Time.

b) Specimen Temperature *vs.* Elapsed Time.

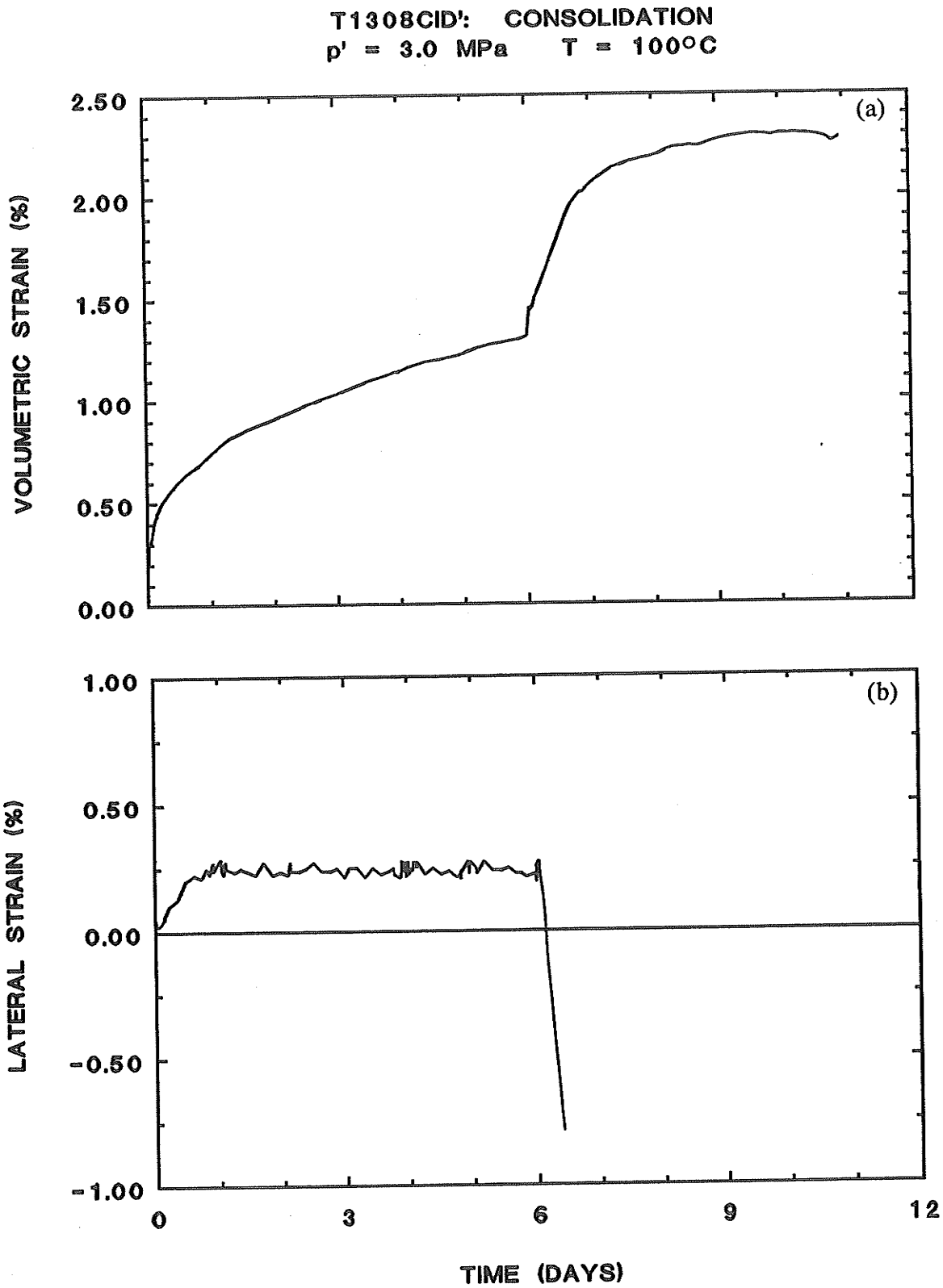

Fig. 5.16 Consolidation T1308. p' = 3.0 MPa, u_b = 1.0 MPa, T = 100°C

a) Volumetric Strain ε_v *vs.* Elapsed Time.

b) Lateral Strain ε_3 *vs.* Elapsed Time.

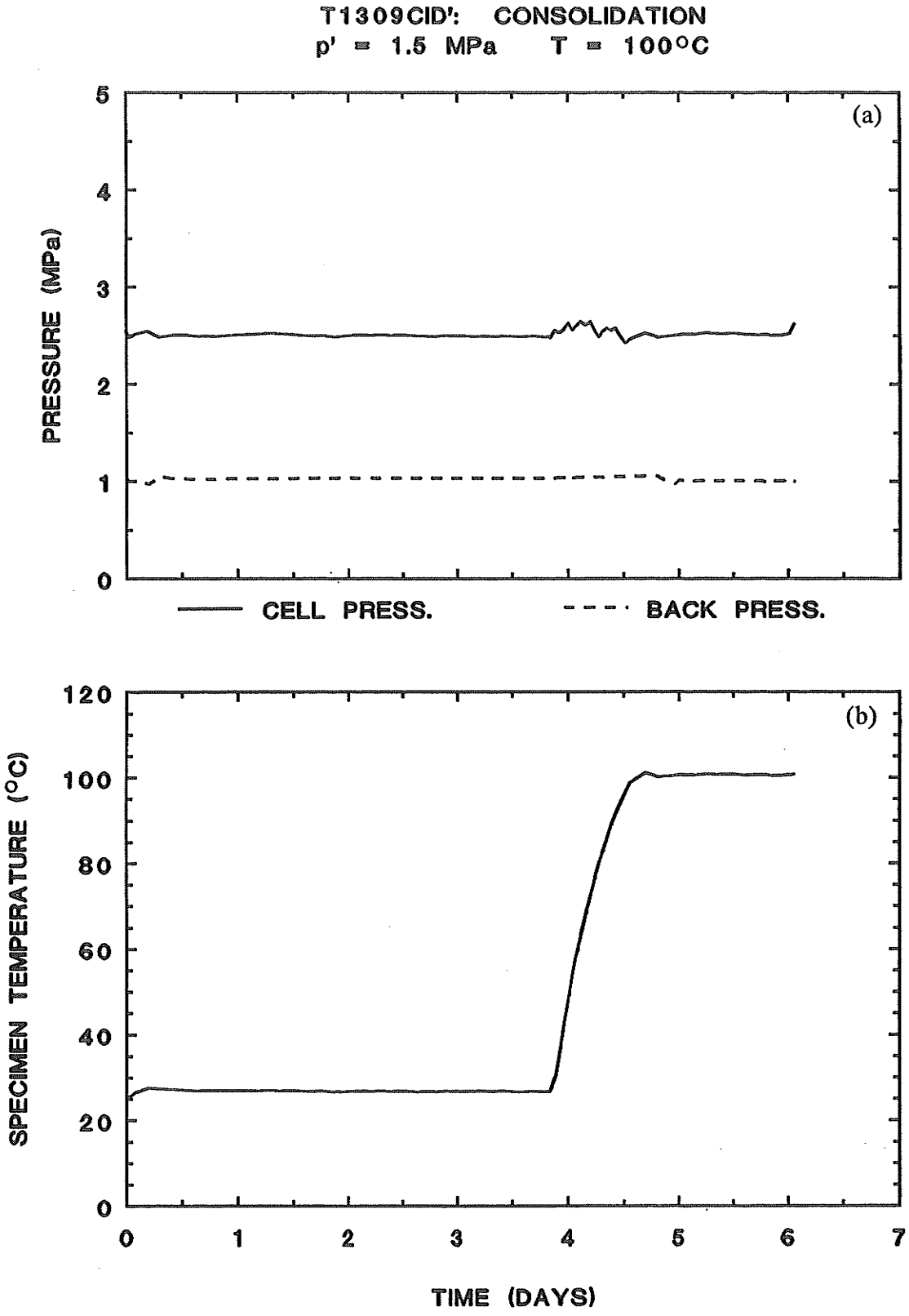

Fig. 5.17 Consolidation T1309. p' = 1.5 MPa, u_b = 1.0 MPa, T = 100°C

a) Cell σ_3 and Back Pressure u_b *vs.* Elapsed Time.

b) Specimen Temperature *vs.* Elapsed Time.

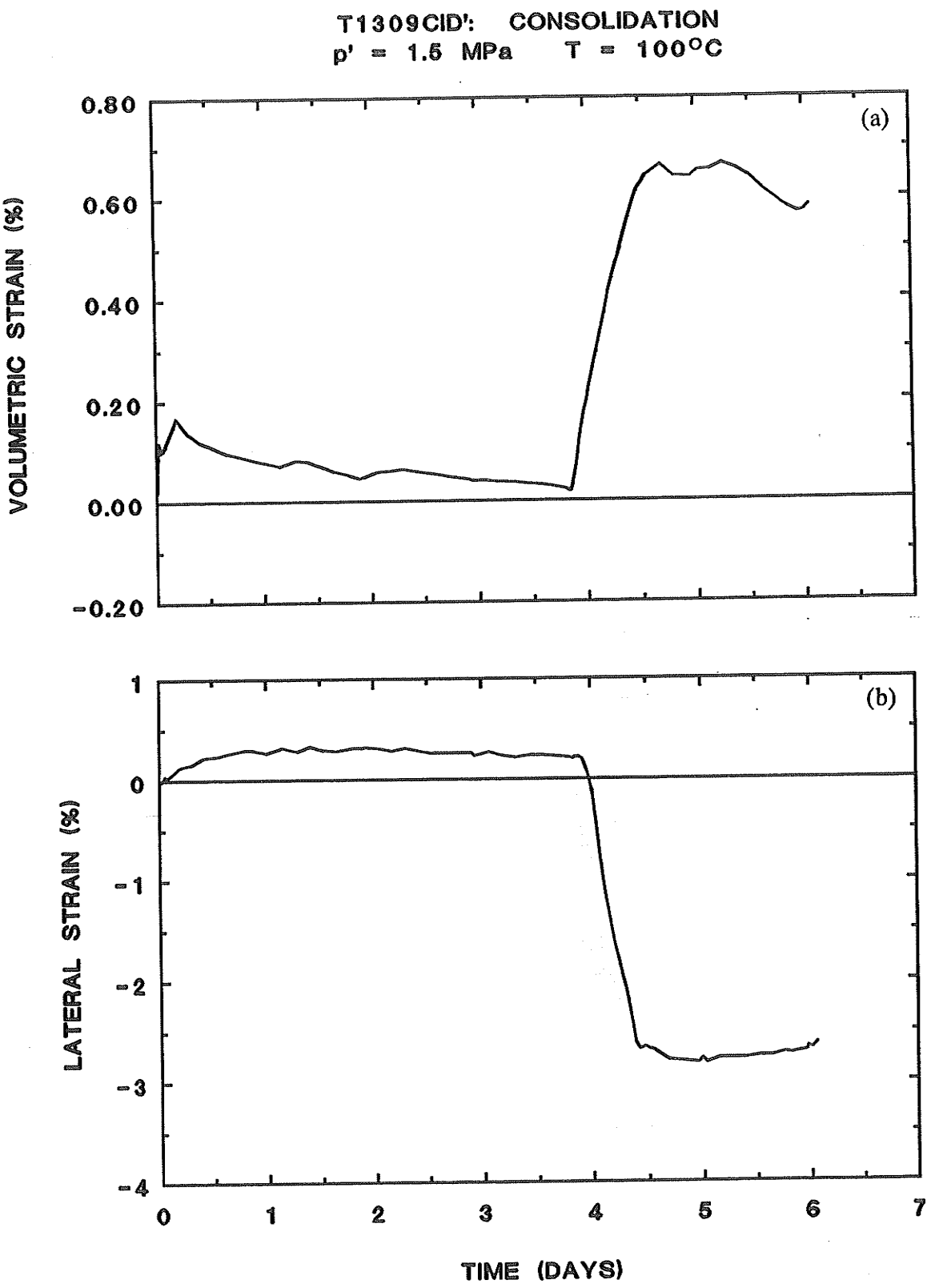

Fig. 5.18 Consolidation T1309. p' = 1.5 MPa, u_b = 1.0 MPa, T = 100°C

a) Volumetric Strain ε_v *vs.* Elapsed Time.

b) Lateral Strain ε_3 *vs.* Elapsed Time.

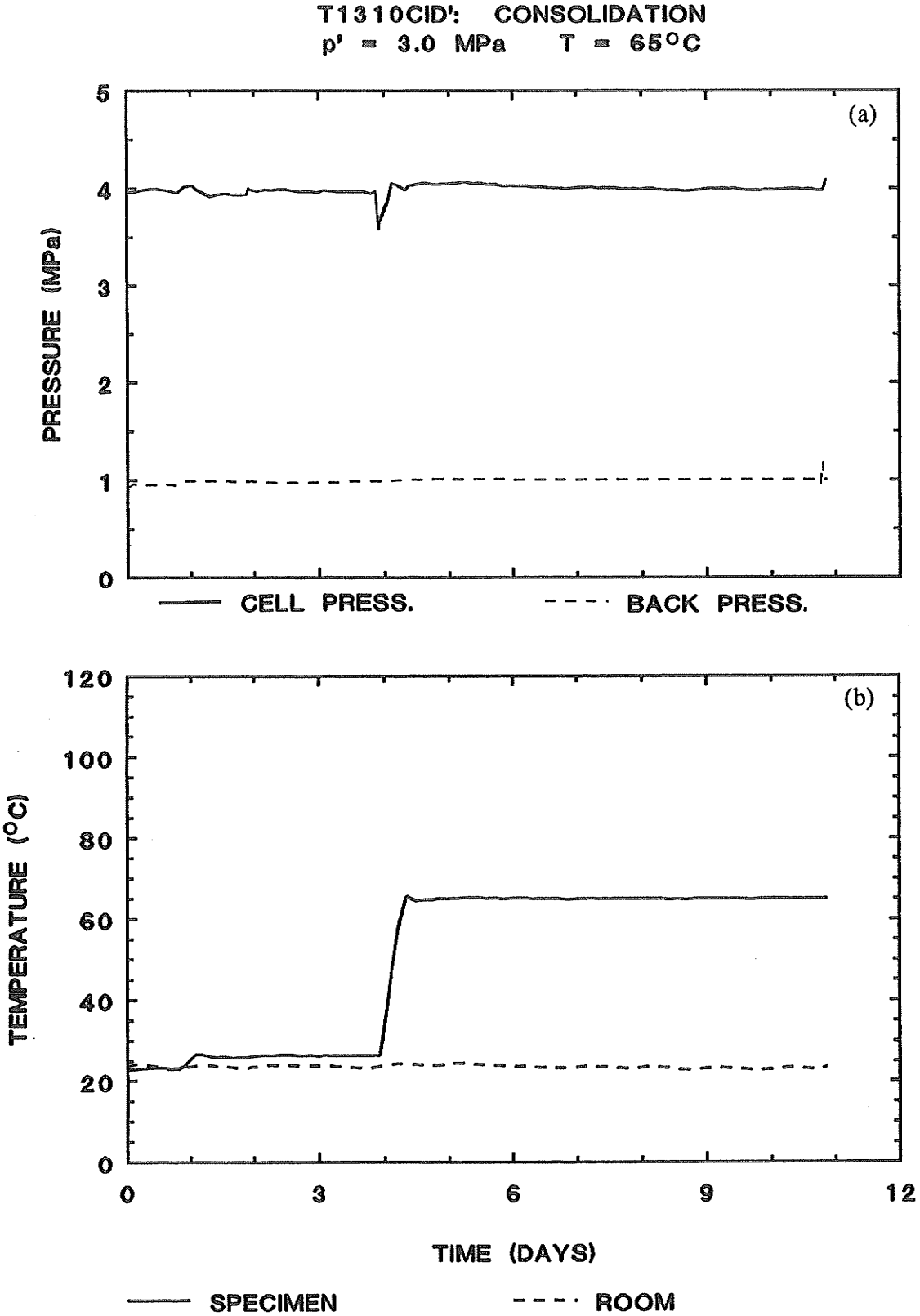

Fig. 5.19 Consolidation T1310. p' = 3.0 MPa, u_b = 1.0 MPa, T = 65°C

a) Cell σ_3 and Back Pressure u_b *vs.* Elapsed Time.

b) Specimen Temperature *vs.* Elapsed Time.

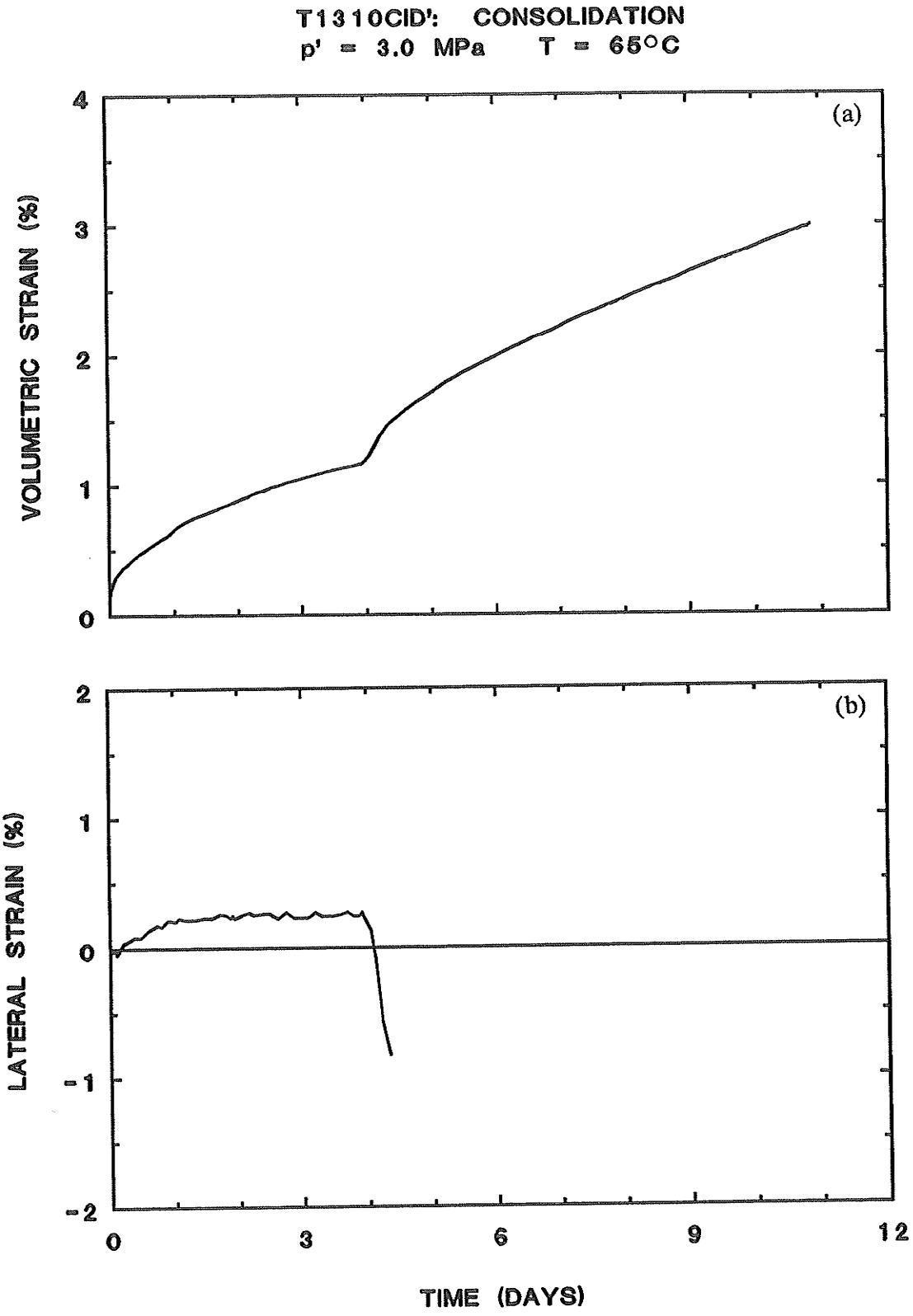

Fig. 5.20 Consolidation T1310. p' = 3.0 MPa, u_b = 1.0 MPa, T = 65°C

a) Volumetric Strain ε_v *vs.* Elapsed Time.

b) Lateral Strain ε_3 *vs.* Elapsed Time.

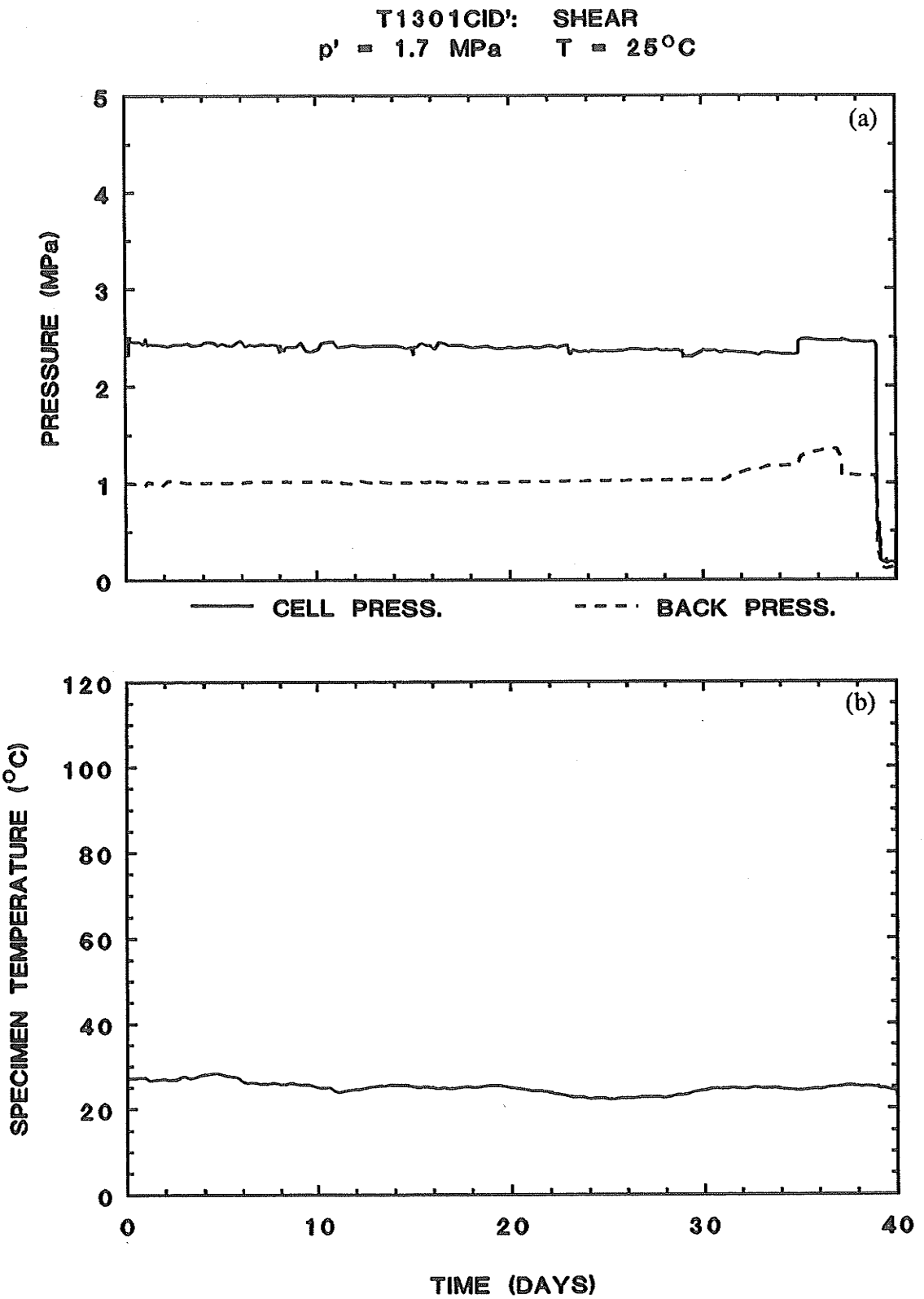

Fig. 5.21 Shear T1301. p' = 1.7 MPa, u_b = 1.0 MPa, T = 25°C

a) Cell σ_3 and Back Pressure u_b *vs.* Elapsed Time.

b) Specimen Temperature *vs.* Elapsed Time.

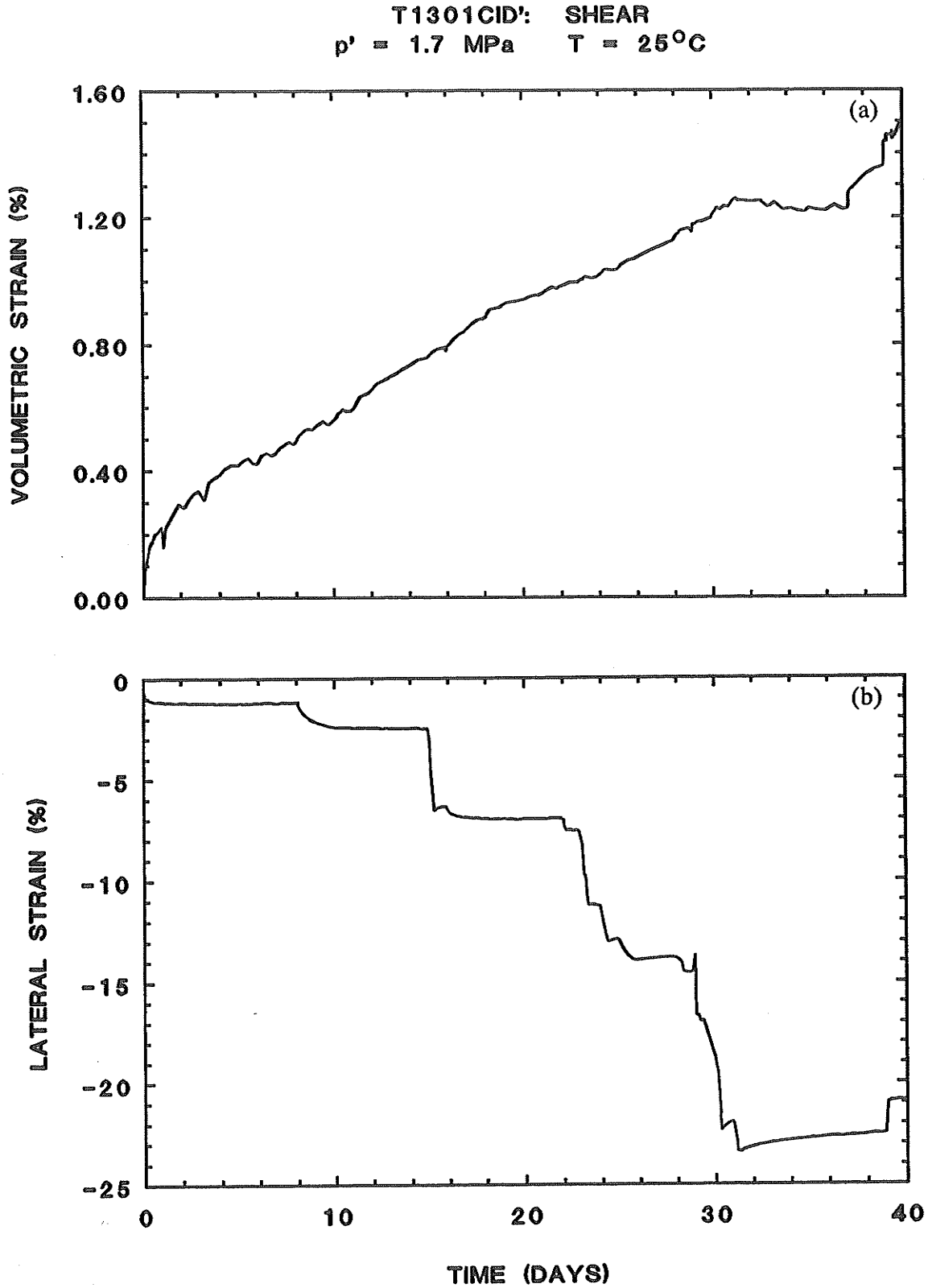

Fig. 5.22 Shear T1301. p' = 1.7 MPa, u_b = 1.0 MPa, T = 25°C

a) Volumetric Strain ε_v *vs.* Elapsed Time.

b) Lateral Strain ε_3 *vs.* Elapsed Time.

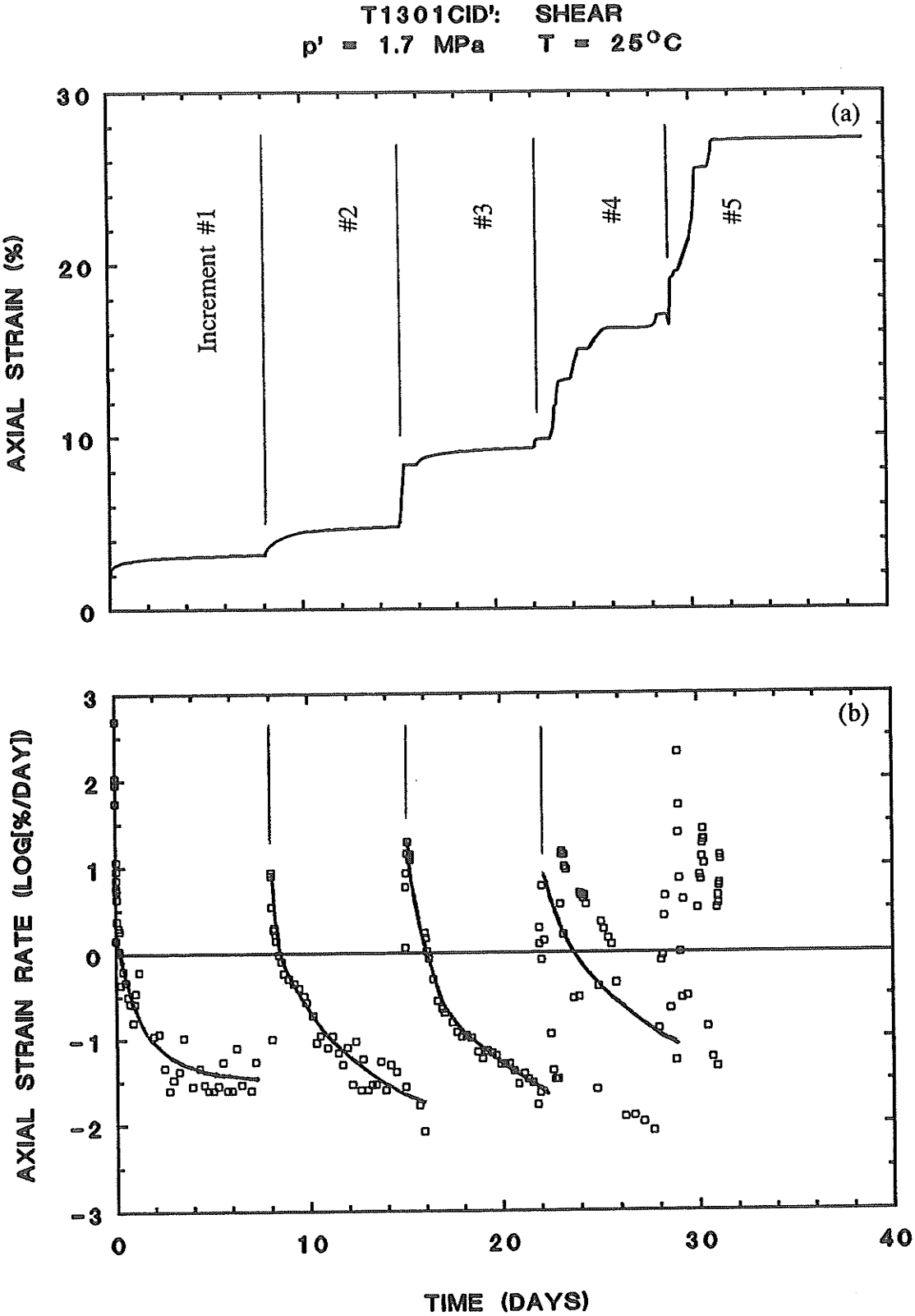

Fig. 5.23 Shear T1301. p' = 1.7 MPa, u_b = 1.0 MPa, T = 25°C

a) Axial Strain ε_1 *vs.* Elapsed Time.

b) Axial Strain Rate log $\dot{\varepsilon}_1$ *vs.* Elapsed Time.

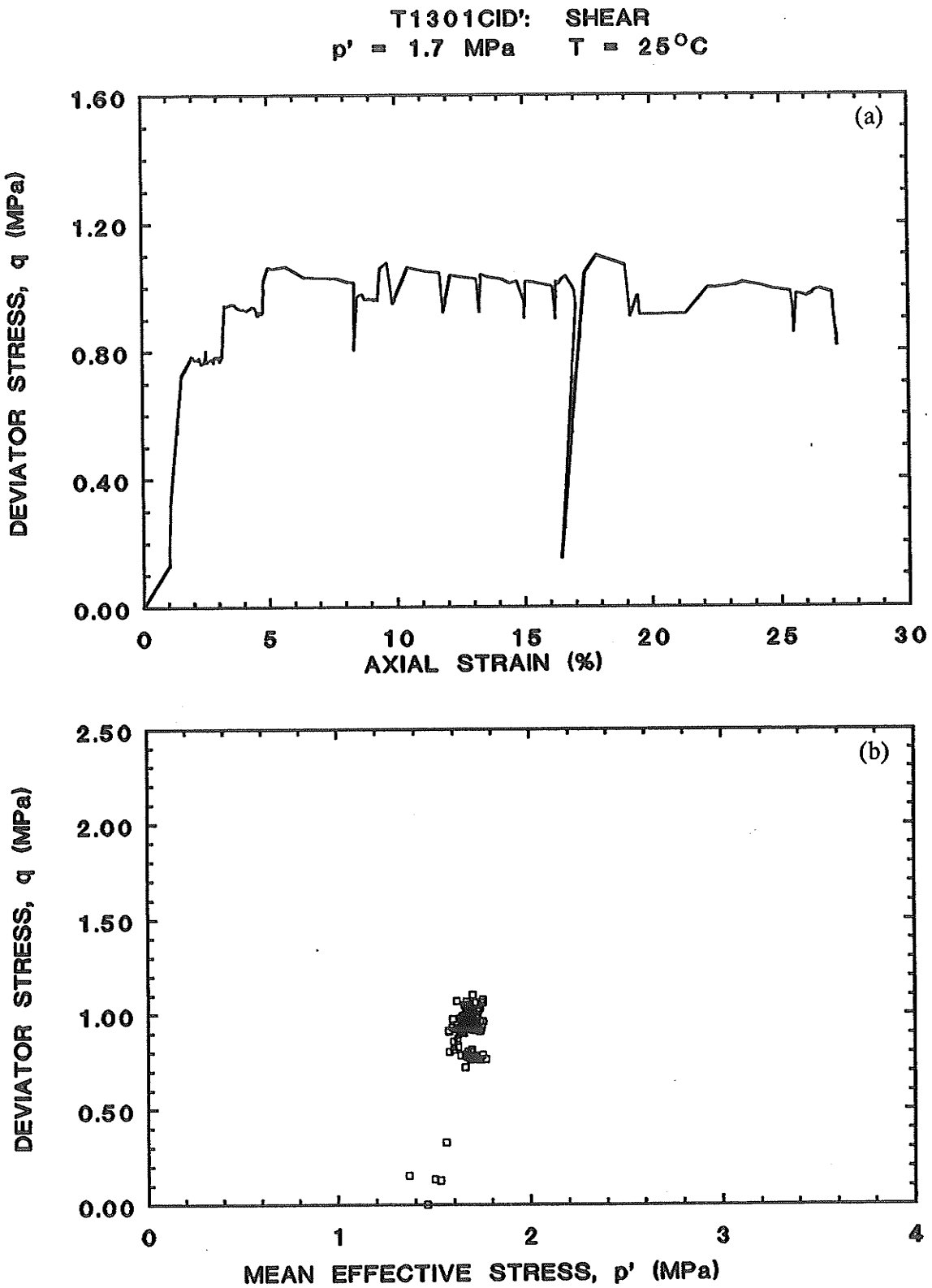

Fig. 5.24 Shear T1301. p' = 1.7 MPa, u_b = 1.0 MPa, T = 25°C

a) Deviator Stress q *vs.* Axial Strain ε_1.

b) Deviator Stress q *vs.* Mean Effective Stress p'.

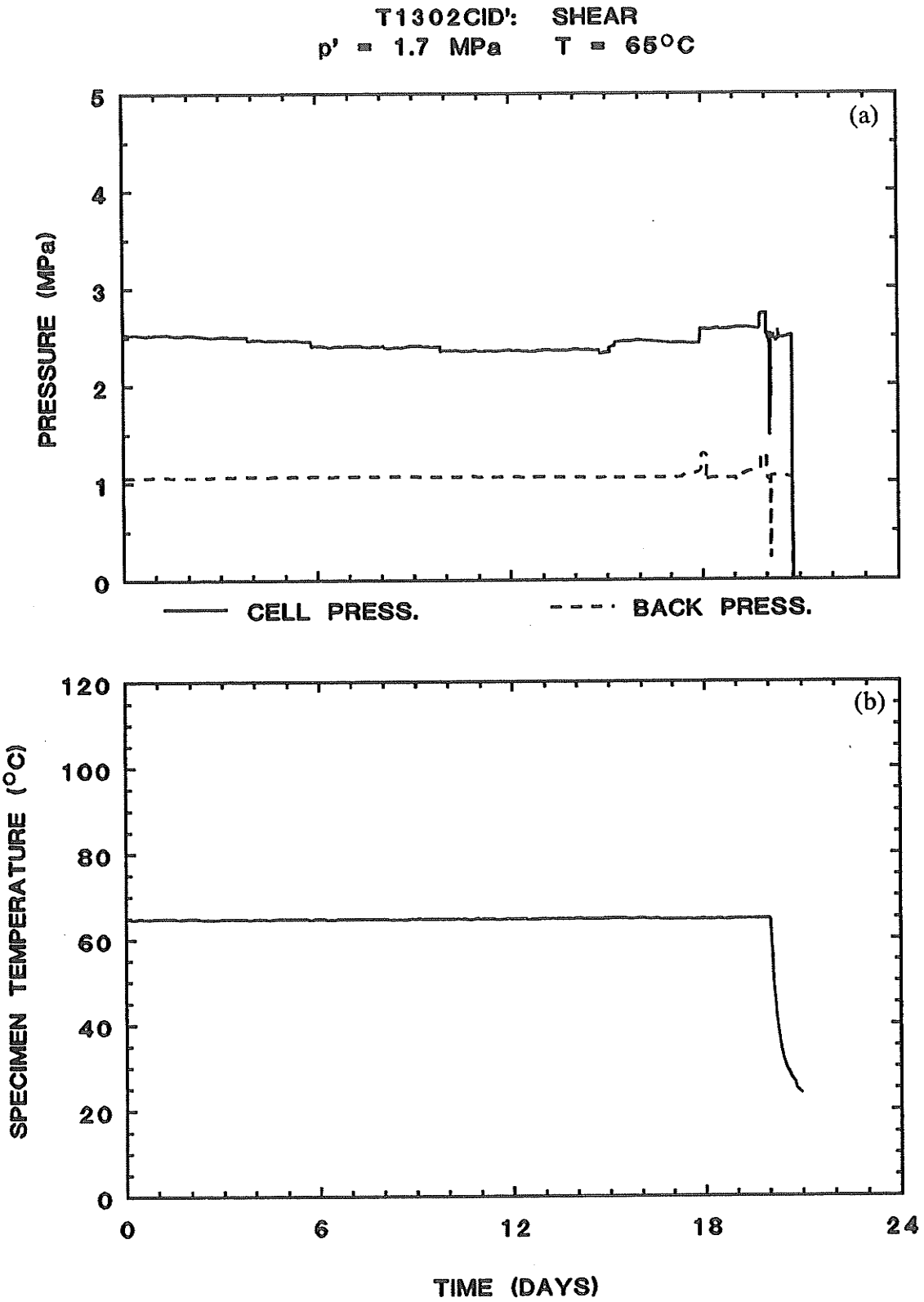

Fig. 5.25 Shear T1302. p' = 1.7 MPa, u_b = 1.0 MPa, T = 65°C

a) Cell σ_3 and Back Pressure u_b *vs.* Elapsed Time.

b) Specimen Temperature *vs.* Elapsed Time.

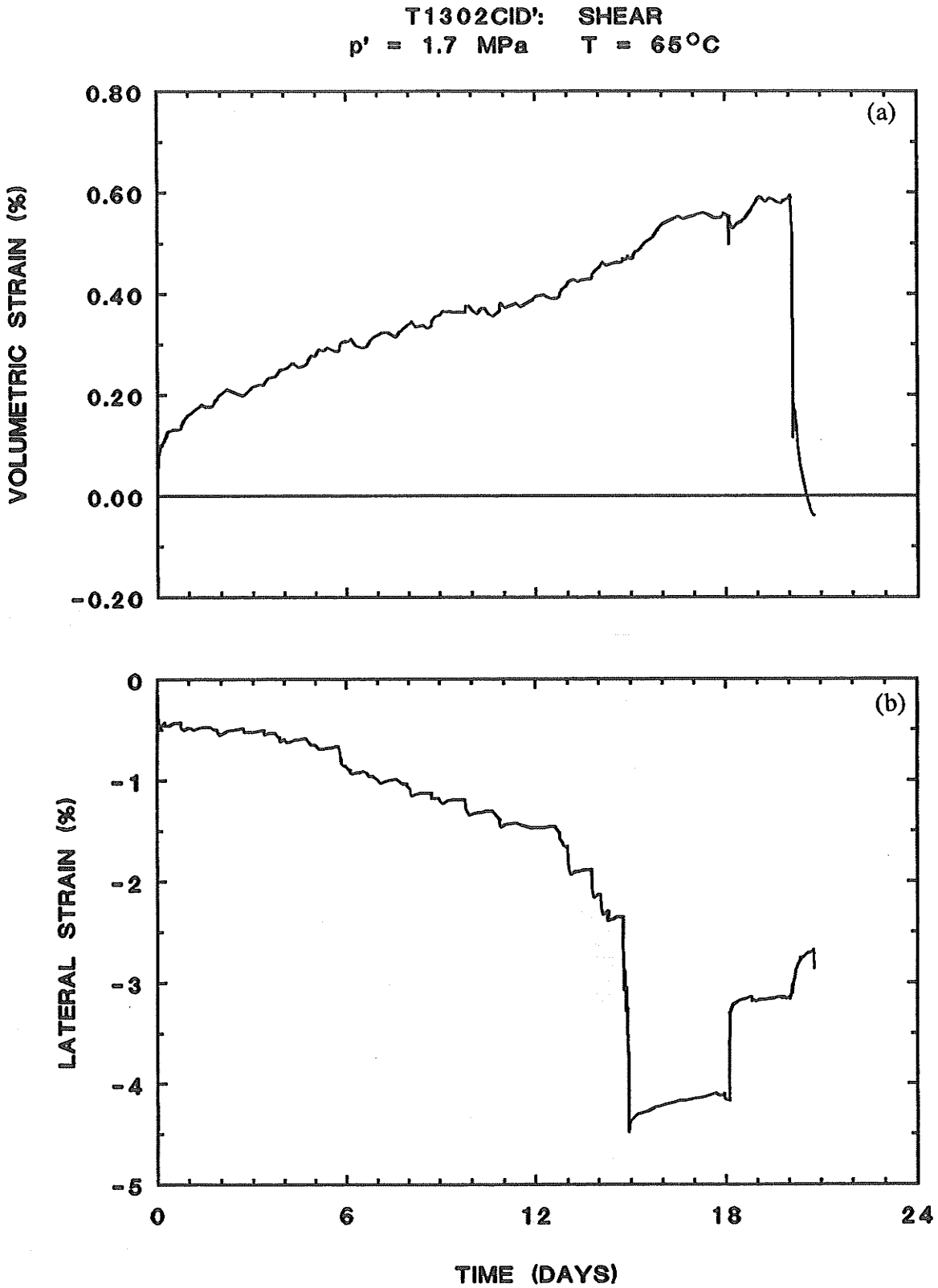

Fig. 5.26 Shear T1302. p' = 1.7 MPa, u_b = 1.0 MPa, T = 65°C

a) Volumetric Strain ε_v *vs.* Elapsed Time.

b) Lateral Strain ε_3 *vs.* Elapsed Time.

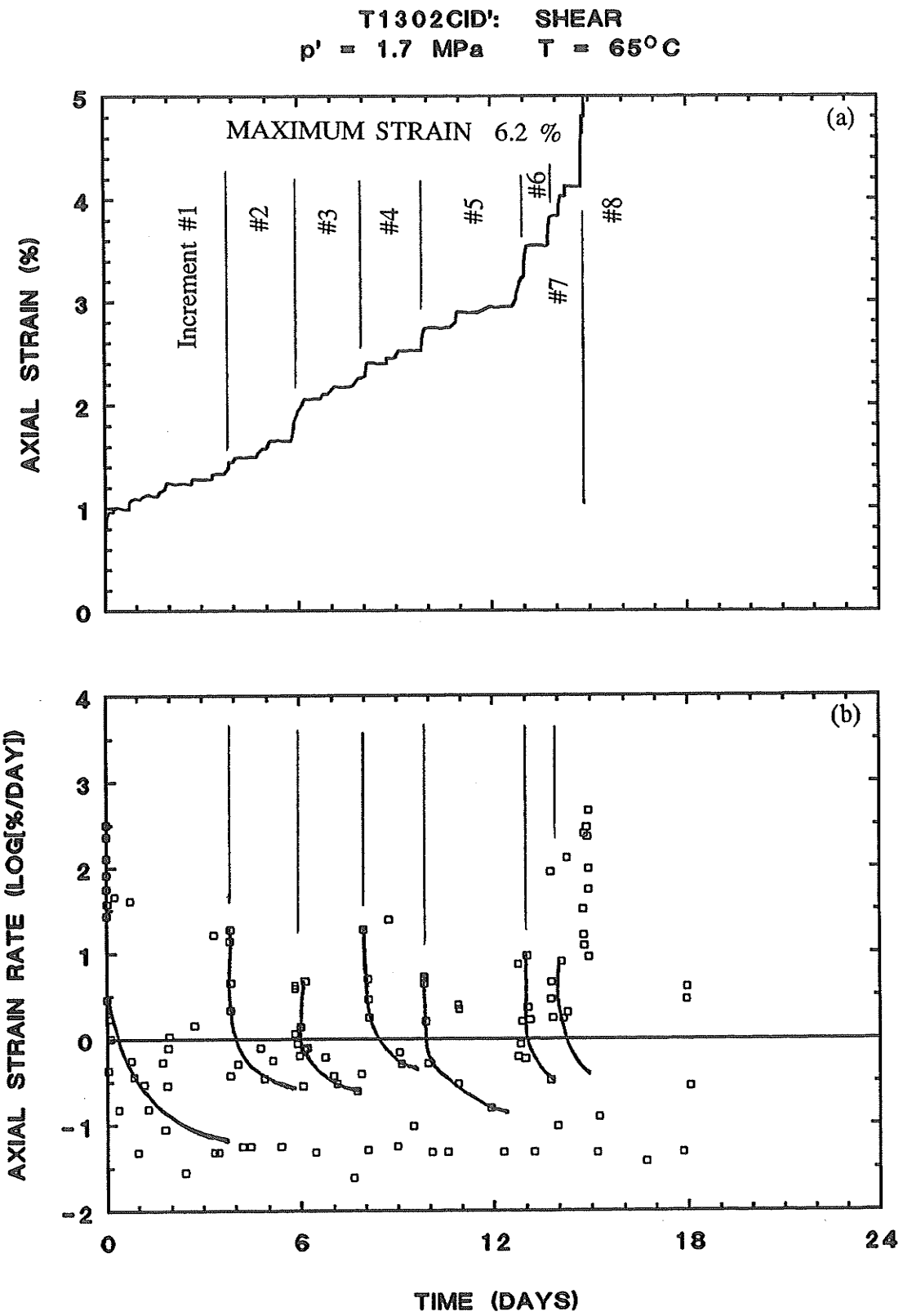

Fig. 5.27 Shear T1302. p' = 1.7 MPa, u_b = 1.0 MPa, T = 65°C

a) Axial Strain ε_1 *vs.* Elapsed Time.

b) Axial Strain Rate log $\dot{\varepsilon}_1$ *vs.* Elapsed Time.

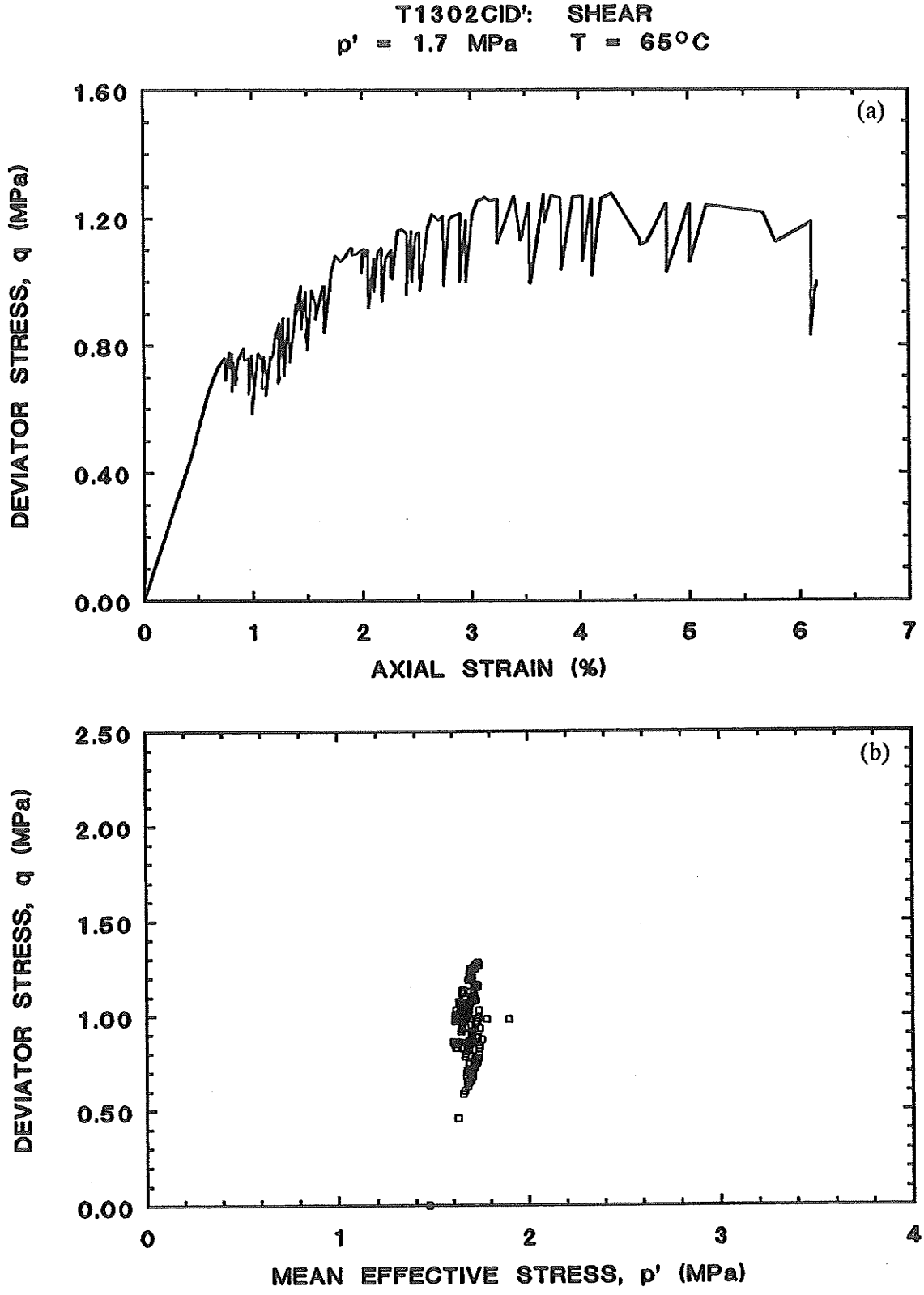

Fig. 5.28 Shear T1302. p' = 1.7 MPa, u_b = 1.0 MPa, T = 65°C

a) Deviator Stress q *vs.* Axial Strain ε_1.

b) Deviator Stress q *vs.* Mean Effective Stress p'.

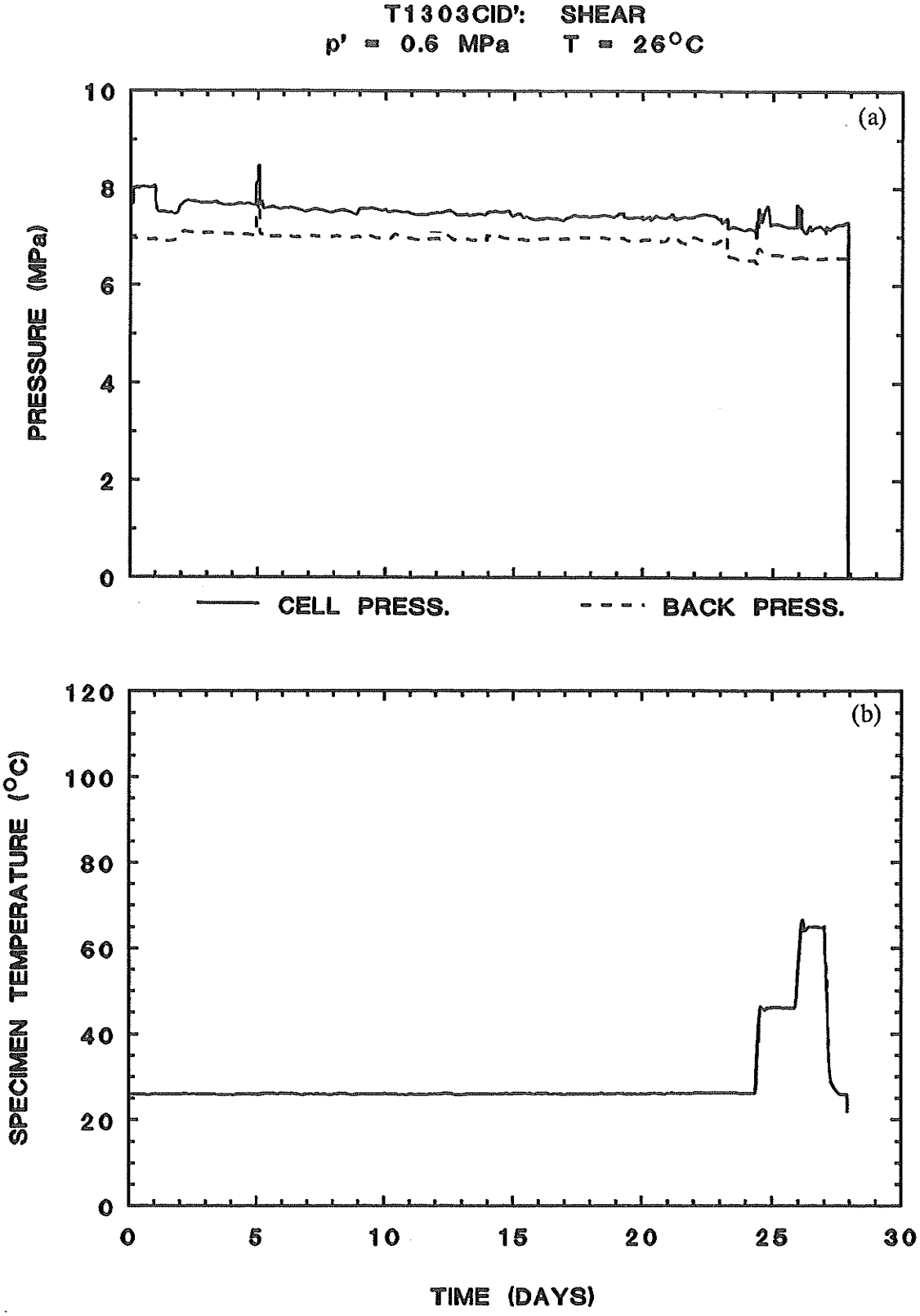

Fig. 5.29 Shear T1303. p' = 0.6 MPa, u_b = 7.0 MPa, T = 26°C

a) Cell σ_3 and Back Pressure u_b *vs.* Elapsed Time.

b) Specimen Temperature *vs.* Elapsed Time.

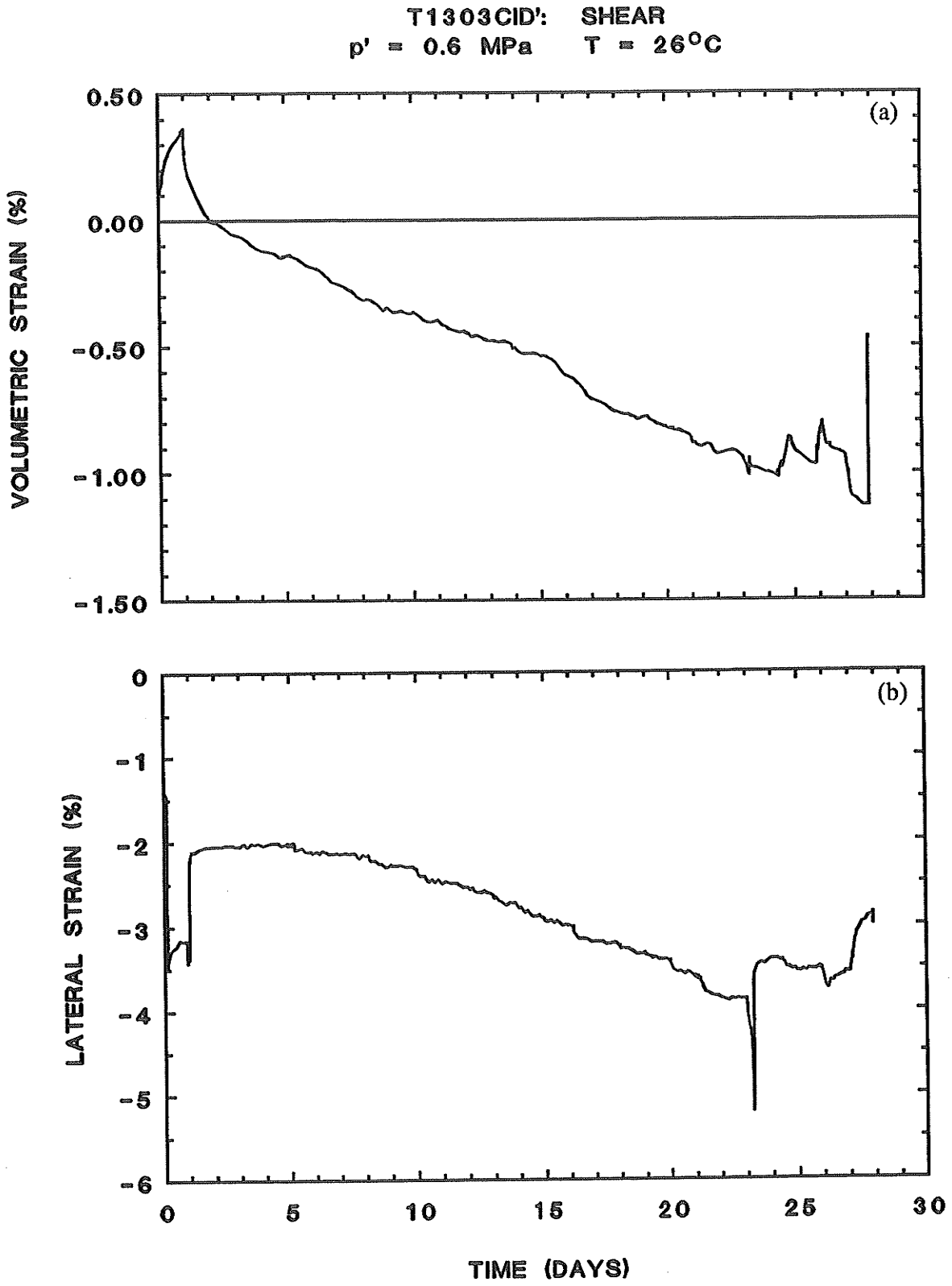

Fig. 5.30 Shear T1303. p' = 0.6 MPa, u_b = 7.0 MPa, T = 26°C

a) Volumetric Strain ε_v *vs.* Elapsed Time.

b) Lateral Strain ε_3 *vs.* Elapsed Time.

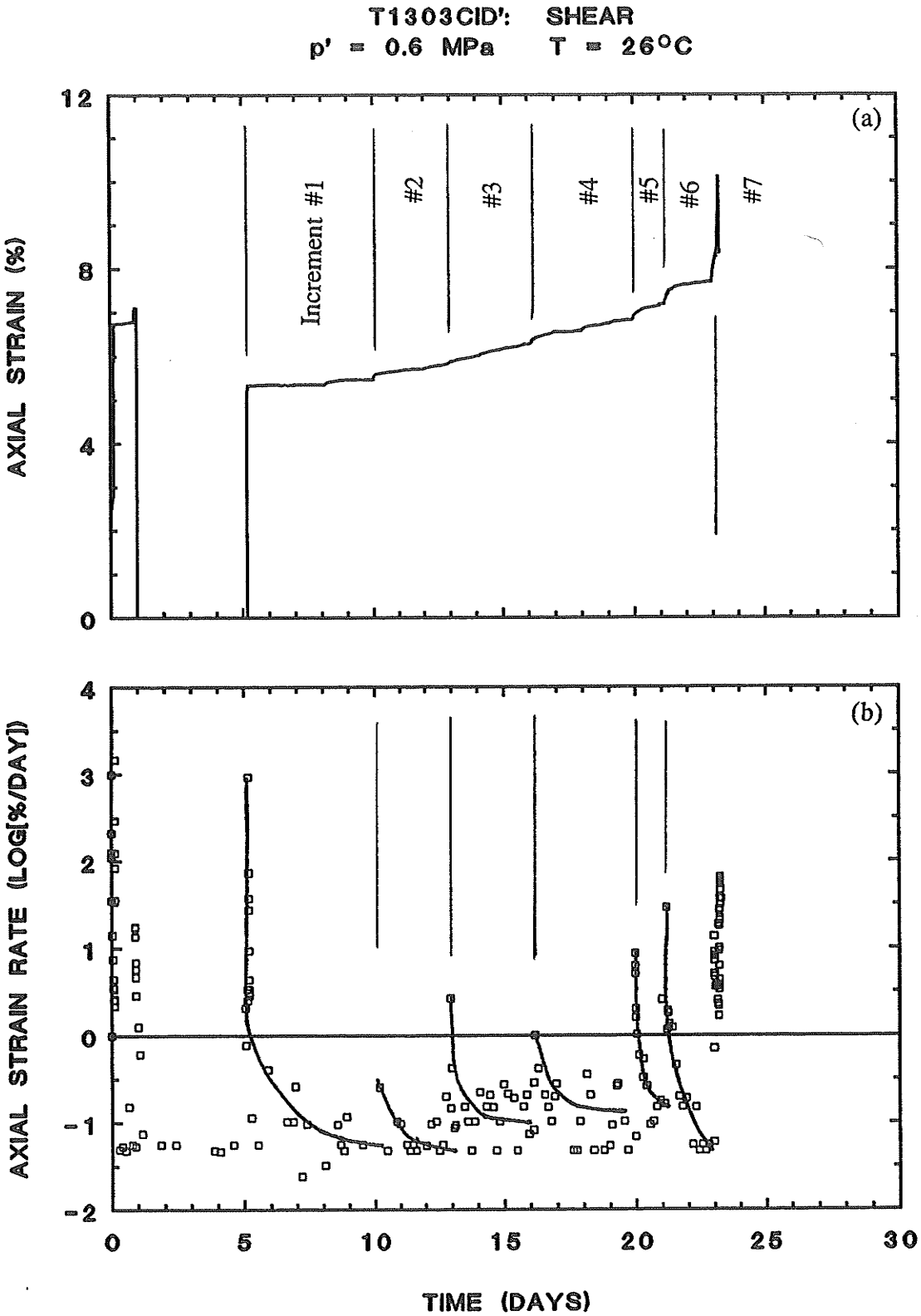

Fig. 5.31 Shear T1303. p' = 0.6 MPa, u_b = 7.0 MPa, T = 26°C

a) Axial Strain ε_1 *vs.* Elapsed Time.

b) Axial Strain Rate log $\dot{\varepsilon}_1$ *vs.* Elapsed Time.

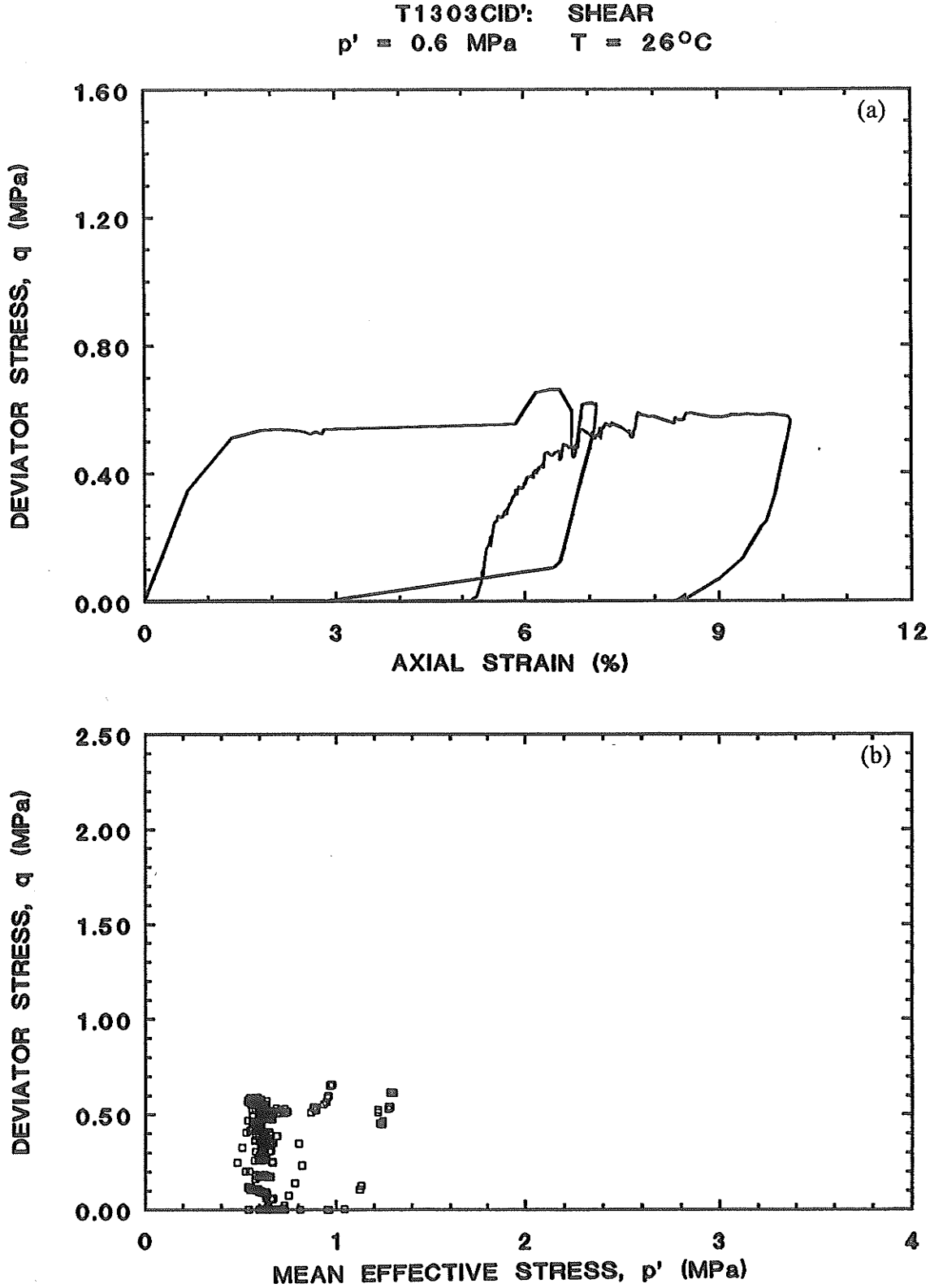

Fig. 5.32 Shear T1303. p' = 0.6 MPa, u_b = 7.0 MPa, T = 26°C

a) Deviator Stress q *vs.* Axial Strain ε_1.

b) Deviator Stress q *vs.* Mean Effective Stress p'.

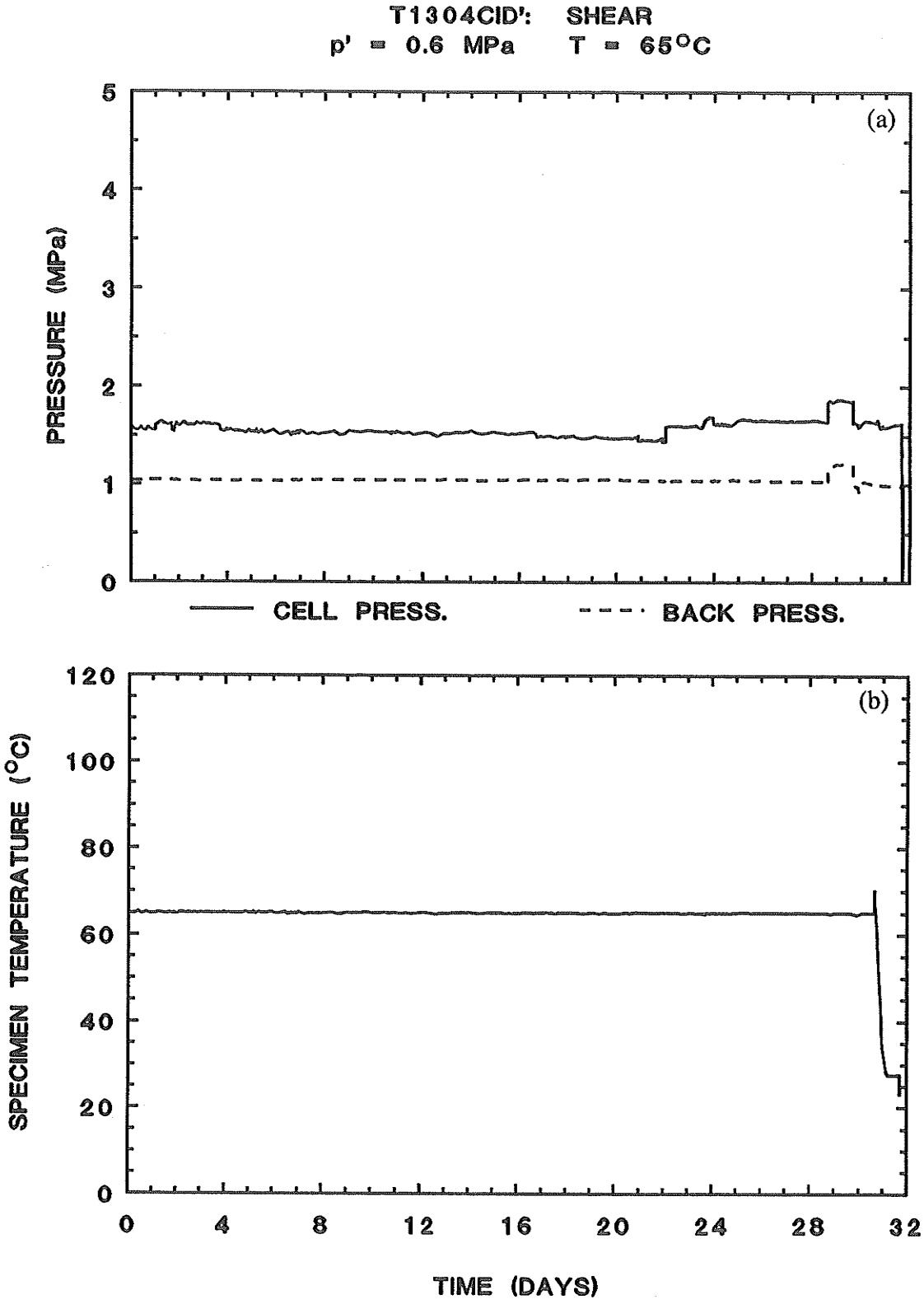

Fig. 5.33 Shear T1304. p' = 0.6 MPa, u_b = 1.0 MPa, T = 65°C
a) Cell σ_3 and Back Pressure u_b *vs.* Elapsed Time.
b) Specimen Temperature *vs.* Elapsed Time.

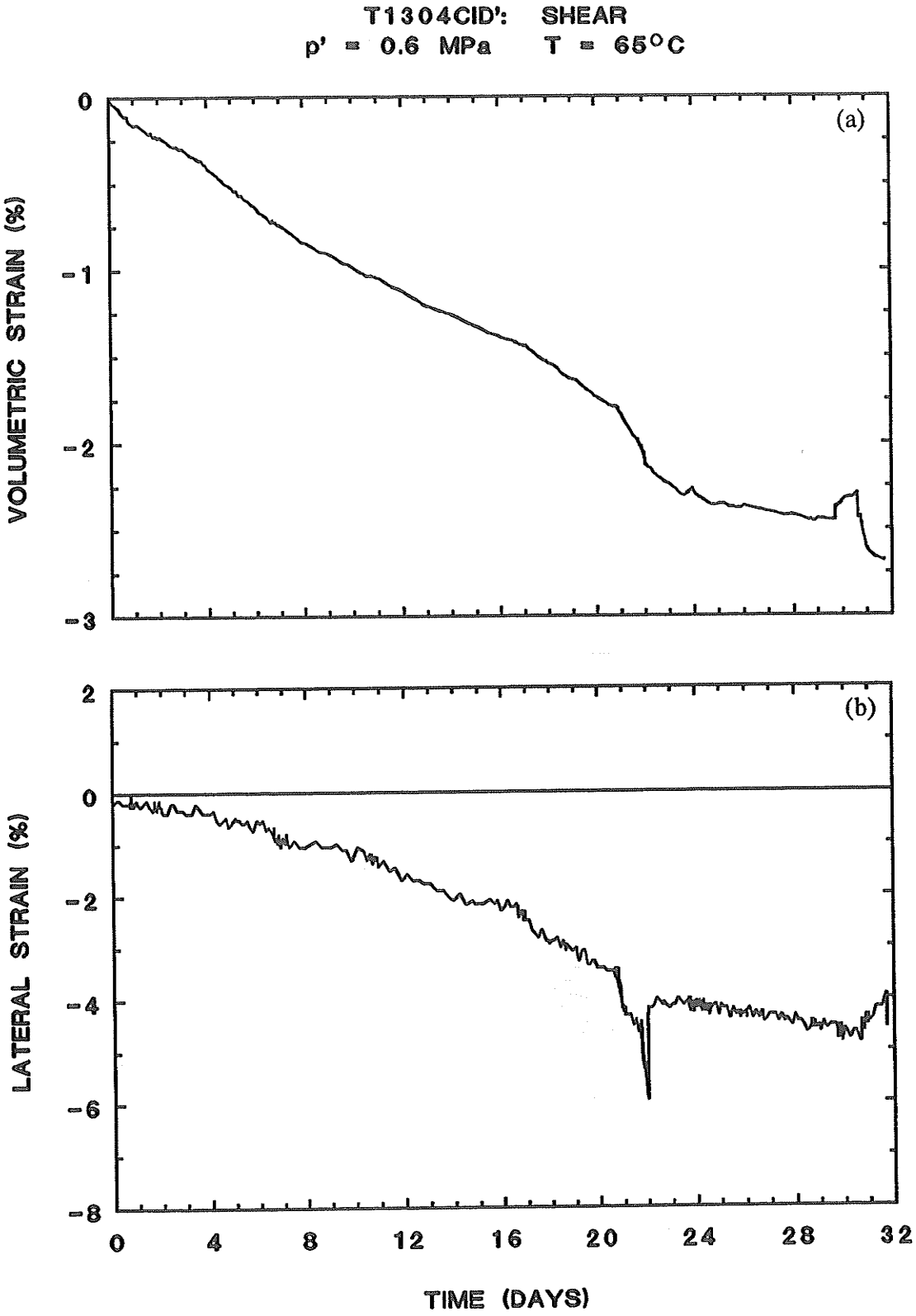

Fig. 5.34 Shear T1304. p' = 0.6 MPa, u_b = 1.0 MPa, T = 65°C

a) Volumetric Strain ε_v *vs.* Elapsed Time.

b) Lateral Strain ε_3 *vs.* Elapsed Time.

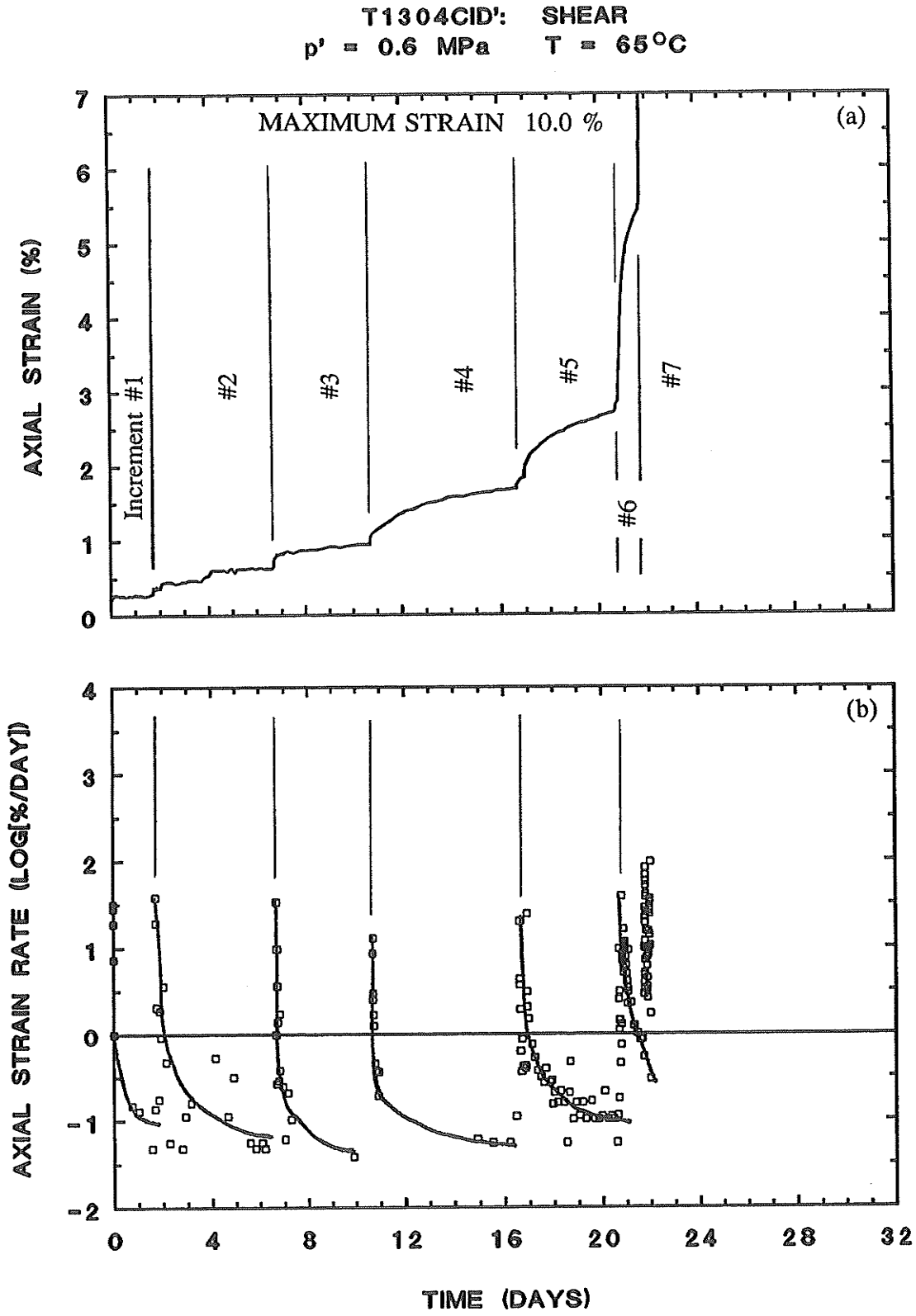

Fig. 5.35 Shear T1304. p' = 0.6 MPa, u_b = 1.0 MPa, T = 65°C

a) Axial Strain ε_1 *vs.* Elapsed Time.

b) Axial Strain Rate log $\dot{\varepsilon}_1$ *vs.* Elapsed Time.

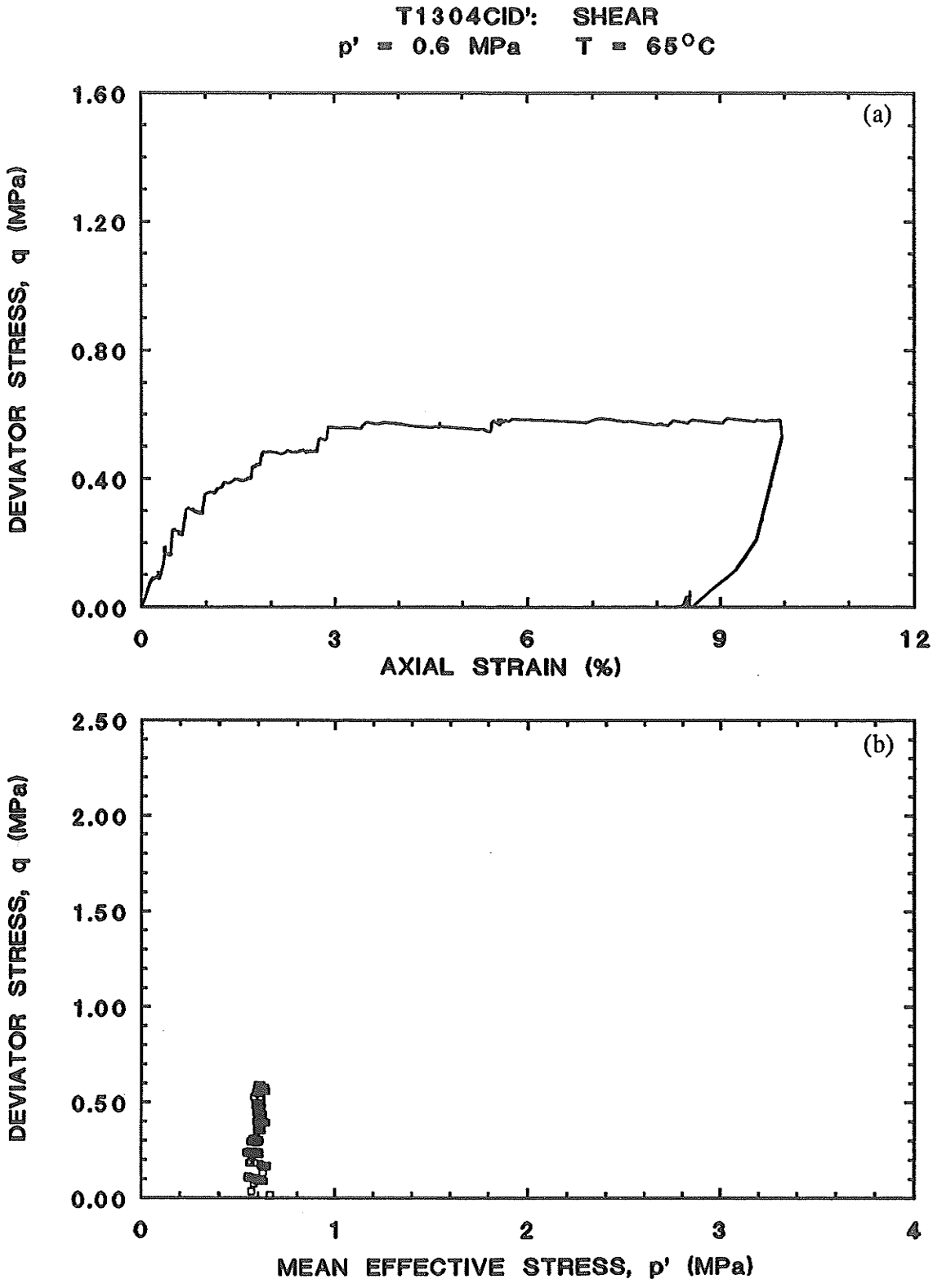

Fig. 5.36 Shear T1304. p' = 0.6 MPa, u_b = 1.0 MPa, T = 65°C

a) Deviator Stress q *vs.* Axial Strain ε_1.

b) Deviator Stress q *vs.* Mean Effective Stress p'.

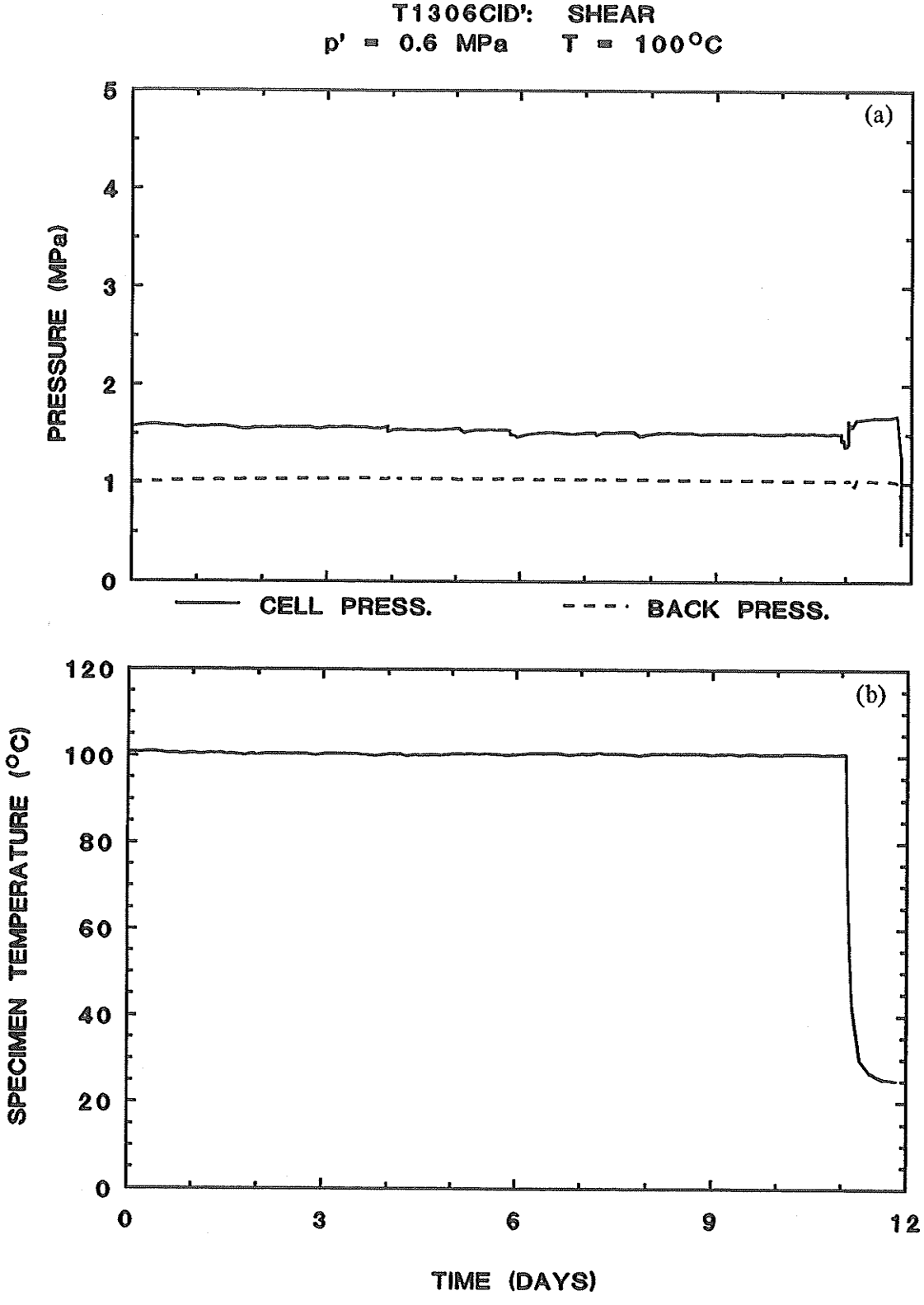

Fig. 5.37 Shear T1306. p' = 0.6 MPa, u_b = 1.0 MPa, T = 100°C

a) Cell σ_3 and Back Pressure u_b *vs.* Elapsed Time.

b) Specimen Temperature *vs.* Elapsed Time.

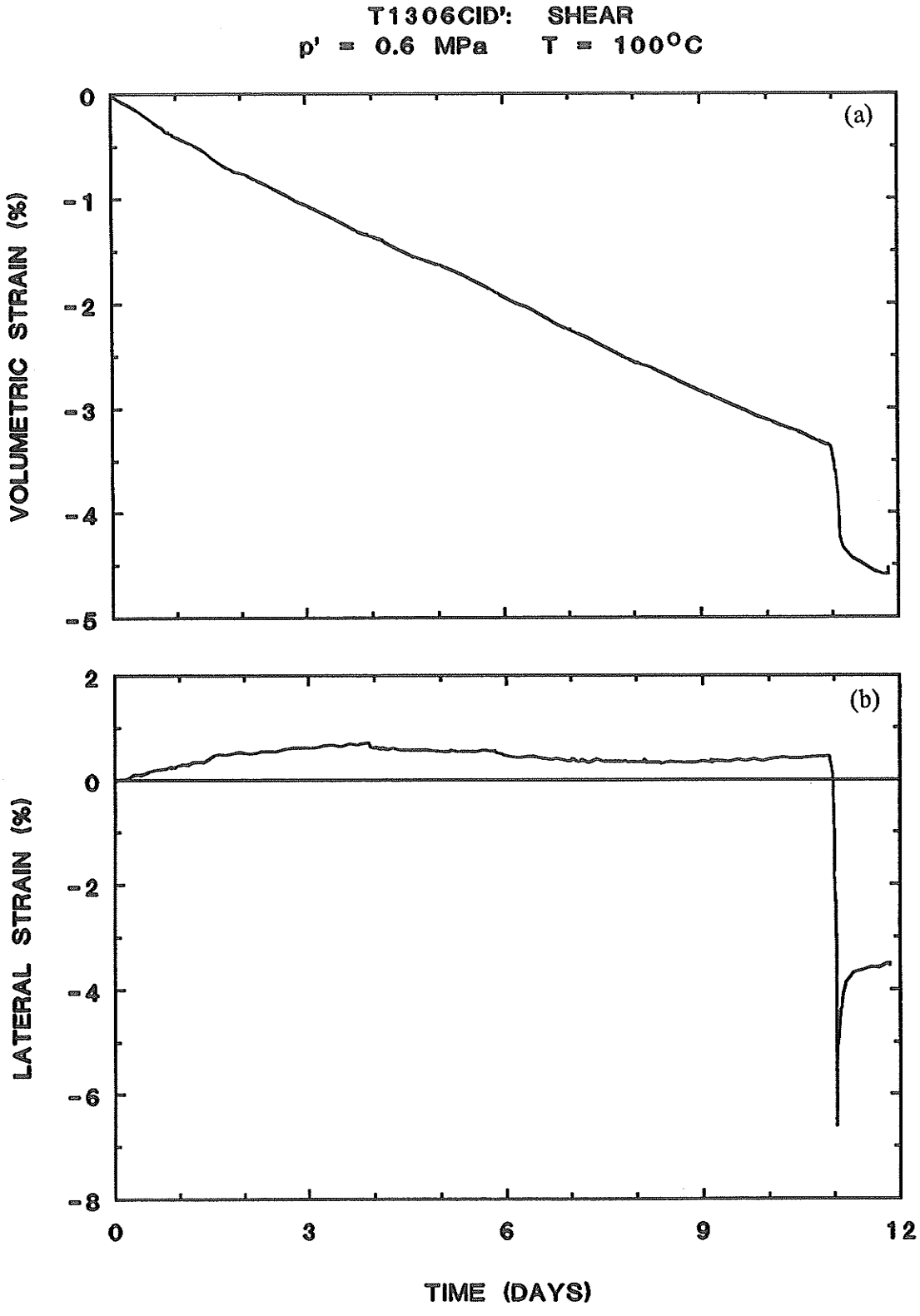

Fig. 5.38 Shear T1306. p' = 0.6 MPa, u_b = 1.0 MPa, T = 100°C

a) Volumetric Strain ε_v *vs.* Elapsed Time.

b) Lateral Strain ε_3 *vs.* Elapsed Time.

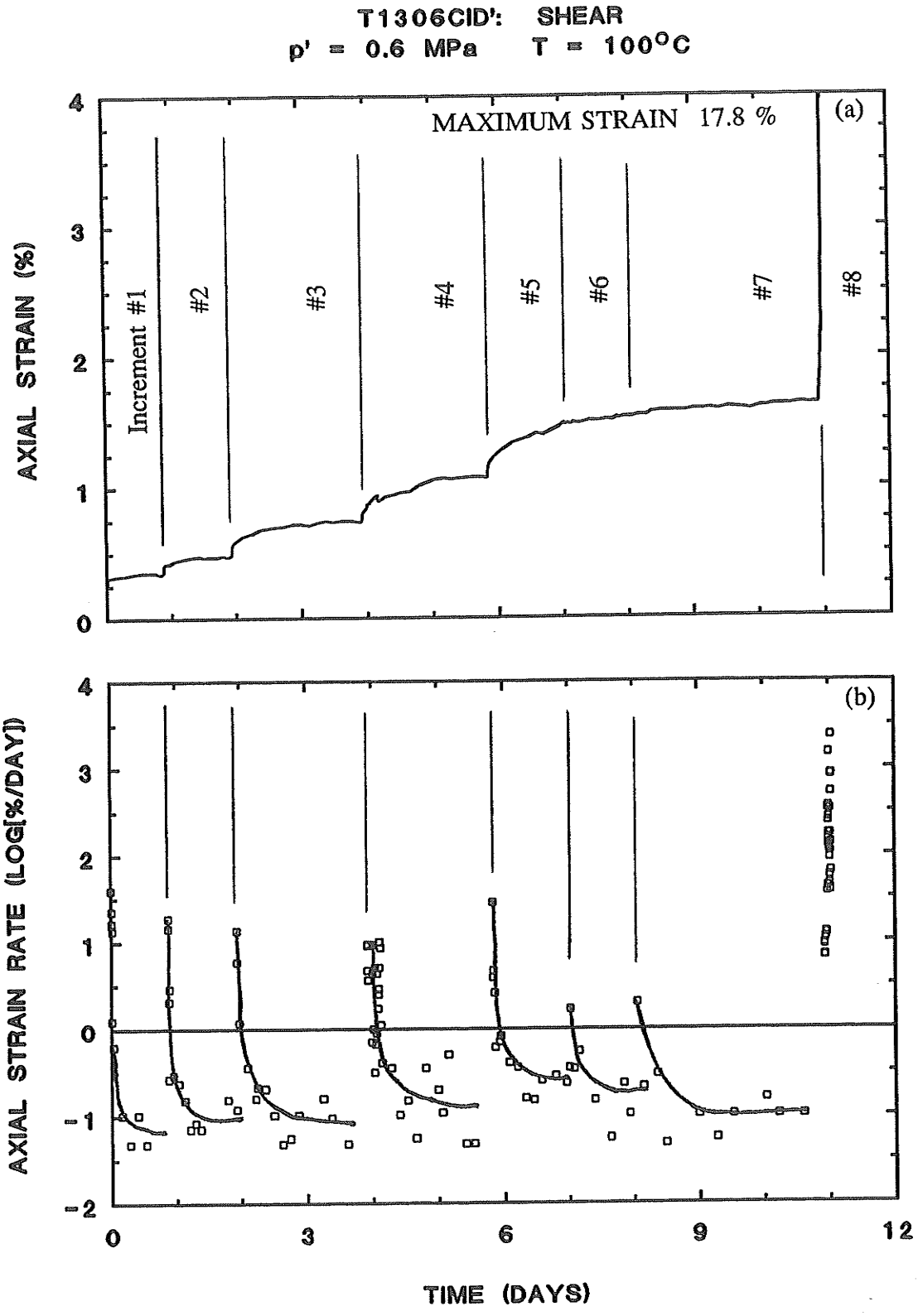

Fig. 5.39 Shear T1306. p' = 0.6 MPa, u_b = 1.0 MPa, T = 100°C

a) Axial Strain ε_1 *vs.* Elapsed Time.

b) Axial Strain Rate log $\dot{\varepsilon}_1$ *vs.* Elapsed Time.

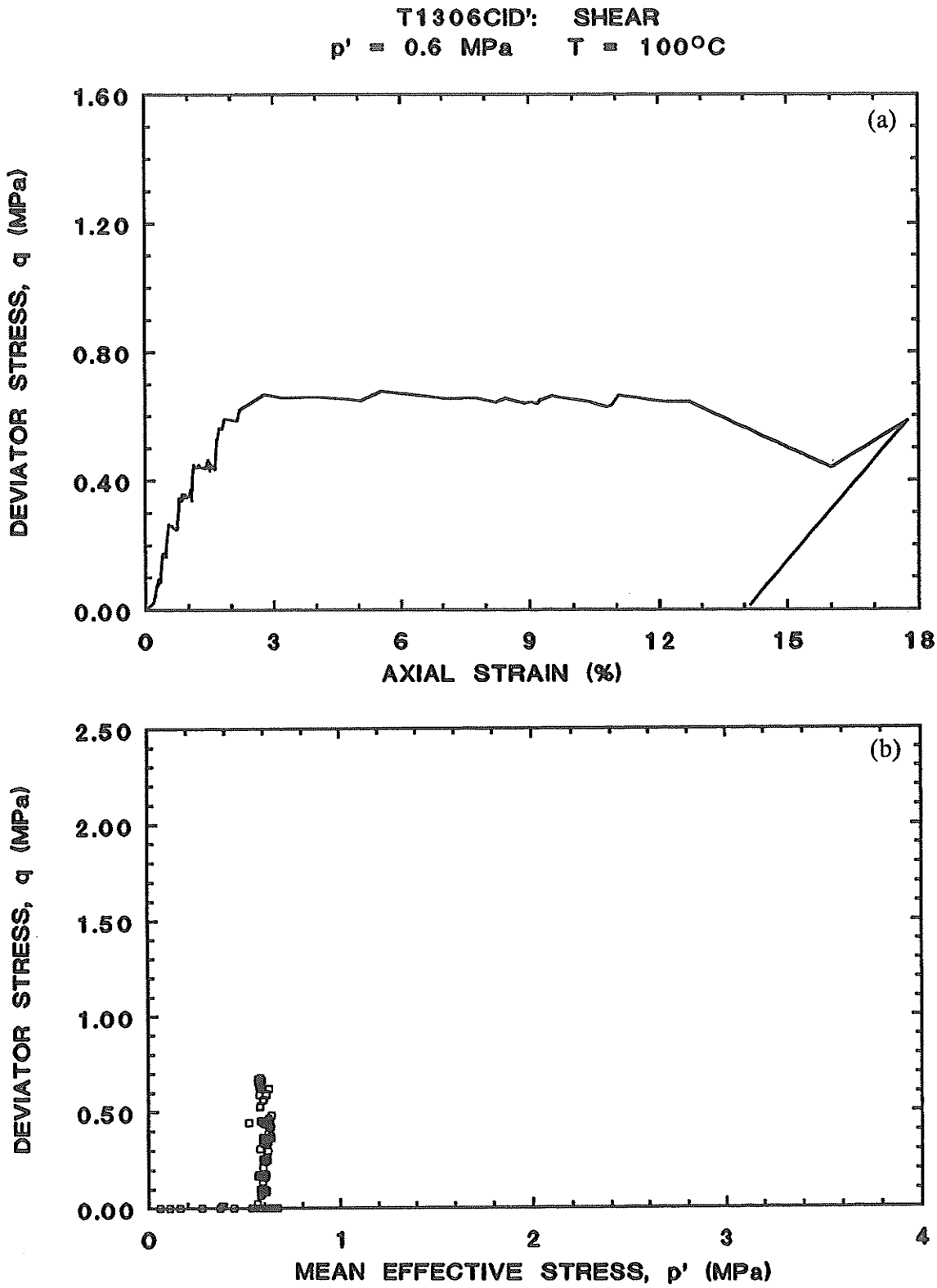

Fig. 5.40 Shear T1306. p' = 0.6 MPa, u_b = 1.0 MPa, T = 100°C

a) Deviator Stress q *vs.* Axial Strain ε_1.

b) Deviator Stress q *vs.* Mean Effective Stress p'.

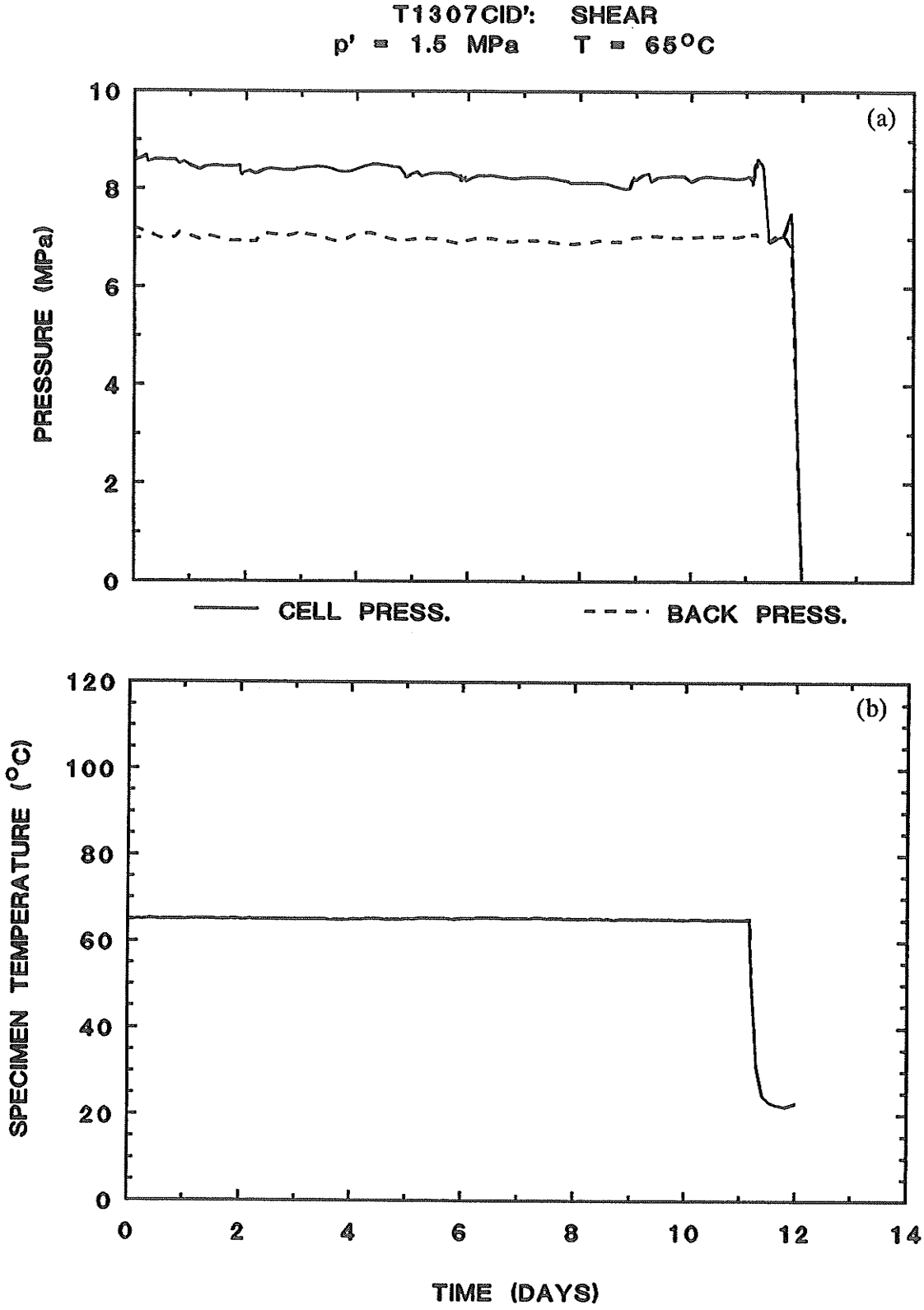

Fig. 5.41 Shear T1307. p' = 1.5 MPa, u_b = 7.0 MPa, T = 65°C
a) Cell σ_3 and Back Pressure u_b *vs.* Elapsed Time.
b) Specimen Temperature *vs.* Elapsed Time.

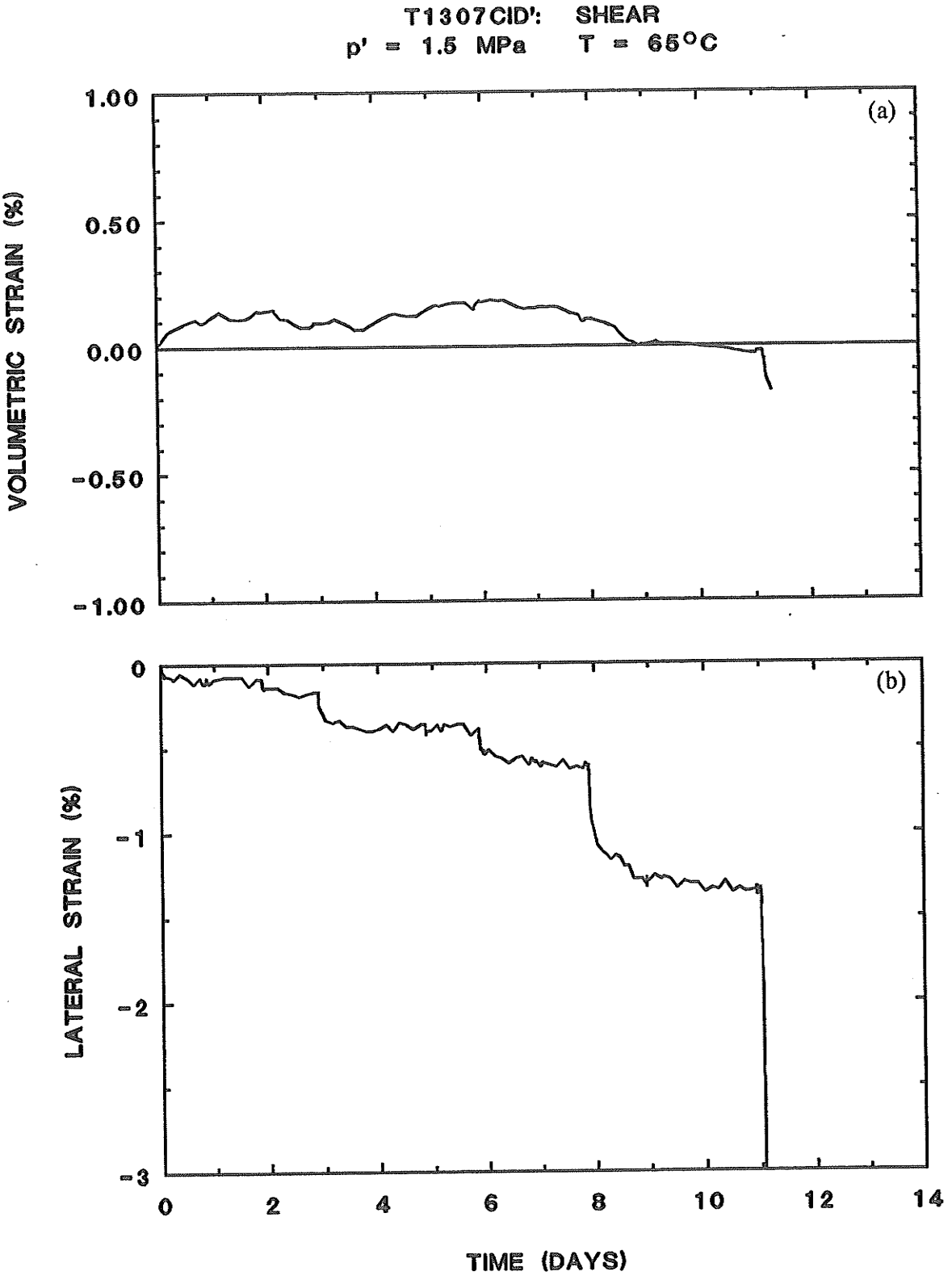

Fig. 5.42 Shear T1307. p' = 1.5 MPa, u_b = 7.0 MPa, T = 65°C

a) Volumetric Strain ε_v *vs.* Elapsed Time.

b) Lateral Strain ε_3 *vs.* Elapsed Time.

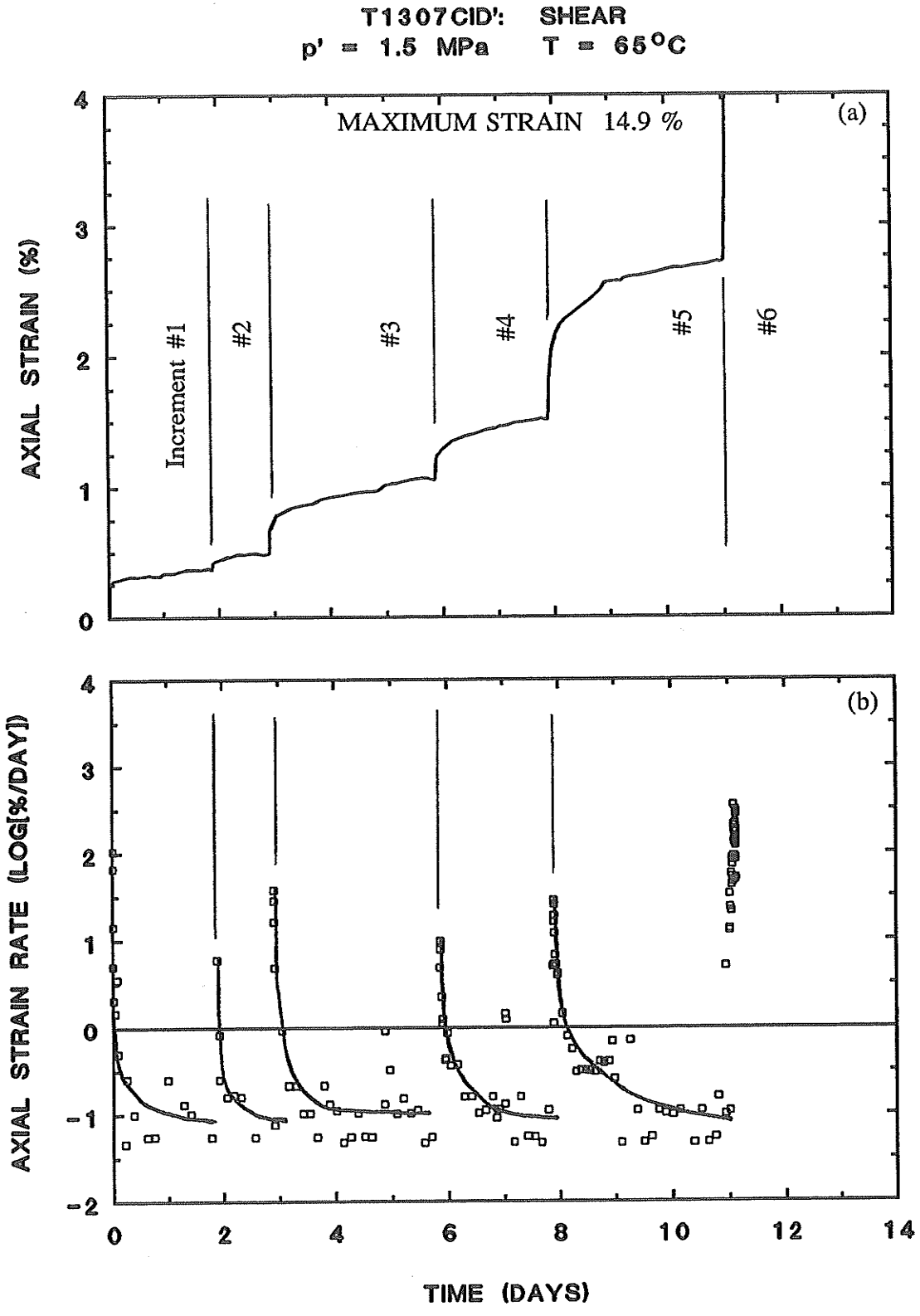

Fig. 5.43 Shear T1307. p' = 1.5 MPa, u_b = 7.0 MPa, T = 65°C

a) Axial Strain ε_1 *vs.* Elapsed Time.

b) Axial Strain Rate log $\dot{\varepsilon}_1$ *vs.* Elapsed Time.

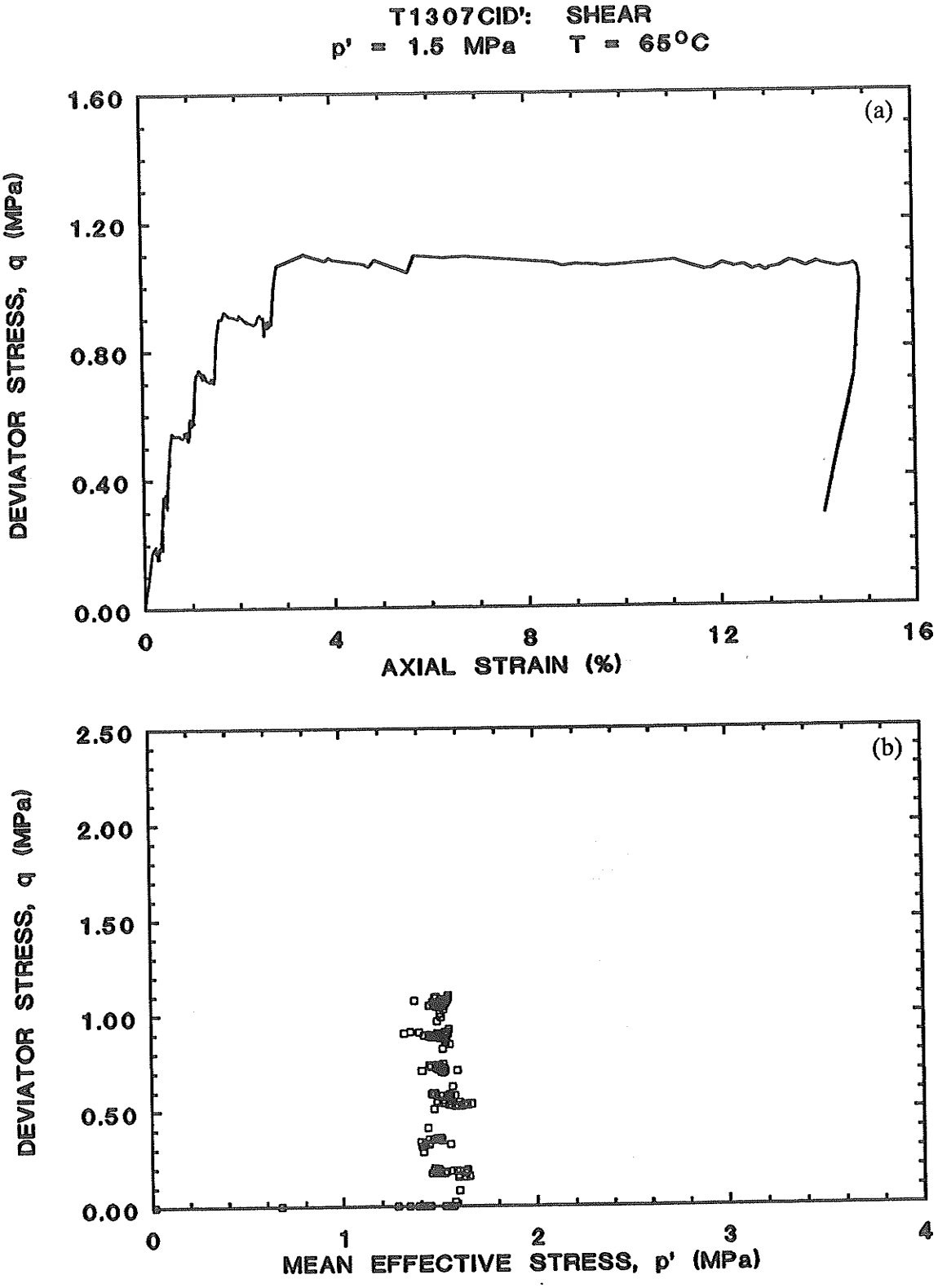

Fig. 5.44 Shear T1307. p' = 1.5 MPa, u_b = 7.0 MPa, T = 65°C

a) Deviator Stress q *vs.* Axial Strain ε_1.

b) Deviator Stress q *vs.* Mean Effective Stress p'.

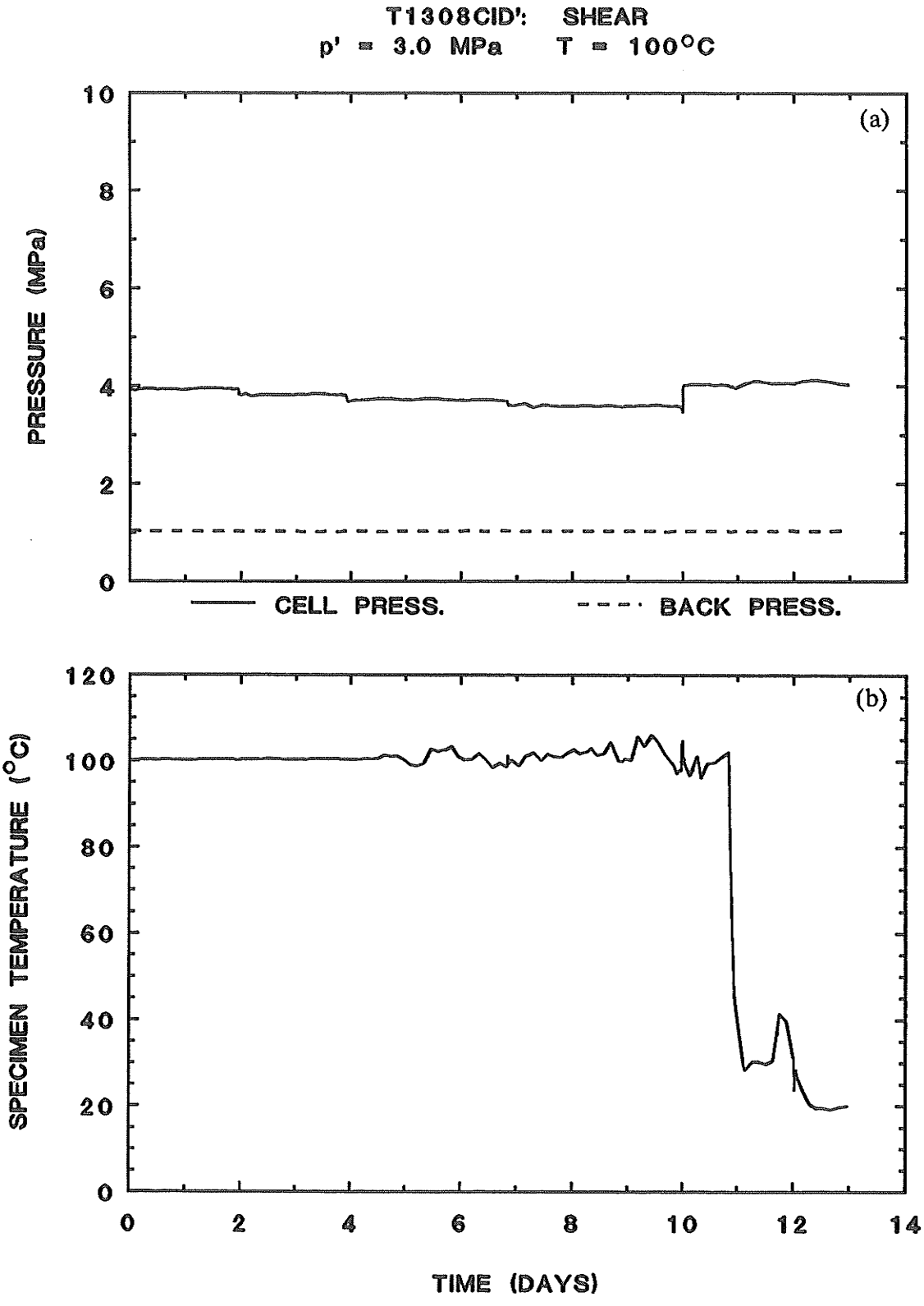

Fig. 5.45 Shear T1308. p' = 3.0 MPa, u_b = 1.0 MPa, T = 100°C

a) Cell σ_3 and Back Pressure u_b *vs.* Elapsed Time.

b) Specimen Temperature *vs.* Elapsed Time.

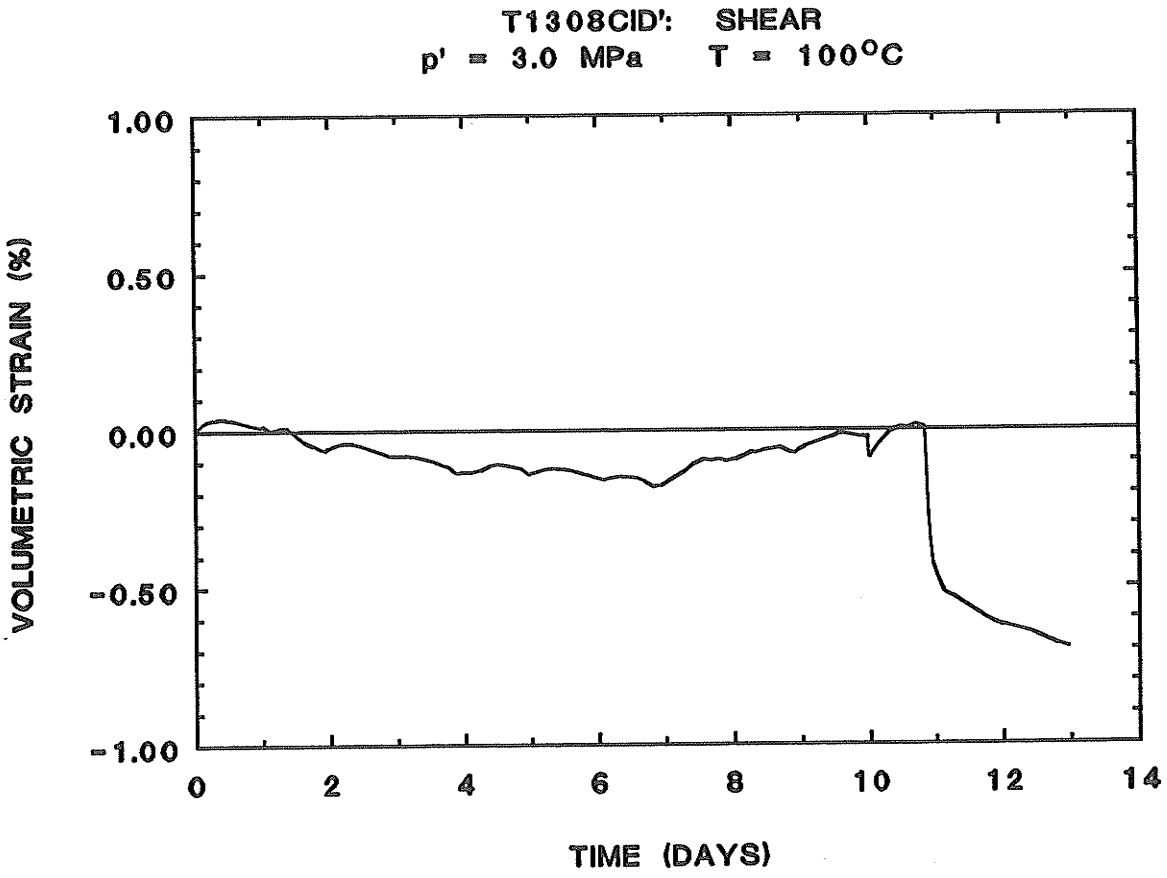

Fig. 5.46 Shear T1308. p' = 3.0 MPa, u_b = 1.0 MPa, T = 100°C
Volumetric Strain ε_v *vs.* Elapsed Time.

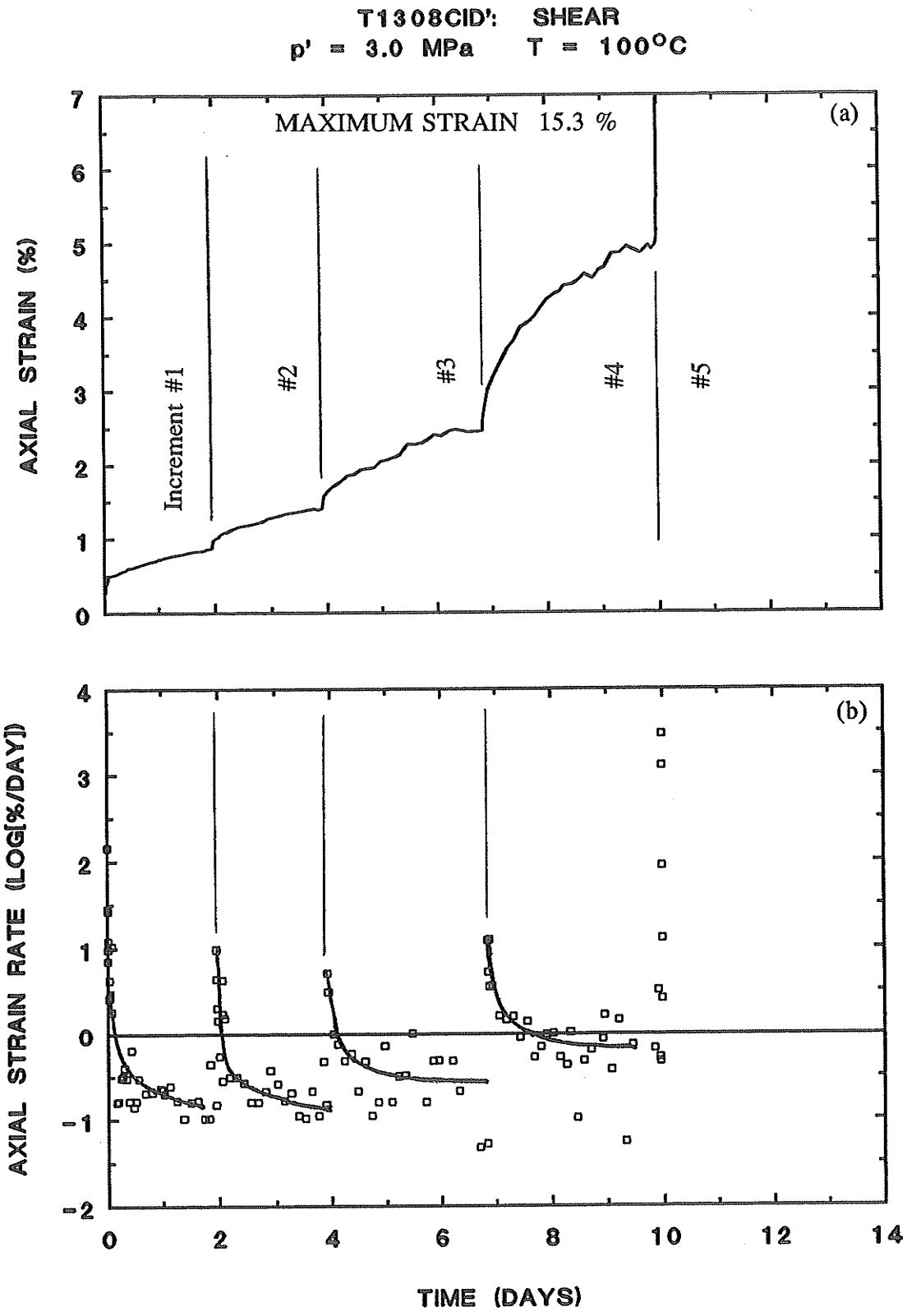

Fig. 5.47 Shear T1308. p' = 3.0 MPa, u_b = 1.0 MPa, T = 100°C

a) Axial Strain ε_1 *vs.* Elapsed Time.

b) Axial Strain Rate log $\dot{\varepsilon}_1$ *vs.* Elapsed Time.

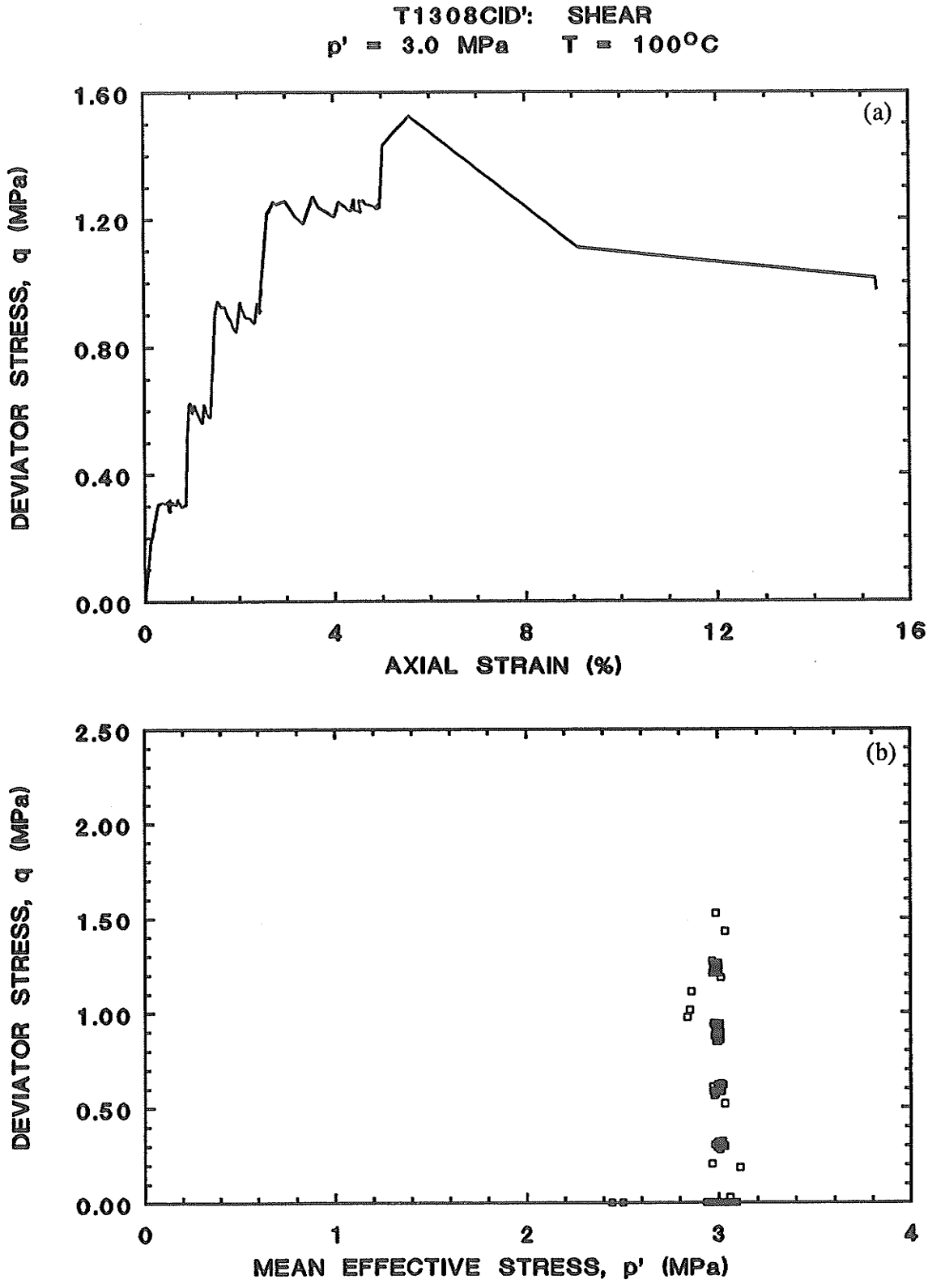

Fig. 5.48 Shear T1308. p' = 3.0 MPa, u_b = 1.0 MPa, T = 100°C

a) Deviator Stress q *vs.* Axial Strain ε_1.

b) Deviator Stress q *vs.* Mean Effective Stress p'.

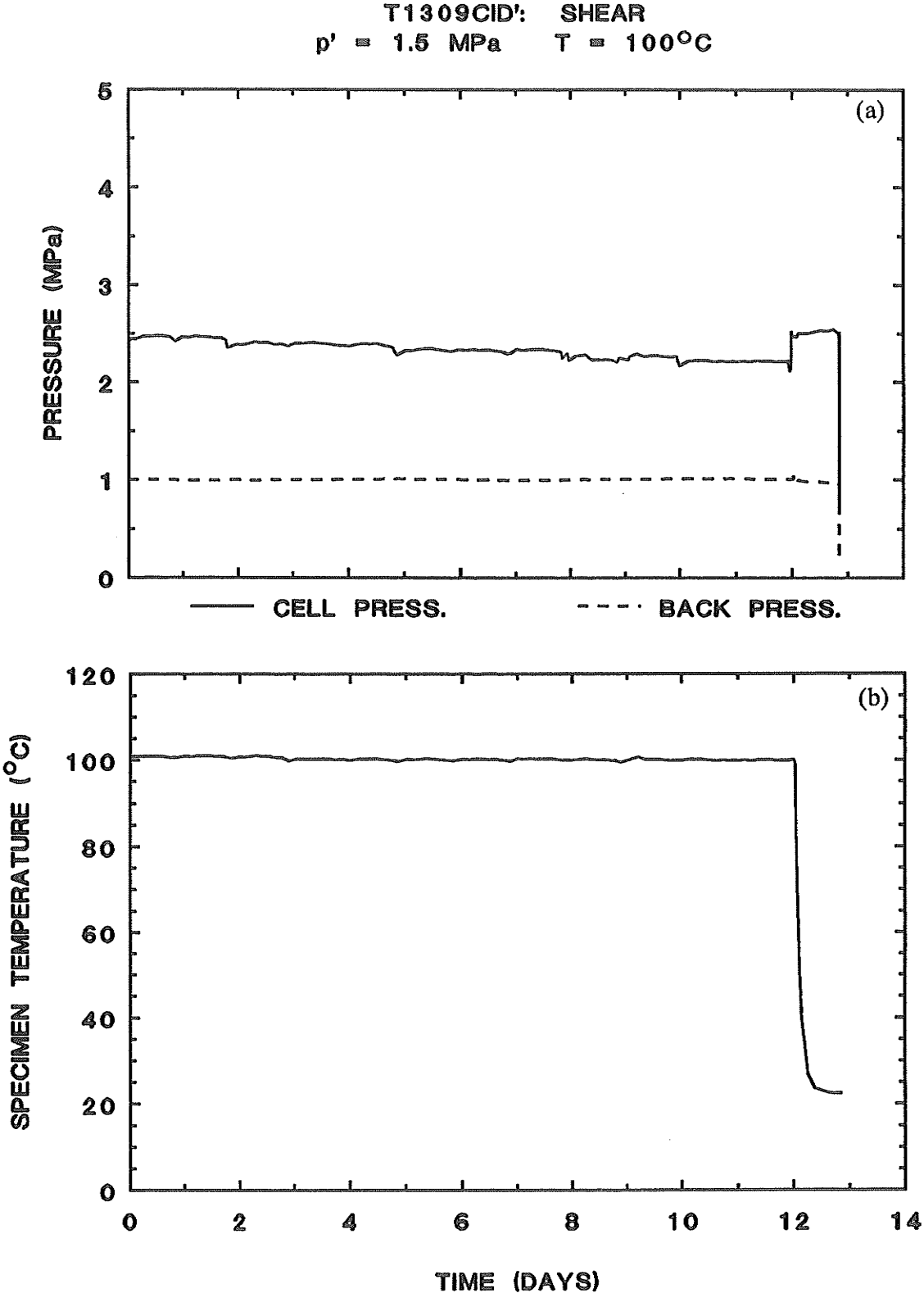

Fig. 5.49 Shear T1309. p' = 1.5 MPa, u_b = 1.0 MPa, T = 100°C
a) Cell σ_3 and Back Pressure u_b *vs.* Elapsed Time.
b) Specimen Temperature *vs.* Elapsed Time.

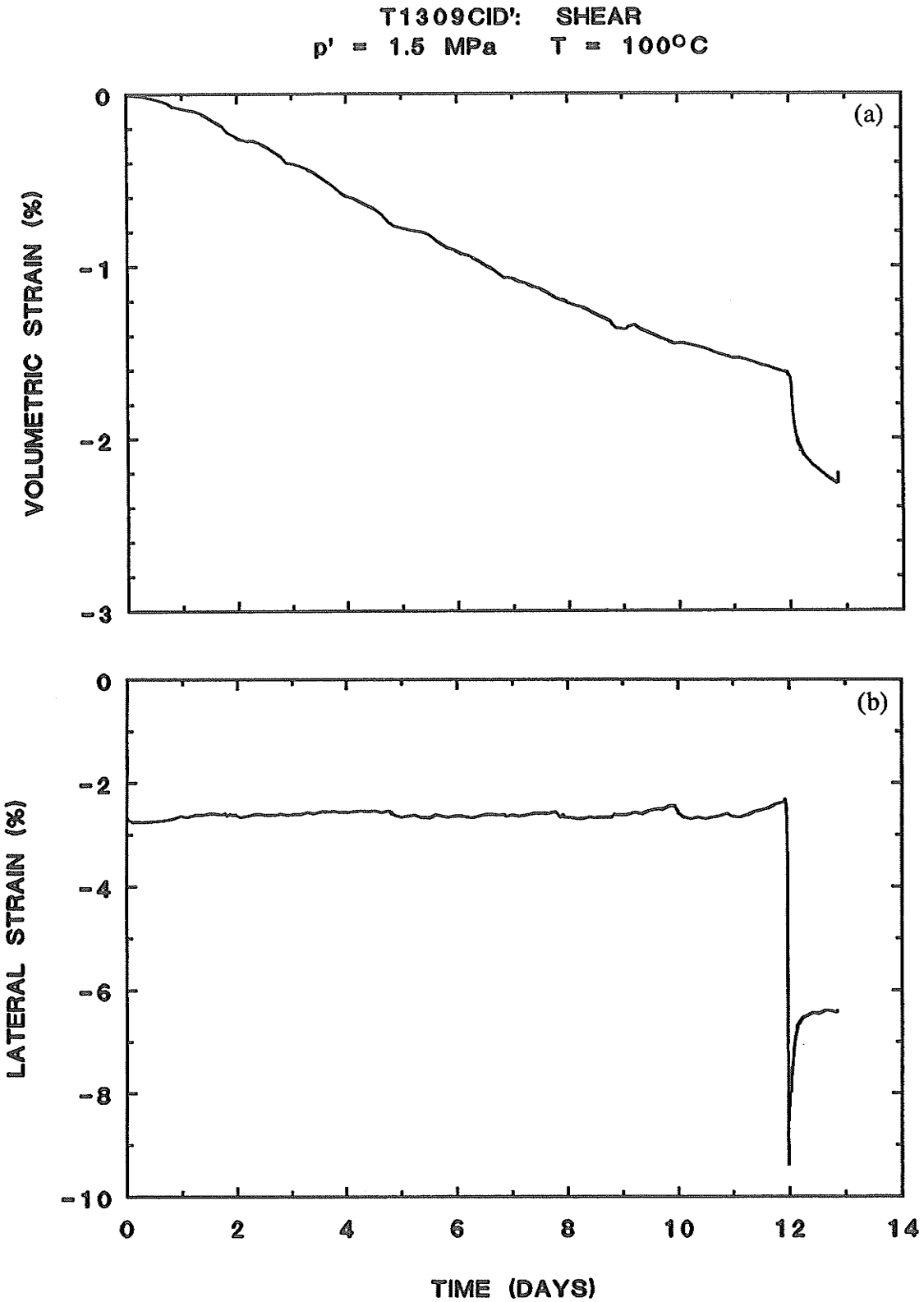

Fig. 5.50 Shear T1309. p' = 1.5 MPa, u_b = 1.0 MPa, T = 100°C

a) Volumetric Strain ε_v *vs.* Elapsed Time.

b) Lateral Strain ε_3 *vs.* Elapsed Time.

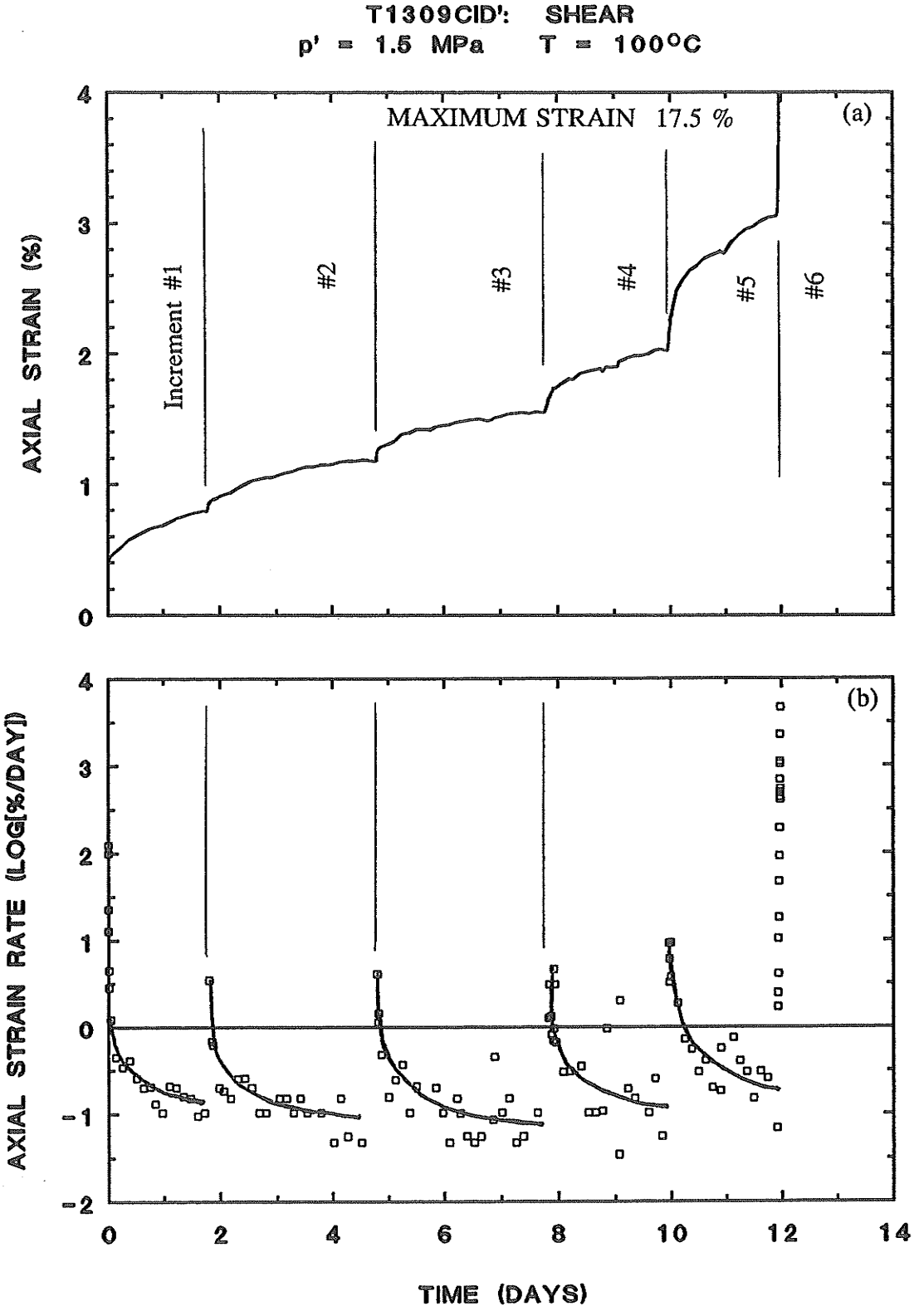

Fig. 5.51 Shear T1309. p' = 1.5 MPa, u_b = 1.0 MPa, T = 100°C

a) Axial Strain ε_1 *vs.* Elapsed Time.

b) Axial Strain Rate log $\dot{\varepsilon}_1$ *vs.* Elapsed Time.

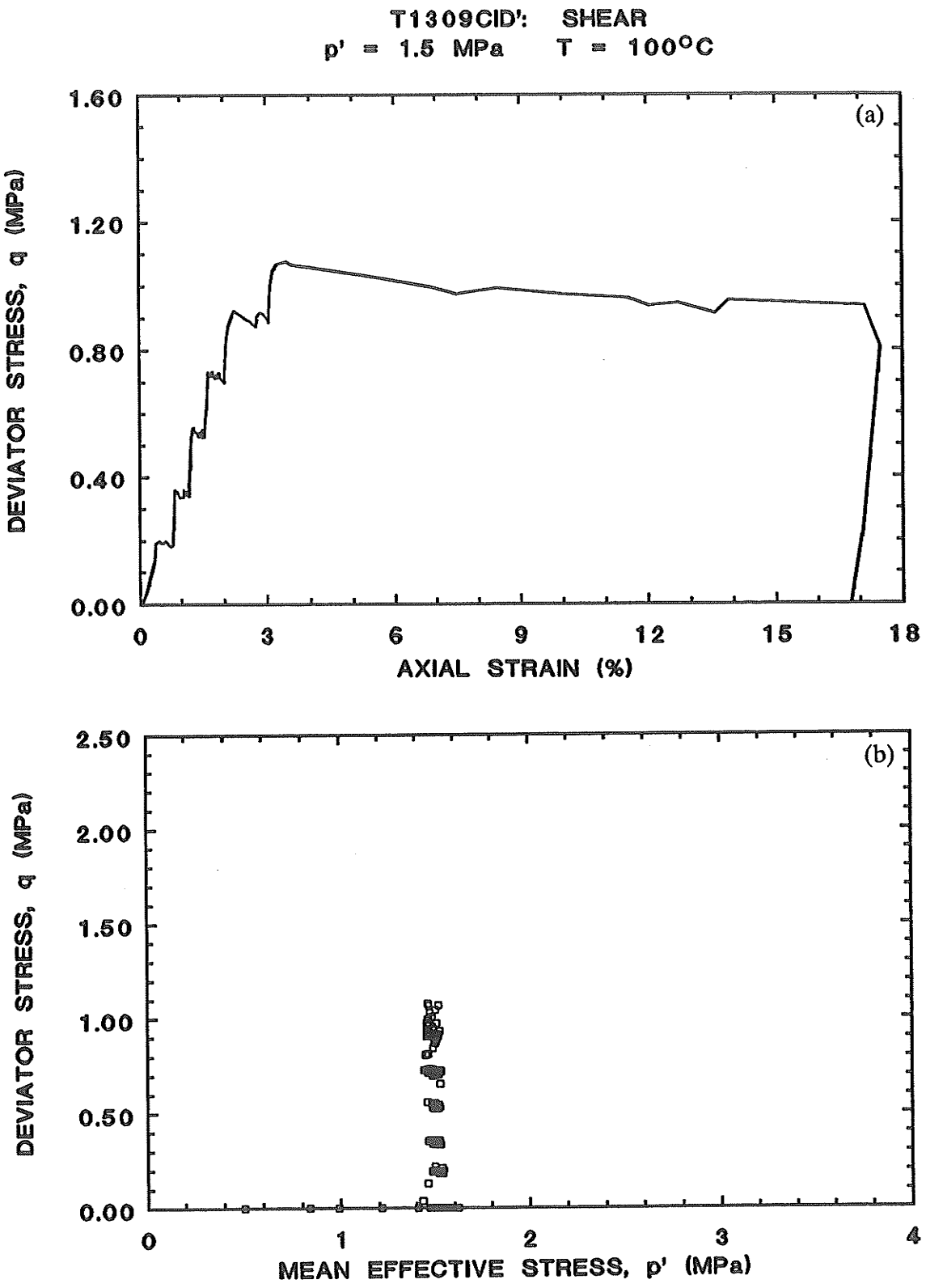

Fig. 5.52 Shear T1309. p' = 1.5 MPa, u_b = 1.0 MPa, T = 100°C

a) Deviator Stress q *vs.* Axial Strain ε_1.

b) Deviator Stress q *vs.* Mean Effective Stress p'.

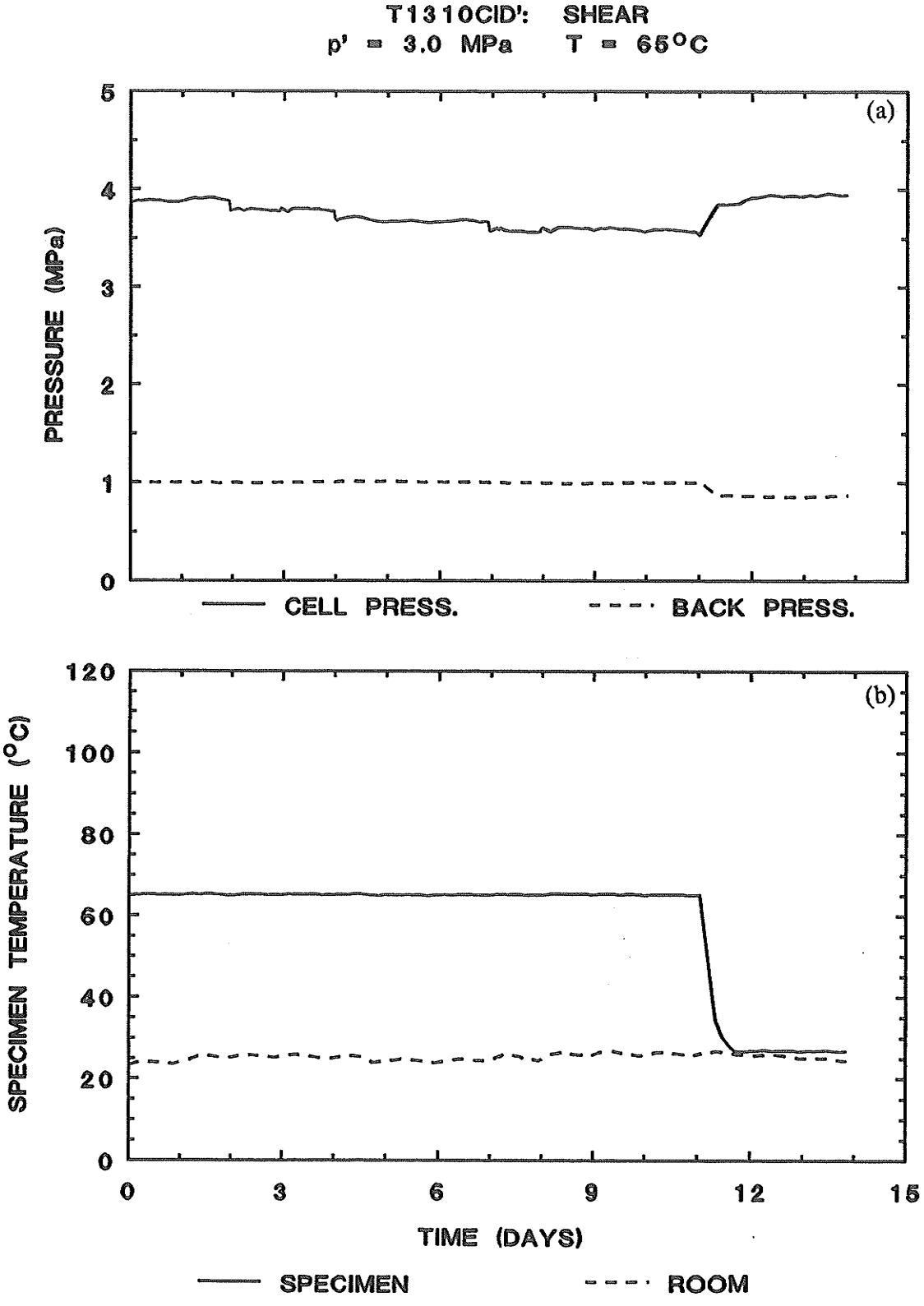

Fig. 5.53 Shear T1310. p' = 3.0 MPa, u_b = 1.0 MPa, T = 65°C

a) Cell σ_3 and Back Pressure u_b *vs.* Elapsed Time.

b) Specimen Temperature *vs.* Elapsed Time.

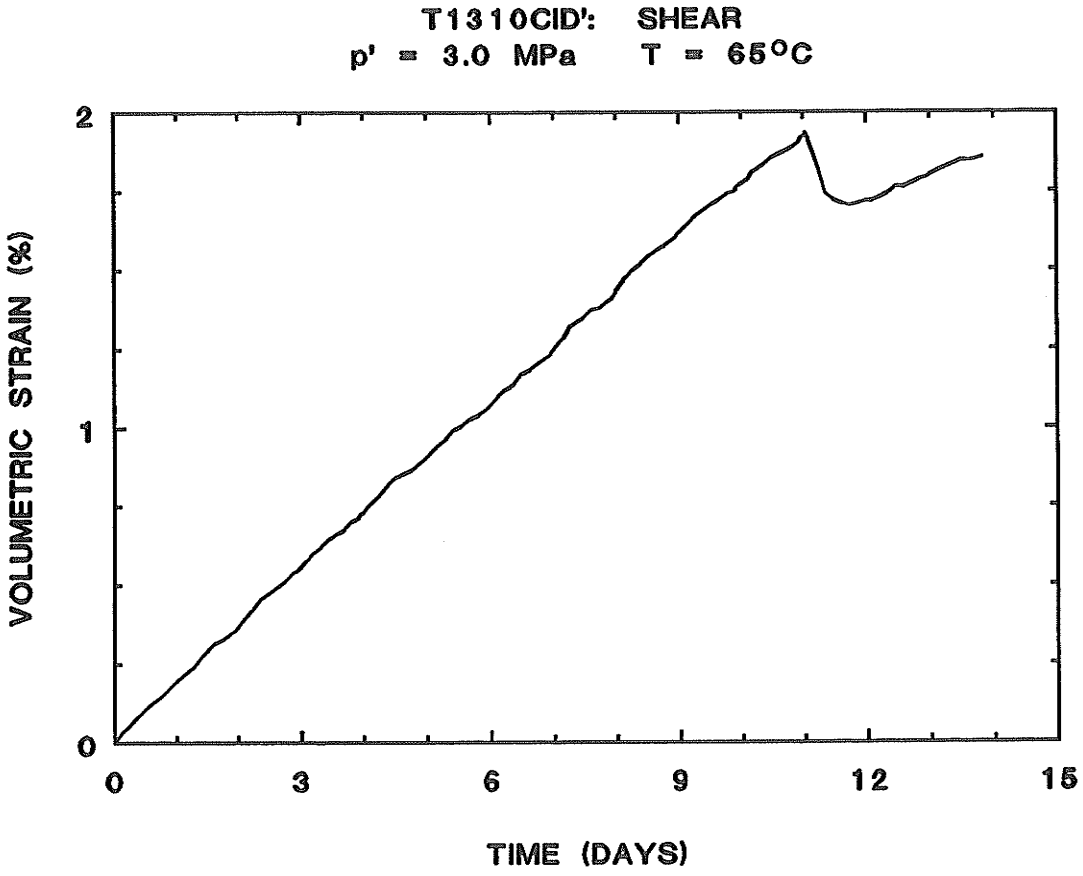

Fig. 5.54 Shear T1310. p' = 3.0 MPa, u_b = 1.0 MPa, T = 65°C
Volumetric Strain ε_v *vs.* Elapsed Time.

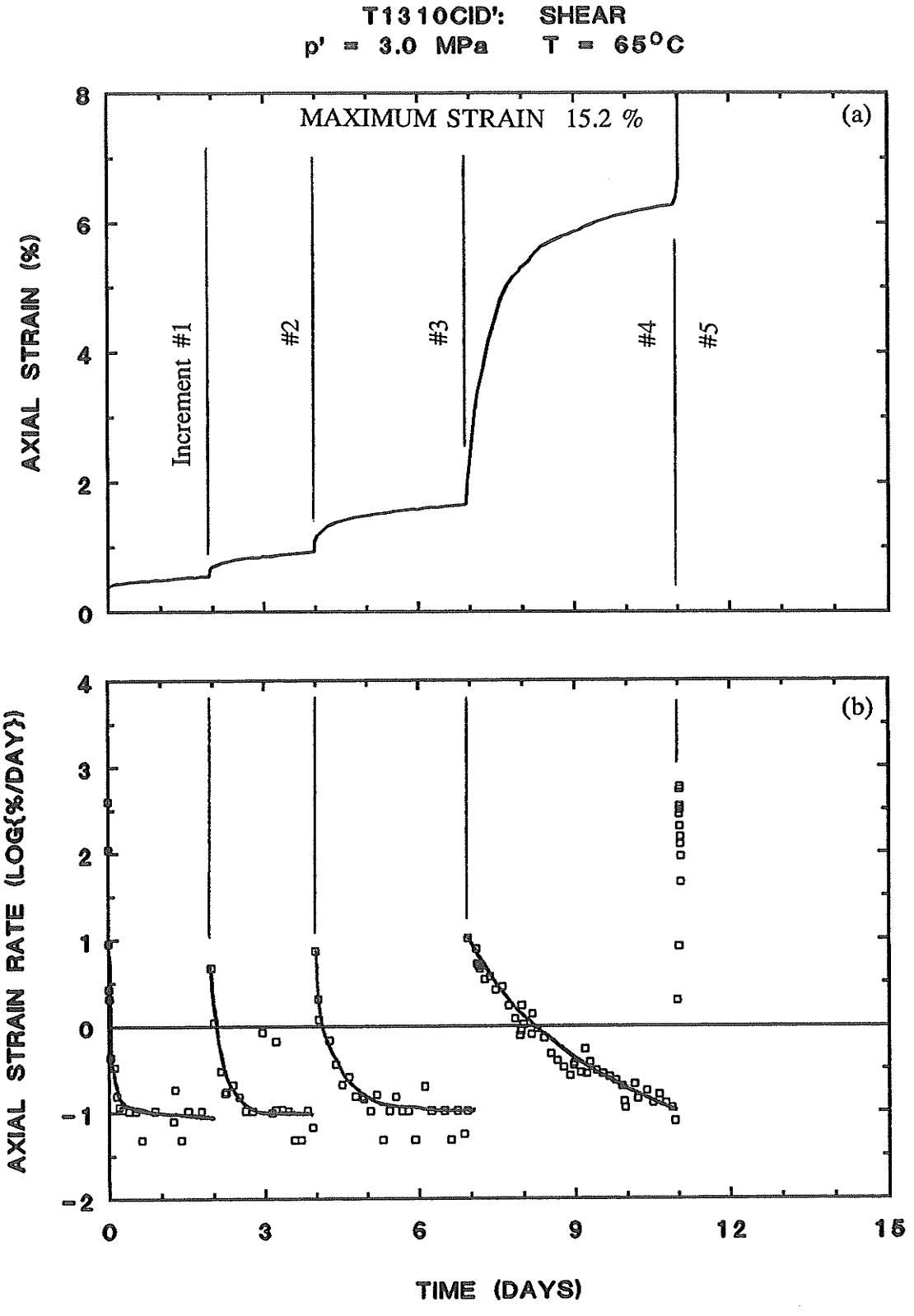

Fig. 5.55 Shear T1310. p' = 3.0 MPa, u_b = 1.0 MPa, T = 65°C

a) Axial Strain ε_1 *vs.* Elapsed Time.

b) Axial Strain Rate log $\dot{\varepsilon}_1$ *vs.* Elapsed Time.

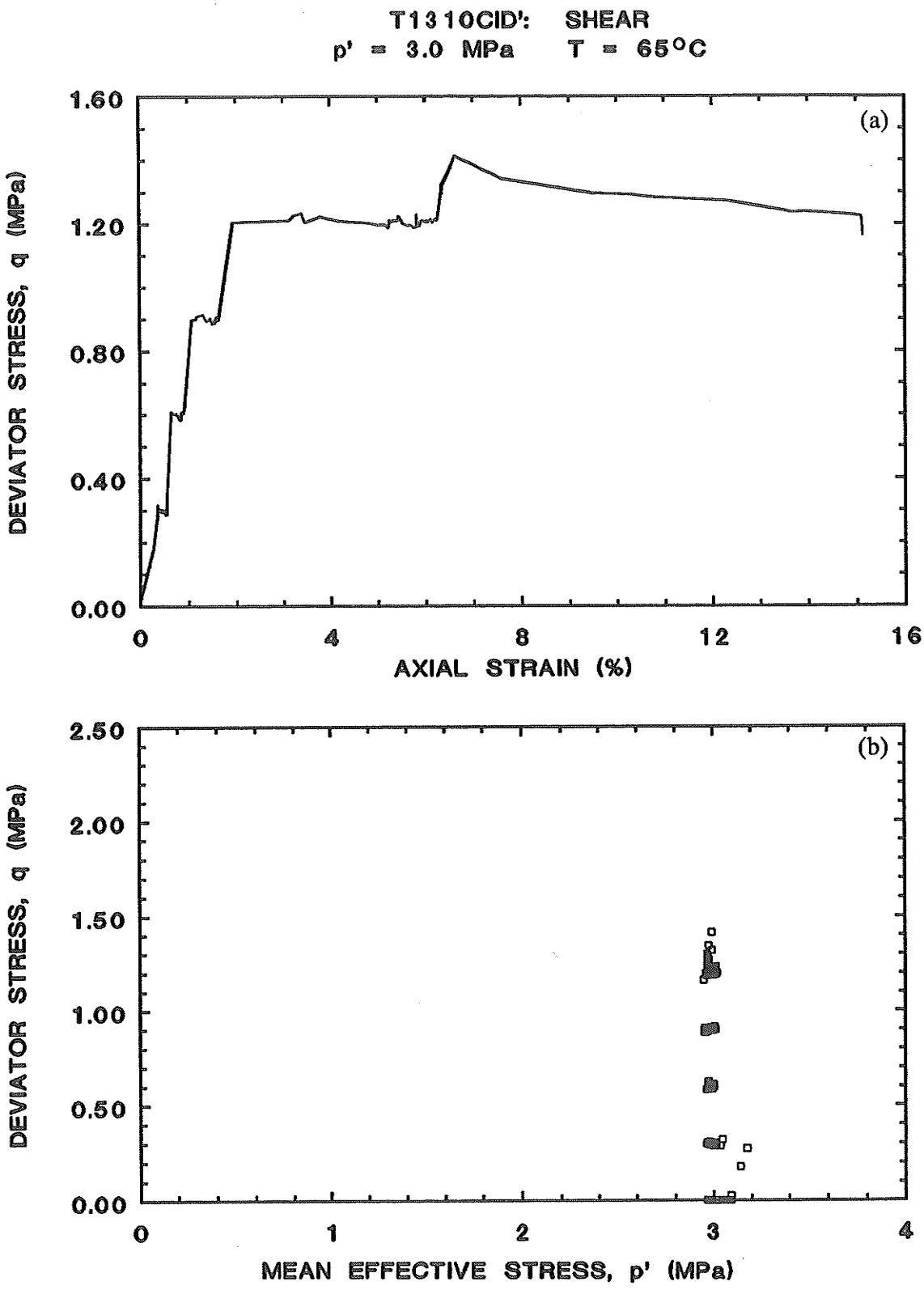

Fig. 5.56 Shear T1310. p' = 3.0 MPa, u_b = 1.0 MPa, T = 65°C

a) Deviator Stress q *vs.* Axial Strain ε_1.

b) Deviator Stress q *vs.* Mean Effective Stress p'.

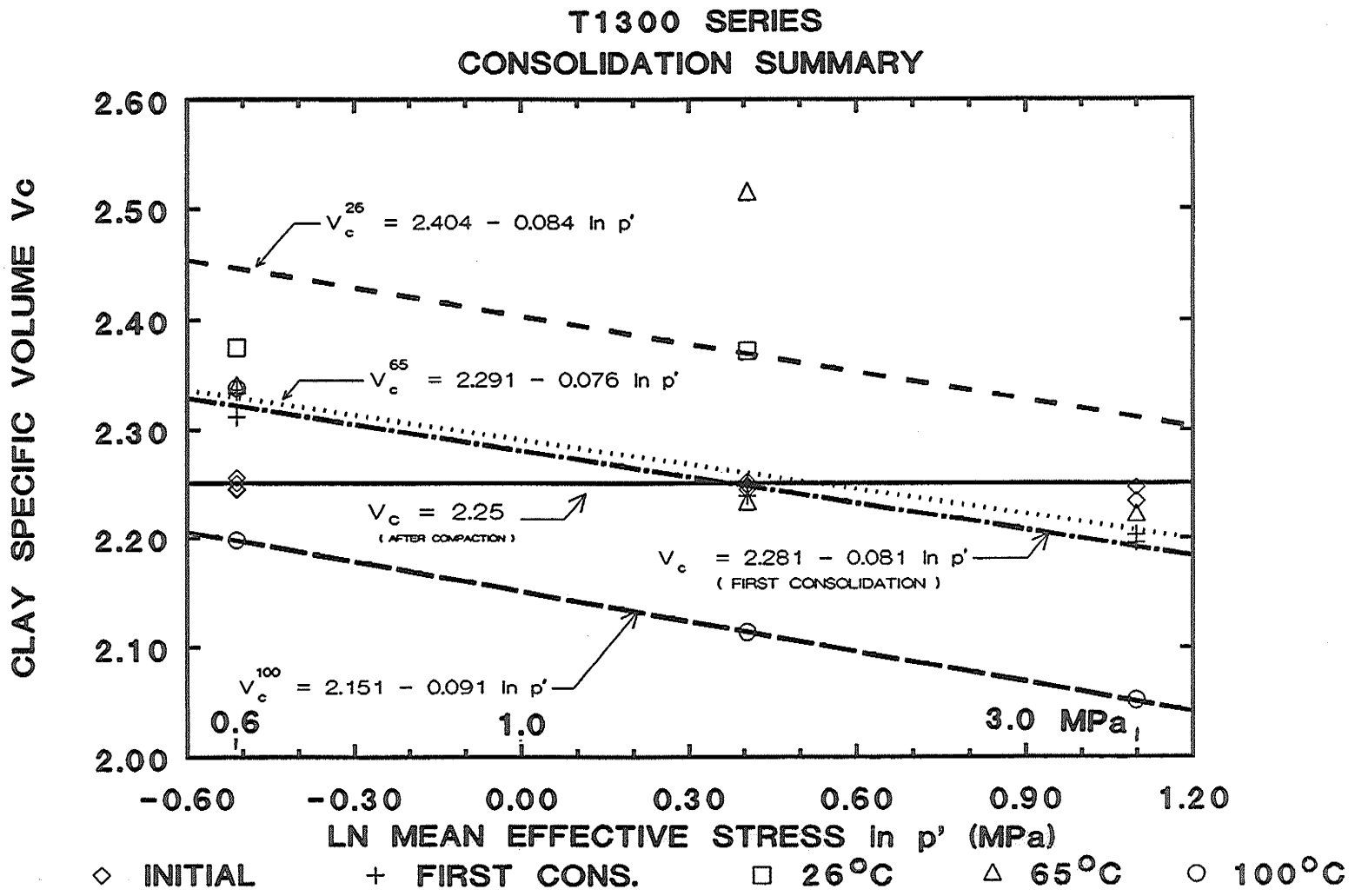

Fig. 5.57 Consolidation Summary for T1300 Series after a) compaction, b) first consolidation period at 26°C, and c) thermal consolidation at 26°C, 65°C, and 100°C.

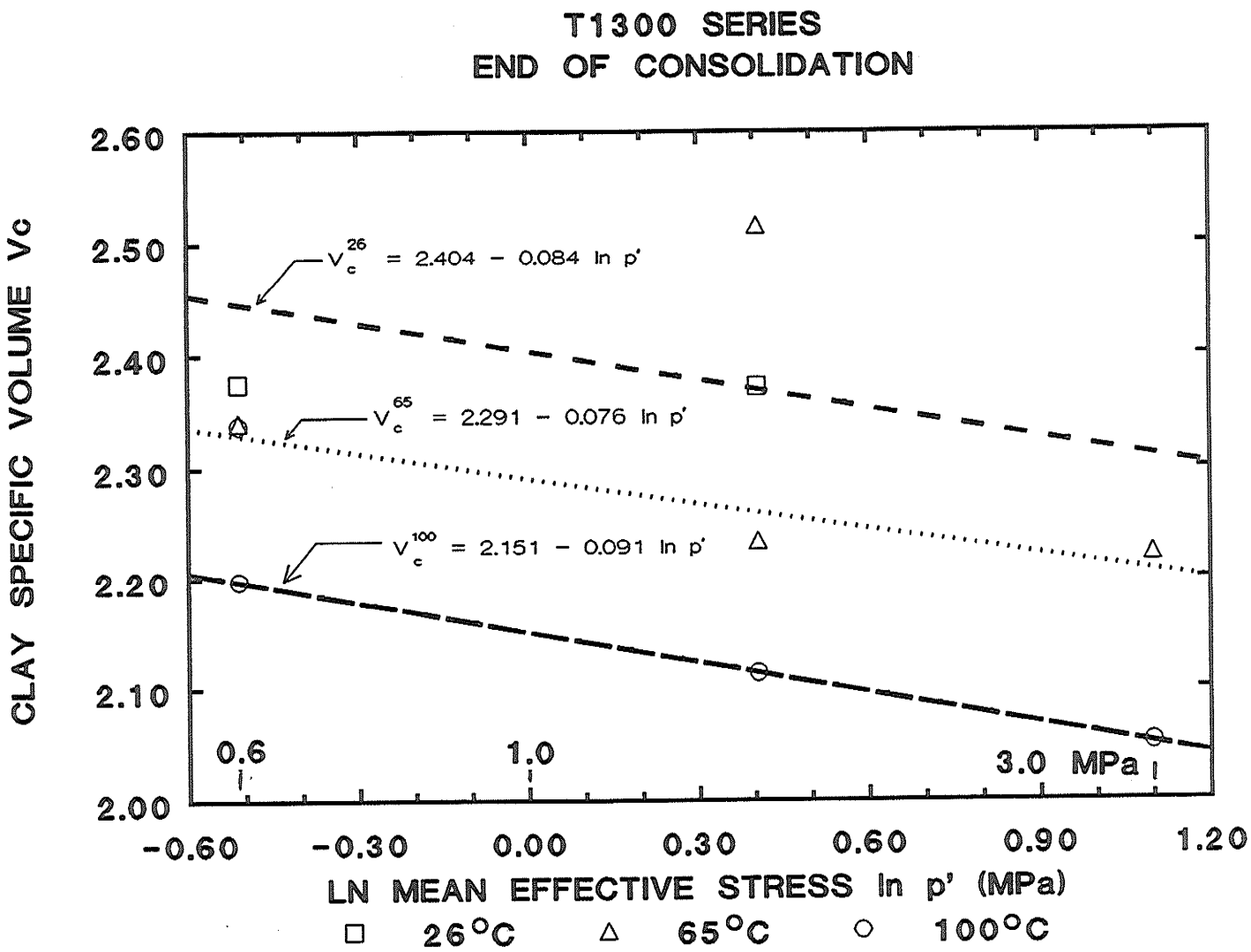

Fig. 5.58 Summary of End of Consolidation results as related to temperature.

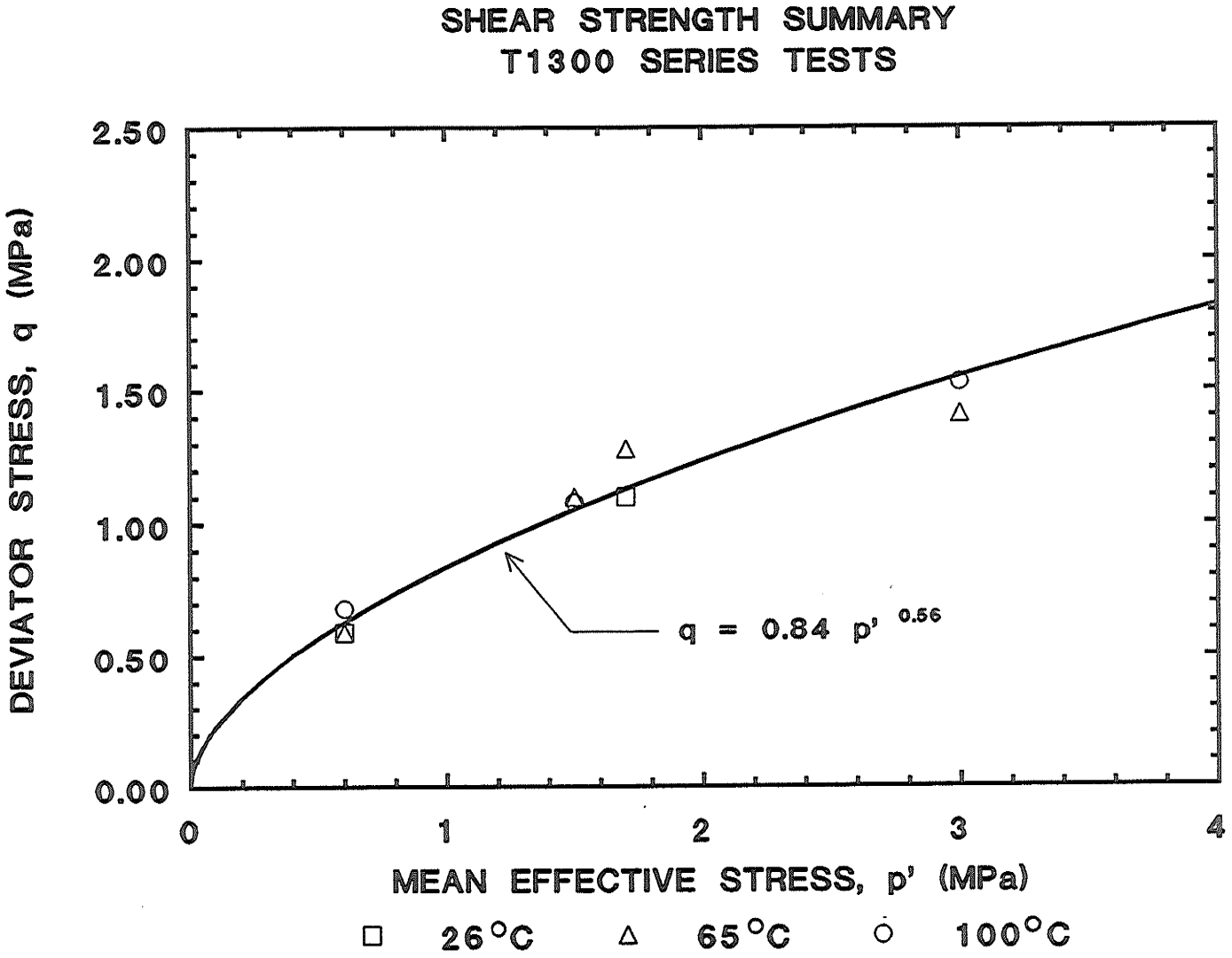

Fig. 5.59 Shear strength summary. Deviator Stress q *vs.* Mean Effective Stress p'.

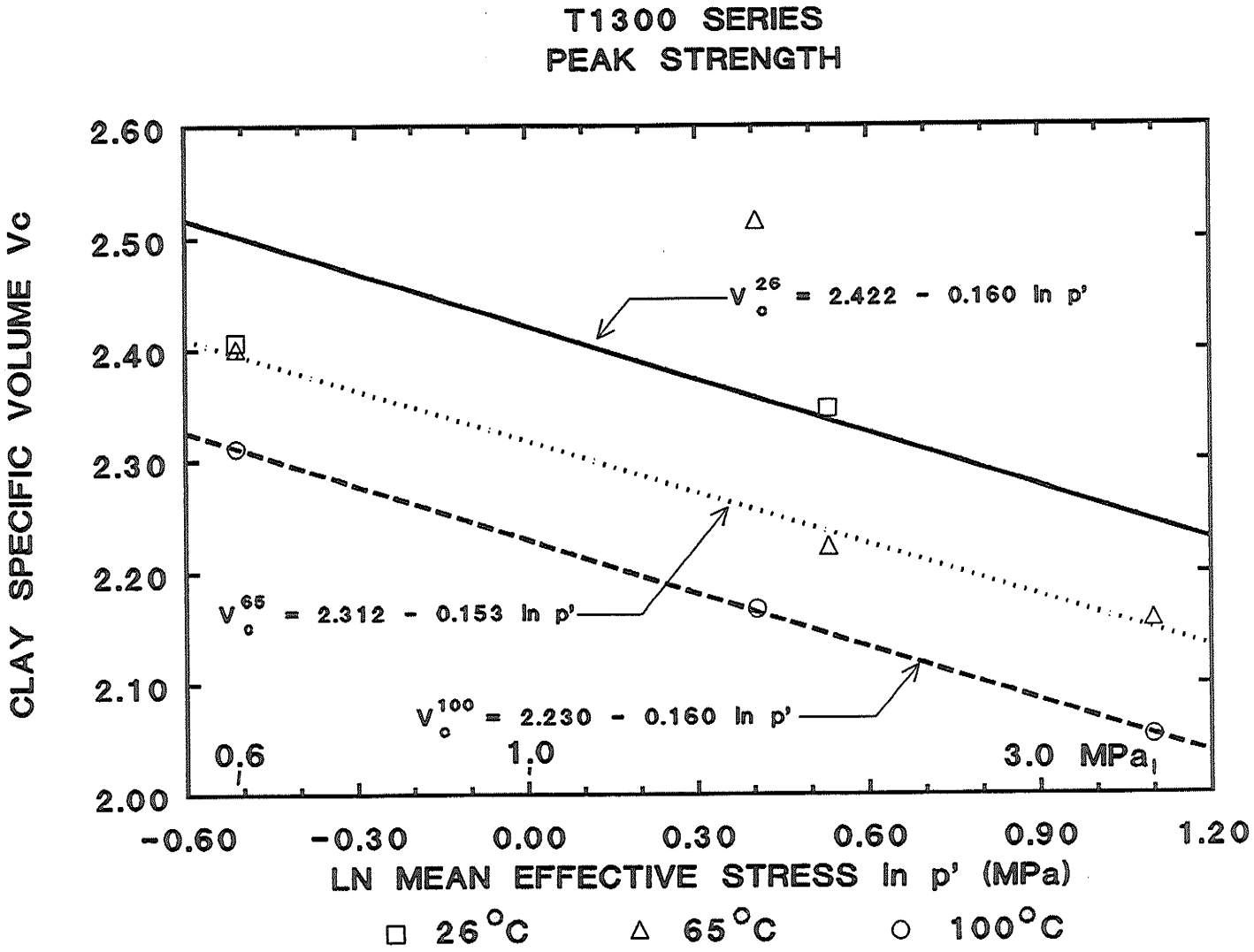

Fig. 5.60 Clay Specific Volume V_c *vs.* Mean Effective Stress ln p' at Peak Strength.

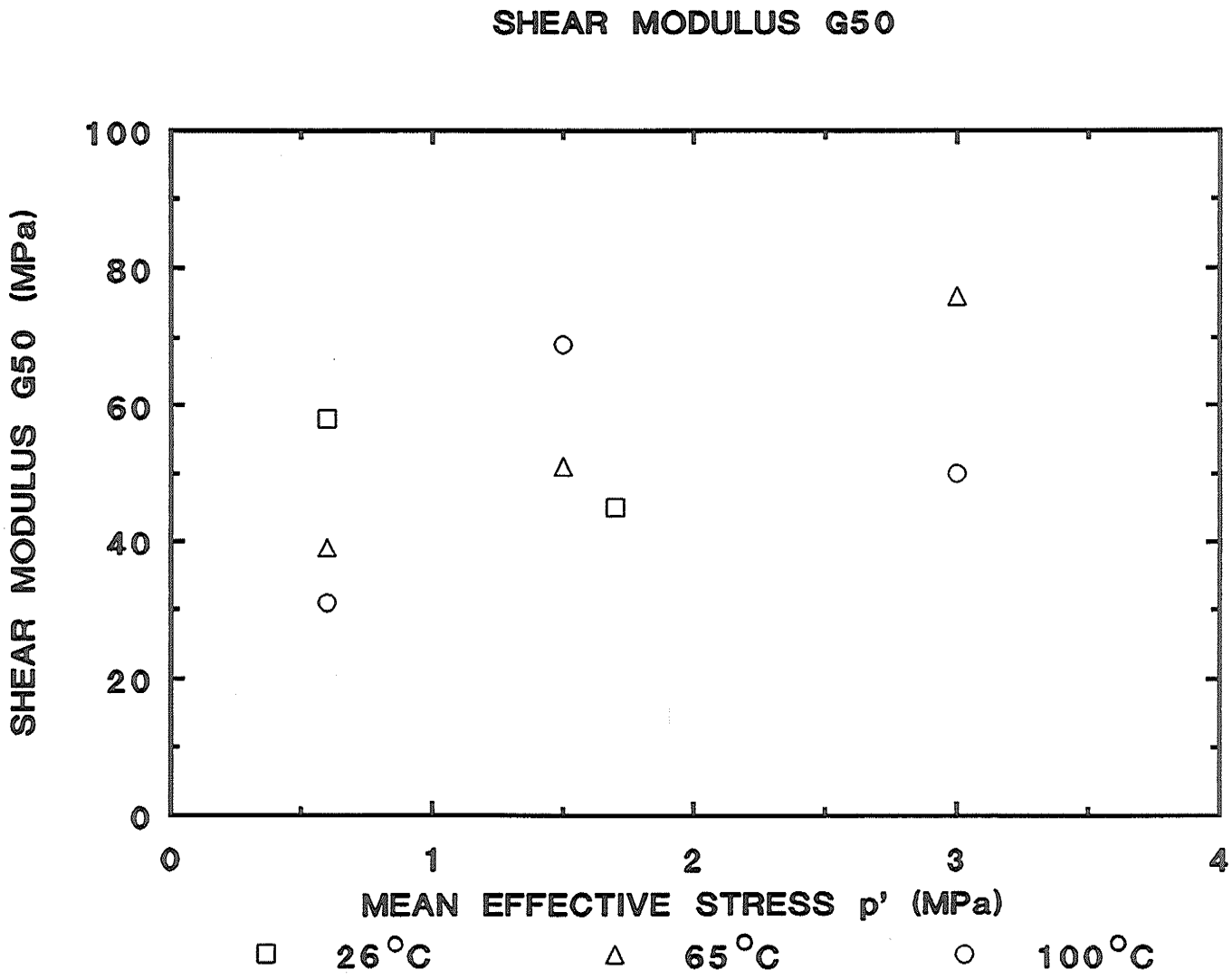

Fig. 5.61 Shear Modulus G_{50} Secant *vs.* Mean Effective Stress p'. Time interval 1-day.

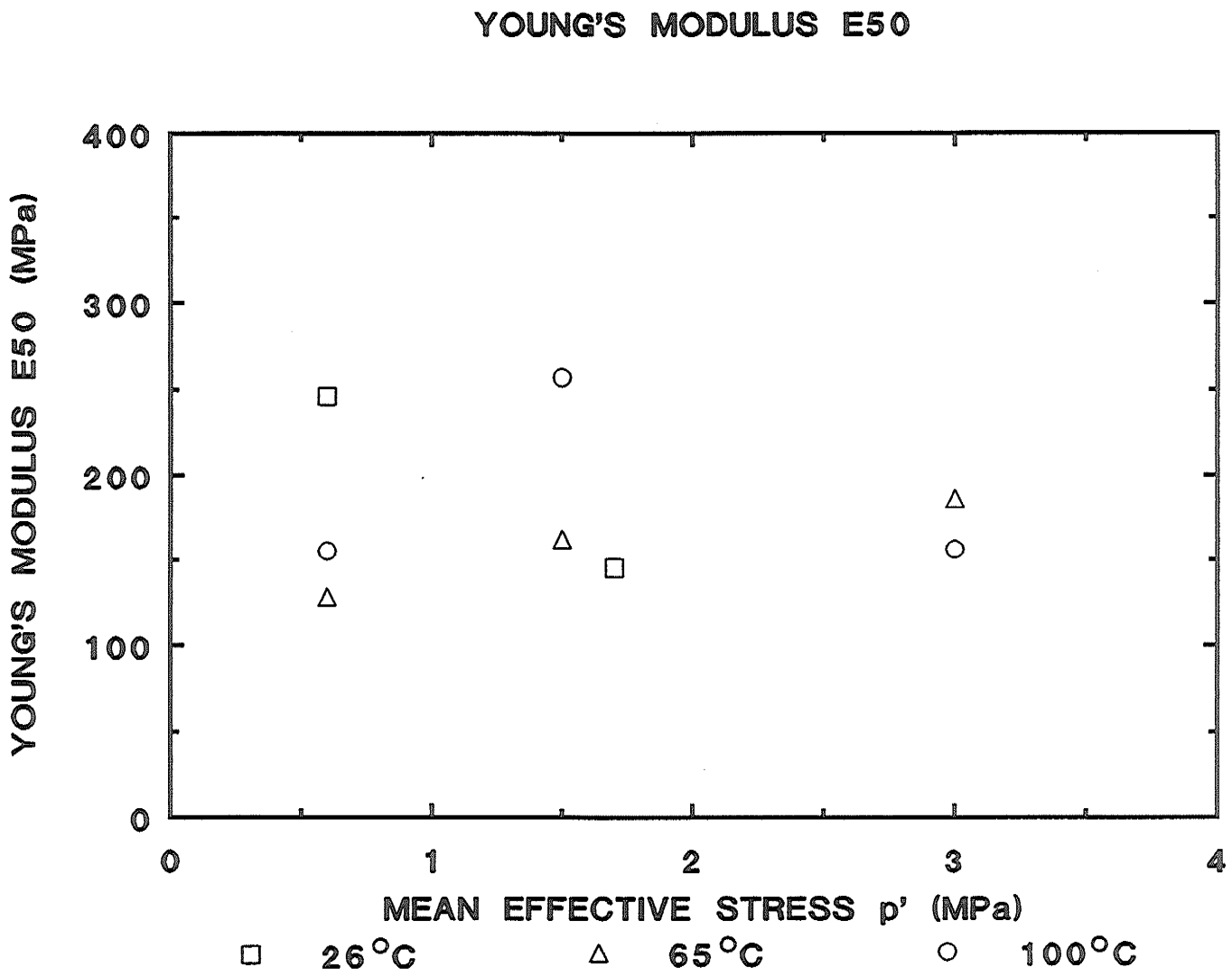

Fig. 5.62 Young's Modulus E_{50} Secant *vs.* Mean Effective Stress p'. Time interval 1-day.

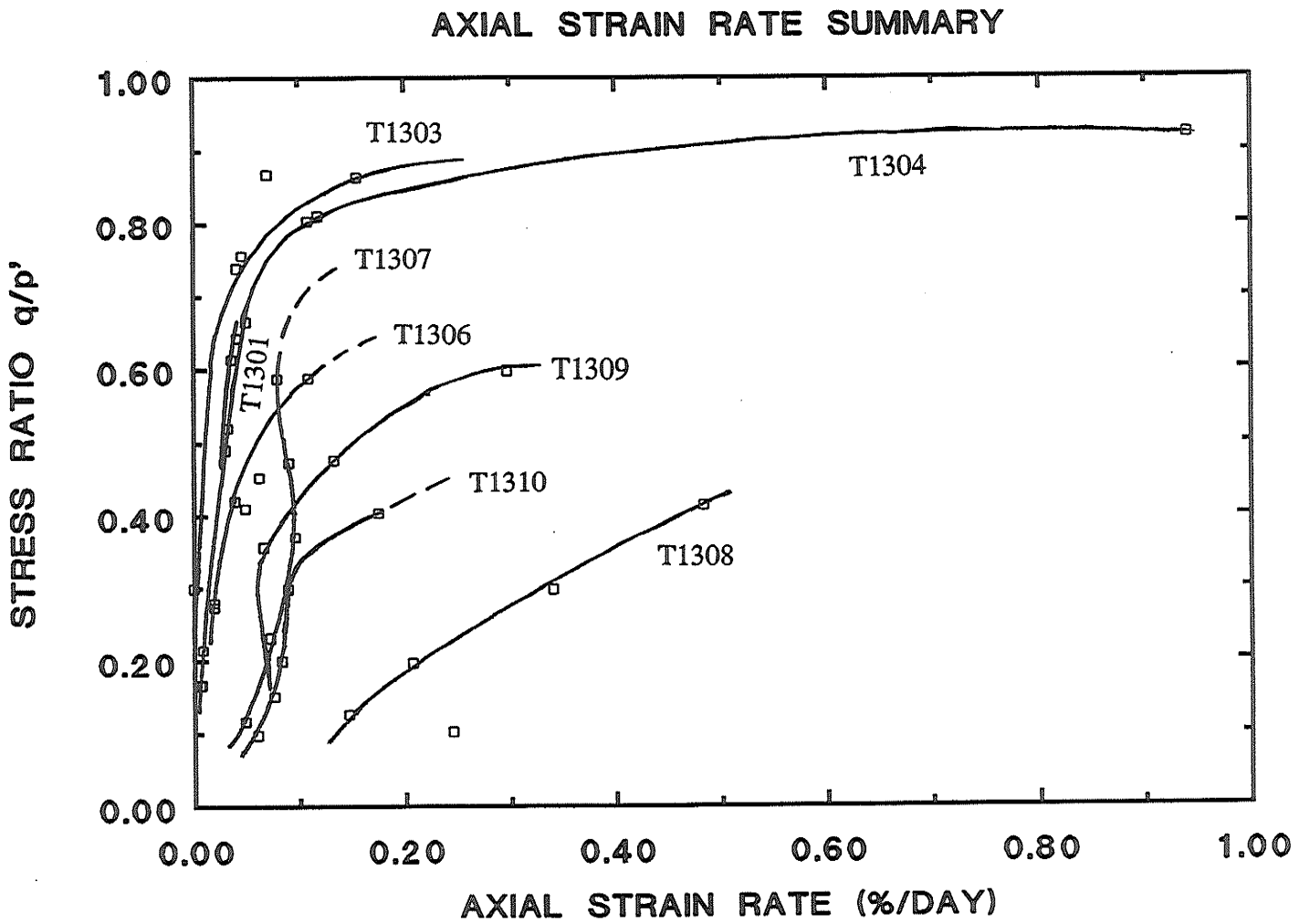

Fig. 5.63 Stress Ratio $\eta = q/p'$ *vs.* Axial Strain Rate $\dot{\varepsilon}_1$.

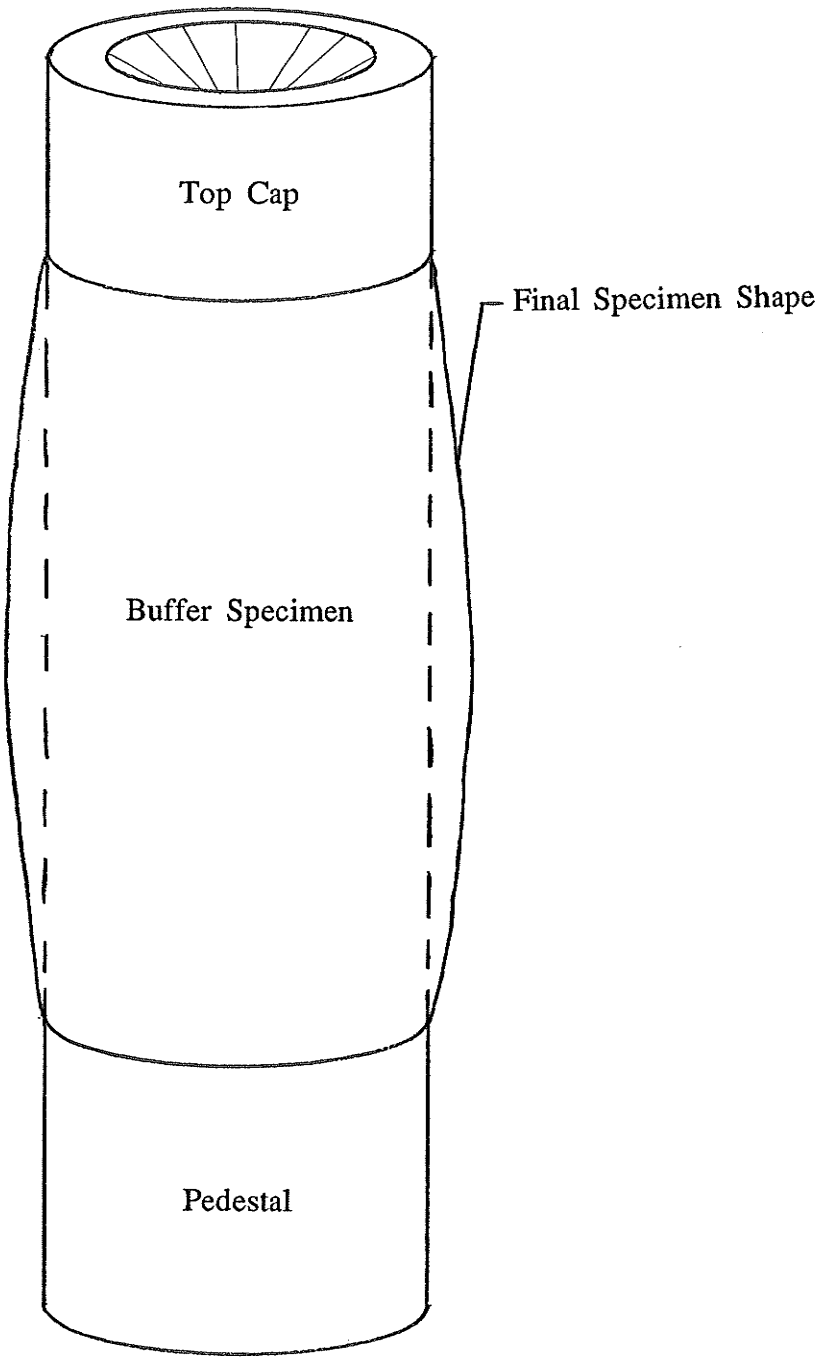

Fig. 5.64 Specimen exhibiting a barrel shape at the end of shear.

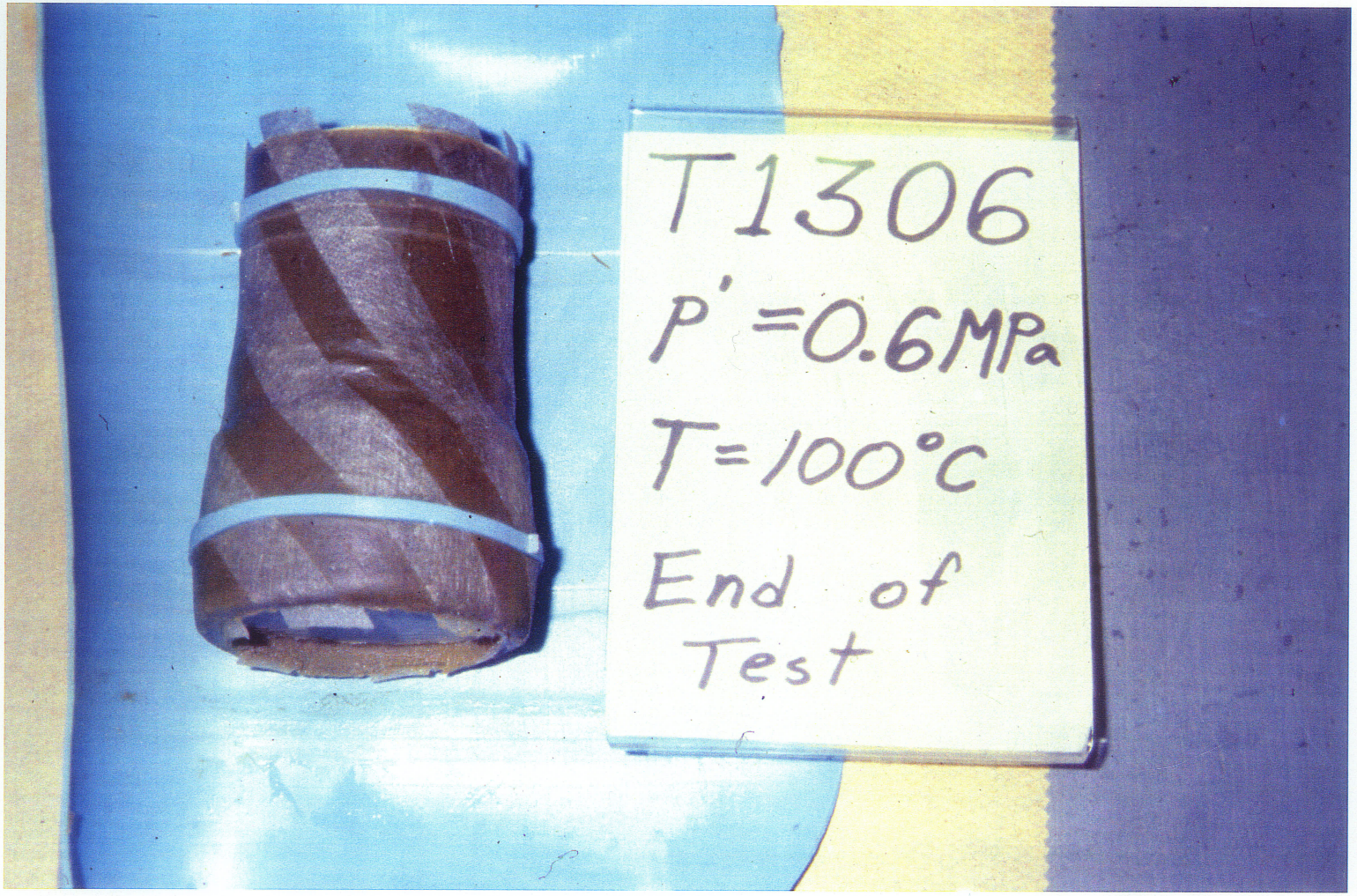

Fig. 5.65 Specimen exhibiting a widened base at the end of shear. Specimen T1306.

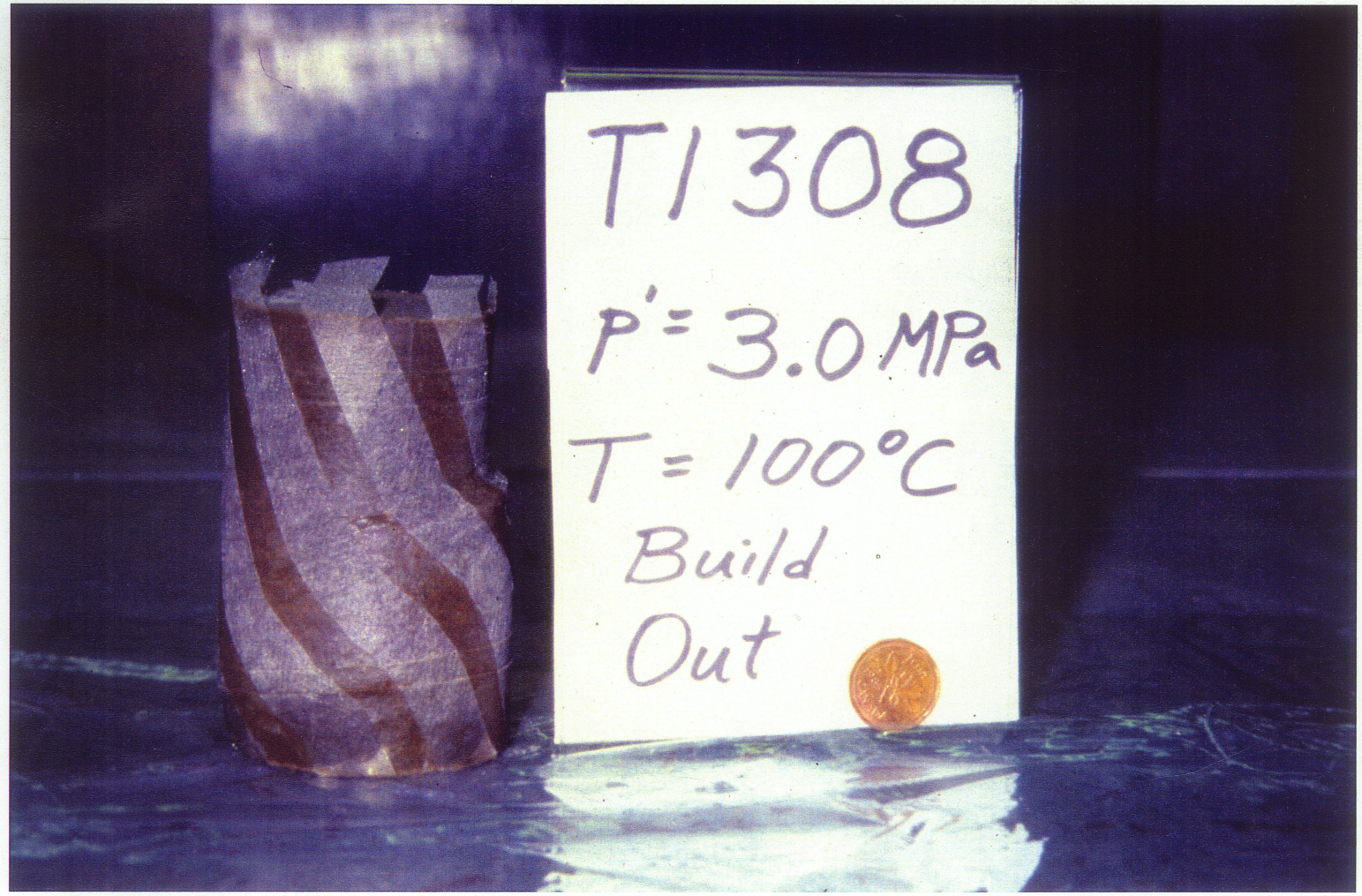

Fig. 5.66 Specimen exhibiting a shear plane at the end of shear. Specimen T1308.

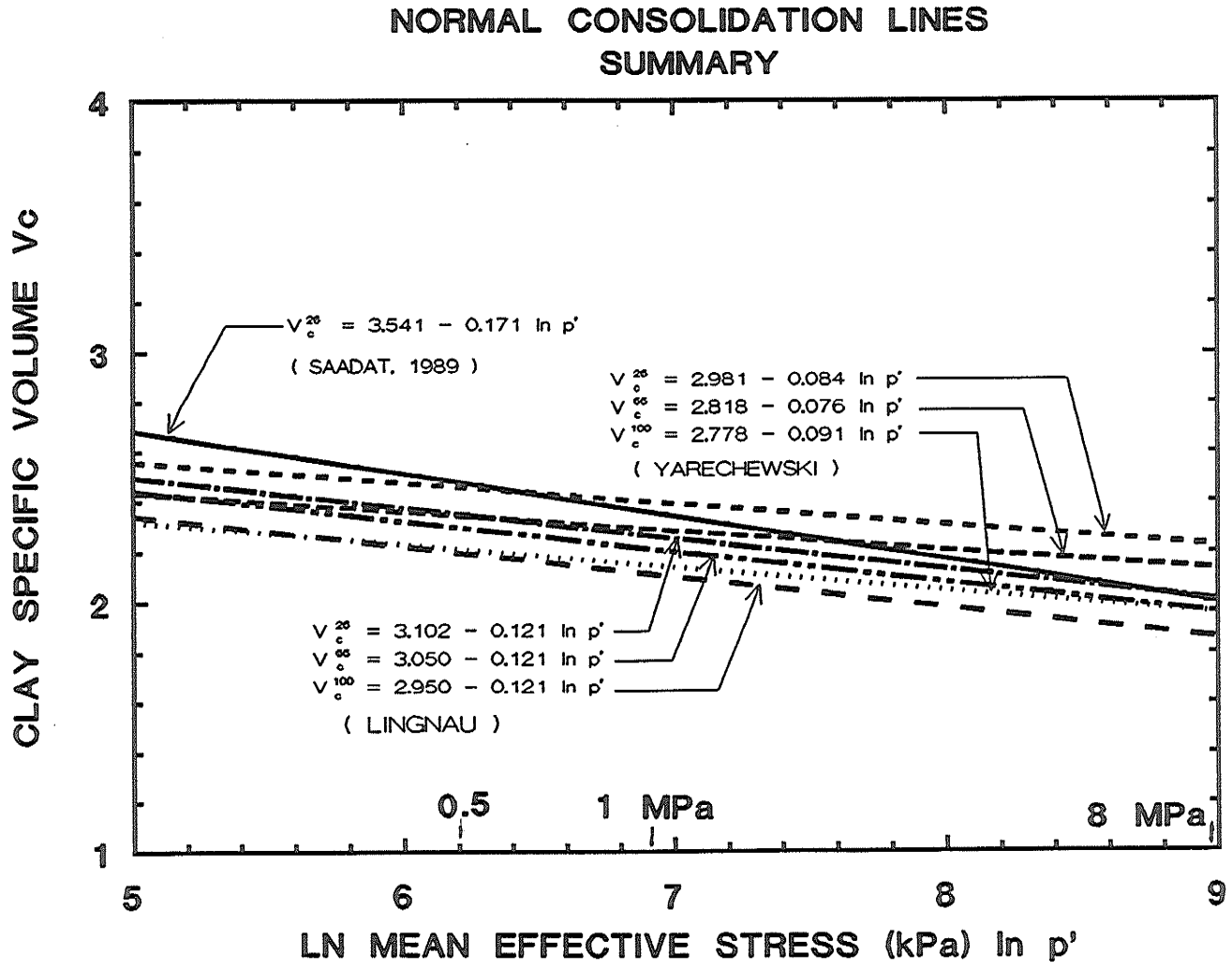

Fig. 6.1 Summary of normal consolidation lines compared with Lingnau and Saadat.

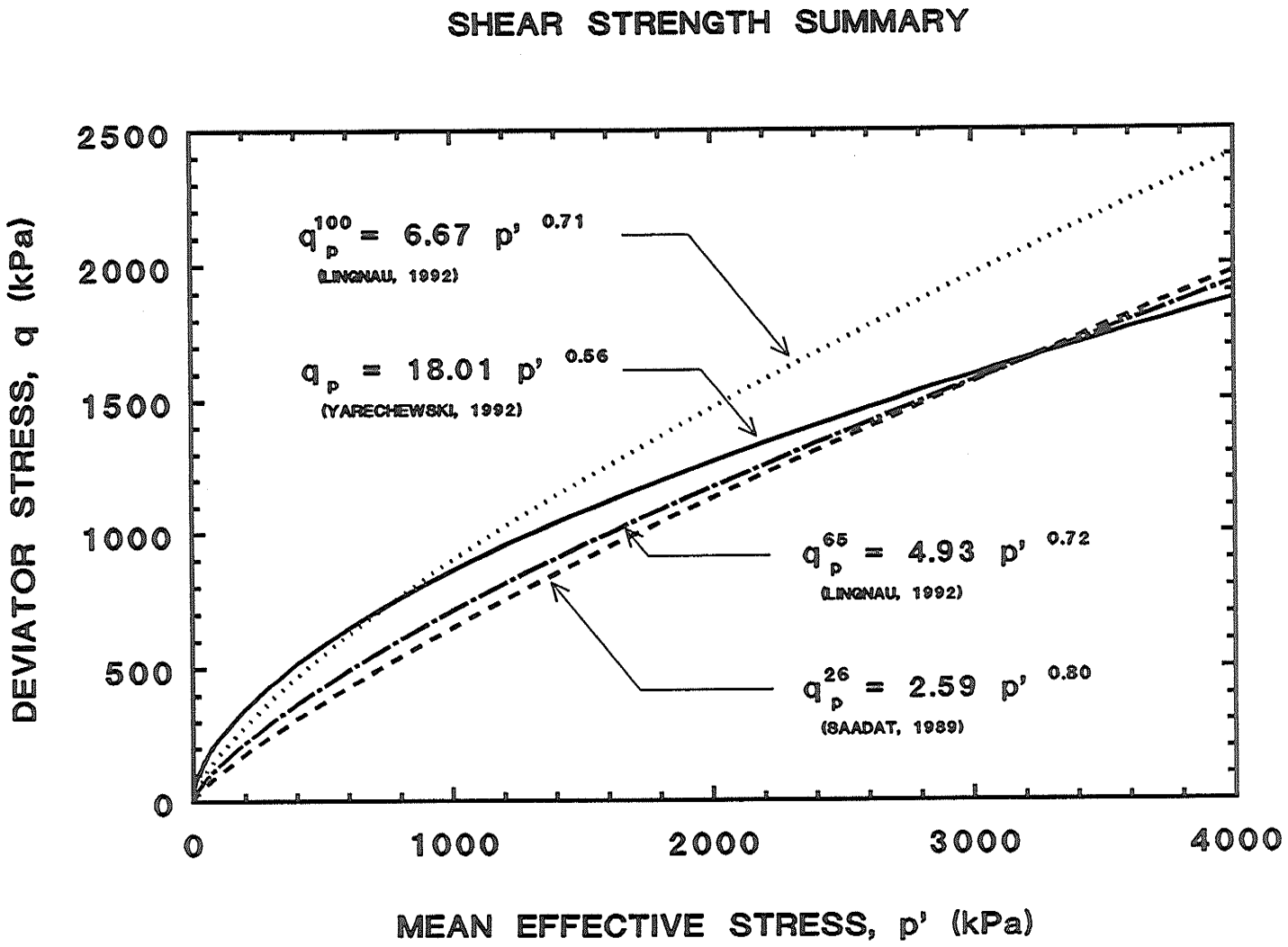

Fig. 6.2 Summary of shear strength results compared with results from Lingnau and Saadat.

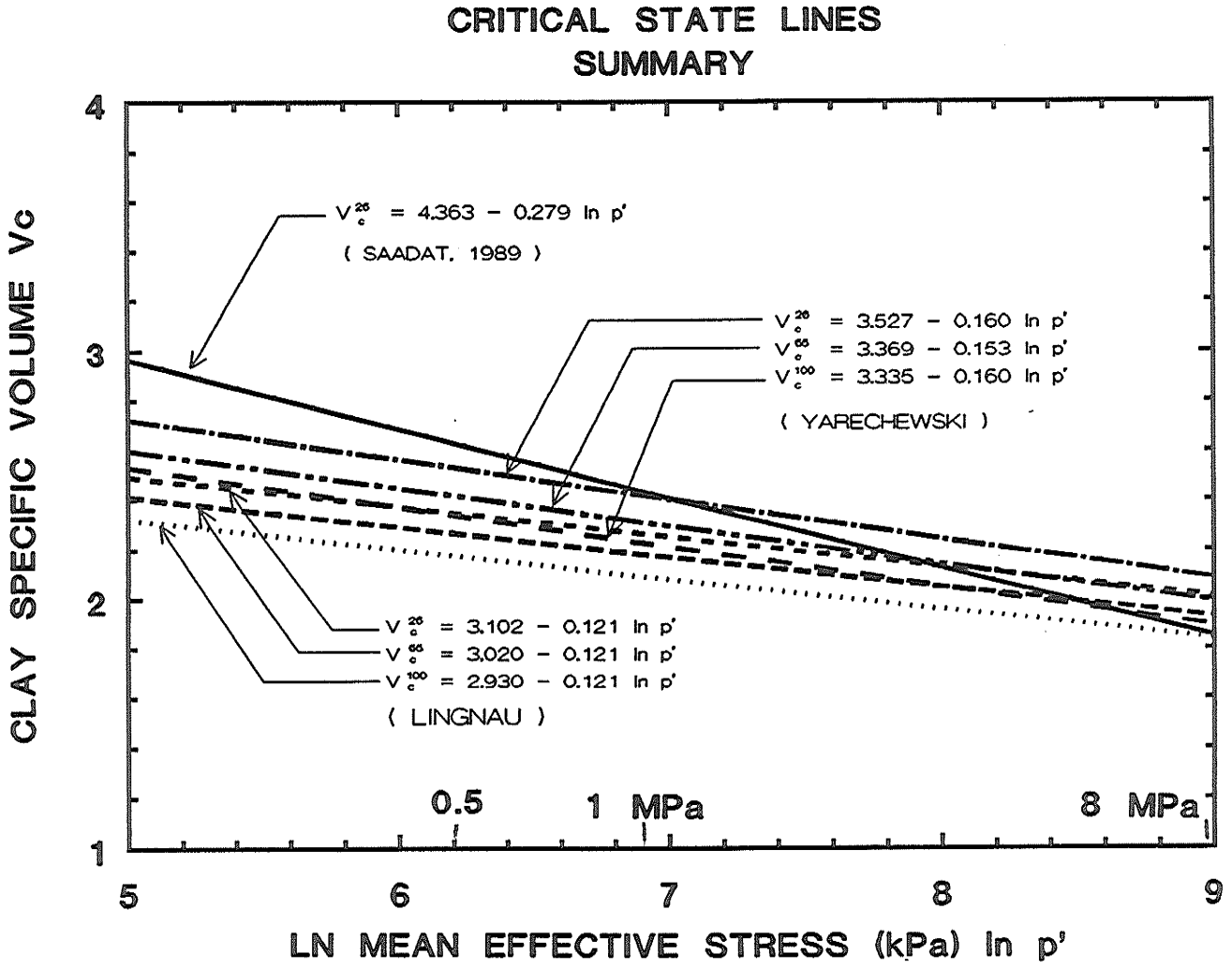

Fig. 6.3 Summary of critical state lines compared with Lingnau and Saadat.